Cellular Effects Nanosilver on Cancer and Non-cancer Cells: Potential Environmental and Human Health Impacts

by

Jessica Sheng

A thesis submitted to the Faculty of Graduate Studies and Research in partial fulfillment of the requirements for the degree of

Master of Science

in

Biology with Specialization in Chemical and Environmental Toxicology

Carleton University
Ottawa, Ontario

Abstract

Nanosilver is extremely small silver particles (1-100 nm in diameter) and have antimicrobial, antifungal, and antiviral properties, which make them one of the most commonly used nanoparticles. There is a lack of biological and toxicological knowledge on the impacts of nanosilver on cellular stress responses, as well as human and environmental health. Nanosilver and ascorbic acid has the potential to be an anticancer therapeutic. In this study, human colon cancer (HCT116) and intestinal epithelial (HIEC-6) cells were used to study nanosilver effects in cancer versus non-cancer cells. Nanosilver increased Nrf2 protein expression and disrupted the cell cycle at the G1 and G2/M phases. Hypoxia attenuated nanosilver-induced oxidative and endoplasmic reticulum stress responses. Nanosilver induced significant mitochondrial oxidative stress in HCT116, whereas it did not in the non-cancer HIEC-6 and nanosilver/sodium ascorbate co-treatment was preferentially lethal to HCT116 cells, which is promising for further research for anticancer therapies.

Acknowledgements

Throughout my Master's degree, I have received so much support from everyone in the lab and from my family. I would like to thank my supervisor Dr. Willmore whose knowledge, support, and guidance has helped navigate my way through my Masters. I would also like to thank Shana Cameron, who I have had the pleasure to work with for the past two years, and who has been a better mentor then I could ever ask for. Furthermore, I would like to thank everyone in the Willmore and Biggar Labs for their valuable expertise, advice, and guidance. Finally, I would like to thank my parents for their constant support.

Table of Contents

List of Tables

List of Figures

List of Acronyms

AhR: Aryl hydrocarbon receptor

APC: Adenomatosis polyposis coli

APS: Ammonium persulfate

ARE: Antioxidant responsive elements

ASK1: Apoptotic-signaling kinase-1

ATF: Activating transcription factor

DMEM: Dulbecco's modified eagle medium,

Dsh: Dishevelled

EGF: Human epidermal growth factor

eIF2α: Eukaryotic initiation factor 2

ER: Endoplasmic reticulum

FBS: Fetal bovine serum

FDA: Food and Drug Administration

GAPDH: Glyceraldehyde 3-phosphate dehydrogenase

GSH: Glutathione

GPx: Glutathione peroxidase

GSK: Glycogen synthase kinase

GST: Glutathione S-transferase

HCT116: Human colon cancer cells

HEK293T: Human embryonic kidney cells

HIEC-6: Human intestinal epithelial cells

HIF: Hypoxic inducible factor

HRE: Hypoxia-response element

IL: Interleukin

IRE1α: Inositol-requiring protein 1α

LEF: Lymphoid enhancer factor

MAPK: Mitogen-activated protein kinase

MDH: Malate dehydrogenase

MTT: 3-(4,5-Dimethylthiazol-2-yl)-2,5-diphenyltetrazolium bromide

nAg: Nanosilver

NCS: Newborn calf serum

NF: Nuclear factor

Nrf: Nuclear Factor erythroid 2 like 2

Nrf2: Nuclear factor erythroid 2 related factor 2

NF-κB: Nuclear factor kappa B

PBS: Phosphate buffered saline

PCP: Planar cell polarity

PERK: Protein kinase RNA-like endoplasmic reticulum kinase

PIM: Precision Medicine Initiative

PVP: Polyvinylpyrrolidone

ROR: Retinoic acid receptor-related orphan receptor

ROS: Reactive oxygen species

RYK: Receptor like tyrosine kinase

SFN: Sulflurophane

SOD: Superoxide dismutase

tBHP: Tert-butyl hydroperoxide

TBHQ: Tert-butylhydroquinone

TCE: Trichloroethanol

TCF: T cell factor

TCE: Tetramethylethylenediamine

TXN: Thioredoxin

UPR: Unfolded protein response

VEGF: Vascular endothelial growth factor

Chapter 1: Introduction

1.1 Nanoparticles

Nanoparticles are extremely small particles that are 1-100 nm in at least one dimension. Many factors can affect the toxicity of nanoparticles such as size, shape, chemical composition, solubility, surface coating and more[1–3]. Nanoparticles due to their small size, have a high surface area to volume ratio which can result in more potentially harmful ions released from the nanoparticle surface[4]. The high surface area to volume ratio can also result in high reactivity due to the relative increase of atoms and molecules that are able to be on the surface for reactions and colloidal instability[5,6]. Studies have shown that the toxicity of nanoparticles may be size-dependent where smaller particles may be more toxic[7,8]. There are various types of nanoparticles such as carbon, metal, polymer-based, and semiconductor-based nanoparticles. Nanoparticles are used in many different applications now such as in food science, cosmetics, electronics, agriculture, and pharmaceuticals.[3,9] Exposure to nanoparticles can occur through exposure to various consumer products. Exposure to nanoparticles commonly occurs through dermal and ingestion exposure, and inhalation from people who work in nanoparticle manufacturing facilities[2,10,11].

Nanoparticles also have clinical applications such as for drug delivery, delivery of mRNA in immunotherapy, cancer, or diseases in the lungs or spleen, and use as therapeutic agents for diseases such as diabetes, neurological disorders, and cancer[12,13]. Currently, the major categories of clinically approved nanomedicines are lipid, polymer, and protein-based particles. Using nanoparticles as a carrier for controlled drug release is a common application in nanomedicine[13]. An excellent review by Bobo and colleagues (2016) has a

list of the United States Food and Drug Administration (FDA) approved nanomedicines as of 2016, which includes use of nanomaterials in treatments of Crohn's disease, arthritis, multiple sclerosis, prostate, ovarian, breast, and pancreatic cancer, hepatitis B and C, fungal infections, and iron deficiency[14]. The nanomaterials' role in these treatments include controlled delivery of drugs, improved stability of proteins, increase in delivery of drugs to disease sites to reduce systemic toxicity, extended release of drugs, increase cell uptake of drugs, biomarker detection assays, and growth of bones by mimicking bone structure to allow for cell adhesion and growth[12,14]. Future directions for nanomedicine look at more complex nanomedicine systems to allow for controlled release, active targeting of diseases, and additional drug approaches for to decrease challenges faced by traditional therapeutics for various diseases with a general goal of less systemic toxicity by more efficient specific disease site targeting and drug accumulation at the disease sites[14].

There are various types of nanoparticles composed of inorganic elements including metals, non-metals, and magnetic elements, polymers, lipids, hydrogels, carbon nanoparticles such as carbon nanotubes, and quantum dots[10,15,16]. Electron transfer can occur between a nanoparticle and a cellular reaction if the conduction band of the nanoparticles is the same as the redox potential of a cellular reaction, which can result in cellular redox reactions resulting in induction of oxidative stress[17].

1.2 Nanosilver

Silver nanoparticles (AgNPs), or nanosilver (nAg), and its compounds have been in use for the past one hundred years as colloidal silver, which have antimicrobial, antiviral, and antifungal properties[18–23]. Studies have found the AgNPs can damage and/or destroy

bacterial membranes, resulting in the antimicrobial effect of AgNPs[19]. It has been found that AgNPs are effective antiviral agents against various viruses such as human immunodeficiency virus, hepatitis B virus, and monkey pox virus through interaction with surface glycoproteins on the virus[23]. AgNPs have been found to have antifungal activity against *Penicillium citrinum*, *Aspergillus niger*, *Trichophyton Mentagrophytes*, and *Candida albicans* by disruption of the fungal cell walls, resulting in cell lysis[22,23].

AgNPs are one of the most commonly used nanoparticles in consumer products[21]. The use of AgNPs has many applications throughout history; such as cosmetics, currencies, jewellery and photography. With the recent advances in technology in the synthesis of nanoparticles, the use of AgNPs in consumer products worldwide has increased greatly[1,2,24,25]. AgNPs are also widely used in, but not limited to, the pharmaceutical, food, cosmetic, and healthcare industries[2,18,21]. In recent studies, the use of AgNPs in nanomedicine, specifically with cancer, has also been shown to be promising[2,26–30]. Surface coatings have been used to prevent aggregation and to help stabilize AgNPs. Coatings include polystyrene, citrate, and polyvinylpyrrolidone (PVP). Citrate and PVP-coated AgNPs have been found to be less toxic than non-coated AgNPs[7]. PVP is a common coating used with AgNPs to prevent aggregation and to increase stability of the nanoparticle[20]. PVP can also aid in the formation of specific nanostructures such as cube or wire shapes and in controlling the size of the nanoparticle formed[31,32].

Several studies have shown the potential applicability of AgNPs for biomedical and pharmaceutical applications[33–35]. AgNPs have been used in the detection of biomarkers in Alzheimer's disease, the targeted imaging of cancer cells, and the identification of pathogens[35]. AgNPs have been used in development and implementation of new AgNP-

based biomedical products such as anticancer agents, drug-delivery platforms, orthopedic materials and devices, bandages, antiseptic sprays, and catheters[2,36]. Other studies show the potential for AgNPs to be used in cellular imaging for cancer diagnostics and therapy[37].

As mentioned previously, ions from the surface of nanoparticles may be released in solution and so to account for silver ion release in AgNPs, controls such as silver nitrate ($AgNO_3$), silver chloride, silver acetate, and silver carbonate have been used. However, most studies use $AgNO_3$ as a control for the release of silver ions from AgNPs.[20]

Inadvertent human exposure to AgNPs can occur through inhalation, dermal contact, and ingestion through contact with consumer products such as clothing, food packing, or medicine, or by exposure in AgNPs production facilities[2,38]. The release of silver ions from these products is dependent on several factors such as product quality, quantity and type of AgNPs coating, pH, and sweat[2]. There is also concern regarding the ability of AgNPs to cross the blood-brain barrier and the placental barrier[2,20]. Another concern is the potential for the development of silver resistance in bacteria, similar to how there is antibiotic resistant bacteria[25]. Antibiotic resistance can also occur from the induction of silver resistance due to "co-selection" in bacteria where bacteria swap DNA with other bacteria that are resistant to different antimicrobials. It has also been found that the main group of silver resistance genes are found nearby antibiotic resistance genes and so silver resistance has been co-selected by antibiotic resistant genes, and so the opposite should occur as well. There are limited studies that have observed silver resistance[25].

Exposure to AgNPs affects mitochondrial function as well. It has been found that AgNPs affects mitochondrial function through the disruption of the electron transport chain[2,24,26,33,39–41]. Studies have shown that exposure to AgNPs resulted in a decrease of

mitochondrial membrane potential (MMP) in various *in vitro* and *in vivo* experiments[41–45]. The decrease of MMP can result in the generation of ROS; therefore, AgNPs may potentially generate ROS through the reduction of MMP. Mitochondrial swelling and uncoupling of oxidative phosphorylation was also observed in the mitochondria isolated from the livers of rats treated with AgNPs[44]. Studies have also found an increase in oxygen consumption in the mitochondria, activation of caspase-3, a key enzyme involved in induction of apoptosis, and also increased apoptosis[41].

Several studies have showed AgNPs can interact with the cellular membrane and induce toxicity. This is the main mechanism of toxicity for the antimicrobial activity of AgNPs. In mammalian cells, AgNPs may alter permeability of the membrane, disrupt the cell membrane structure, and induce lysis of cellular membranes[40]. AgNPs has also been shown to interact with and induce damage to DNA, DNA strand breaks, DNA damage induced by oxidative stress, apoptosis, and chromosomal aberrations in various mammalian cell lines[26,35,40,41]. Several studies have shown that the cytoxicity, DNA damage, and apoptosis induced by AgNPs were through membrane lipid peroxidation, ROS, and oxidative stress[2,24,39]. It has been shown that AgNPs interact with DNA to stop the cell cycle and lead to apoptosis[2].

Although various studies have shown various nanoparticles have shown cytotoxic effects, it's difficult to make a blanket statement that all these nanoparticles are toxic due to the variety of methods and different cell lines used resulting in a lack of consistency. It is also unclear how much of the toxicity of the nanoparticle is a result from the release of the metal ions and how much is related to the actual nanoparticle. For example, AgNPs has been shown to induce toxicity, but it's unclear how much of the toxicity may be attributed

to the release of silver ions[1,2,9]. Nanomaterials can also act as a Trojan horse by releasing ions once inside the cell which can then interact with intracellular components. Metallic nanoparticles in solution may result in release of metal ions where increased surface area to volume ratio results in more metal ions released[4,46]. Studies have shown these released metal ions can be a major source of toxicity of the nanoparticle[46]. In a biological system, the release of ions from metallic nanoparticles can participate in two reactions to produce ROS: the Fenton-type reaction and Haber-Weiss-type reaction where the Fenton-type reaction is the main mechanism of production of free radicals by metallic nanoparticles. In the Fenton-type reaction, the metal ions can react with hydrogen peroxide to produce oxidized metal ions and hydroxyl radicals. In the Haber-Weiss-type reaction, oxidized metal ions react with hydrogen peroxide to produce hydroxyl radicals[4,47].

1.3 Nanosilver and Environmental Toxicology

As the industrial use of AgNPs increases, so does the environmental contamination and human exposure to AgNPs. Metal-based nanoparticles have high surface-area to volume ratio and the higher the surface area to volume ratio, the greater the potential for interaction with serum, saliva, or mucus, as well as risk of releasing potentially harmful metal ions, which are silver ions in the case of AgNPs[1]. The smaller the nanoparticle, the higher the surface area to volume ratio is which results in an increase release of silver ions. Other factors such as pH, the surface coating, or the formation of a protein corona can also affect release of silver ions.

The increase in use of AgNPs also means that AgNPs is inevitably released into the environment, which can lead to bioaccumulation in organisms or can be found in aquatic

environments. AgNPs will sediment in aquatic environments where the concentration of AgNPs in sediments are approximately be 0.19–470.65 μg/kg while the concentration for fresh water was approximately 0.03–2.79 ng/L[48,49]. A study has calculated predicted environmental concentrations of AgNPs: 0.5−2 ng/L in surface waters, 32–111 ng/L in sewage treatment plant waste, and 1.3–4.4 mg/kg in sewage sludge, with a prediction of exponential increase every year[50]. However, there is currently a lack of data to confirm these values.

AgNPs are used in various fabric and textile products and so washing of these products can result in releasing AgNPs into the aquatic environment so there is a concern regarding the effect AgNPs have on aquatic organisms[8]. Studies have suggested one key route of environmental exposure to AgNPs comes from the wastewater network release from consumer products such as textiles, cleaning agents, cosmetics, and medical products[48]. Another study found that 17-22% of manufactured AgNPs ended up in soil, 7-16% ended up in water, 3-4% in air, and 48-58% was either recycled, incinerated, and landfilled[50]. This can have impacts on aquatic or terrestrial ecosystems.

As mentioned previously, it's also important to keep in mind that the mechanism of AgNP toxicity is complex. Release of silver ions, aggregation, surface oxidation, and disruption or loss of the surface coating if available can affect how AgNPs interact with the environment and in biological systems[40].

Plants may take up and accumulate elements where other animals may consume the plant and transfer of the accumulated elements may occur. It's important to determine if this occurs with AgNPs and assess any negative effects it may have. Studies have found accumulation of AgNPs in plant tissue where the nanoparticle size had no significant effect

on accumulation. In plants, AgNP exposure has been shown to alter chloroplast structure, inhibit the Benson-Bassham-Calvin cycle, produce ROS resulting in oxidative stress, delay germination, decrease plant biomass, and reduce root growth[51]. Nanoparticle size dependent phytotoxicity where smaller nanoparticles induced greater phytotoxicity, and damaged chlorophyll[51,52].

Toxicity studies in nematodes have showed conflicting results on the survival after exposure to AgNPs, partially due to aggregation at higher concentrations. However, AgNPs have been showed to induce germ cell degradation and accumulation in tissues has been observed, which suggest potential trophic movement of the AgNPs[50].

Studies looking at annelids showed AgNPs exposure had no effect on mortality on some species, but a few other studies found increased mortality. As in nematodes, earthworms exposed to AgNPs resulted in a significant decrease in reproduction and accumulation of silver in the tissue. Oxidative stress, changes in behaviour, and other general defense responses are induced by AgNP treatment as well[50].

In zebrafish, it has been shown that exposure to AgNPs decreased the ATPase pump activity in the gills and intestines[51]. AgNPs induced an increase in lipid peroxidation in erythrocytes, hepatocytes, and in the gills of fish[53]. It has also been shown that AgNPs can accumulate in gills and liver of fish, which can induce oxidative stress[52]. Accumulation of silver after exposure to both AgNPs or silver nitrate occurs in fish gills, however, some studies showed lower accumulation occurred with the AgNPs exposure compared to the silver nitrate and some studies showed the opposite[54]. Studies have looked at silver ion toxicity in fish *in vivo* and showed high toxicity in certain fish species. However, few studies have looked at the effects AgNPs has in these species. In these studies, AgNPs

affects development such as induction of spinal cord deformities, cardiac arrhythmia, and general survival[52].

A review by Courtois and colleagues (2019) looks at the impact of AgNPs exposure through sewer sludge has on microorganisms, plants, and earthworms found in the soil[50]. AgNPs can alter soil properties, such as altering the soil microbiome diversity and biomass, inhibiting plant growth, and inhibiting invertebrate reproduction. The main form of silver found in sewer sludge is silver sulfide (Ag_2S), created when the AgNPs react with sulfides produced by anaerobic bacteria in sewers. However, Ag_2S has low solubility and is stable, so release of silver ions is lower, potentially decreasing the overall toxicity of the silver[50].

Autotrophic ammonia-oxidizing bacteria (AOB) are responsible for the rate limiting step, ammonia oxidation, in nitrification in terrestrial and aquatic systems. AgNPs have been shown to inhibit activity of soil AOB[51,55]. Studies have also found inhibition of growth, reduction of nitrifying activity, reduction of bacterial activity, and anti-bacterial effects of AgNPs against important soil bacteria. However, it's important to be cautious when drawing conclusions from these *in vitro* experiments, as they do not take into account the complex nature of the environment the bacteria are found in[50].

Although AgNPs is used so widely, there is much biological and toxicological knowledge lacking regarding AgNP exposure and associated risks to human health or the environment[2]. Once released into the environment, AgNPs can be modified in many ways such as oxidation, aggregation, sulfurization, and/or chlorination, which can affect how AgNPs behaves and makes it difficult to determine the fate of AgNPs in the enviornment[8]. Another issue regarding the evaluation of toxicity of AgNPs is whether the resulting toxicity is due to the release of silver ions or from the nanoparticle itself[1,2,8,9]. For this

study, there will be a focus on the effect that AgNPs may have on human or environmental health and the role AgNPs plays in cancer versus non-cancer human cells.

1.4 Physiological Effects of Nanosilver

It is important to keep in mind that the mechanism of toxicity of AgNPs can be complex due to various characteristics of AgNPs. AgNPs release silver ions and, as previously mentioned, it is difficult to determine if effects seen are due to the ionic silver or the AgNPs. Aggregation of AgNPs may be able to affect the cytotoxicity and how AgNPs may interact with biological systems and biomolecules. The surface of AgNPs can undergo oxidation to form silver oxide which presents another issue of whether the toxicity is due to the nanoparticle or due to the silver oxide formed and released[40].

Exposure to AgNPs or ionic silver can result in deposition of the silver particles and aggregated silver particles in the human body which results in a blue-gray colour in the affected areas of skin[20,56]. This condition is known as argyria and it can be local or general, and in some cases, it is reversible, but in a specific case of a patient treated with a wound dressing containing AgNPs, the argyria took over 3 years to reduce. Studies looking at patients treated with AgNP wound dressings found blood levels of silver in the range of 70-1500 mg/kg body weight in humans. Studies that used guinea pigs and rats showed no changes except for a weak sensitizing effect when exposed to AgNPs dermally for 24 hours at 0.04 to 400 mg/kg bodyweight for guinea pigs and 2000 mg/kg bodyweight for rats[56].

Studies have also showed AgNP exposure to human dermal fibroblasts (NHDFs) and normal human epidermal keratinocytes (NHEKs) aided in the healing process through decrease in expression of various factors such as inflammatory cytokines, and vascular

endothelial growth factor (VEGF). Decreased inflammation and faster healing was observed in dermal exposure of AgNPs in mice[20]. AgNPs are commonly used in wound dressings due to the antimicrobial effects of AgNPs[56]. Argyria can occur after dermal exposure to AgNPs, however, only a weak sensitizing effect is seen in guinea pigs and rats[56]. Other studies have showed AgNPs to be cytotoxic to keratinocytes and fibroblasts[2].

In humans, exposure to AgNPs results in transportation of the AgNPs to the liver and the blood stream. In rats exposed to AgNPs, AgNP levels were highest in the liver and spleen, and lower in the testis, kidneys, brain, and lungs[20,41]. *In vitro* and *in vivo* studies looking at the effects of AgNPs on the liver showed decreased liver enzyme activity and levels, lesions in chicken liver, DNA damage in the liver, apoptosis of liver cells and general cytotoxicity[41]. Studies have also shown AgNPs, due to its small size, can cross the blood brain barrier, where AgNP acts as a neurotoxin. In various *in vivo* and *in vitro* studies, AgNPs injected into the blood stream passed through the blood brain barrier and induced neurotoxicity[7,41]. AgNPs have been showed to induce inflammation and cytotoxicity in *in vivo* and *in vitro* lung tissue[41,57]. AgNPs have also been showed to be cytotoxic to keratinocytes and fibroblasts[2].

Angiogenesis involves the formation of blood vessels which is essential for survival of cells and especially in cancer cells to obtain nutrients in tumours. Angiogenesis is crucial for normal growth and wound healing processes and an imbalance of growth factors can cause various diseases[20,58]. There are various factors involved in angiogenesis, such as VEGF, acidic fibroblast growth factor (FGF-1), basic fibroblast growth factor (FGF-2), and angiopoietin[20]. There are also inhibitors of angiogenesis, such as endostatin and angiostatin[20]. Exposure to AgNPs has been found to inhibit VEGF, which induces growth

of blood vessels, induced cell proliferation, increase in inflammation, and migration, in various cell lines, and rats[59].

Studies have showed that AgNPs play a role in reducing inflammation at the site of the wound and facilitates early healing of the wound[60]. Silver nitrate in wound dressings irritate the skin and so by using AgNPs, the continuous release of silver ions makes the wound dressing antimicrobial without the skin irritation[23,61]. The AgNPs accelerated healing of wounds by increasing expression of collagen, growth factors, and improved growth of epithelial cells[62]. AgNPs have also been found to induce the differentiation of fibroblasts into myofibroblasts, resulting in wound contraction, increases the healing rate, and induces proliferation and relocation of keratinocytes[60].

Studies in mice and *in vivo* angiogenesis models such as the chick chorioallantoic membrane assay (CAM), Matrigel implant, and aortic ring, showed AgNPs had anti-angiogenesis effects. It is proposed that AgNPs targets the activation of the HIF signaling pathway, which is involved in angiogenesis. An increase of angiogenesis after exposure to AgNPs has been reported in one study that looked at mice[63]. With this exception, all other studies are in agreement that AgNPs inhibits angiogenesis[20,58].

1.5 Nanosilver and Protein Interactions

Due to the size of nanoparticles, it's possible for smaller particles of AgNPs to penetrate cells and interact with biomolecules such as proteins. Proteins can bind to the surface of nanoparticles through adsorption to form a surface coating of proteins called the protein corona which can then also affect the reactivity of the nanoparticle[64]. It has been proposed that the interactions between nanoparticles and proteins is dynamic where the

protein corona formed is dependent on the protein's affinity for surface exchange. Proteins with low affinity form a soft protein corona with loosely bound proteins quickly over seconds or minutes while proteins with high affinity form a hard protein corona with tightly bound coronas over hours. The protein corona formed can also affect how nanoparticles behave in biological systems[64,65]. The conformational changes and disruption of function of proteins can be caused by the protein corona formed with the nanoparticle. The nanoparticle-protein corona can also affect the folding of proteins and can affect protein aggregation. It has also been proposed that nanoparticles may potentially act as a chaperone and prevent protein aggregation[64].

AgNPs and ionic silver have high binding affinity to thiols, or sulfide groups (S-H), to form Ag-S bonds[20,40,51,66]. Studies have showed that binding to thiol groups induces protein misfolding in bacteria[51]. There are various important proteins that contain thiol groups such as glutathione, thioredoxin, metallothioneins, thioredoxin peroxidase, and superoxide dismutase and it is possible that AgNPs can bind to these proteins. However, there is currently a lack of literature studying these proteins' interaction with AgNPs[20,66].

Several studies have showed AgNPs interact with various proteins such as haemoglobin, serum albumin, metallothioneins, copper transporters, glyceraldehyde 3-phosphate dehydrogenase (GAPDH), malate dehydrogenase (MDH), and bacterial proteins. Studies have also shown AgNPs may disrupt copper, iron, and zinc homeostasis[45,51,67–72]. Various studies looked at the interaction of AgNPs with human and bovine haemoglobin (Hb) where exposure to AgNPs induced altered secondary protein structure in humans and both secondary and tertiary protein structure in bovine Hb[73–75]. The AgNPs were found to bind to the heme group in a study looking at human Hb[74].

However, another study found that AgNPs did not induce structural changes in Hb[66]. AgNPs have also been shown to competitively bind to copper transport proteins, disrupting protein function in *Drosophila melanogaster*[67]. There are mixed results on AgNPs adsorbing to metallothionein proteins where in mice macrophage cells, the AgNPs did not adsorb onto the metallothioneins[76] and another UV-vis spectroscopy and transmission electron microscopy (TEM) study, AgNPs were shown to adsorb to metallothionein-1[77]. A study looking at the interactions between AgNPs and GAPDH and MDH showed AgNP binds to the thiol groups and induced structural changes, resulting in inhibition of protein activity[51].

1.6 Nanosilver and Cellular Stress Responses

It is generally accepted that AgNPs induces oxidative stress in various *in vivo* and *in vitro* studies[2,24,39]. Metal nanoparticles in general are able to form superoxide, by donating an electron to oxygen, which can then result in a cascade of generation of other ROS such as hydroxyl radical, nitric oxide, organic radicals, peroxyl radicals, and alkoxy radicals[41]. Various methods have been used to measure oxidative stress induced by AgNPs. Most studies use the fluorescent dye, 20,70-dichlorodihydrofluorescein diacetate (H_2DCFDA), however, there are potential issues with the reliability of the dye where it is unclear how much fluorescence is due to background and how much is the actual ROS. Other methods include the CellROX and MitoSOX fluorescent probes to detect ROS in the cytoplasm and mitochondria, respectively[20].

Studies have showed AgNP treatment resulted in an increase in ROS in a variety of human cancer and non-cancer cell lines[18,53,78–82]. However, some studies have also found

no change or a decrease in production of ROS after exposure to AgNPs in various cell lines[83–88].

Studies have shown exposure to AgNPs induces activation of the UPR. AgNPs induced increased levels of GRP78, phosphorylated PERK, phosphorylated eIF2-α, and phosphorylated IRE1α, spliced XBP1, cleaved ATF-6, CHOP, JNK and caspase 12[20,89]. Studies have also found AgNPs induces upregulation of ER stress marker genes such as CHOP, XBP1, and homocysteine-inducible ER protein with ubiquitin-like domain 1 (HERPUD1)[20,89].

Currently, there are very few studies that look at the effects of AgNPs on the hypoxic response. One study showed AgNPs inhibits HIF-1 accumulation and suppresses expression of HIF-1 target genes in breast cancer cells (MCF-7) and also found the protein levels of HIF-1α and HIF-1β decreased[90].

Another recent study looked at the effect AgNPs had on prostate cancer (PC-3) cells and showed AgNPs can induce the hypoxic response in cells by inducing an increase in HIF-1α expression. This induction of the hypoxic stress response in the cells is suggested to activate the AMP-activated protein kinase (AMPK)/mammalian target of the rapamycin (mTOR) autophagic pathway[91].

1.7 Nanosilver and Cancer

Cancer involves cells in the body that divide uncontrollably without stopping and spread into surrounding tissues. Cancer is primarily caused by environmental factors and different types of cancer can behave very differently. Tumours, in different tissues, can vary in environmental and physiological characteristics as well, which make each type of

cancer unique as well as posing a problem for developing therapeutics. Cancer is one of the leading causes of death according to the World Health Organization (WHO) and so it is important to recognize the growing global cancer crisis and study new techniques and therapeutics to combat cancer, such as with nanoparticles[92]. Current anticancer therapies have limited effectiveness, undesired toxic effects, and lack of generality[34] and so it is important to develop more effective and safe alternatives to current anticancer treatments such as incorporating the use of nanomedicine on its own or in conjunction with other existing treatments.

Many studies have showed that AgNPs have anticancer effects against various cell lines including: human fibrosarcoma, skin carcinoma, mouse melanoma, cervical cancer, breast cancer, prostate cancer, human lung cancer, human ovarian cancer, lymphoma, and liver cancer cell lines[2,18,26,29,30,37,41,93,94]. AgNPs induce toxicity to cancer cells through various mechanisms including reducing mitochondrial function, production of ROS, deregulation of the cell cycle, induction of apoptotic genes, chromosome aberration, and DNA damage[94]. Figure 1 shows the mechanisms of toxicity AgNPs have on cancer cells.

Many studies have showed biologically synthesized AgNPs from plants induced greater toxicity and inhibition of cell proliferation in cancer cells compared to non-cancer cells. It is proposed that AgNPs synthesized biologically from plants may be healthier due to the non-toxic nature of the source of the capping material as well as less time consuming and environmentally friendly[29,30,33,41,93,95].

AgNPs also have low systemic toxicity, which makes AgNP a potential anticancer agent[41]. However, the mechanisms which AgNPs affect cellular responses is complex due to the characteristics of the nanoparticles: size, shape, release of silver ions, aggregation

and surface oxidation can all affect how AgNPs interact with biological systems. For AgNPs to be considered as an anticancer therapy, or as a co-treatment for anticancer therapy, the mechanisms of action for the nanosilver must be completely understood and a system for characterization of AgNPs must be in place.

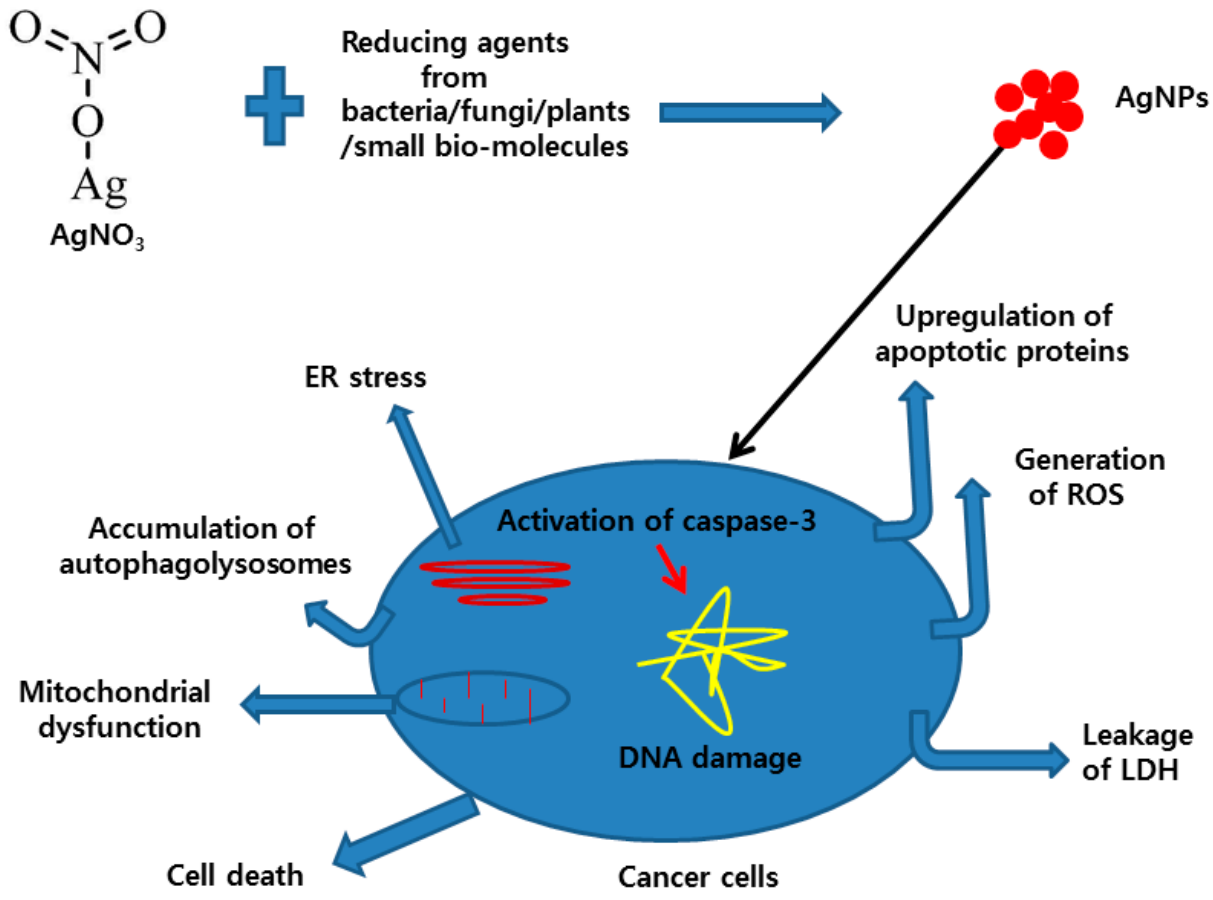

Figure 1. The possible mechanisms of AgNP-induced cytotoxicity in cancer cell lines. ER: Endoplasmic reticulum stress; LDH: lactate dehydrogenase; ROS: reactive oxygen species. **(**Zhang, X.-F.; Liu, Z.-G.; Shen, W.; Gurunathan, S. Silver nanoparticles: synthesis,

characterization, properties, applications, and therapeutic approaches. Int. J. Mol. Sci. 2016, 17, 1534. https://doi.org/10.3390/ijms17091534).

1.8 Ascorbic Acid and Cancer

Many studies have shown that ascorbic acid, on its own, has anti-cancer effects[96]. Mechanisms include scavenging ROS, inducing cytotoxicity against tumour cells through selectively produced ROS, prevention of glucose metabolism, and the regulation of HIF expression[97].

It has been shown that high dose intravenous administration of ascorbic acid, on its own or in combination with traditional chemotherapies, are effective anticancer therapies in various case studies clinical trials in cancer patients and in various animal studies. It has also been shown that intravenous ascorbic acid administration decreased the side effects resulting from traditional chemotherapies, in clinical studies[97,98].

A recent study looked at the effects of combined treatment of ascorbic acid (vitamin C) treatment with AgNP treatment in rat parotid glands. AgNP treatments, on their own, resulted in cytotoxic effects. However, when the rats were treated with both ascorbic acid and AgNPs, a decrease in toxic effects was observed in non-cancer parotid glands in rats[99]. Currently there is a lack of knowledge on the effects that AgNPs cotreated with ascorbic acid have on cancer cells or models.

It was proposed that AgNPs includes the production of ROS, as well as release of ions that may be toxic, and that the ascorbic acid decreases the production of ROS[99]. Oxidative stress has been suggested to be closely linked to cancer and with ascorbic acid being a potent antioxidant, ascorbic acid treatment can decrease ROS that may harm crucial

biomolecules. Intravenous treatment of ascorbic acid in cancer patients has been shown to decrease oxidative stress, in general. This may indicate that the ascorbic acid cotreatment with AgNPs can decrease the toxic effects in non-cancer cells while being anticancer through other mechanisms[98].

AgNPs, as mentioned previously, has also been found to have anticancer effects[2,26–30]. It's important to study the effect of co-treatment of ascorbic acid and AgNPs in cell cultures and study the cellular response pathways to determine if ascorbic acid and AgNPs may act synergistically to be a potential anticancer therapy.

1.3 Cellular Stresses

1.9 Oxidative Stress

Oxidative stress occurs when the production of reactive oxygen species (ROS) exceeds the capacity of the cell to detoxify them with antioxidant systems. ROS are common by-products of metabolism and so biological systems have antioxidants in order to detoxify ROS products to prevent cell and tissue damage[71].

The most common ROS generated in biological systems as metabolic waste are superoxide radicals ($O_2•^-$), hydrogen peroxide (H_2O_2), hydroxyl radicals (•OH), and singlet oxygen ($^1O_2$)[71,100]. Superoxides are formed by the reduction of triplet oxygen ($^3O_2$) through enzymatic mediation by oxidases or non-enzymatically in the electron transport chain in the mitochondria. In biological systems, superoxide can be enzymatically converted into H_2O_2 by superoxide dismutase (SOD) or non-enzymatically into H_2O_2 and $^1O_2$. H_2O_2, in the presence of reduced transition metals, can be converted into •OH, which are very reactive or H_2O_2 can also be converted into water by enzymes such as CAT or glutathione

peroxidase (GPx)[101]. Due to their high reactivity, ROS can quickly transition between different ROS through electron transfer. The main sources of ROS in biological systems are from cellular respiration and metabolic processes. Enzymes and organelles can also produce ROS as metabolic by-products. NADPH oxidases (NOX) are proteins that are responsible for transfer of electrons across membranes to oxygen to generate superoxide[100]. Mitochondrial ROS occurs due to oxidative phosphorylation where free radicals can be generated through reactions with oxygen and electrons from NADH or FADH. Environmental stresses such as certain chemicals, UV, and heavy metals, can also generate ROS[71].

ROS have also been found to be important secondary messenger molecules in various regulatory signaling pathways such as regulation of vascular smooth muscle relaxation or monitoring of oxygen tension. H_2O_2 is now a recognized as a secondary messenger used by protein kinases and in signal transduction pathways at low levels in the cell[102]. Some ROS also play a role in building cellular structures for defense against pathogens.[71,101] ROS can also play a role in elimination of pathogens, aid in wound healing, and repair processes[103]. Oxidative stress can also be induced by reactive nitrogen species such as nitric oxide (NO•), nitrogen dioxide (NO_2), and dinitrogen trioxide (N_2O_3)[103].

Cells have an antioxidant system to protect against ROS-induced damage which include antioxidant enzymes: SOD, catalase (CAT), glutathione (GSH), GPx, and thioredoxin (TXN). These enzymes are responsible for breaking down harmful ROS into less harmful components[71,103]. Other antioxidants include vitamin E, lipoic acid, N-acetyl-L-cysteine, and ubiquinones[41]. An excellent review by He and colleagues (2017) covers the antioxidant system and its mechanisms to maintain redox homeostasis in detail[103].

Oxidative stress has been shown to be harmful to lipids, proteins, lipoproteins, and DNA. ROS can react with biomacromolecules such as lipids, proteins, carbohydrates, and nucleic acid and induce potentially irreversible damage[100]. Exposure to ROS can result in lipid peroxidation, protein oxidation, amino acid modification, DNA single- and double-strand breaks and base modification, and carbohydrate monosaccharide modification and strand breaks[71,100]. Lipid peroxidation results in damage to cell membranes and lipoproteins. Protein oxidation can result in structural changes of the proteins which can lead to decrease or inhibition of enzymatic activity. Oxidative stress can induce DNA lesions, mainly the formation of 8-oxo-2′-deoxyguanosine (8-OHdG), which can result in mutagenesis or loss of epigenetic information[71]. This damage that ROS can induce can play a role in development or progression of various diseases such as cardiovascular disease, neurological diseases such as Alzheimer's disease, respiratory diseases, kidney diseases, rheumatoid arthritis, and in the development of cancer[71,100,103].

A transcription factor involved in the oxidative stress response pathway is Nrf2 (also known as Nuclear Factor, Erythroid 2 Like 2 or NFE2L2)[104,105]. Nrf2 is the master regulator of the oxidative stress response and is activated by oxidants and has been found to regulate the expression of various genes through antioxidant responsive elements (AREs) involved in the cellular defense against oxidative stress. AREs are transcriptional elements found in close proximity to several genes that encode various antioxidant enzymes such as glutathione peroxidase (GPX-1), heme oxygenase-1 (HO-1), cytochrome P450, Nrf1, and glutathione S-transferase (GST).[104,106,107] Upregulation of Nrf2 may be indicative of oxidative stress.

1.10 Hypoxic Stress

The Earth's atmosphere is comprised of 21% oxygen (normoxia). Hypoxic stress occurs under low oxygen environments and hypoxic stress is a relevant stress in cancer as cancerous cells in tumours are often in hypoxic microenvironments. The hypoxic stress can also be induced chemically by exposing cells to metals such as cobalt, cadmium, nickel or manganese[105]. These metals interfere with the oxygen sensing

Hypoxia inducible factors (HIFs) are a group of transcription factors that play an important role in oxygen homeostasis and are expressed during hypoxic stress. HIF-1 is the most well-understood HIF and has been found to control more than hundred genes involved in cell proliferation, cell survival, apoptosis, angiogenesis, and more. HIF-1 proteins have been found to bind to the hypoxia-response element (HRE). HIF-1 subunit alpha (HIF-1α) is one of three HIF-1 subunits and is broken down under normoxia (regular atmospheric oxygen conditions) with a short half-life of less than five minutes[108–110].

Generation of ROS, especially H_2O_2, results in stabilization and activation of HIF-1α, therefore oxidative stress may affect the hypoxic stress response.HIF-1α activity is also regulated by various molecules such as growth factors, cytokines, and some ROS such as nitric oxide and hydrogen peroxide[109,111].

HIF-1α is regulated by various post-translational modifications such as hydroxylation, ubiquitination, methylation, acetylation, and phosphorylation[109,112]. Under normoxic conditions, HIF-1α is hydroxylated and acetylated at the oxygen-dependent degradation domain (ODDD) of HIF-1α, resulting in ubiquitination then degradation of HIF-1α via the ubiquitin-proteasome pathway[112,113]. Under hypoxic conditions, HIF-1α can be acetylated by co-activator p300 to increase stability via suppression of

polyubiquitylation. Methylation of HIF-1α results in destabilization of the protein. Phosphorylation of HIF-1α has many various purposes, dependent on location of the post-translational modification. Phosphorylation regulates protein stability, activity, subcellular localization, and plays roles in binding interactions. Phosphorylation can increase or decrease HIF-1α stability, for example, phosphorylation by cyclin-dependent kinases increases stability while phosphorylation by Polo-like kinase 3 (PLK3) destabilizes HIF-1α and marks HIF-1α for degradation under normoxia[113].

HIF-1α also plays a role in survival of cancer cells as it is a transcription factor for genes involved in angiogenesis, cell proliferation and survival, glucose metabolism, and iron metabolism. Diseases such as cancer and cardiac arrest create hypoxic microenvironments and so HIF-1α plays a role in these diseases[109,114]. The role HIF-1α plays in metabolism means HIF-1α expression can affect metabolic diseases such as obesity, type 2 diabetes, and non-alcoholic fatty liver disease[114].

1.11 Endoplasmic Reticulum Stress

The endoplasmic reticulum (ER) in cells is where proteins that are destined to be membrane-bound or secreted are synthesized and folded into their functional forms[115]. Thus, the ER is the organelle that forms the starting point for the secretory protein pathway of synthesis. The ER is responsible for many important functions, such as protein folding, protein and lipid synthesis, and calcium storage[89]. Proteins, after synthesis, must be folded by chaperone proteins, which occurs in either the cytosol, ER or the mitochondria. Each cellular compartment has its own unique set of chaperone proteins. Unfolded proteins are

capable of aggregating and becoming toxic and so there are generally systems in place to prevent misfolded or unfolded proteins[116].

ER stress occurs when there is an accumulation of unfolded proteins which can be caused by a variety of reasons, including lack of nutrients, exposure to hypoxic conditions, disruption in function of various chaperones and enzymes involved in the folding process, and aggregation of unfolded proteins[115]. The UPR is a signaling pathway that is activated in response to ER stress, which occurs when there is a buildup of misfolded or unfolded proteins due to the disruption to the homeostasis maintained in the ER. The UPR is activated to decrease ER stress and return the cell to homeostasis. If homeostasis can't be established, or if the proteins build up to the point where they start to aggregate within the cell, it can lead to cell death by apoptosis[105,117].

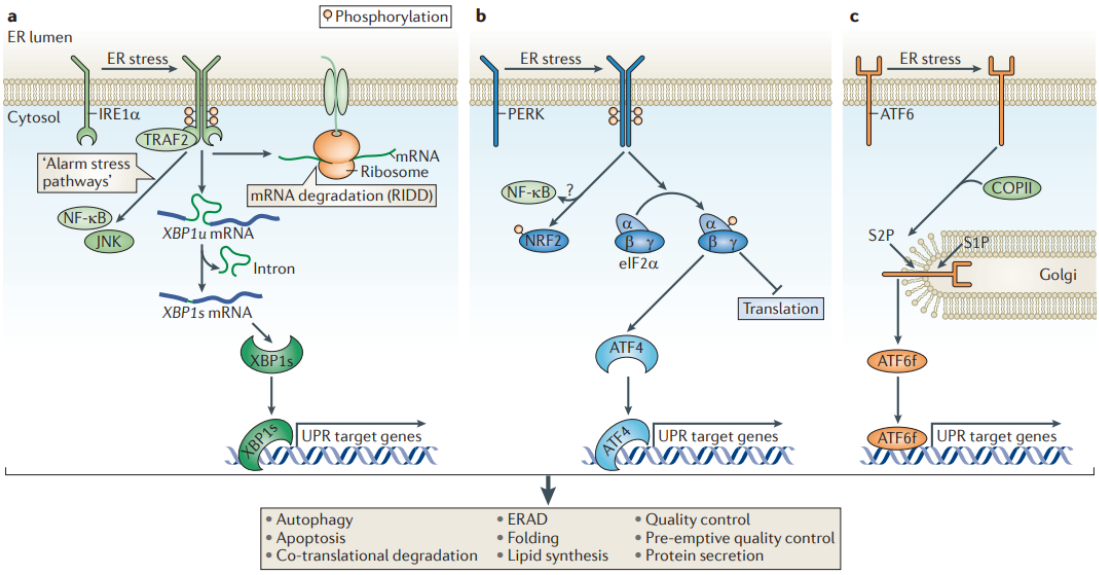

Figure 2. The unfolded protein response (UPR) has three stress sensors: inositol-requiring protein 1α (IRE1α), protein kinase RNA-like endoplasmic reticulum (ER) kinase (PERK) and activating transcription factor 6 (ATF6), where each sensor is responsible for a signaling cascade for restoring homeostasis to protein folding function. General outcomes

of the UPR are shown at the bottom of the figure. (Hetz, C. The unfolded protein response: controlling cell fate decisions under ER stress and beyond. Nat Rev Mol Cell Biol 13, 89–102 (2012). https://doi.org/10.1038/nrm3270).

The UPR involves the signaling from key ER stress sensors including inositol-requiring protein 1α (IRE1α), protein kinase RNA-like endoplasmic reticulum (ER) kinase (PERK) and activating transcription factor 6 (ATF6). These sensors are responsible for transmitting information regarding the ability of the ER to fold proteins[118,119]. GRP78/BiP/ HSP5A is a protein that is responsible for inhibiting the previously mentioned ER stress sensors and releases them when there is buildup of unfolded proteins in the ER. GRP78 then switches to its chaperone function and activates the ER stress sensors[118]. The pathway for each sensor is shown in Figure 1.

When IRE1α is activated, it splices the *XBP1* mRNA, which results in the transcription of XBP1, which is a transcription factor that is involved in regulation of the transcription of genes that are involved in protein folding, degradation, and quality control pathways[117,118,120,121].

When PERK is activated, it phosphorylates eukaryotic initiation factor 2 (eIF2α) and potentially nuclear factor erythroid 2-related factor 2 (Nrf2), which is a transcription factor that is normally involved in the oxidative stress response pathway[106,118]. The phosphorylation of eIF2α results in a reduction in global protein synthesis and for the translation of transcription factor ATF4, which is responsible for regulation of genes controlling autophagy, cell cycle arrest, apoptosis, amino acid metabolism, and antioxidant responses.[118,122,123]. ATF4 is not only involved in the UPR, it is a downstream effector

protein for other pathways, such as the oxidative stress response pathway, and the amino acid response pathway which to amino acid deprivation[123].

ATF6 is a transcription factor located in the ER that is activated by ER stress. When the cell experiences ER stress, ATF6 is transported then processed by proteases at the Golgi apparatus to release the cytosolic domain fragment ATF6f. The ATF6f is regulates the expression of genes that encode ER-associated protein degradation (ERAD) components, such as EDEM1, p97, SEL1L, gp78, UBE2J1, UBE2G2, HERP and DERLIN1 and the *XBP1* gene[118,124]. ATF6 and spliced XBP1 are responsible for regulation of the expression of chaperones such as GRP78/BiP and GRP94 in response to ER stress[118].

When the ER stress is too much for the UPR to restore homeostasis, ER stress-induced apoptosis can result. There are three main ER-induced apoptosis pathways: IRE1/apoptosis signal-regulating kinase 1 (ASK1)/c-Jun N-terminal kinase (JNK) pathway, the caspase-12 kinase pathway, and the C/EBP homologous protein (CHOP)/GADD153 pathway[125]. For this study, expression of both ER stress markers, ATF4 and XBP1 will be observed in cell culture.

1.12 Cross-Talk Between Cellular Stresses

These cellular stresses do not occur in isolation effects from each stress also interact with each other in "cross-talking". Cross-talk can occur when a single factor responds to multiple stresses, or when factors that respond to different stresses interact with each other either synergistically or antagonistically. When more than one stress is encountered simultaneously, the latter occurs most commonly.

It is important to study the "cross-talk" that occurs as a result of the interaction of different stresses. The ER stress response, oxidative stress and inflammatory responses often interact and facilitate progression of various diseases[126]. The UPR also produces ROS and so ER stress can also result in production of oxidative stress. Oxidative stress can also induce ER stress by inducing misfolding of proteins in the ER[127]. The generation of the ROS, H_2O_2, results in stabilization and activation of HIF-1α and so oxidative stress may induce hypoxic stress. Hypoxic and oxidative stress can also induce ER stress by inducing unfolded or misfolded proteins[20]. Prolyl-hydroxylases (PHDs) are enzymes that promotes proteasome degradation of HIF-1α and it has been found that ATF4 and XBP1 expression can upregulate the degradation of PHDs, resulting in increase in HIF-1α expression and so ER stress can affect the hypoxic stress response as well[128].

1.4 Wnt Signaling

Wnt proteins, a family of which includes what were originally named the int and Wingless family of genes, where the name Wnt is a combination of the int and Wingless[129]. The Wnt family consists of secreted glycoproteins and are involved in cell differentiation, polarization, apoptosis, proliferation, polarity and migration and are highly conserved across species[130,131]. Wnt signaling has been found to have roles in embryonic development, and tissue regeneration of bone marrow, skin, and the intestine, and as well as in various diseases such as breast, prostate, and colon cancer, Parkinson's, Alzheimer's, and type II diabetes[131,132].

It has been found that Wnt proteins are insoluble due to the proteins being palmitoylated[133]. Palmitoylation is a post translational modification that plays a role in

communication between cell surfaces[134]. Porcupine (PORCN) is an acyl-transferase that responsible for attaching palmitoleic acid to Wnt ligands which then mediates transport of Wnts for extracellular export for downstream signaling[135,136]. Wntless (Wls) is a Wnt protein that is responsible for the secretion for various Wnt proteins[137,138].

The Wnt signaling pathway consists of three pathways: canonical Wnt/ β-catenin, non-canonical Wnt/planar cell polarity (PCP), and non-canonical Wnt/calcium pathway[130,132]. These three pathways are activated when a Wnt protein binds to Wnt receptors from the Frizzled family of proteins[139].

1.13 Canonical Wnt/β-catenin Pathway

β-catenin, a transcription cofactor protein involved in the canonical Wnt/β-catenin pathway is normally degraded by the glycogen synthase kinase (GSK) 3β/adenomatosis polyposis coli (APC)/Axin complex when there is no Wnt signaling[139,140]. β-catenin is also a major part of the cadherin protein complex which is responsible for regulation of cell adhesion and cell migration[141].

The canonical pathway is activated when Wnt proteins bind to the Frizzled and lipoprotein receptor-related protein 5/6 (LRP5/6) receptor complex which is present at the surface of cells. This results in the receptors transducing a signal to various proteins, including the recruitment of Axin by the Dishevelled (Dsh) protein. Dsh also releases β-catenin from the degradation complex where β-catenin translocates to the nucleus to control transcription[141]. Axin eliminates the GSK3/APC/Axin complex which results in accumulation of β-catenin. β-catenin then translocates into the nucleus from the cytoplasm and can bind to transcription factors from the lymphoid enhancer factor/T cell factor

(LEF/TCF) family to activate transcription of Wnt-specific genes[139,140,142]. Activation of this pathway results in activation of signaling and increase in cell proliferation[143].

1.14 Non-canonical Wnt/PCP Pathway

Non-canonical Wnt signaling pathways are β-catenin-independent and are responsible for cell adhesion and migration[144]. The two main non-canonical Wnt pathways are the Wnt/PCP and Wnt/calcium pathways. Neither of these two pathways associated with the LRP receptors, but both bind to Frizzled receptors and activate Dsh[132,140,145]. Some studies have shown non-canonical Wnt signaling can compete with the Wnt/β-catenin pathway by suppressing the Wnt/β-catenin pathway[146].

The Wnt/PCP pathway was discovered through *Drosophila* studies looking at mutations of the Frizzled and Dsh genes. When Wnt ligands bind to Frizzled receptors, activation and recruitment of Dsh occurs, resulting in upregulation of cell adhesion and migration genes. Mutations in these genes affected the orientation of the epithelial structures such as cuticle hairs and sensory bristles of the *Drosophila*[132,140,147].

The Wnt/calcium pathway has roles during embryogenesis including: dorsal axis formation, ventral patterning, regulation of tissue separation, heart formation, and gastrulation[147]. In the Wnt/calcium pathway, Wnt ligands bind Frizzled receptors and alternative receptors, receptor like tyrosine kinase (RYK) or retinoic acid receptor-related orphan receptor (ROR). Activation of this pathway results in cell migration and inhibition of the canonical Wnt/β-catenin pathway through the G-protein dependent release of calcium and activation of calcium-sensitive proteins such as protein kinase C, JNK and calmodulin kinase II[132,147,148]. Binding of certain Wnt and Frizzled receptors can result in

release of calcium ions from the ER. Wnt5a is an example of a Wnt protein that can potentially induce release of intracellular calcium ions and also plays an important role in carcinogenesis[147,149].

1.15 Wnt Signaling and Cancer

Upregulation of the canonical Wnt/ β-catenin pathway occurs during development and is normally downregulated any other time. Activation of the canonical pathway when development is not occurring can result in increase of risk of cancer.

Studies has shown the Wnt/β-catenin pathway regulates expression of various angiogenic factors, which aid in cancer cell survival, such as VEGF-A, VEGF-C, and Ribosomal Protein S15a (RPS15A), which recently has been shown to induce angiogenesis which aids in cancer cell survival. Wnt3a, a Wnt ligand in the canonical pathway, has been shown to increase levels of RPS15A[130]. Wnt signaling is involved in various cancer cell lines such as leukemia, colorectal cancer, breast, cancer cells and cancer stem cells[130,135].

1.5 Research Significance

With the increase of use of AgNPs in consumer products, it is important to understand how AgNPs may interact with cellular processes after exposure. Studies have also shown that AgNPs has anticancer properties[2,26–30]. It is important to explore the potential of nanoparticles in regard to developing new cancer therapies, either by using AgNPs on its own, or in combination with other therapies. To develop anti-cancer therapies that use AgNPs, it is important to understand the cellular effects that AgNPs may have in terms of endoplasmic reticulum (ER) stress, mitochondrial stress, and oxidative stress, as

well as determine what kind of cross-talk occurs between these stresses in both cancer and non-cancer cell lines. The effects that AgNPs has on these cellular stress responses are also important to study, due to the increase of exposure to humans from AgNPs in the environment.

1.6 Hypothesis

I hypothesize that AgNP treatments will induce cellular stress responses such as the ER stress, oxidative stress, and hypoxic stress responses, and as well as crosstalk of stress responses, in different cell lines. The focus will be on human colon cell lines, both cancerous (HCT116) and non-cancerous (HIEC-6) human intestinal epithelial cells. Studies have shown both AgNPs and ascorbic acid have greater effects and toxicity in cancer cells relative to non-cancer cells, so I predict that AgNP treatments will induce greater stress responses in human colon cancer cells compared to non-cancer human intestinal epithelial cells and that AgNPs and ascorbic acid will act synergistically with AgNPs to preferentially cause colon cancer cells to expire, compared to normal colon cancer cells.

1.7 Objectives

The first objective of this thesis was to investigate the relationships between AgNPs, at non-toxic concentrations, and the various cellular stresses that it may or may not cause, in human colon cancer and non-cancer cells. To determine the effects AgNPs had on cellular stress responses, cytoplasmic and mitochondrial oxidative stress, ER stress markers, hypoxic stress marker HIF1-α were measured. The second objective was to

determine potential cross-talk that may occur between these cellular stress responses in human cancer and non-cancer cells, due to AgNP exposure, in order to determine if AgNPs have potential environmental or human health impacts. To determine effects of AgNPs on cross-talk, the experiments involving measuring ER stress and oxidative stress were conducted under normoxia and hypoxia. The third objective was to determine differences in the effects of AgNP treatment alone and AgNPs co-treated with ascorbic acid on cancer versus non-cancer human colon cells. To determine the effect of AgNPs, ascorbic acid, and combined treatment, experiments relating to cell viability, cell cycle, and Wnt signaling were used for HCT116 cells.

Chapter 2: Methods and Materials

2.1 Characterization of Nanosilver

In our study, polyvinylpyrrolidone (PVP) coated 10 nm nanosilver (BioPure^{TM}) obtained from NanoComposix was used for all experiments. The nanosilver was diluted in purified water and was 10.6 ± 2.1 nm in diameter under transmission electron microscopy (TEM) (Figure 3 and Table 1).

Table 1. Characteristics of PVP coated 10 nm nanosilver (BioPure^{TM}) obtained from the certificate of analysis provided by NanoComposix (San Diego, California) (product number: AGPO10, lot number: SDC0111). Mass concentration obtained with Thermo Fisher X Series 2 ICP-MS and spectral properties obtained by Agilent 8453 UV-Visible Spectrometer by NanoComposix.

Characteristic	Value
Diameter (nm)	10.6 ± 2.1
Coefficient of Variation (%)	20.0
Surface Area (m^2/g)*	50.4
Mass Concentration (Ag) (mg/mL)	1.02
Particle Concentration (particles/mL)*	$1.6 * 10^{14}$
Molar Particle Concentration (particle # mol/L)	$2.6 * 10^{-7}$
Endotoxin Concentration (EU/mL)	< 5
Hydrodynamic Diameter (nm)	27
Zeta Potential (mV)**	-24
pH	7.4
Silver purity (%)	99.99
Particle Surface Coating	PVP 40 kDa (polymer)
Solvent	USP Purified Water

**Calculated values*

***Concentration of nanosilver may be too low to obtain high accuracy measurements and so the charge magnitude may be greater than reported here*

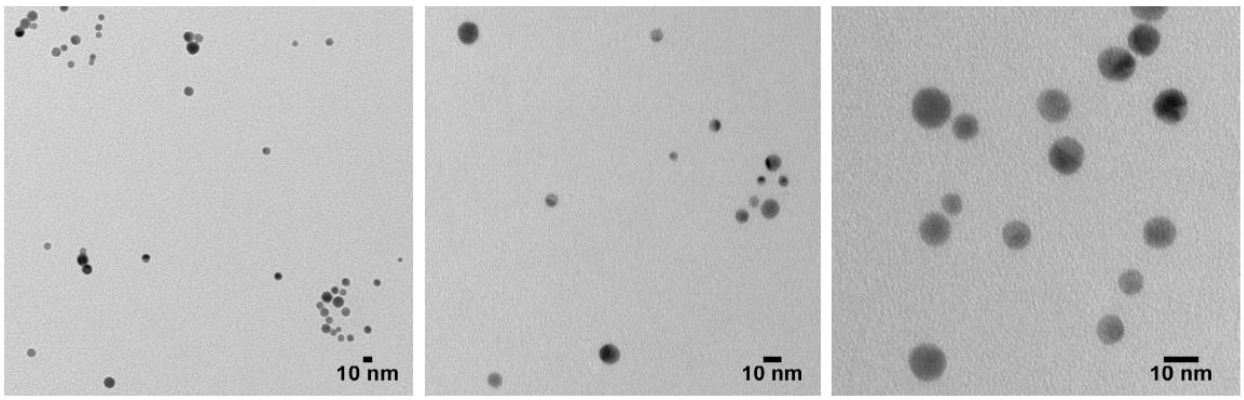

Figure 3. Transmission electron microscope (TEM) image of PVP coated 10 nm nanosilver (BioPure^{TM}) obtained from NanoComposix. Images obtained by NanoComposix using the JEOL 1010 TEM and modified via ImageJ. NanoComposix (San Diego, California).

Figure 4 shows the size distribution of the nanosilver obtained from NanoComposix where the average diameter was 10.6 ± 2.1 nm.

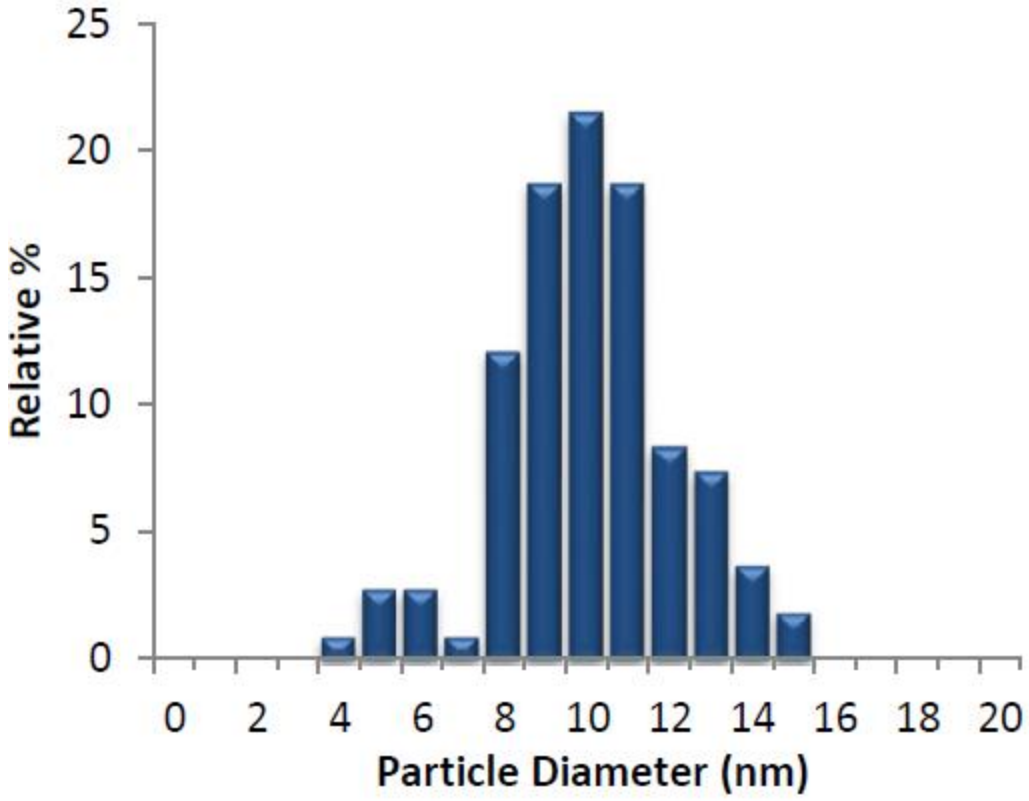

Figure 4. Size distribution of PVP coated 10 nm nanosilver (BioPureTM) obtained from NanoComposix (San Diego, California).

Figure 5 shows the NanoComposix provided UV-visible spectrometer data, which indicates no aggregation of the nanosilver. Max optical density was 174.1 and the peak wavelength was 389 nm.

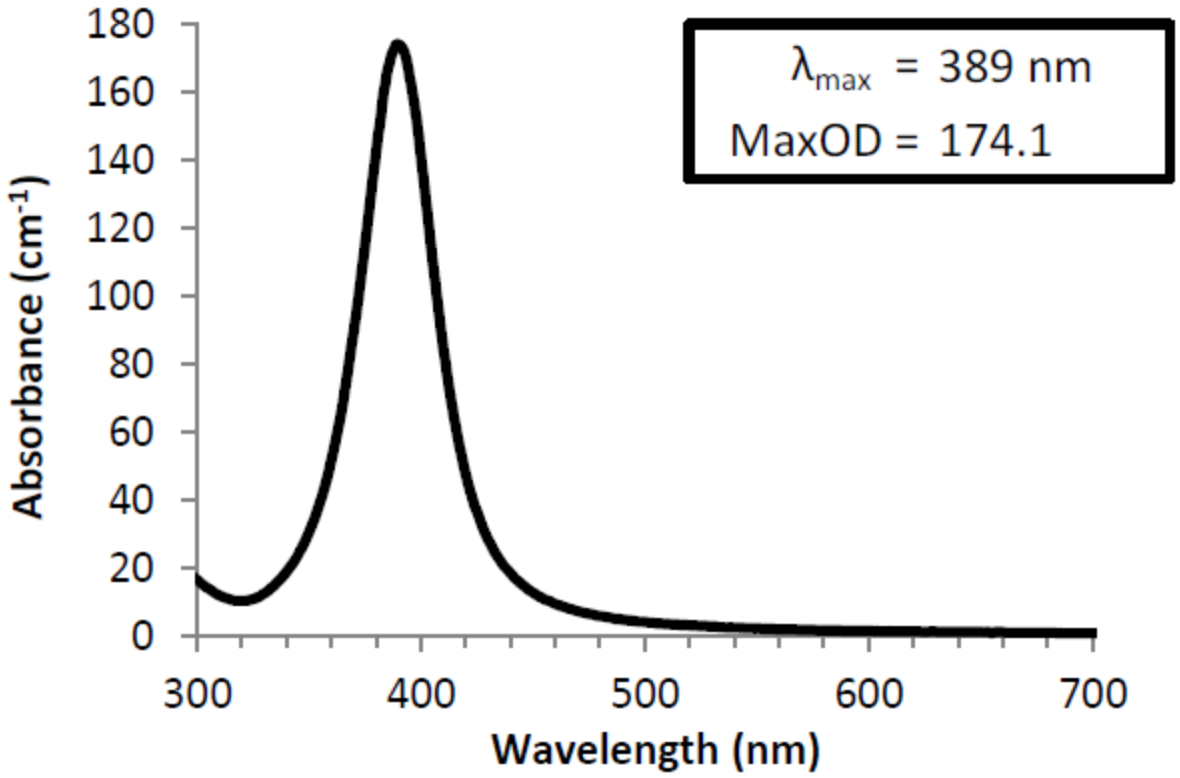

Figure 5. Optical properties of PVP coated 10 nm nanosilver (NanoComposix, BioPure™) obtained by NanoComposix (San Diego, California) using Agilent 8453 UV-Visible Spectrometer.

No aggregation was observed from the UV-Visible spectrometer data obtained in this study for the nanosilver (Figure 6). The peak absorbance was 0.974 at 391 nm.

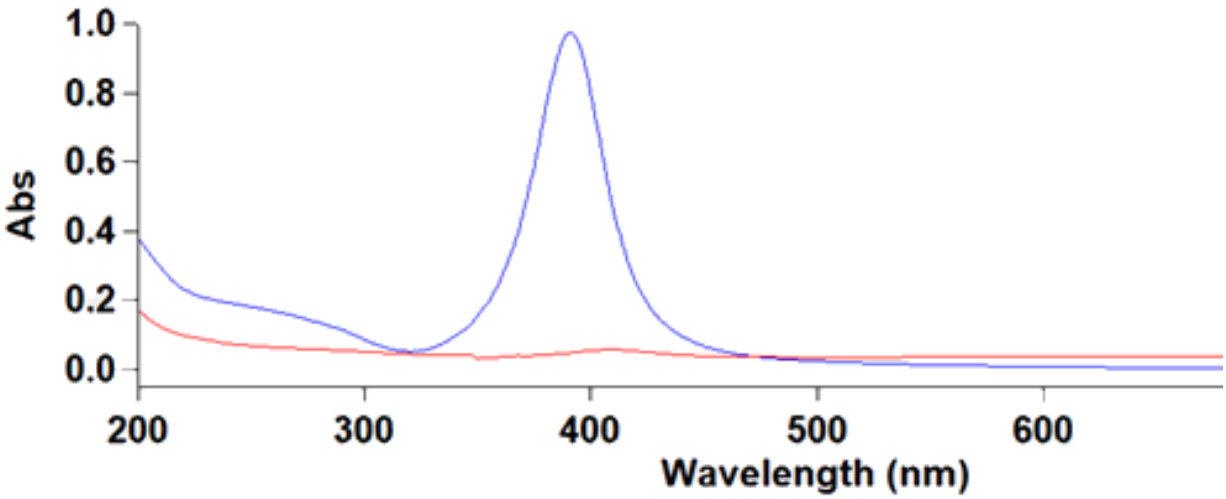

Figure 6. Optical properties of PVP coated 10 nm nanosilver (BioPure^{TM}, NanoComposix, San Diego, California) using the Cary 100 Bio UV-Visible Spectrophotometer (Agilent Technologies, Santa Clara, California). Maximum wavelength was 391 nm and peak absorbance was 0.974.

2.2 Cell Culture

HCT116 and HEK293T cells were grown to confluence in T75 (75 cm^2) flasks with 5% fetal bovine serum (FBS) and 5% newborn calf serum (NCS) in Dulbecco's Modified Eagle Medium (DMEM) media (Wisent, Saint-Jean-Baptiste de Rouville, Quebec) and incubated at 37°C with 5% CO_2 in a Thermo Forma Series II Incubator (Thermo Forma, Waltham, Massachusetts). HIEC-6 cells were grown in T25 (25 cm^2) and T75 (75 cm^2) cell culture flasks in HIEC-6-specific media (5% Premium FBS, 1% HEPES buffer solution (1 M), 1% GlutaMAX (100x), 0.001% human epidermal growth factor (EGF) (Gibco, Thermo Fisher Scientific, Waltham, Massachusetts), in Opti-MEM (Gibco, Thermo Fisher Scientific, Waltham, Massachusetts) media). Cells were used in experiments and were approximately 70-80% confluent on the day of harvest.

2.3 Harvesting Cells

Generally, cells were harvested either under the biosafety cabinet with trypsin or on the bench on ice using cell scrapers. Hypoxic samples were harvested in a hypoxic workstation. In the biosafety fume hood, the media from the plates or wells was removed and then plates or wells were gently rinsed once with PBS and the PBS was removed. Trypsin was then added enough to cover the bottom of the plate (1 mL for T75 flasks or 0.5 mL for T25 flasks) or well for up to 5 minutes at room temperature for HCT116 and HEK293T cells and for 5 minutes in the incubator at 37°C with 5% CO_2 for HIEC-6 cells. An appropriate amount of media was added to the plates or wells and gently pipetted up and down to disperse the cells. The harvested cells were collected in 1.5 mL Eppendorf tubes.

For harvesting using cell scrapers, the plates had the media dumped and rinsed with PBS three times. PBS (700 µL) was added to each plate and cell scrapers were used to gently scrape the cells off into the PBS. The cells were then collected in labeled 1.5 mL Eppendorf tubes to be processed depending on the experiment and protocol

2.4 ICP-MS

The AgNPs (10 nm, PVP-coated) was diluted in DMEM media (5% NCS, 5% FBS) to concentrations of 1, 5, and 10 µg/mL in a cell culture dish and was incubated at 37 °C and 5% CO_2 for 0, 6, and 24 hours. The solution was collected in a centrifuge tube and then centrifuged at 25,400 rpm for 2 hours at 4 ^{o}C in a Beckman Type 100 Ti centrifuge (Beckman Coulter, Brea, California). The supernatant was removed without disturbing the

pellet at the bottom of the tube. This was also done with $AgNO_3$ at concentrations of 0, 0.05, 0.1, 1, 2, and 5 µg/mL. Nitric acid was added (1% nitric acid) to the samples and the samples were measured with ICP-MS. ICP-MS was used to was used to determine the concentrations of $AgNO_3$ to use as a control for AgNP treatments by determining the amount of silver ions released by AgNP and $AgNO_3$. The ICP-MS was used in the lab of Dr. Alexandre Poulain (Biology, University of Ottawa).

2.5 MTT

MTT (3-(4,5-dimethylthiazol-2-yl)-2,5-diphenyltetrazolium bromide) assays were used to determine viability of HCT116 and HIEC-6 cells. Cells were cultured in 96 well plates. HIEC-6 cells were plated at 20,000 cells/well one day before treatment. HCT116 cells were plated at 10,000 cells/well one day before treatment. Cells were treated 24 hours before adding in the 10 µL of 5 mg/mL MTT to each well which contained 100 µL media. After 1-hour incubation at 37ºC, the media and MTT solution was taken out of the wells and replaced with 100 µL of 100% dimethyl sulfoxide (DMSO) in each well. The plate was slightly shaken to dissolve the purple crystals at the bottom of the wells. Absorbance was measured at 570 nm and 630 nm using a PowerWave XS microplate reader (BioTek Instruments, Winooski, Vermont). Absorbance values at 630 nm were subtracted from the absorbance values at 570 nm to control for scratches on the plate. Absorbance values from wells with cells with no MTT were subtracted from the 570 nm absorbance values to control for the cells in the wells.

2.6 Flow Cytometry

For flow cytometry experiments that involved staining, at least one sample needed to be untreated but unstained, and one sample untreated but stained. After treatment and harvest of samples for flow cytometry, the samples in Eppendorf tubes were spun down at 1,000 x g and had the media removed and the cell pellet was rinsed in PBS once. The cell pellets were then resuspended in 200 µL of flow buffer (0.5% BSA, 2 mM EDTA in PBS). The BD Accuri C6 flow cytometer (BD, Franklin Lakes, New Jersey) from Dr. Bruce McKay (Biology, Carleton University) was used. Before running samples, autoclaved MilliQ water was run for 10 minutes, decontamination solution (0.5% bleach in autoclaved MilliQ water) for 2 minutes and then autoclaved MilliQ water again for 2 minutes with fluidics set to fast to wash the flow cytometer. Samples were pipetted into a 96-well plate and then run at either slow, medium, or fast fluidics, making sure that the events per second do not exceed 1,500. A minimum of 10,000 gated live events were measured. Using the BD Accuri C6 software, the FSC vs SSC plot was used to gate live versus dead cells and debris. Histograms of count versus various channels was used to measure fluorescence. These channels included FL1 was for green, GFP, FL2 for red, propidium iodide (PI), FL4 for CellROX Deep Red (cytosolic ROS) and MitoSOX (mitochondrial ROS). See Appendix for examples of gated flow cytometry data.

2.7 DNA Purification

Mito and Cyto roGFP plasmids were purified using the Wizard® *Plus* Midipreps DNA Purification System (Promega, Madison, Wisconsin) protocol. To obtain the

concentration of the DNA, a NanoDrop Cary 100 Bio UV-Visible Spectrophotometer (Agilent Technologies, Santa Clara, California) was used.

2.8 PEI Transfection

Stock polyethylenimine (PEI) working solution (10 mg/mL) was made by dissolving 10 mg of PEI (Sigma-Aldrich, St. Louis, Missouri) in 1 mL of RNase-free and DNase-free MilliQ (double-distilled) water. Stocks of 10 mg/mL PEI solution were diluted in RNase-free and DNase-free MilliQ water to make a working PEI solution (1 mg/mL). The solution was vortexed thoroughly for at least one minute.

Before transfection, the PEI solution was warmed to room temperature and vortexed thoroughly. HEK293T cells were plated at 332,500 cells/well (70-80% confluency) the day before transfection.

The working PEI solution (10 µL) was added per 100 µL of Opti-MEM required. In a sterile tube, 4 µg of DNA was added per 100 µL Opti-MEM. The diluted PEI was vortexed for 5 seconds then added to the diluted DNA. The mixture was vortexed for 10 seconds every 3 minutes for 15 minutes. The mixture was added drop-wise to the plates of cells and the cells were incubated at 37°C with 5% CO_2 for 48 hours.

2.9 Mito roGFP and Cyto roGFP

For the mito and cyto roGFP experiments, HEK293T cells were transfected via PEI transfection with mito- or cyto-roGFP plasmids (see Appendix for Mito- and Cyto-roGFP plasmids) (see above for protocol). The Mito and Cyto roGFP plasmids were purified using

the Wizard® Plus Midipreps DNA Purification System (Promega, Madison, Wisconsin) (see above).

HEKT293T cells were chosen as they were ideal for transfection of these plasmids as they have high transfection efficiency and have been shown to work in this cell line. HEK293T cells transfected with the mito or cyto roGFP plasmids were plated at 237,500 cells/well in 6-well plates one day before treatment. Cells were harvested by trypsinization and spun down at 1,000 x g and resuspended in PBS. The samples were spun down and resuspended in 200 µL of flow buffer then run through the flow cytometer for data analysis (see above).

2.10 CellROX

HCT116 and HIEC-6 cells were used for the CellROX (Thermo Fisher Scientific) experiments, where CellROX measures cellular oxidative stress from the cytosol. Cells were plated for 70-80% confluency on the day of harvest. Cells were plated on a 24-well plate and treated, the day after plating, for 24 hours as this was the most optimal treatment time. HIEC-6 cells were plated at 87,000 cells/well one to two days before treatment. HCT116 cells were plated at 50,000 cells/well 2 days before treatment. The positive control used for CellROX experiments was 2 hour treatment of 25 µM and 50 µM hydrogen peroxide (H_2O_2). The negative control was 5 mM N-acetylcysteine (NAC) treatment 2 hours prior to the positive control treatments.

One hour before harvest, the cells were incubated with 3.75 µM CellROX in media for 1 hour in the dark at 37°C and 5% CO_2. Before harvest, the wells that were stained with CellROX were rinsed with PBS three times, otherwise the wells were rinsed once with

PBS. Cells were harvested by trypsinization after treatment. Cells were spun down, resuspended in PBS, spun down again and then resuspended in flow buffer (0.5% BSA and 2 mM EDTA in PBS). The samples were then run on the flow cytometer (see above). Example of flow data analysis can be found in the Appendix (Figure A9).

2.11 MitoSOX

HCT116 and HIEC-6 cells were used for MitoSOX (Thermo Fisher Scientific) experiments. Cells were plated for 70-80% confluency on the day of harvest. Cells were plated on a 24-well plate and treated the day after plating for 24 hours. HIEC-6 cells were plated at 87,000 cells/well one to two days before treatment. HCT116 cells were plated at 50,000 cells/well 2 days before treatment. The positive control used for the MitoSOX experiments was 30 minute treatments of 5 µg/mL and 15 µg/mL antimycin A. The negative control for the MitoSOX experiments was 5 mM NAC treatment 2 hours before the positive control treatment, which was the antimycin A treatment.

Cells were harvested by trypsinization after 24 hours of treatment. Cells were spun down and resuspended in PBS. The PBS was removed and the cell pellets were resuspended in freshly prepared 1 µM MitoSOX (in 1 X PBS). Samples were then incubated at 37°C with 5% CO_2 for 30 minutes. After incubation in the MitoSOX solution, 0.5 mL PBS was added to the tube, the cell pellets were spun down and resuspended with PBS to remove the MitoSOX solution. The cell pellets were spun down and resuspended in 100 µL of flow buffer and then run on the flow cytometer (see above). Example of flow data analysis can be found in the Appendix (Figure A10).

2.12 Bromodeoxyuridine (BrdU) Staining

HCT116 cells were grown in 6 cm plates to approximately 70-80% confluency on the day of harvest. HCT116 cells were plated at 600,000 cells/well in 6 cm plates one day before treatment. Cells were treated for 24 hours and the 30 μM BrdU and removed one hour prior to harvest by replacing with untreated media. Cells were harvested via trypsinization. Cells were spun down and resuspended in PBS and kept on ice when possible. The PBS was removed, and the cell pellets were resuspended in ice-cold 70% ethanol and stored at -20°C for a minimum of 30 minutes and up to a week before processing the samples.

After incubating in ethanol, the ethanol was removed after spinning down the cells at 1,000 x g. Samples were rinsed once in PBS and then resuspended in 0.7 mL of PBS with 50 μg/mL RNase A and incubated at 37°C for 30 minutes in the dark. After, 0.7 mL of PBS was added to the samples, spun down then resuspended in 0.7 mL of ice cold 0.1 N HCl containing 0.7% Triton X-100 and cooled on ice for 15 minutes in the dark. Then 0.7 mL of PBS was added to the samples, the samples were spun down and resuspended in 0.7 mL of sterile distilled water and incubated at 97°C in a hot block for 15 minutes in the dark (the samples were covered in tin foil on the hot block) then cooled immediately for 15 minutes on ice in the dark. Samples were spun down and resuspended in 0.7 mL PBS containing 0.5% Tween 20. The samples were spun down and resuspended in 50 μL of HBT (PBS, 5% FBS and 0.5% Tween 20) containing 1:100 dilutions of anti-BrdU secondary antibody (Thermo Fisher Scientific; Invitrogen BrdU Monoclonal Antibody (MoBU-1), Alexa Fluor 488) and incubated in the dark at room temperature for 30 minutes except for the no treatment/no stain sample and the no treatment/propidium iodide (PI)

sample. After, 1 mL of HBT was added to the samples and spun down and resuspended in 150 µL of HBT then spun down and resuspended in 200 µL of PBS with 50 µg/ml RNase A and 20 µg/mL PI except for the no treatment, no stain sample and the no treatment, BrdU sample. The samples were stored for a minimum of 30 minutes or overnight at 4°C in the dark. Before running the samples, the samples were filtered using cell strainers and then run on the flow cytometer (see above) to analyze for BrdU incorporation. Example of flow data analysis for Brdu experiments can be found in the Appendix (Figure A11).

2.13 HCT116-XBP1/ATF4 Experiments

The HCT116-XBP1 cell line was transfected with mNeonGreen through viral infection and fluoresces when *XBP1* splicing occurs. The HCT116-ATF4 cell line was transfected with mScarlet through viral infection and fluoresces when ATF4 translation occurs.[150] (See Figure A5 and A7 in the Appendix for the plasmids)

HCT116-XBP1 and HCT116-ATF4 cells were obtained from Dr. Bruce McKay (Biology Department, Carleton University). Cells were plated at 30,000 cells/well in 24 well plates 48 hours prior to harvest. The cells were treated 24 hours prior to harvest by replacing the media from the wells with the treatments that were dissolved in media. After the cells were harvested, the fluorescence was analyzed using flow cytometry where the fluorescence of the treated cells was compared to the fluorescence of the non-treated cells, stained sample to determine relative change in ER stress. Example of data analysis for HCT116-XBP1 and HCT116-ATF4 can be found in the Appendix (Figure A6 and A5)

2.14 Western Blotting

Proteins were obtained through urea protein extraction or cell fractionation. HCT116 cells were plated at 1,500,000 cells per plate in 10 cm plates 48 hours before harvest. Cells were treated 4 hours before harvest and hypoxic treatments were at 5% CO_2 and 1% O_2 in a triple gas incubator (Thermo Forma Series II Incubator). A Western blot time course experiment using various concentrations of tert-Butylhydroquinone (TBHQ) and observing the expression of Nrf2 found the 4-hour treatment elicited the greatest response (Figure A15 from the Appendix).

Cells were harvested using cell scrapers into 1 X PBS. For any hypoxia treated samples, the PBS was bubbled in nitrogen for 5-10 minutes prior to scraping cells. Hypoxic samples were harvested as quickly as possible. The samples then underwent urea extraction or cytosolic and nuclear cell fractionation. Total protein for each sample was quantified using the BCA assay (Pierce™, ThermoFisher Scientific, Ottawa, Ontario, Canada) protocol.

Various treatments were used as positive and negative controls. Tert-butylhydroquinone (TBHQ) is an antioxidant and Nrf2 activator and was used as a positive control for Nrf2 protein expression. Sulforaphane (SFN), a Nrf2 activator was used as a positive control. 2,3,7,8-tetrachlorodibenzodioxin (TCDD), a AhR activator, was used as a positive control. Hypoxia treatments were used as control for HIF1-α and to determine the effects of hypoxia on the cancer cells, HCT116, which are commonly found in hypoxic tumour microenvironments. SA and AgNPs treatments were to determine the effect that SA and SA co-treatment has on cancer cells to determine the potential of AgNP and SA for anticancer therapeutics.

2.14.1 Urea Extraction

After harvesting, the cells were spun down at 1,000 x g for 1-2 minutes. The PBS was removed and 100 µL of 8 M urea was added to cells in a 10 cm plate or 70 µL to cells in a 6-well plate. The tubes were then flicked to thoroughly resuspend and lyse the cell pellets in the urea. The tubes were then put on a rotator at 4°C overnight. The next day, the samples were ultracentrifuged at 100,000 x g for 1 hour at 4°C and the supernatant was removed and stored in 1.5 mL Eppendorf tubes. Protein determination was done on the samples using BCA assay and standards were made up in 8 M urea. The BCA assay was used to determine protein-loading amounts for making gels for Western blotting.

2.14.2 Cytosolic and Nuclear Cell Fractionation

Before harvesting, 1.5 mL Eppendorf tubes were labelled, and the weights of each empty tube was recorded. After harvesting, the samples were spun down at 680 x g for 10 minutes and the supernatant was carefully discarded. The tubes with the cell pellets were weighed and the weight from the tubes were subtracted to obtain the weight of the cell pellet. If fractionation was to be done later, the cell pellets were flash frozen in liquid nitrogen. The tubes were dropped into a container of liquid nitrogen for 1 minute. The cell pellet was resuspended in four times the cell pellet volume equivalent (4 mL of buffer A for every gram of cell pellet). Fresh buffer A (10 mM KCl, 10 mM HEPES, and 1.5 mM $MgCl_2$, pH 7.9, with 1 mM DTT, 0.5 mM PMSF, and 1 × protease inhibitor added right before use) was made up. The samples were incubated at 4°C for 15 minutes. Then 1% NP-40 (10 µL NP-40 + 990 µL Buffer A) was added to the cell suspensions to make a final concentration of 0.1% NP-40 (V/V). The tubes were flicked 13-15 times to open the cell

membrane. The samples were centrifuged at 680 x g for 10 minutes and the supernatant was collected into new labeled 1.5 mL Eppendorf tubes, this is the cytosolic fraction. The pellets were washed with 150 µL of buffer A (protease inhibitor does not need to be added for the Buffer A washing step), spinning at 680 x g for 10 minutes with the supernatant discarded. The pellets were resuspended in 40 µL RIPA (radioimmunoprecipitation assay) buffer (Pierce™, ThermoFisher Scientific, Ottawa, Ontario) (1 mM DTT, 0.5 mM PMSF, 1 × protease inhibitor) and vigorously mixed by flicking the tubes 10-15 times. The samples were incubated at 4°C for 30 minutes. The samples were centrifuged at 14,000 x g for 30 minutes at 4°C. The supernatant was collected and collected as the nuclear fraction in new labeled tubes. The nuclear and cytosolic fractions were stored at -80°C until needed. β-tubulin (Developmental Studies Hybridoma Bank (DSHB), Iowa City, Iowa) and lamin B (Santa Cruz, Dallas, Texas) were blotted for using Western blotting to check for proper cytosolic and nuclear separation, respectively. The BCA assay was used to determine protein-loading amounts to load into gels for Western blotting.

2.14.3 BCA Assay

In a 96 well plate, standards made up using the BCA assay (Pierce™, ThermoFisher Scientific) protocol was pipetted in triplicates of 25 µL. Sample cell lysate was pipetted in duplicates of 2.5 µL cell lysate and 22.5 µL MilliQ water. If cell fractionation was used, triplicate of 2.5 µL Buffer A and 22.5 µL MilliQ water, and 2.5 µL RIPA buffer and 22.5 µL MilliQ water were used as the lysis buffer controls. If urea extraction was used, the standards were made up in 8 M urea buffer instead of MilliQ water. The BCA assay Reagent A was mixed with the Reagent B at a 1:4 ratio and 200 µL of the solution was

added to each well. The plate was incubated for 30 minutes at 37°C. The plate was read at 562 nm and protein amounts were calculated.

2.14.4 Running Mini SDS-PAGE Gels

After determining the protein amounts for the samples using the BCA assay, the samples were made up to either 20, 30, or 40 μg of protein, depending on the targeted protein for blotting, and 2 x Laemmli sample buffer (5% β-mercaptoethanol) (Sigma-Aldrich, St. Louis, Missouri) was added to the samples at a 1:1 ratio. The samples were incubated at 100°C in an Isotemp heating block (Fisher Scientific) for 5 minutes. The samples after cooling were spun down at 800 x g for 1 minute to get rid of bubbles then loaded on Mini SDS-PAGE 8% or 10% gels. 2,2,2-trichloroethanol (TCE) (0.5%) was added to the resolving gel for normalization. Gels were run in resolving buffer (Bio-Rad, Hercules, California) 1 X Tris/glycine/SDS buffer) at 150 Volts for approximately an hour until the desired band distance was reached.

The Bio-Rad (Hercules, California) mini-gel apparatus was used to make mini SDS-PAGE gels using the Bio-Rad Protogel, Protogel Resolving Buffer, and Protogel Stacking Buffer (National Diagnostics, Atlanta Georgia) with 8% gels used for the aryl hydrocarbon receptor (AhR) blots and 10% gels used for all other experiments. TCE (0.5%) was added to all gels for normalization. Ammonium persulfate (APS) (30%) and tetramethylethylenediamine (TEMED) (Thermo Fisher Scientific, Waltham, Massachusetts) was added to the gels for polymerization of the gels.

After running, the gel was imaged for TCE normalization using the Image Lab (Bio-Rad, Hercules, California) software. Bio-Rad Immun-Blot PVDF membranes were used

for protein transfer. Proteins were transferred at 180 mA for 16-20 hours overnight. Blots were blocked with 10% dry milk (Carnation, Markham, Ontario) in TBST (tris-buffered saline with 0.1% Tween 20) for 1 hour on a rocker at 4°C then rinsed thoroughly with TBST until no milk was left.

2.14.5 Antibodies

Primary antibodies were diluted in TBST with 5% milk or 5% BSA, or just TBST and 0.1% sodium azide depending upon the recommendation for each antibody. The primary antibody in TBST was put on the blot overnight up to 3 nights over the weekend, shaking at 4°C depending on the antibody used. Blots were then washed with TBST 5 times for 5 minutes each.

Secondary antibodies were diluted in TBST with 5% milk, 5% BSA, or just TBST depending on the recommendation for each antibody. The secondary antibody was put on the blot for 1 hour or overnight shaking at 4°C depending on the primary antibody used. Blots were then washed with TBST shaking at 4°C, 5 times for 5 minutes each.

A Kimwipe was used to dab the edges of the blot to remove the wash. Then 300 µL of the peroxide reagent was mixed with 300 µL of the Luminol/Enhancer reagent of the Bio-Rad Clarity Western ECL Blotting Substrate (Bio-Rad, Hercules, California) and added to the blot for 5 minutes. The blot was then imaged using a Molecular Imager Gel Doc XR+ documentation system (Bio-Rad, Hercules, California).

Table 2. Primary antibodies, their brand, and the dilution used. Sodium azide (0.1%) was added to primary antibodies to prevent bacterial or fungal growth. Dry non-fat milk (0.5%) or bovine serum albumin (BSA) (0.5%) was added according to recommendations for each antibody.

Primary Antibody	Brand	Dilution
AhR	Invitrogen (JM34-10)	1:1,000
Lamin B	Santa Cruz (sc-M-20)	1:1,000
Nrf1	Novus (NBP2-55915)	1:1,000
Nrf2	Santa Cruz (sc-C-20)	1:1,000
β-tubulin	Developmental Studies Hybridoma Bank (DSHB) (E7)	1:1,000
HIF1-α	Cell Signaling (D2U3T)	1:1,000
β-catenin	Novus (NBP1-54467)	1:1,000
Wntless/GRP177	Novus (NBP1-59013)	1:1,000
PORCN	Novus (NBP1-59677)	1:1,000
Wnt5a	Novus (NBP2-24752)	1:1,000
Wnt3a	Santa Cruz (sc-136163) Novus (NBP1-19050)	1:500 (Santa Cruz) 1:1,000 (Novus)

Table 3. Secondary antibodies, their brand, and the dilution used. Dry non-fat milk (0.5%) or bovine serum albumin (BSA) (0.5%) was added according to recommendations for each antibody.

Secondary Antibody	Brand	Dilution
Goat-anti-rabbit	Abcam (Ab 6721)	1:10,000
Goat-anti-mouse	Dako (P0447)	1:5,000
Mouse-anti-goat	Santa Cruz (sc-2354)	1:2,000

2.14.6 Densitometry

The Image Lab (Bio-Rad, Hercules, California) software was used for densitometry of protein bands obtained from Western Blotting. Protein bands were normalized to TCE images or to β-tubulin bands. Each protein band was normalized to the control and the normalized data was analyzed for statistical significance.

2.15 Quantitative Polymerase Chain Reaction (qPCR)

HCT116 cells were plated at 600,000 cells/plate in 6 cm plates 48 hours before harvest. The cells were treated for 4 hours before harvest. At harvest time, the cells on the plates were quickly rinsed with PBS that was warmed to 37^{o}C and lysed on the plate immediately. Using the Aurum Total RNA Mini Kit (BioRad, Hercules, California), the total ribonucleic acid (RNA) was extracted. Using the Cary 100 Bio UV-Visible Spectrophotometer (Agilent Technologies, Santa Clara, California), the quality of the RNA was determined by Nanodrop and by visualization on an agarose gel with 1% bleach). Using the iScipt cDNA Synthesis Kit (BioRad, Hercules, California), 1 µg of RNA was converted to complementary deoxyribonucleic acid (cDNA). Then using Sso Advanced Universal SYBR Green (BioRad, Hercules, California), qPCR was performed at 60^{o}C, and data was analyzed using the CFX manager software (BioRad, Hercules, California). For validation of the qPCR primers, a thermal gradient, an agarose gel of the amplicons from the thermal gradient, and standard curve was used. A melt curve for each plate was used to determine specificity and make sure there were no primer dimers. Each plate had a non-template control with DNase/RNase free water for each primer pair.

Table 4 shows the primer sequences and the quantity of cDNA used for each primer pair. Data was analyzed using the Standard error, one-way ANOVA, and the Dunnett's test. Samples were tested for purity; the OD260/280 was between 1.8-2.0.

Table 4. Primer sequences and the amount of cDNA used in the qPCR reaction for each primer pair.

Gene Target	Primer Sequence	Amount of cDNA per Reaction
Nrf 1 (NFE2L1)	Forward: 5'-CTG GAG GAG GAA TTT GAC TCT G-3' Reverse: 5'-GAG GAA GAG GAG GAG GAA GAA-3'	500 ng
Nrf 2 (NFE2L2)	Forward: 5'-CCG GCA TTT CAC TAA ACA CAA G-3' Reverse: 5'-CAG AAT CAC TGA GGC CAA GTA G-3'	250 ng
AhR	Forward: 5'-TCA ACA GCA ACA GTC CTT GG-3' Reverse: 5'-TCC AAT TTT CAA ACA TGC CA-3'	250 ng
WLS	Forward: 5'-GGA CAT TGC CTT CAA GCT AAA C-3' Reverse: 5'-CAT TTC AGT CCA CTC AGC AAA C-3'	500 ng
WNT3A	Forward: 5'-GAC TTC CTC AAG GAC AAG TAC G-3' Reverse: 5'-GGC ACC TTG AAG TAG GTG TAG-3'	1000 ng
WNT5A	Forward: 5'-CCC AGG ACC CGC TTA TTT ATA G- 3' Reverse: 5-'GGT TCC GGT TGC AAT TCT TG-3'	1000 ng
PORCN	Forward: 5'-CTC CTT CCA CTT CAG CAA CTA T-3' Reverse: 5'-CCA TTC CAG GTG ATC CTT CTC-3'	1000 ng
GAPDH	Forward: 5'-CTT TGG TAT CGT GGA AGG ACT C-3' Reverse: 5'-GAG GCA GGG ATG ATG TTC TG-3'	10 ng

2.16 Statistics

Standard error of the mean (SEM), one-way ANOVA, and Dunnett's tests were conducted using the SigmaPlot software. Treatments were all compared to controls. Values shown in the figures under the results section represent the mean ± SEM. Biological replicates were used for all experiments. Statistical significance is indicated by *$p<0.05$, **$p<0.01$, and ***$p<0.001$.

Chapter 3: Results

3.1 Determining Silver Ion Equivalents

Using ICP-MS, the amount of silver ions released at 0.05, 0.1, 1, 2, and 5 µg/mL $AgNO_3$ in DMEM media with 5% FBS and 5% NCS was determined, and a standard curve was made (Figure 7A). Using ICP-MS, the equivalent $AgNO_3$ concentrations was determined for 1, 5, and 10 µg/mL AgNP (Figure 7B).

Table 2 shows the equivalent $AgNO_3$ concentrations at 1 and 10 µg/mL AgNP at 4 and 24 hours. The proposed $AgNO_3$ equivalents for 20 µg/mL was calculated using the line equation from Figure 7. Sample calculations for determining the $AgNO_3$ equivalents are provided in the Appendix.

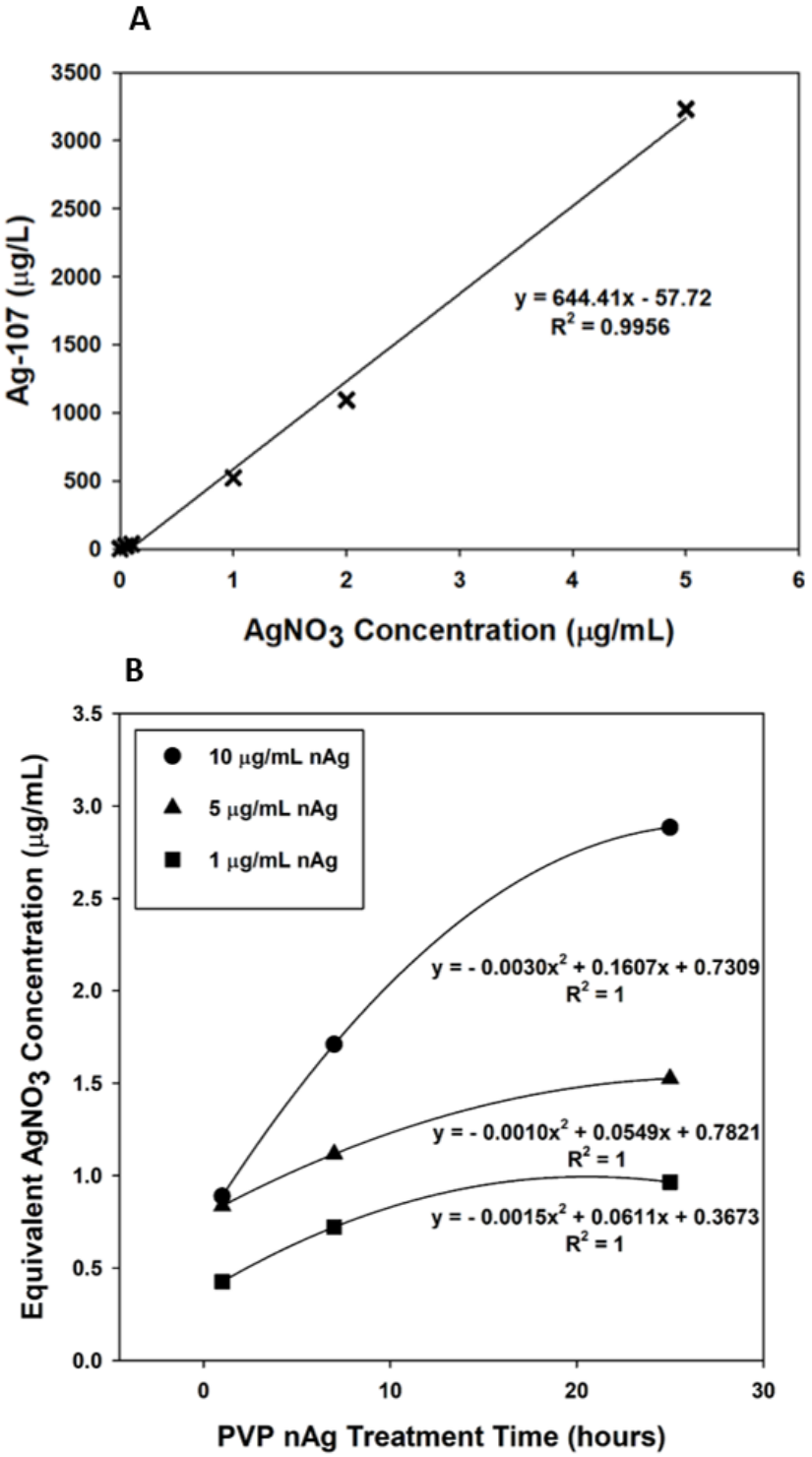

Figure 7. Using ICP-MS to determine equivalent concentrations of $AgNO_3$ based on silver (Ag-107) ions released by silver nitrate ($AgNO_3$) and nanosilver (nAg). A) Standard curve for Ag-107 ions released by 0.05, 0.1, 1, 2, 5 µg/mL $AgNO_3$ using ICP-MS was determined.

A linear line of best of fit was used: y = 644.41x – 57.72, where R^2 = 0.9956. B) Determining the equivalent $AgNO_3$ concentrations for different treatment times of 1, 5, and 10 µg/mL of 10 nm PVP coated nAg. A polynomial line of best fit was used: for 1 µg/mL nAg, $y = -0.0015x^2 + 0.0611x + 0.3673$ where $R^2 = 1$, for 5 µg/mL nAg, $y = -0.0010x^2 + 0.0549x + 0.7821$, where $R^2 = 1$, and for 10 µg/mL nAg, $y = -0.003x^2 + 0.1607x + 0.7309$, where $R^2 = 1$. 1 replicate. Samples were prepared by S. Cameron from Carleton University and samples were run on the ICP-MS by Alexandre Poulain at the University of Ottawa.

Table 2. Determining silver nitrate ($AgNO_3$) equivalent concentrations for 1, 10, 20, 30 µg/mL of 10 nm PVP coated nanosilver (nAg) for 4 and 24 hours using ICP-MS. From Figure 7B (List of Figures), the equation: $y = -0.0015x^2 + 0.0611x + 0.3673$ was used to determine the $AgNO_3$ equivalent at 1 µg/mL nAg and the equation $y = -0.003x^2 + 0.1607x + 0.7309$ was used to determine the $AgNO_3$ equivalent at 10 µg/mL nAg. The $AgNO_3$ equivalent for 30 µg/mL nAg for 4 hours was calculated using the equation $y = 0.5808x^{0.3487}$ from Figure A1 (Appendix). Sample calculations for proposed $AgNO_3$ at 20 and 30 µg/mL are found in the Appendix.

Time (hr)	**$AgNO_3$ equivalent (µg/mL) at 1 µg/mL nAg**	**$AgNO_3$ equivalent (µg/mL) at 10 µg/mL nAg**	**Proposed $AgNO_3$ equivalent (µg/mL) at 20 µg/mL nAg**	**Proposed $AgNO_3$ equivalent (µg/mL) at 30 µg/mL nAg**
4	0.586	1.326	1.783	1.902
24	0.924	2.860	5.367	N/A

3.2 Cell Pictures and Determining Cell Viability

Figure 8 and Figure 9 shows pictures of cells HCT116 cells at 10 x and 20 x magnification treated with 1, 10, 20, and 30 µg/mL 10 nm PVP-coated nAg and 0.5, 1, 1.5, and 2 µg/mL $AgNO_3$ for 24 hours. Cells at the highest $AgNO_3$ concentration looked slightly shriveled and unhealthy. As the concentration of AgNP treatment increased, the HCT116 looked to become stressed.

Figure 10 and Figure 11 shows pictures of cells HIEC-6 cells at 10 x and 20 x magnification treated with 1, 10, 20, and 30 µg/mL AgNP and 0.5, 1, 1.5, and 2 µg/mL $AgNO_3$ for 24 hours. Cells at the highest $AgNO_3$ and AgNP concentrations looked relative to controls, normal and unstressed.

The EC_{50} of $AgNO_3$ for HCT116 cells was 1.645 ± 0.0286 µg/mL (Figure 12A) and the EC_{50} of $AgNO_3$ for HIEC-6 cells was higher at 17.972 ± 0.356 µg/mL (Figure 12B). The viability of HCT116 cells significantly decreased at 1.5 µg/mL $AgNO_3$, while the HIEC-6 cells decreased significantly at 20 µg/mL $AgNO_3$.

Cell viability was determined by conducting MTT assays for HCT116 and HIEC-6 cell lines. The EC_{50} of $AgNO_3$, AgNP, SA, and SA and AgNP combined treatments were determined for HCT116 and HIEC-6 cells by using the MTT assay and 24-hour treatments. Treatments were made up in the appropriate media for HIEC-6 or HCT116 cells and no treatment samples were made up of just media.

The EC_{50} of AgNPs for HCT116 cells was 78.431 ± 0.703 µg/mL. Cell viability was significantly different at 75 µg/mL AgNPs (Figure 13A). The EC_{50} of AgNPs for HIEC-6 cells could not be calculated as no statistical differences were found for up to 125 µg/mL AgNP treatment (Figure 13B).

The EC_{50} of sodium ascorbate (SA) for HCT116 cells treated for 24 hours was 5.375 ± 0.918 mM μg/mL. Cell viability was significantly different starting at 4 mM SA (Figure 14A). The EC_{50} of SA for HIEC-6 treated for 24 hours was 3.775 ± 0.00803 mM. Cell viability was significantly different starting at 3.25 mM SA (Figure 14).

The EC_{50} for HCT116 treated with constant 10 μg/mL of AgNPs with varying concentrations of SA up to 10 mM was 0.726 ± 0.204 mM SA. All treatments were significantly different than the control (Figure 15). The EC_{50} for 10 μg/mL of AgNPs with varying concentrations of SA up to 10 mM. Treatments were statistically different at 0.1 mM SA + 10 μg/mL AgNPs and higher (Figure 15).

The EC_{50} for HCT116 treated with constant 1 mM SA and varying concentrations of AgNPs was 86.33 ± 2.70 μg/mL. Cell viability was shown to be statistically different after 10 μg/mL AgNP + 1 mM SA (Figure 16). The EC_{50} for HIEC-6 treated with constant 1 mM SA and varying concentrations of AgNPs could not be calculated as no statistical differences were shown for up to 125 μg/mL AgNP treatment. HIEC-6 cell viability was not statistically different at any treatment tested (Figure 16).

The higher concentrations of $AgNO_3$ equivalents calculated from the ICP-MS curve (Table 2 and Figure 7) were too toxic and so were not used for experiments; the highest equivalent dose (5.367 μg/mL) (Table 2) was highly toxic and resulted in almost 100 % cell death (Figure 12). Instead, a range of $AgNO_3$ values that encompasses a simple and reasonable range of silver ion release (0.5 – 2 μg/mL) was used for experiments. Further experiments for silver ion equivalents should be conducted.

The AgNP treatment concentrations were chosen based on the EC_{50} and MTT assay results (Figure 13). I chose a sublethal concentration of 30 μg/mL for most experiments,

below the EC_{50} value that did not seem to stress the cells too much. The SA co-treatment concentration was chosen based on the MTT using constant 10 µg/mL AgNPs and varying SA concentrations (Figure 15). The 1 mM SA and 10 µg/mL was used as this concentration was sublethal to the HIEC-6 and induced the greatest difference in cell death between the HCT116 and HIEC-6 cells with greater cell death in the cancer HCT116 cells.

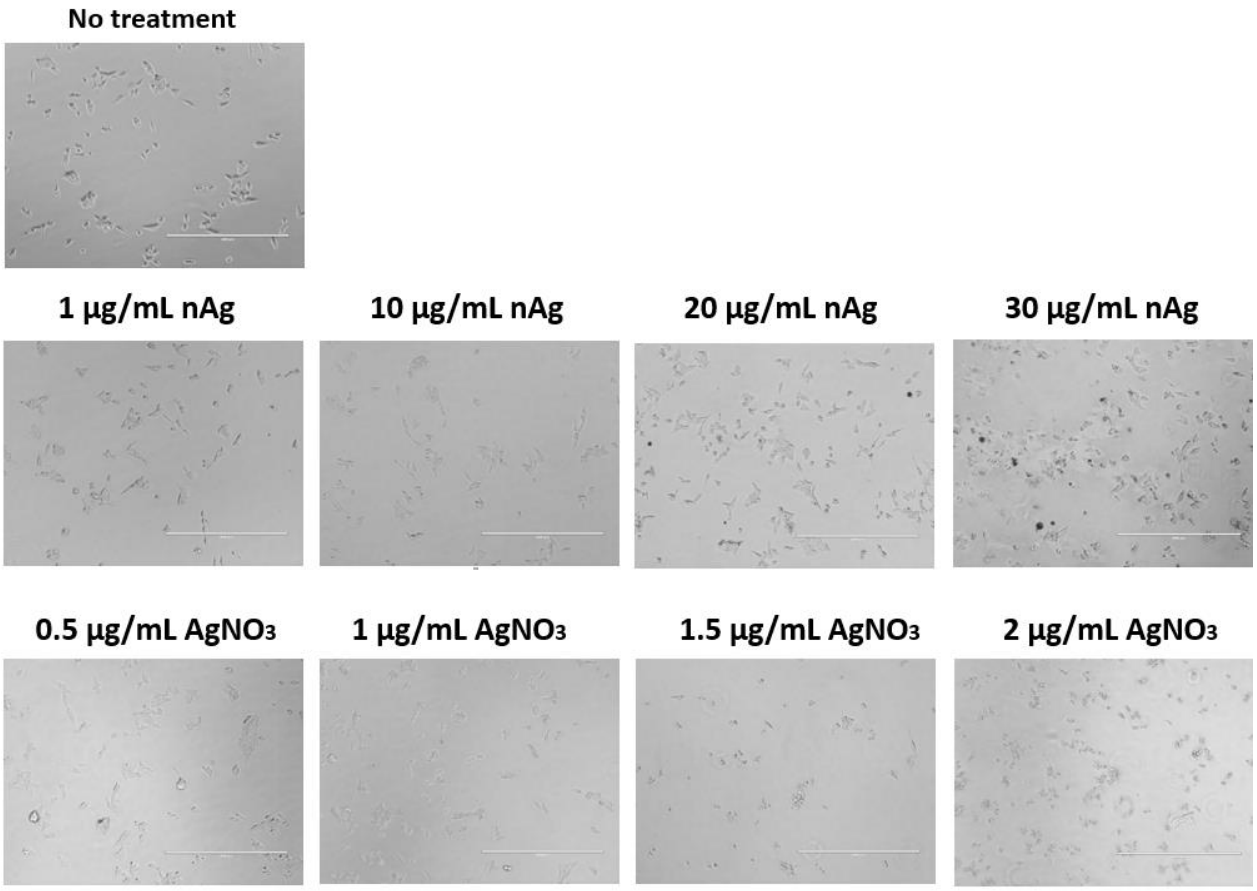

Figure 8. Pictures of HCT116 cells treated with 1, 10, 20, and 30 µg/mL 10 nm PVP-coated nanosilver (nAg) and 0.5, 1, 1.5, and 2 µg/mL silver nitrate ($AgNO_3$) for 24 hours. All cells were in HCT116 media. No treatment was in just media. Pictures were taken with the EVOS M5000 microscope (Model # AMF5000) (ThermoFisher Scientific, Waltham, Massachusetts). Scale bars are 400 µm in length.

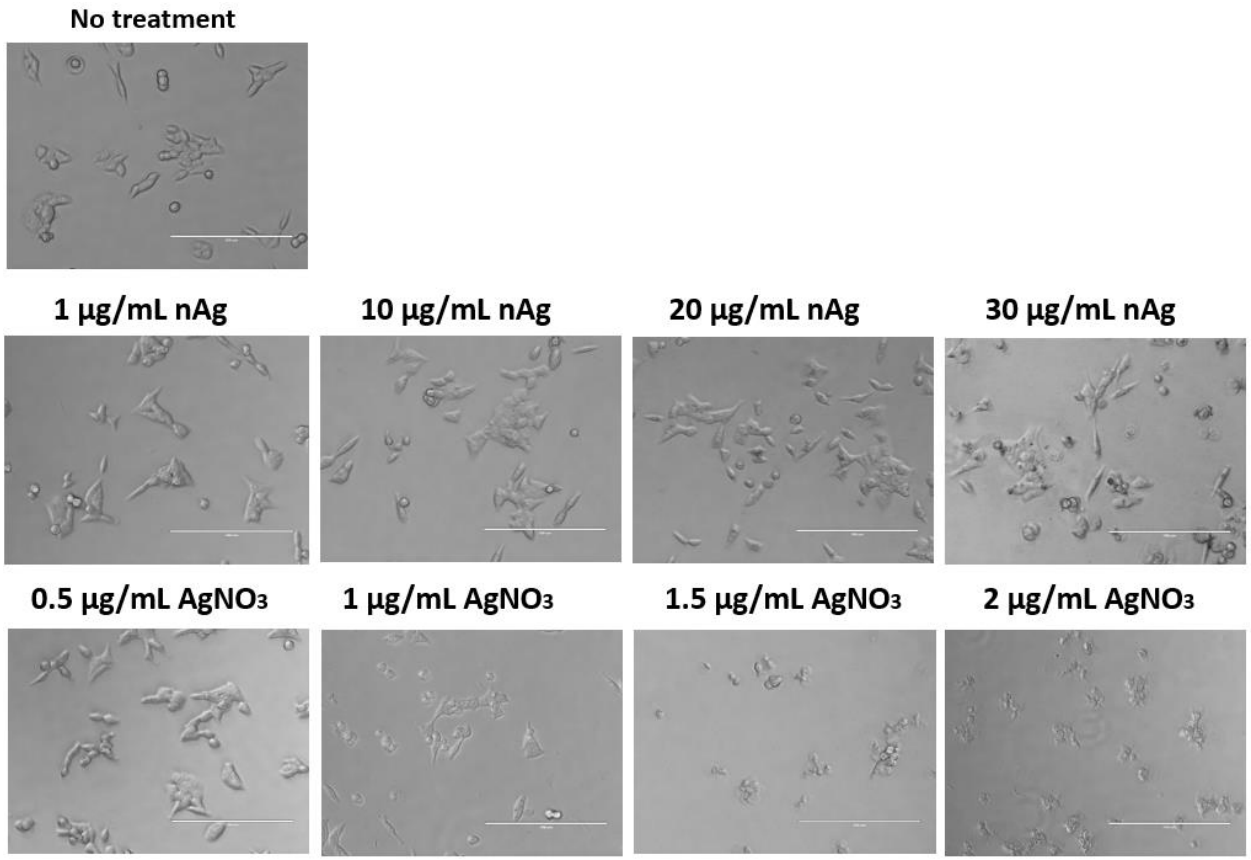

Figure 9. Pictures of HCT116 cells treated with 1, 10, 20, and 30 µg/mL 10 nm PVP-coated nanosilver (nAg) and 0.5, 1, 1.5, and 2 µg/mL silver nitrate ($AgNO_3$) for 24 hours. All cells were in HCT116 media. No treatment was in just media. Pictures were taken with the EVOS M5000 microscope (Model # AMF5000) (ThermoFisher Scientific, Waltham, Massachusetts). Scale bars are 200 µm in length.

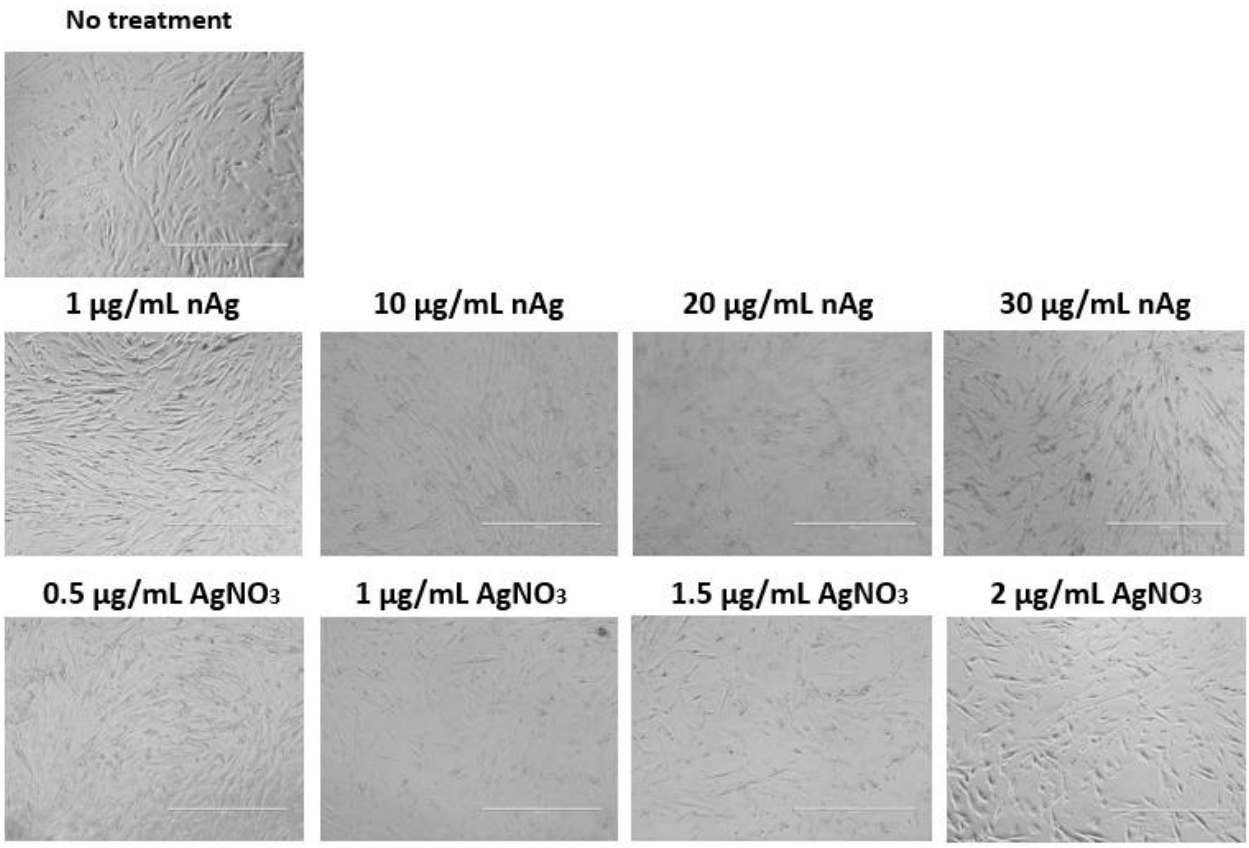

Figure 10. Pictures of HIEC-6 cells treated with 1, 10, 20, and 30 µg/mL 10 nm PVP-nanosilver (nAg) and 0.5, 1, 1.5, and 2 µg/mL silver nitrate ($AgNO_3$) for 24 hours. All cells were in HIEC-6 media. No treatment was in just media. Pictures were taken with the EVOS M5000 microscope (Model # AMF5000) (ThermoFisher Scientific, Waltham, Massachusetts). Scale bars are 400 µm in length.

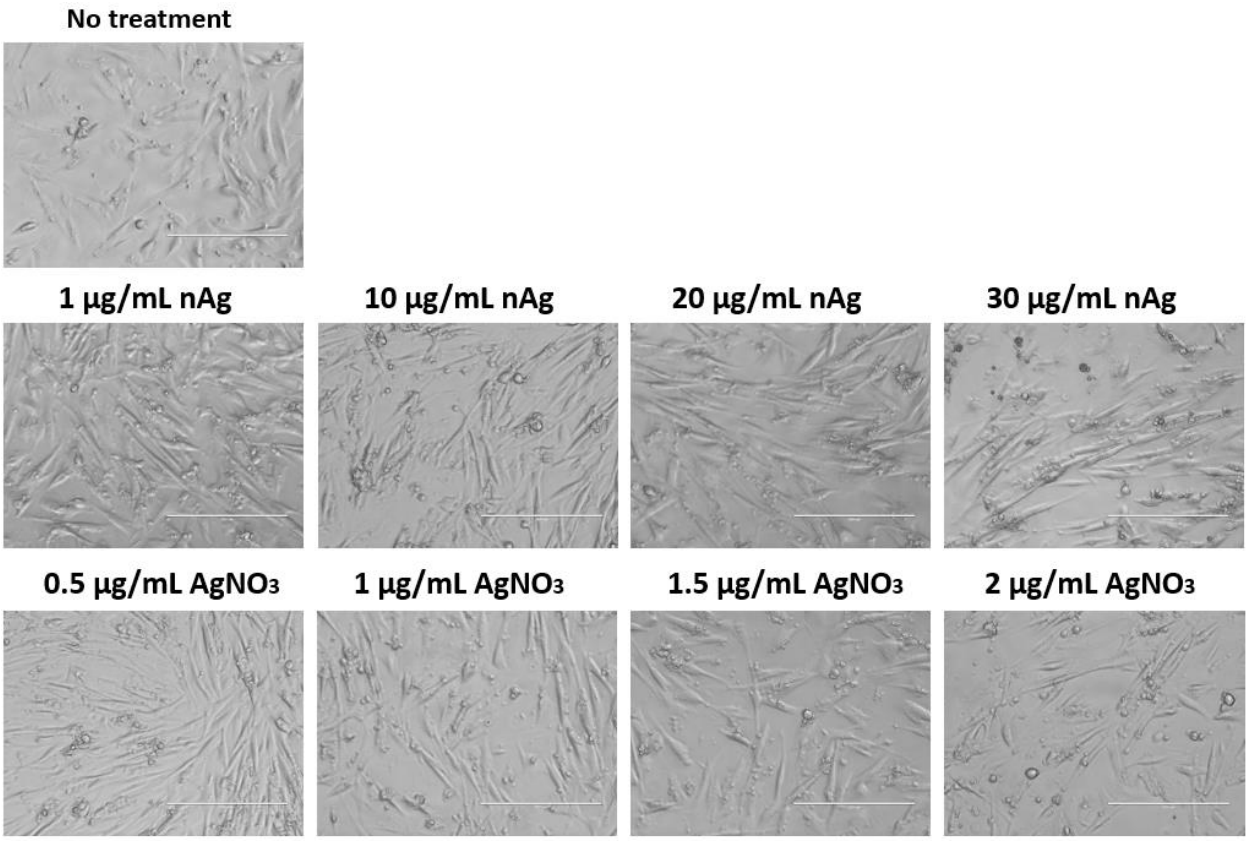

Figure 11. Pictures of HIEC-6 cells treated with 1, 10, 20, and 30 µg/mL 10 nm PVP-coated nanosilver (nAg) and 0.5, 1, 1.5, and 2 µg/mL silver nitrate ($AgNO_3$) for 24 hours. All cells were in HIEC-6 media. No treatment was in just media. Pictures were taken with the EVOS M5000 microscope (model # AMF5000) (ThermoFisher Scientific, Waltham, Massachusetts). Scale bars are 200 µm in length.

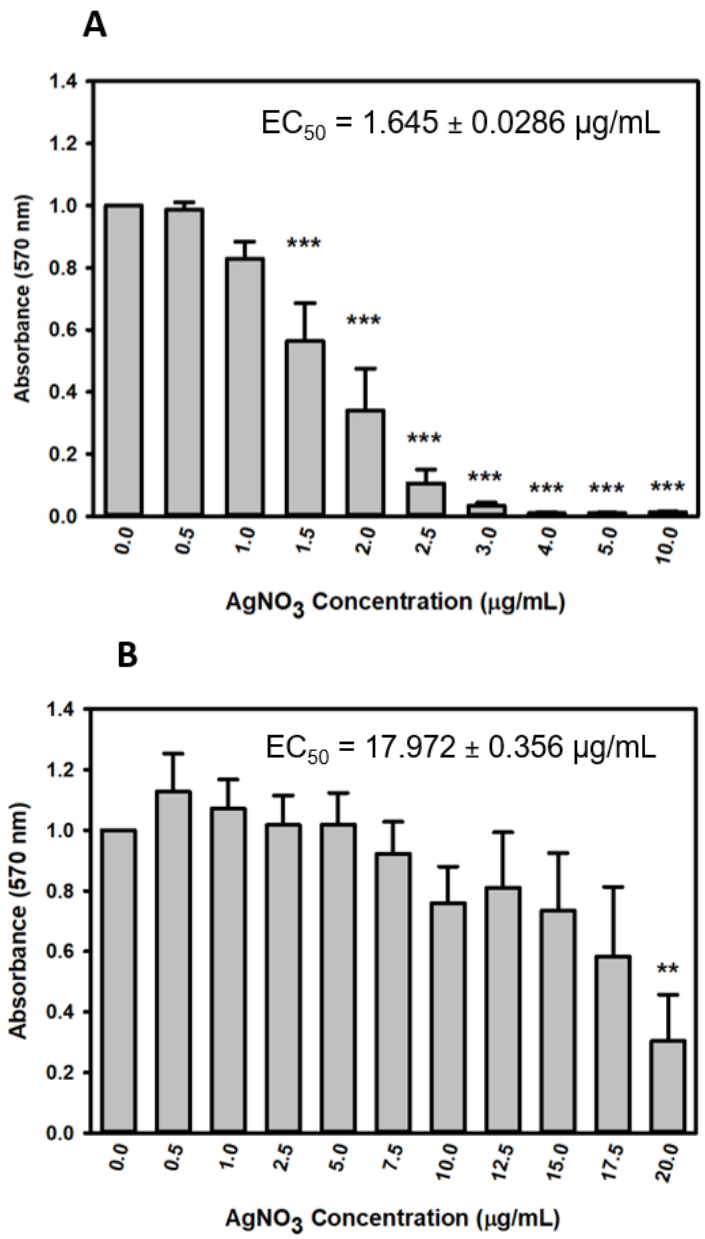

Figure 12. Determining cell viability in HCT116 and HIEC-6 cells using the MTT assay. All treatments were made up in HCT116 or HIEC-6 media. No treatment was only media. Cells were treated with varying concentrations of silver nitrate ($AgNO_3$) for 24 hours. A) HCT116 $AgNO_3$ EC_{50} = 1.645 ± 0.0286 µg/mL. 1.0, 2.0, 2.5, 3.0, 4.0, 5.0, and 10.0 µg/mL $AgNO_3$ treatments were significant. 7 replicates. B) HIEC-6 $AgNO_3$ EC_{50} = 17.972 ± 0.356 µg/mL. 6 replicates. Standard error, Standard error, one-way ANOVA, and Dunnett's test were used (*$p<0.05$, **$p<0.01$, ***$p<0.001$).

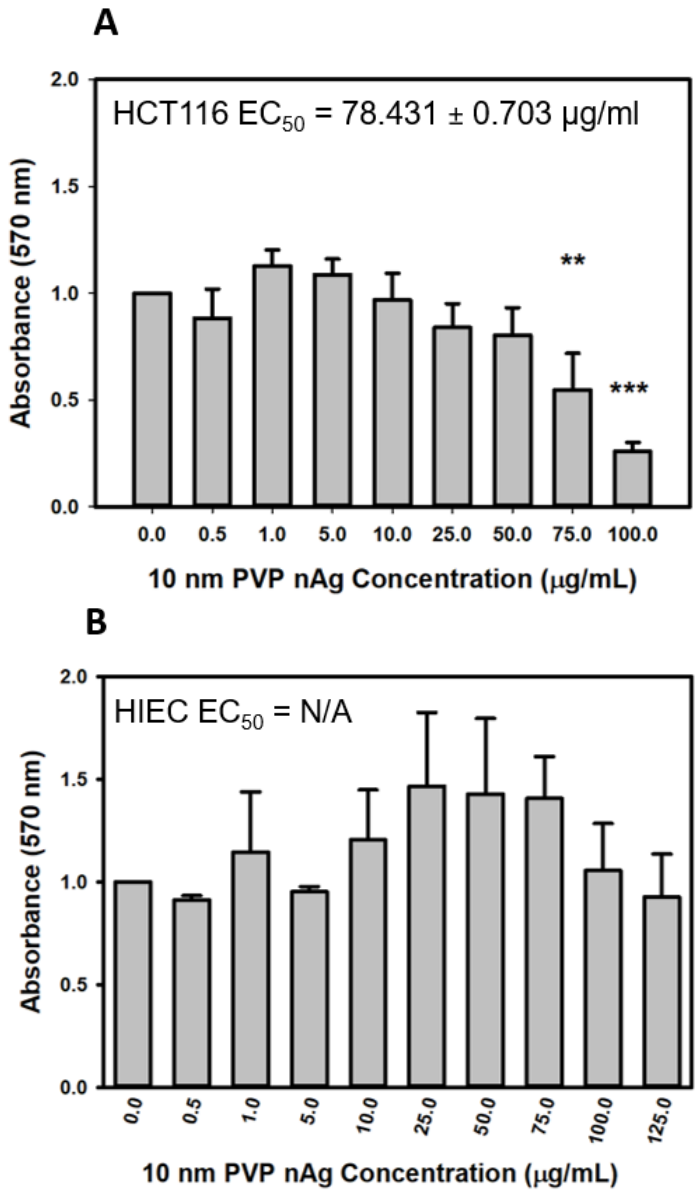

Figure 13. Determining cell viability in HCT116 and HIEC-6 cells treated with 10 nm PVP coated nanosilver (nAg) for 24 hours using the MTT assay. All treatments were made up in HCT116 or HIEC-6 media. No treatment was only media. Cells were treated with nAg for 24 hours. A) HCT116 nAg EC_{50} = 78.431 ± 0.703 µg/mL. 3 replicates B) HIEC-6 nAg EC_{50} not applicable. Four replicates. Standard error, Standard error, one-way ANOVA, and Dunnett's test were used.

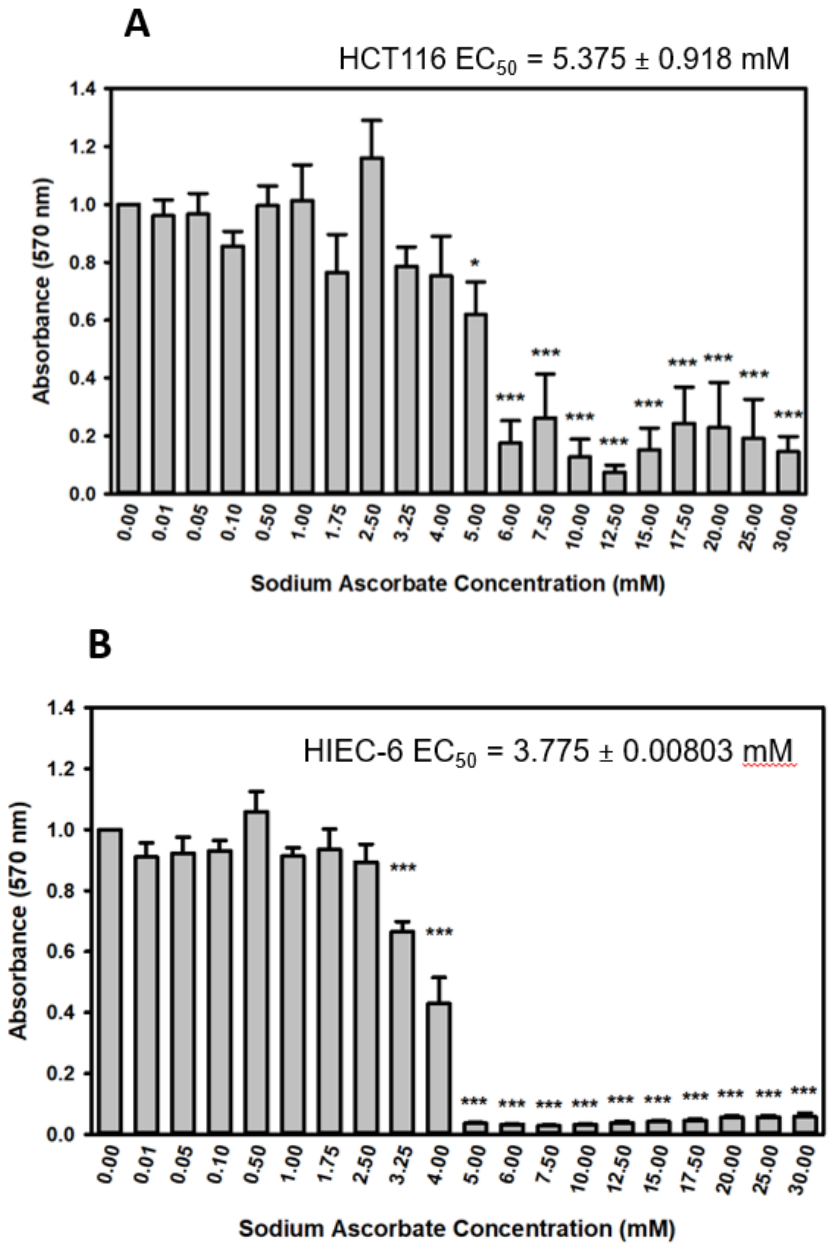

Figure 14. Determining cell viability in HCT116 and HIEC-6 cells treated with sodium ascorbate (SA) using the MTT assay. All treatments were made up in HCT116 or HIEC-6 media. No treatment was only media. Cells were treated with varying concentrations of sodium ascorbate (SA) for 24 hours. A) HCT116 SA EC_{50} = 5.375 ± 0.918 mM. 3-6 replicates. B) HIEC-6 SA EC_{50} = 3.775 ± 0.00803 mM. 3 replicates. Standard error, one-way ANOVA, and Dunnett's test were used (*p<0.05, **p<0.01, ***p<0.001).

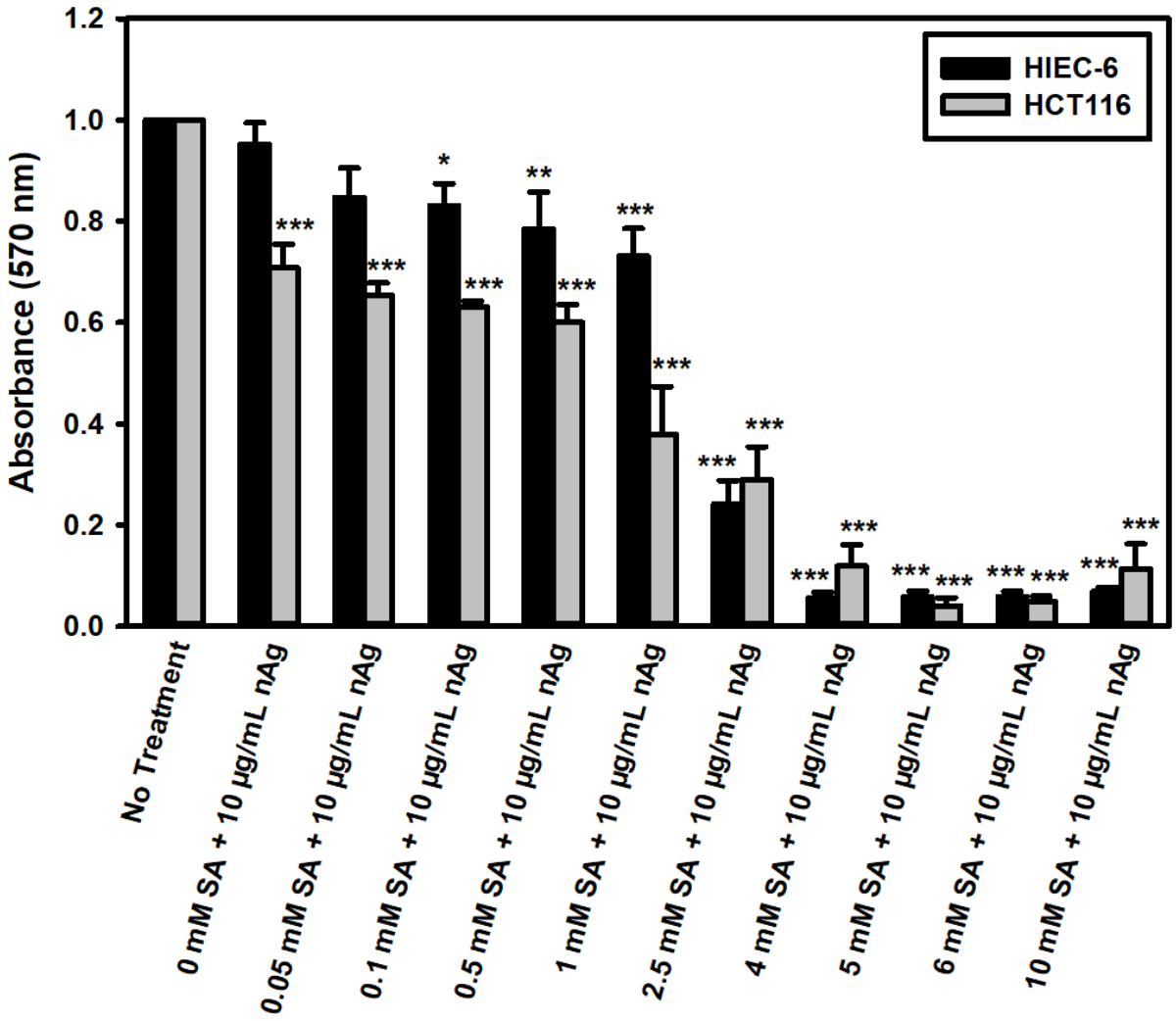

Figure 15. Determining cell viability in HCT116 and HIEC-6 cells treated with constant 10 µg/mL of 10 nm PVP coated nanosilver (nAg) with varying concentrations of sodium ascorbate (SA) using the MTT assay. All treatments were made up in HCT116 or HIEC-6 media. No treatment was only media. Cells were treated with a constant 10 µg/mL of 10 nm PVP coated nAg with varying concentrations of SA for 24 hours. HCT116 SA EC_{50} = 0.726 ± 0.204 mM. HIEC-6 SA EC_{50} = 1.802 ± 0.366 mM. Standard error, one-way ANOVA, and Dunnett's test were used (*$p<0.05$, **$p<0.01$, ***$p<0.001$). HCT116 had 3-5 replicates. HIEC-6 had 3 replicates.

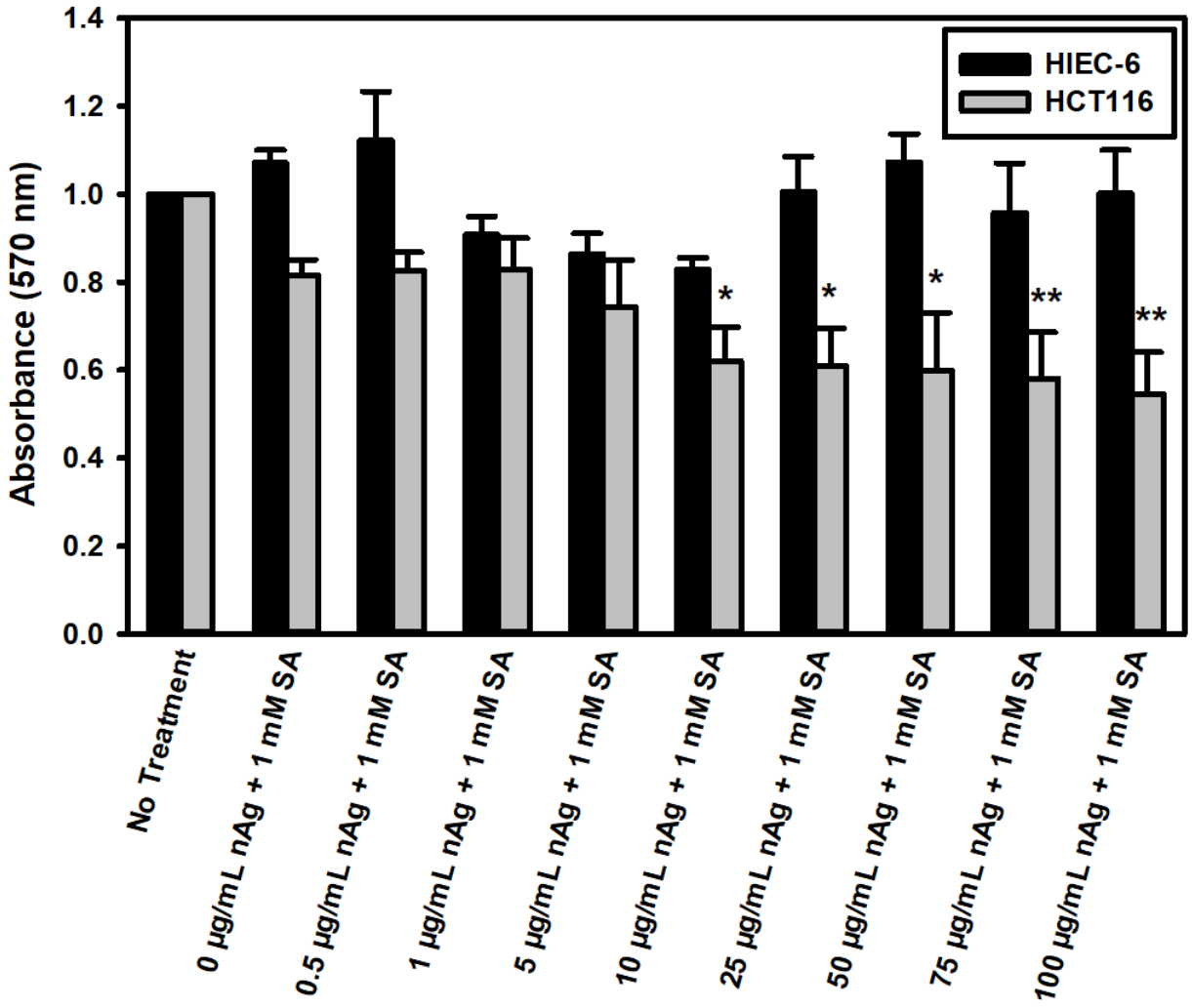

Figure 16. Determining cell viability in HCT116 and HIEC-6 cells using the MTT assay. Cells were treated with a constant 1 mM sodium ascorbate (SA) and varying concentrations of 10 nm PVP coated nanosilver (nAg) for 24 hours. All treatments were made up in HCT116 or HIEC-6 media. No treatment was only media. HCT116 nAg EC_{50} = 86.333 ± 2.696 µg/mL. HIEC-6 nAg EC_{50} = N/A. Standard error, one-way ANOVA, and Dunnett's test were used (*$p<0.05$, **$p<0.01$, ***$p<0.001$). HCT116 had 4 replicates. HIEC-6 had 3 replicates.

3.3 Nanosilver and the Oxidative and Hypoxic Stress Responses

3.3.1 Mito- and Cyto-roGFP

Mito- and Cyto-roGFP transfected HEK293T cells were used to determine the effect that AgNPs has on cytosolic and mitochondrial oxidative stress. A time course experiment was conducted for both the Mito-roGFP transfected HEK293T cells with 30 minutes, 1 hour, and 2 hour treatments. (Figure 17). Based on these results, I chose to use the 2-hour treatment time as it yielded the least variable results and showed the most potential to show viable results.

The 2-hour AgNP treatments had no effect on the fluorescence emitted by the Mito-roGFP transfected HEK293T cells. Negative control dithiothreitol (DTT), and positive controls tert-butyl hydroperoxide (tBHP), and antimycin A (AA), did not induce any significant changes either. (Figure 18). No significant changes in fluorescence were seen in any of treatments for the 2-hour treated Cyto-roGFP transfected HEK293T cells either (Figure 19).

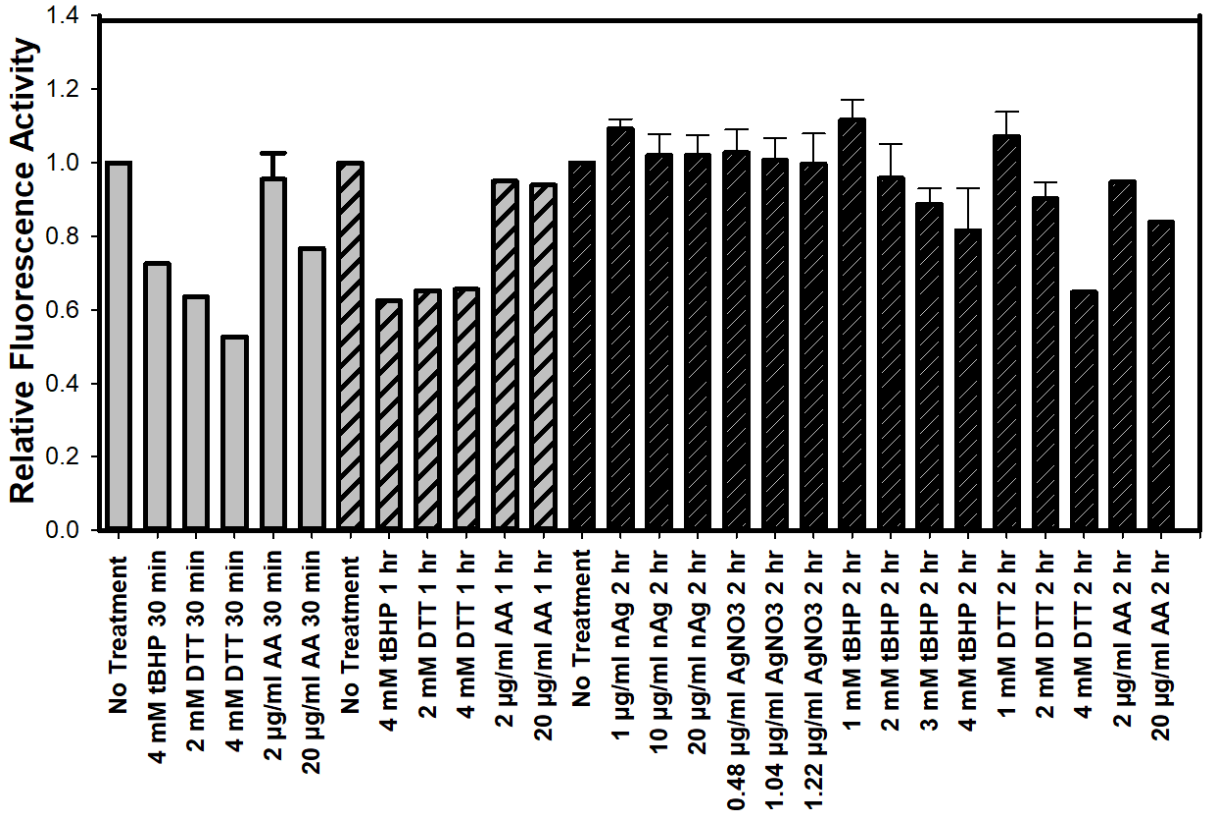

Figure 17. Time course treatments show that 2-hour treatments seem to have more of an effect on mitochondrial oxidative stress than 30 min or 1 hour treatments in HEK293T cells transfected with fluorescent Mito-roGFP. Cells were treated for 30 min, 1 hour, and 2 hours. All treatments were made up in HEK293T media. No treatment was only media. Negative control dithiothreitol (DTT), and positive controls tert-butyl hydroperoxide (tBHP), and antimycin A (AA) were used. No significance was found using one-way ANOVA, and the Dunnett's test. 1-9 replicates. Treatments with no error bars have only one replicate.

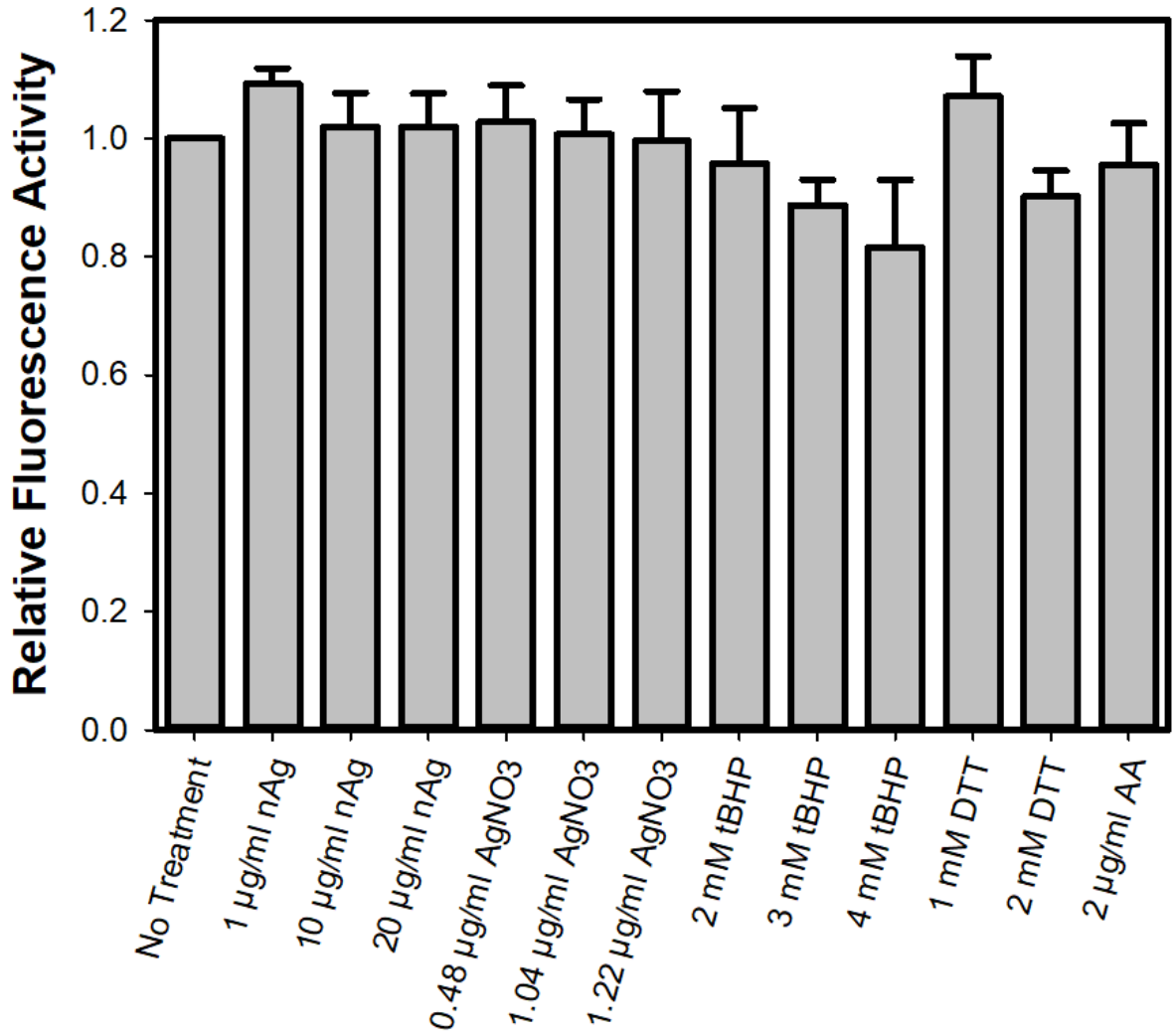

Figure 18. Determining the effect of 10 nm PVP coated nanosilver (nAg) on mitochondrial oxidative stress in HEK293T cells transfected with fluorescent Mito-roGFP. Cells were treated for 2 hours. Cells were treated with positive control antimycin A (AA) for 30 minutes. All treatments were made up in HEK293T media. No treatment was only media. Negative control dithiothreitol (DTT), and positive controls tert-butyl hydroperoxide (tBHP), and antimycin A (AA) were used. Standard error, one-way ANOVA, and the Dunnett's test were used. 3-9 replicates.

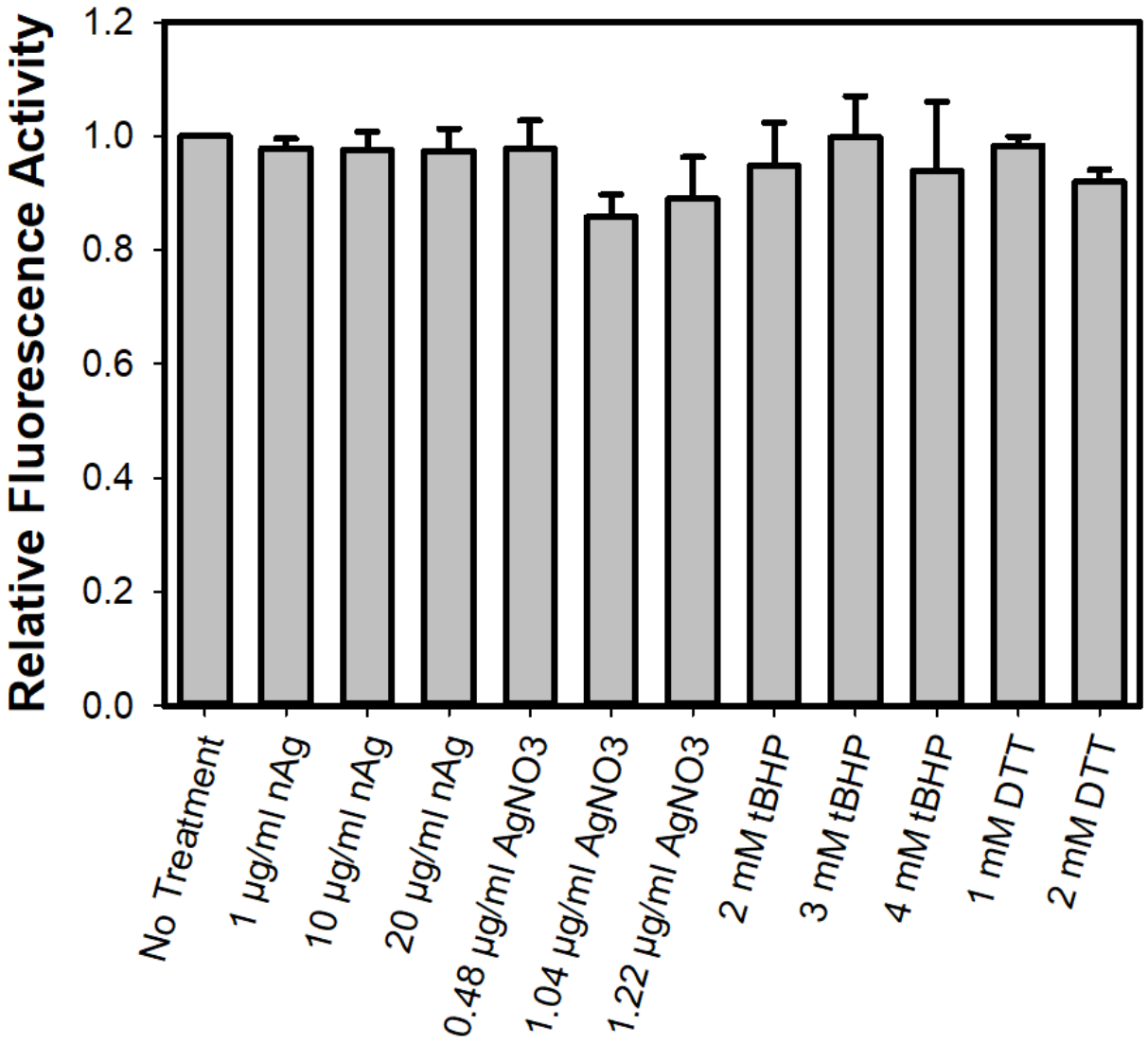

Figure 19. Determining the effect of 10 nm PVP coated nanosilver (nAg) on cellular oxidative stress in HEK293T cells transfected with fluorescent Cyto-roGFP. Cells were treated for 2 hours. All treatments were made up in HEK293T media. No treatment was only media. Negative control dithiothreitol (DTT), and positive control tert-butyl hydroperoxide (tBHP). Standard error, one-way ANOVA, and the Dunnett's test were used. 3-9 replicates.

3.3.2 CellROX

I found only the positive control 25 μM H_2O_2 treatment to be significantly increased cytoplasmic oxidative stress in the HCT116. A slight decrease in cytoplasmic oxidative stress was observed in the AgNP treatments and slight increase in cytoplasmic oxidative stress was observed in the $AgNO_3$ treatments (Figure 20).

I found that the AgNP treatment in HCT116 cells stained with CellROX after 24-hour treatment under normoxia induced slight increase of cytoplasmic oxidative stress. (Figure 21A). No change to cytoplasmic oxidative stress was observed for AgNP and $AgNO_3$ treatments under hypoxia and no significant differences were found in any treatments, including the 25 μM H_2O_2 control.

Treatments under hypoxia were conducted to mimic the hypoxic tumour microenvironment that cancer cells usually are in. Under hypoxia, attenuation of cytoplasmic oxidative stress was seen for all treatments including the positive control, relative to the normoxic treatments (Figure 21B).

AgNP did not induce changes in cytoplasmic oxidative stress in HIEC-6 for the 4 hour and 24 hour treatments under normoxia and hypoxia. The positive controls, 25 μM H_2O_2 and 50 μM H_2O_2 treatments were significantly different relative to the control (Figure 22A). Under hypoxia, slight attenuation of oxidative stress in the positive and negative controls was observed in the HIEC-6 cells Figure 22B.

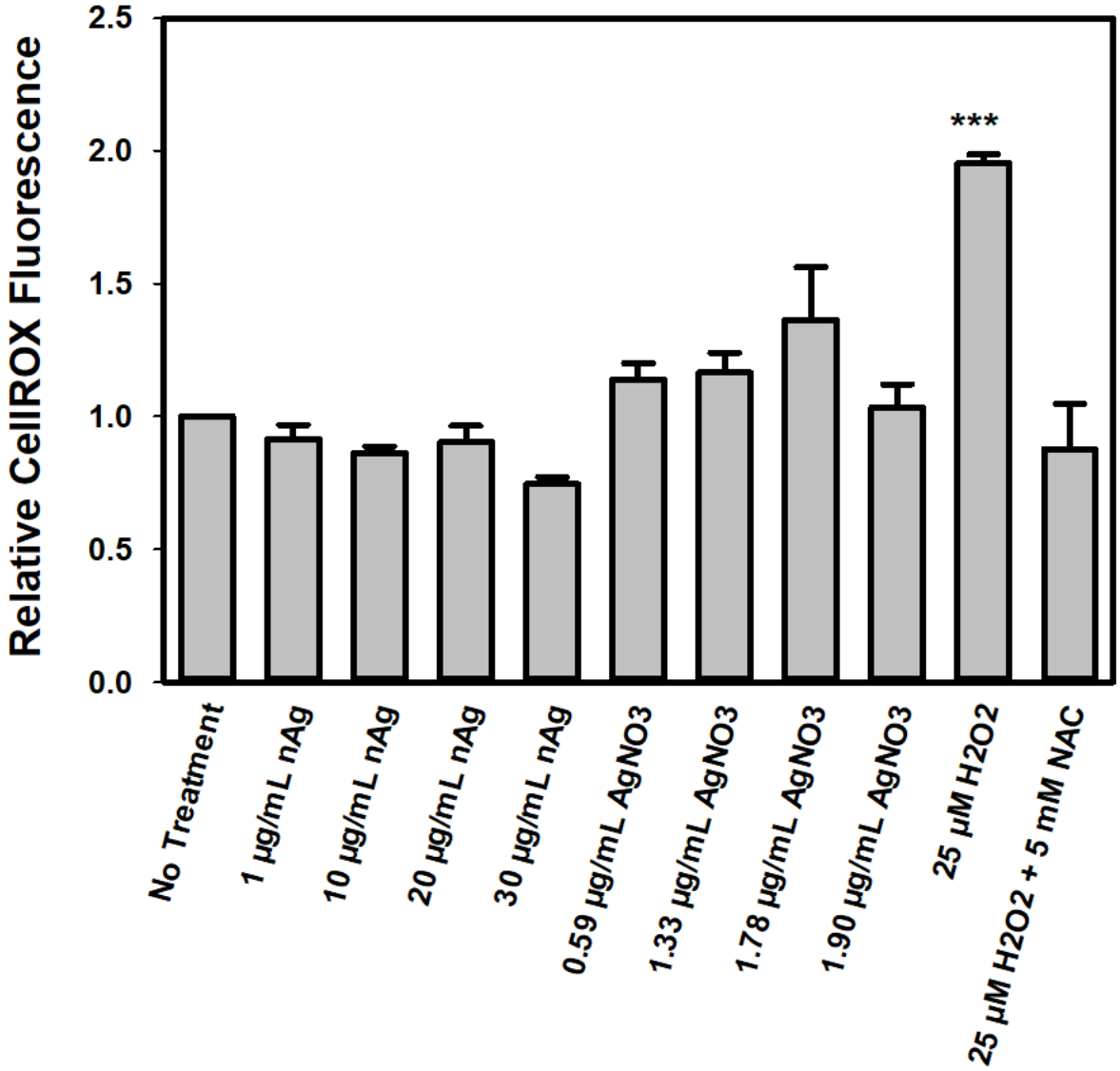

Figure 20. Determining the effect that 10 nm PVP coated nanosilver (nAg) has on cellular oxidative stress in HCT116 cells stained with CellROX. All treatments were made up in HCT116 media. No treatment was only media. Positive control H_2O_2 treatment was for 2 hours before harvest and negative control NAC was added 4 hours before treatment. HCT116 treated for 4 hours under normoxic conditions (21% O_2, 5% CO_2). Standard error, one-way ANOVA, and Dunnett's test were used (*$p<0.05$, **$p<0.01$, ***$p<0.001$). 3-5 replicates.

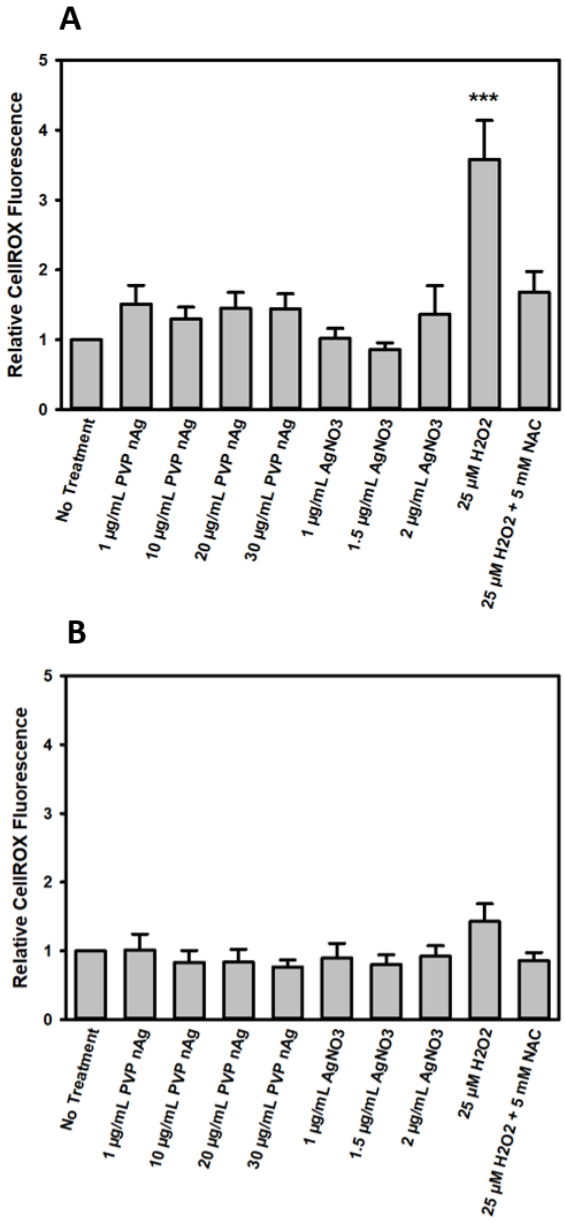

Figure 21. Determining the effect that 10 nm PVP coated nanosilver (nAg) has on cellular oxidative stress in HCT116 cells stained with CellROX. All treatments were made up in HCT116 media. No treatment was only media. Positive control H_2O_2 treatment was on for 2 hours before harvest and negative control NAC was added 4 hours before treatment. A) HCT116 treated for 24 hours under normoxia. 3-7 replicates. B) HCT116 cells treated for 24 hours under hypoxia. 3-4 replicates. Standard error, one-way ANOVA, and Dunnett's test were used (*$p<0.05$, **$p<0.01$, ***$p<0.001$).

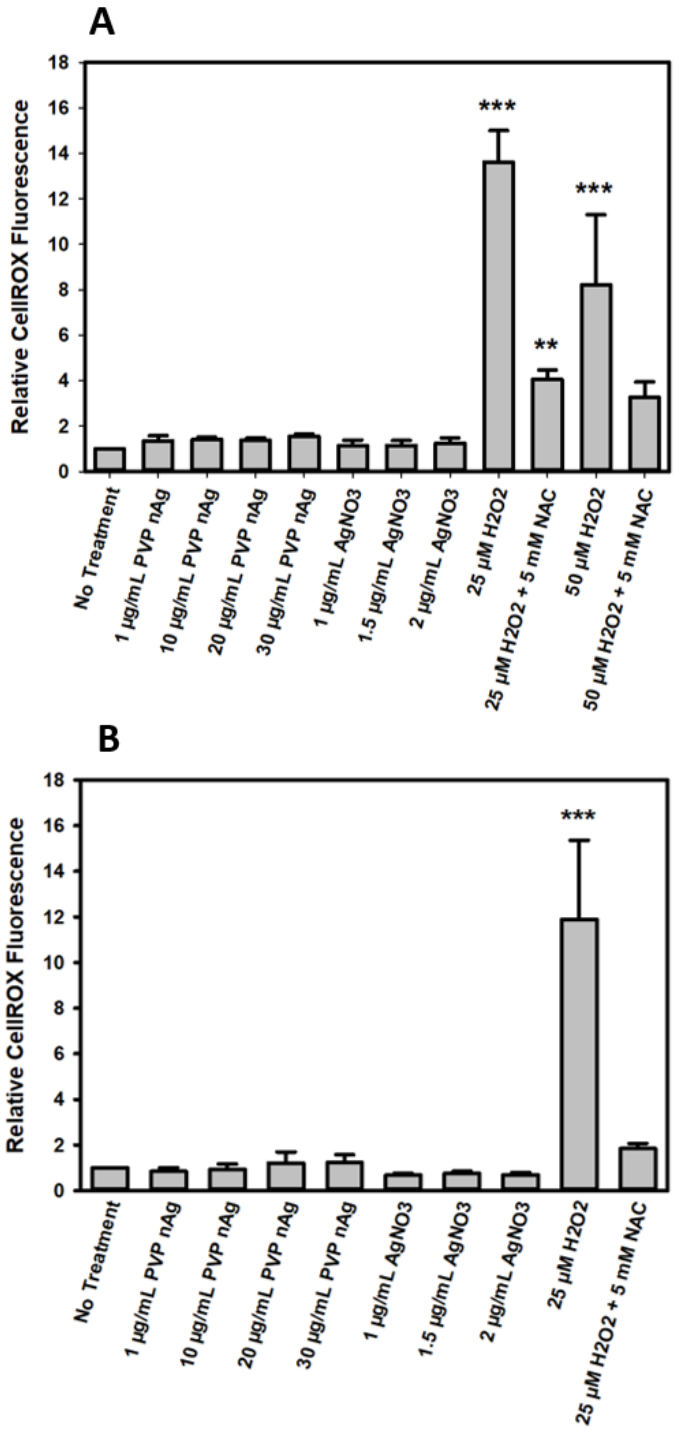

Figure 22. Determining the effect that 10 nm PVP coated nanosilver (nAg) has on cellular oxidative stress in HIEC-6 cells stained with CellROX. All treatments were made up in HIEC-6 media. No treatment was only media. Positive control H_2O_2 treatment was for 2 hours before harvest and negative control NAC was added 4 hours before treatment. A)

HIEC-6 cells were treated for 24 hours under normoxia conditions. 3-5 replicates. B) HIEC-6 cells were treated for 24 hours under hypoxia. 3 replicates. Standard error, one-way ANOVA, and Dunnett's test were used (*$p<0.05$, **$p<0.01$, ***$p<0.001$).

3.3.3 MitoSOX

HCT116 cells stained with MitoSOX after 4-hour treatment under normoxia showed variable increase and decrease in AgNP treatments and slight increase in $AgNO_3$ treatments. Only the positive control 15 µg/mL AA was significantly different (Figure 23).

HCT116 cells stained with MitoSOX after 24-hour treatment under normoxia showed a significant dose-dependent increase in the AgNP treated cells and the highest 2.0 µg/mL $AgNO_3$ treatment. Both 20 and 30 µg/mL AgNP was significantly different. The 10, 20, and 30 µg/mL AgNP had 1.3, 1.8, and 2.0-fold increases in fluorescence relative to the control, respectively. The 2.0 µg/mL $AgNO_3$ treatment had a 3.5-fold increase. The 15 µg/mL AA and 15 µg/mL AA with 5 mM NAC co-treatment were significantly different (Figure 24A). Under hypoxia, AgNPs had little to no effect relative to the control and only 2.0 µg/mL $AgNO_3$ and the 15 µg/mL AA with 5 mM NAC co-treatment were significantly different (Figure 24B).

HIEC-6 cells stained with MitoSOX after 4-hour treatment under normoxia showed the 30 µg/mL AgNPs induced a non-significant increase in mitochondrial oxidative stress relative to the control. No treatments were statistically significant (Figure 25).

HIEC-6 cells stained with MitoSOX after 24-hour treatment under normoxia showed a slight increase in fluorescence for the AgNPs treatments. $AgNO_3$ had a slight dose-dependent increase in fluorescence. The 5 and 15 µg/mL AA treatments were significantly different (Figure 26A). Under h ypoxia, variable results with AgNPs were observed: 1, 10, and 30 µg/mL AgNP saw an increase while 20 µg/mL AgNP had no change. AA treatments induced increase in fluorescence. No treatments were significantly different (Figure 26B).

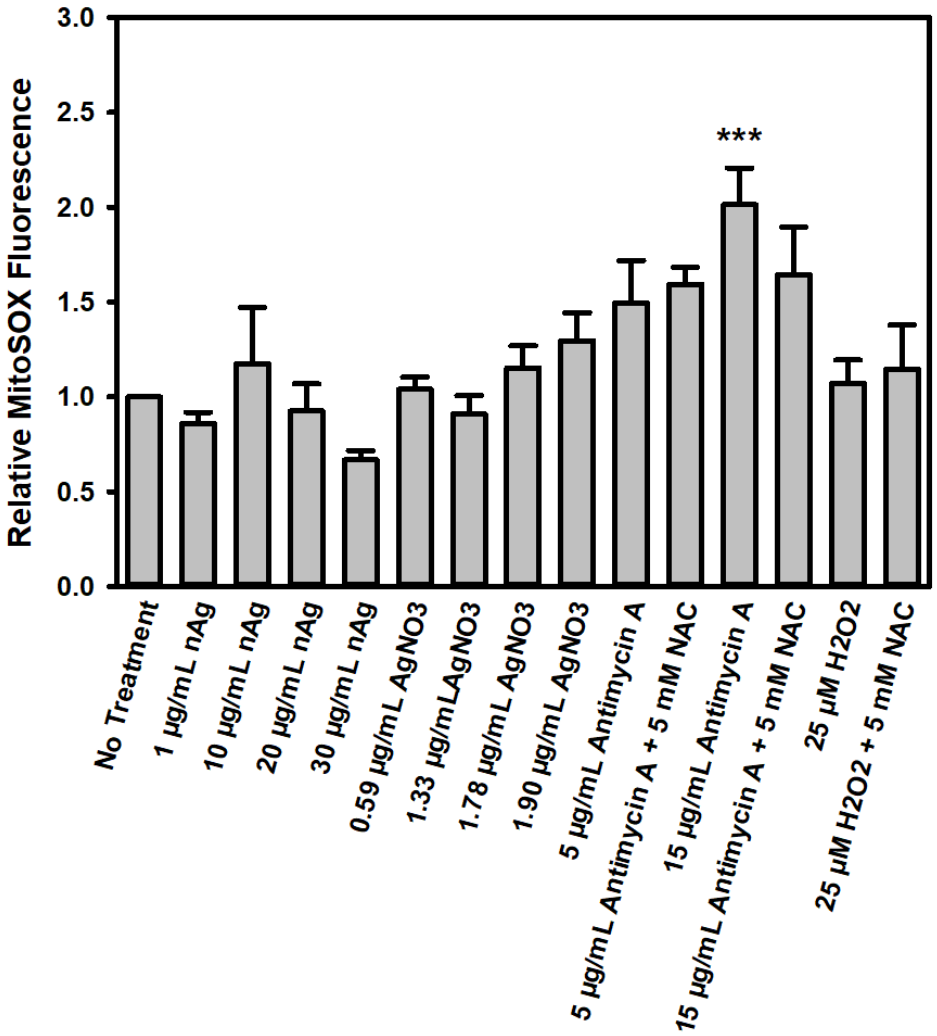

Figure 23. Determining the effect that 10 nm PVP coated nanosilver (nAg) has on mitochondrial oxidative stress in HCT116 cells stained with MitoSOX. All treatments were made up in HCT116 media. No treatment was only media. Positive control H_2O_2 treatment was for 2 hours before harvest and negative control NAC was added 4 hours before AA treatment. Cells were treated with AA 30 minutes before harvest and NAC was treated 2 hours before AA treatment. HCT116 cells were treated for 4 hours under normoxic conditions (21% O_2, 5% CO_2). No treatments showed significant cellular oxidative stress. Standard error, one-way ANOVA, and Dunnett's test were used (*$p<0.05$, **$p<0.01$, ***$p<0.001$). 3 replicates.

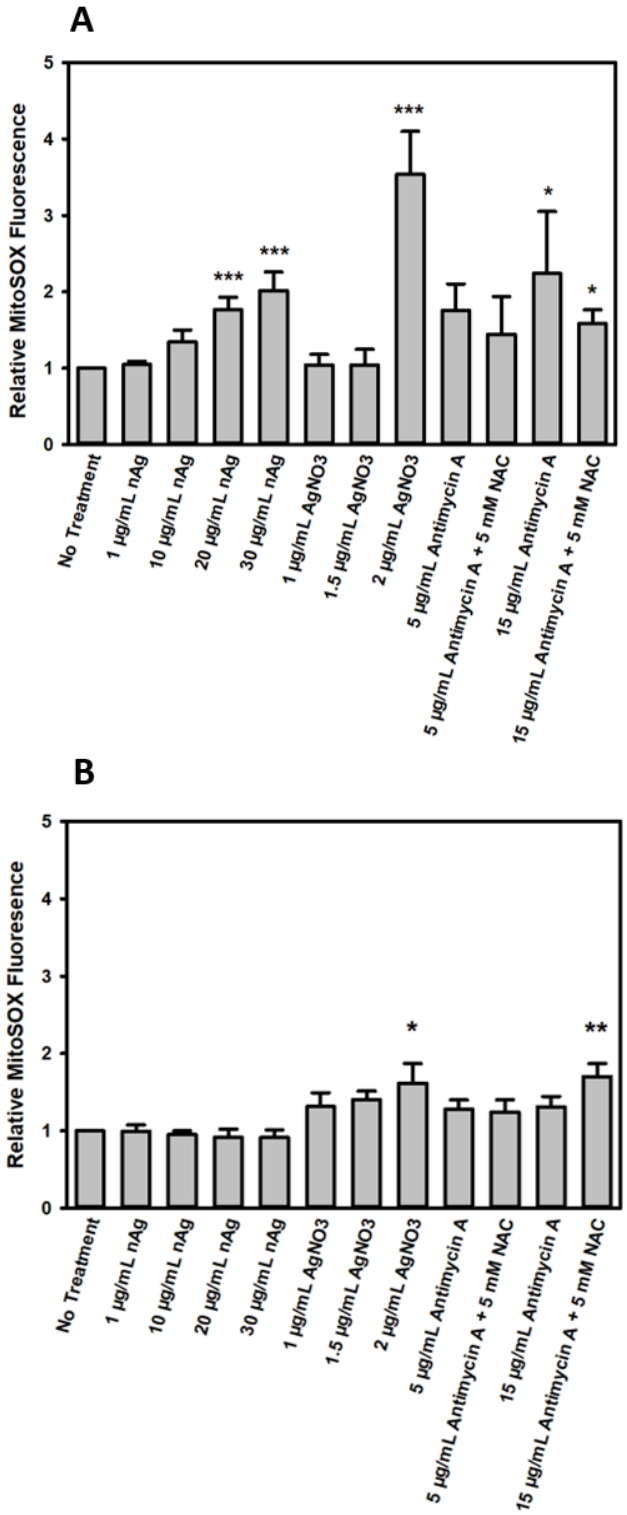

Figure 24. Determining the effect that 10 nm PVP coated nanosilver (nAg) has on mitochondrial oxidative stress in HCT116 cells stained with MitoSOX. All treatments were made up in HCT116 media. No treatment was only media. Positive control H_2O_2 treatment

was for 2 hours before harvest and negative control NAC was added 4 hours before AA treatment. A) HCT116 cells were treated for 24 hours under normoxia. 3-7 replicates. B) HCT116 cells were treated for 24 hours under hypoxia. 6 replicates. Standard error, one-way ANOVA, and Dunnett's test were used (*$p<0.05$, **$p<0.01$, ***$p<0.001$).

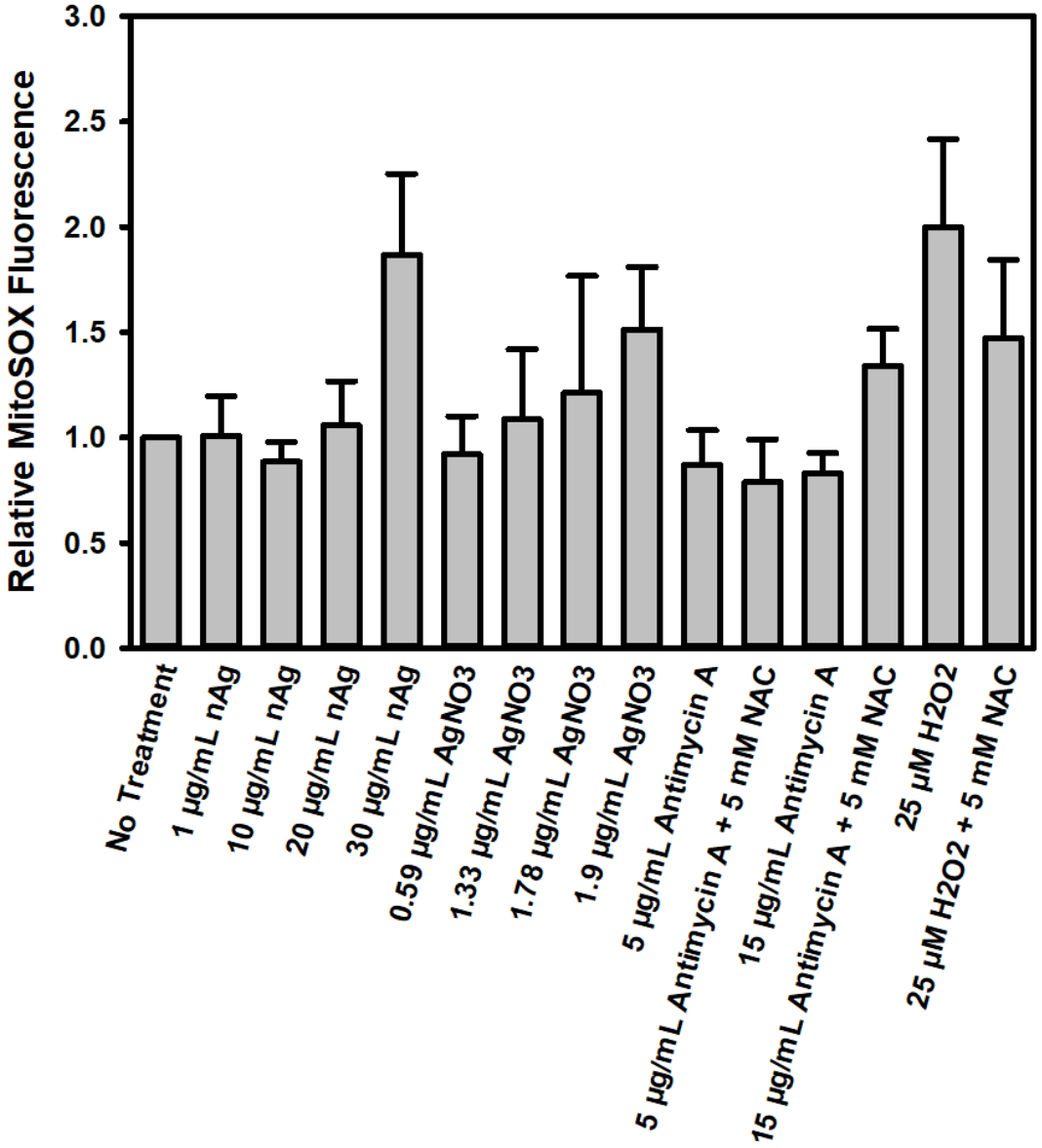

Figure 25. Determining the effect that 10 nm PVP coated nanosilver (nAg) has on mitochondrial oxidative stress in HIEC-6 cells stained with MitoSOX. All treatments were made up in HIEC-6 media. No treatment was only media. Positive control H_2O_2 treatment was for 2 hours before harvest and negative control NAC was added 4 hours before positive control AA treatment. AA was added 30 minutes before harvest. HIEC-6 cells were treated for 4 hours under normoxia. Standard error, one-way ANOVA, and Dunnett's test were used. 3 replicates.

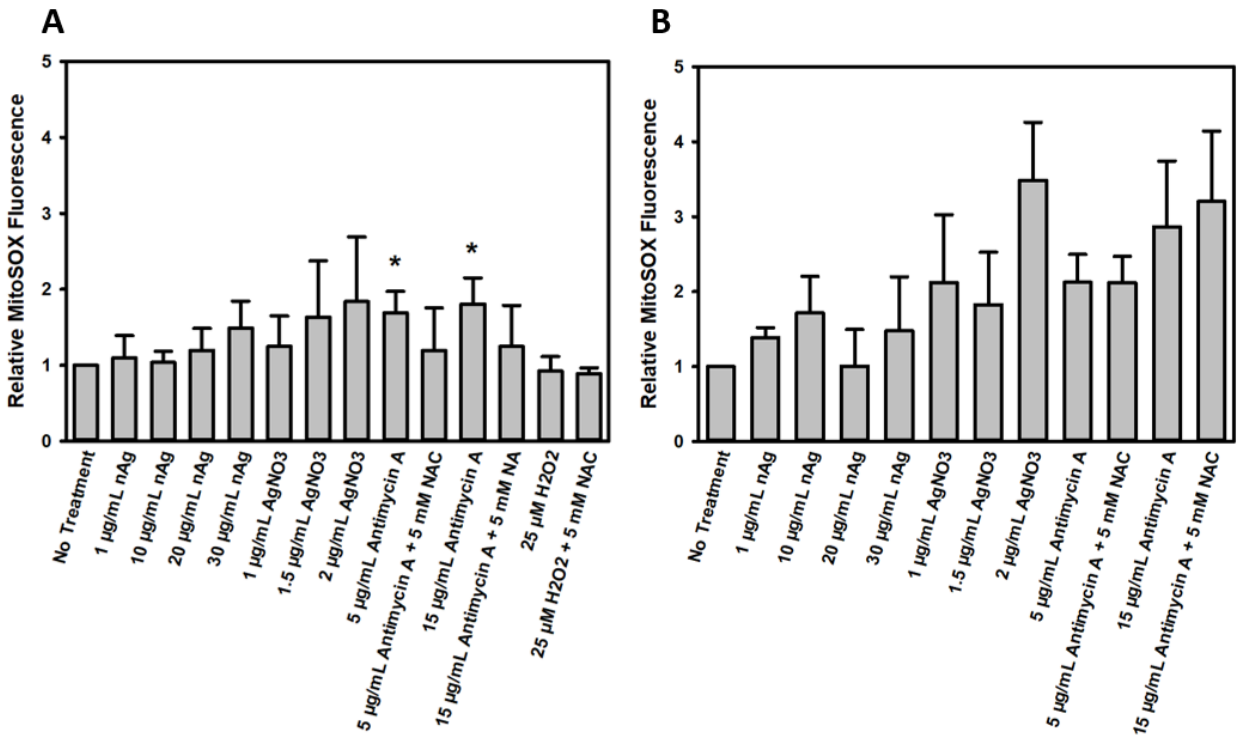

Figure 26. Determining the effect that 10 nm PVP coated nanosilver (nAg) has on mitochondrial oxidative stress in HIEC-6 cells stained with MitoSOX. All treatments were made up in HIEC-6 media. No treatment was only media. Positive control H_2O_2 treatment was for 2 hours before harvest and negative control NAC was added 4 hours before positive control AA treatment. AA was added 30 minutes before harvest. A) HIEC-6 cells were treated for 24 hours under normoxia. 4-5 replicates. B) HIEC-6 cells were treated for 24 hours under hypoxia. 4-5 replicates. Standard error, one-way ANOVA, and Dunnett's test were used (*$p<0.05$, **$p<0.01$, ***$p<0.001$).

3.3.4 Nrf1 and Nrf2 Expression

Treatment time for all Western blots were for 4 hours based on the time course experiment done with Nrf2 expression (Figure A15). The 4-hour treatment yielded the highest protein expression out of times tested (0.5 – 24 hour).

Western blotting for Nrf1 protein expression for 4-hour treatments in HCT116 showed that AgNPs induced a non-significant increase of Nrf1 expression. All other treatments induced a slight non-significant increase in Nrf1 expression relative to the control. No changes were significant (Figure 27).

Using qPCR, gene expression of Nrf1 for 4-hour treatments in HCT116 showed no significant changes in gene expression. All treatments decreased Nrf1 gene expression relative to the no treat control. The AgNP treatments decreased gene expression more than the $AgNO_3$ treatments (Figure 28).

Western blotting for Nrf2 protein expression for 4-hour treatments in HCT116 showed a significant dose-dependent increase in Nrf2 expression after AgNP treatment up to 3.5-fold in the nuclear fraction. Nuclear Nrf2 expression after $AgNO_3$ treatments were relatively constant. The positive controls, TBHQ and SFN treatments also induced significant increase in Nrf2 expression in the nuclear fraction. Other treatments also increased expression of nuclear Nrf2. No significant changes in Nrf2 expression occurred in the cytosolic fraction (Figure 29).

Using qPCR, no significant changes in Nrf2 gene expression were found. The AgNP, $AgNO_3$, hypoxia, SA, and SA with AgNP treatments induced slight increase in gene expression relative to the no treatment control (Figure 30).

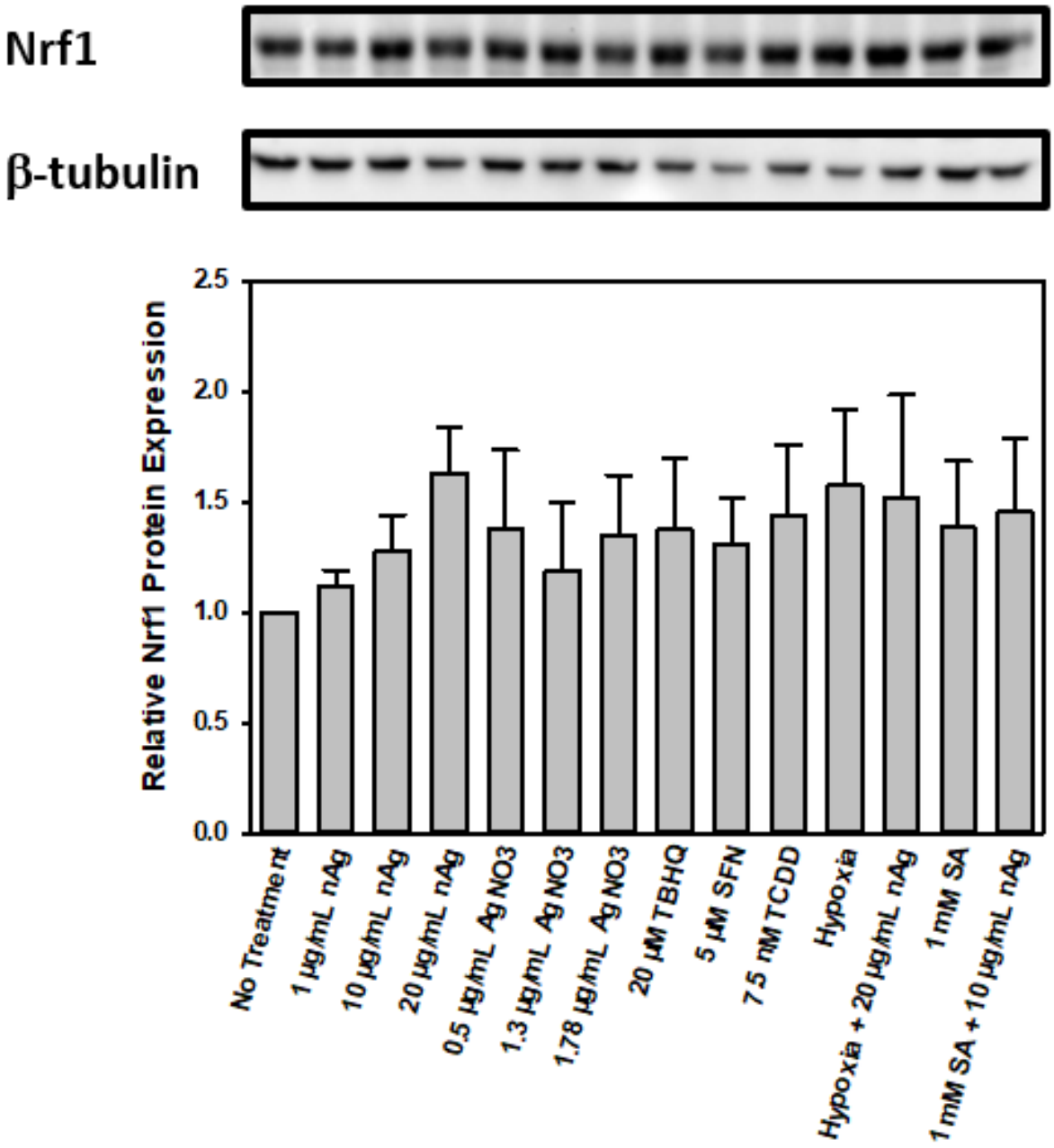

Figure 27. Western blots for Nrf1 protein expression in using urea extraction from HCT116 cells treated for 4 hours. Protein expression of each sample was normalized to β-tubulin. Nrf1 band at 95 kDa. Standard error, one-way ANOVA, and the Dunnett's test were used. 3 replicates.

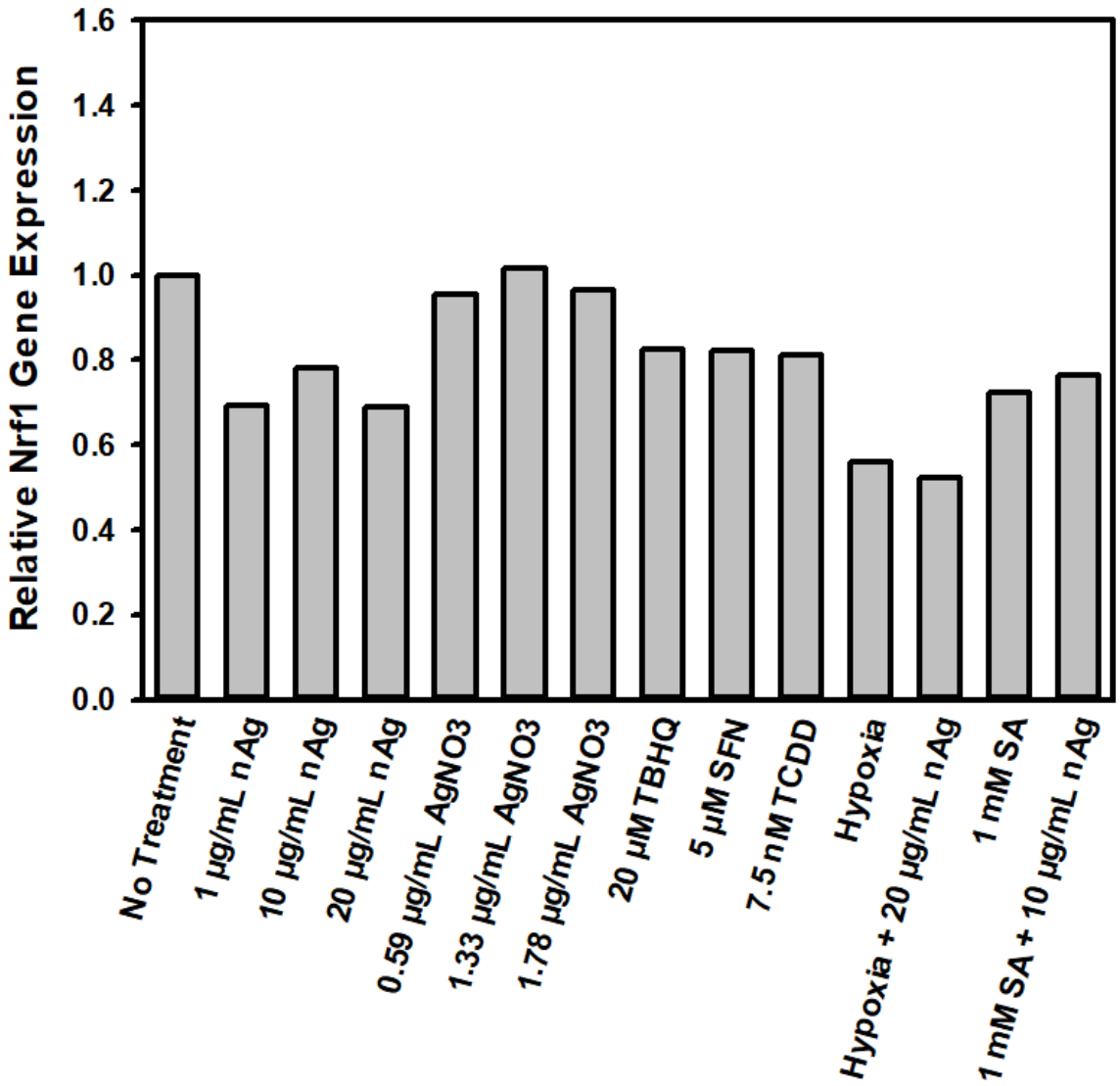

Figure 28. Using qPCR to determine Nrf1 gene expression in HCT116 cells treated for 4 hours. One-way ANOVA, and the Dunnett's test were used. 2 replicates.

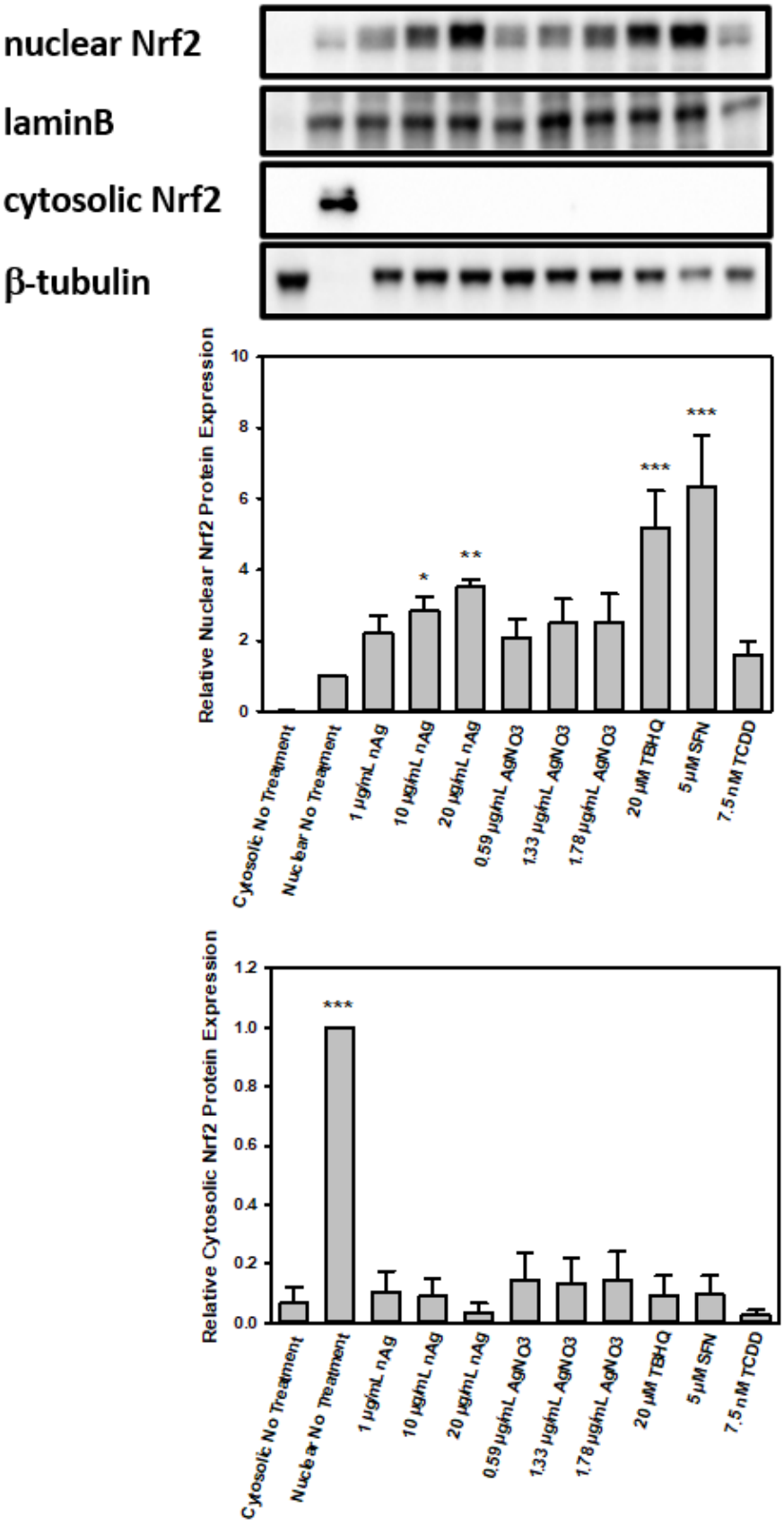
nuclear Nrf2
laminB
cytosolic Nrf2
β-tubulin
Relative Nuclear Nrf2 Protein Expression
Relative Cytosolic Nrf2 Protein Expression
Cytosolic No Treatment
Nuclear No Treatment
1 µg/mL nAg
10 µg/mL nAg
20 µg/mL nAg
0.59 µg/mL AgNO3
1.33 µg/mL AgNO3
1.78 µg/mL AgNO3
20 µM TBHQ
5 µM SFN
7.5 nM TCDD

Figure 29. Western blotting for Nrf2 protein expression in nuclear and cytosolic fractions from HCT116 cells treated for 4 hours. Protein expression of each sample was normalized to β-tubulin. Nrf2 band at 100 kDa. Standard error, one-way ANOVA, and the Dunnett's test (*$p<0.05$, **$p<0.01$, ***$p<0.001$). 3-7 replicates.

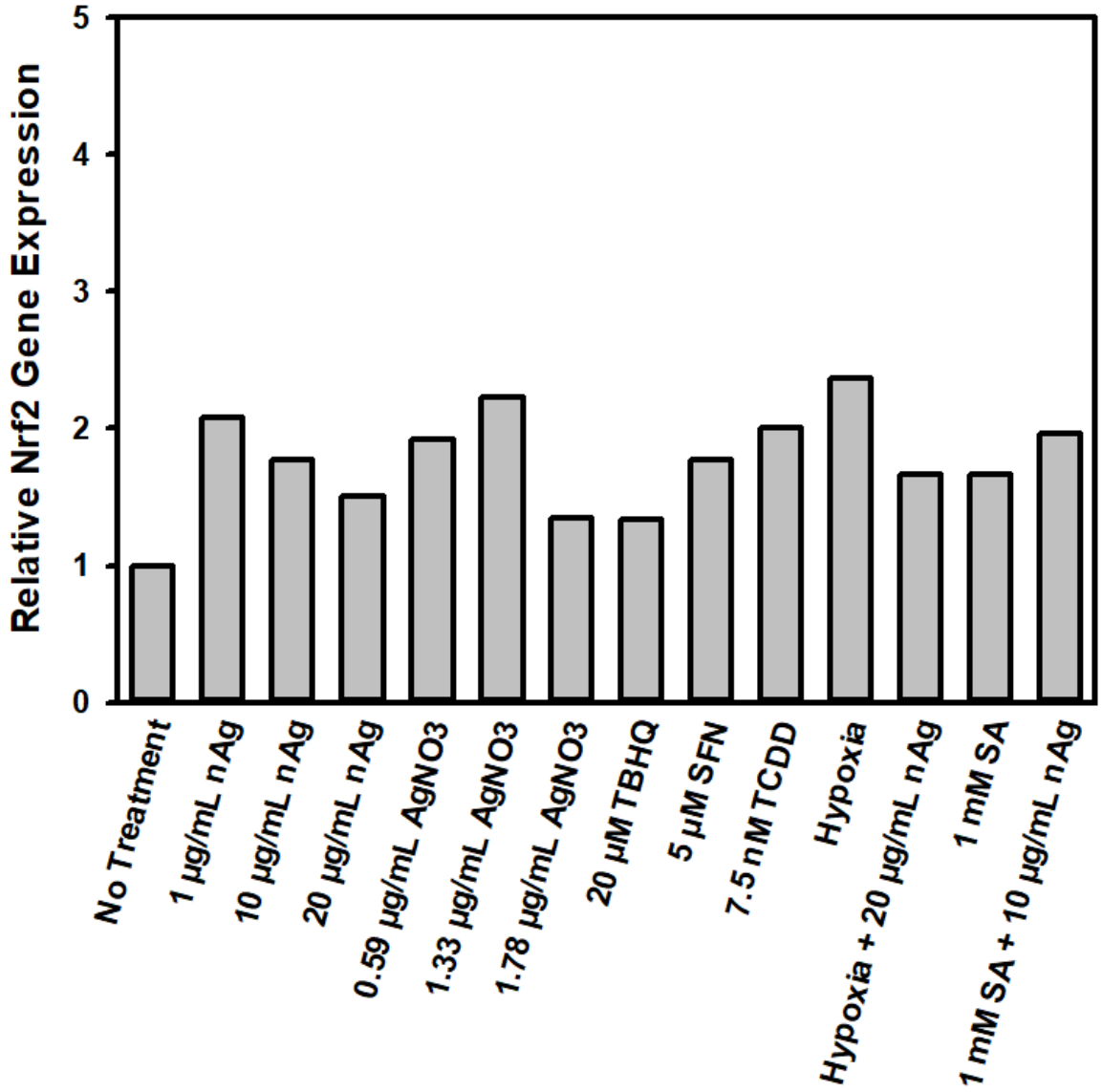

Figure 30. Using qPCR to determine Nrf2 gene expression in HCT116 cells treated for 4 hours. One-way ANOVA, and the Dunnett's test were used. 2 replicates.

3.4 Nanosilver and the Endoplasmic Reticulum Stress Response

3.4.1 HCT116-XBP1

A time course experiment was conducted to determine optimal treatment time to determine the effects on the ER stress response in HCT116-XBP1 cells (Figure 31). HCT116-XBP1 cells were treated with ER stress inducers, 200 nM thapsigargin, 10 µg/mL tunicamycin, and 3 mM DTT for 2, 4, 16, and 24 hours. The 24 hour of 200 nM thapsigargin treatment induced a significant and the greatest amount of fluorescence, with a 12.9-fold change relative to the control (Figure 31).

HCT116-XBP1 cells were treated at different AgNP and $AgNO_3$ concentrations, and 200 nM thapsigargin for 24 hours under both normoxic (21% oxygen) and hypoxic (1% oxygen) conditions. Under both hypoxic and normoxic conditions, only 1.5 and 2.0 µg/mL $AgNO_3$, and the positive control 200 nM thapsigargin treatments significantly increased XBP1 splicing. HCT116-XBP1 cells treated for 24 hours under hypoxic conditions did not result in significant *XBP1* splicing in AgNP treated cells, however, the 1.5 µg/mL and 2 µg/mL $AgNO_3$ and positive control 200 nM thapsigargin treatments showed significant *XBP1* splicing. Attenuation of ER stress was seen under hypoxia for every treatment relative to the normoxic treatments (Figure 32).

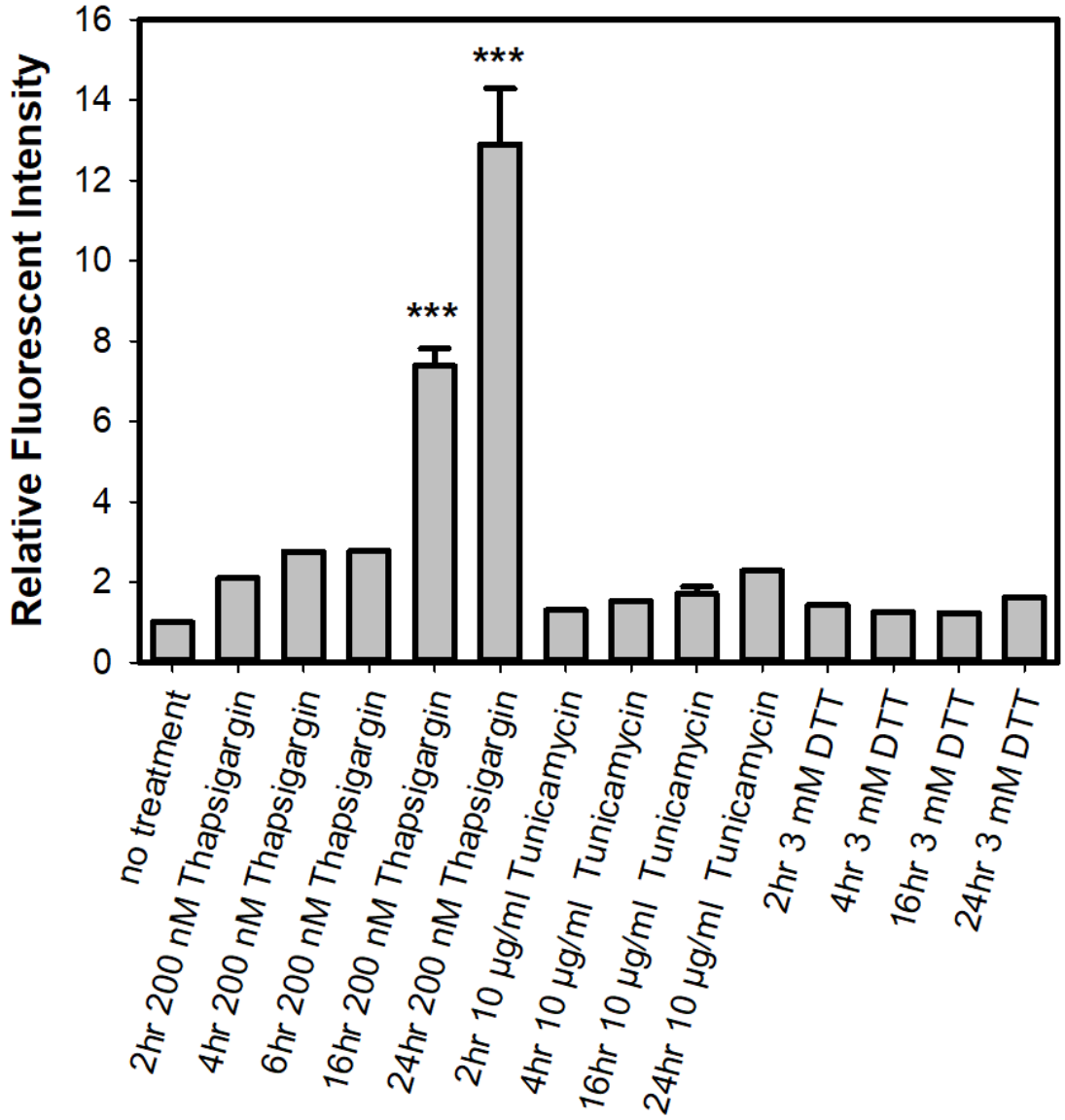

Figure 31. Time course treatment for effects of known ER stress inducers, thapsigargin, tunicamycin, and dithiothreitol (DTT) treatments in HCT-XBP1 cells for *XBP1* splicing. All treatments were made up in HCT116 media. No treatment was only media. 1-8 replicates. Standard error, one-way ANOVA, and the Dunnett's test (*p<0.05, **p<0.01, ***p<0.001) were used.

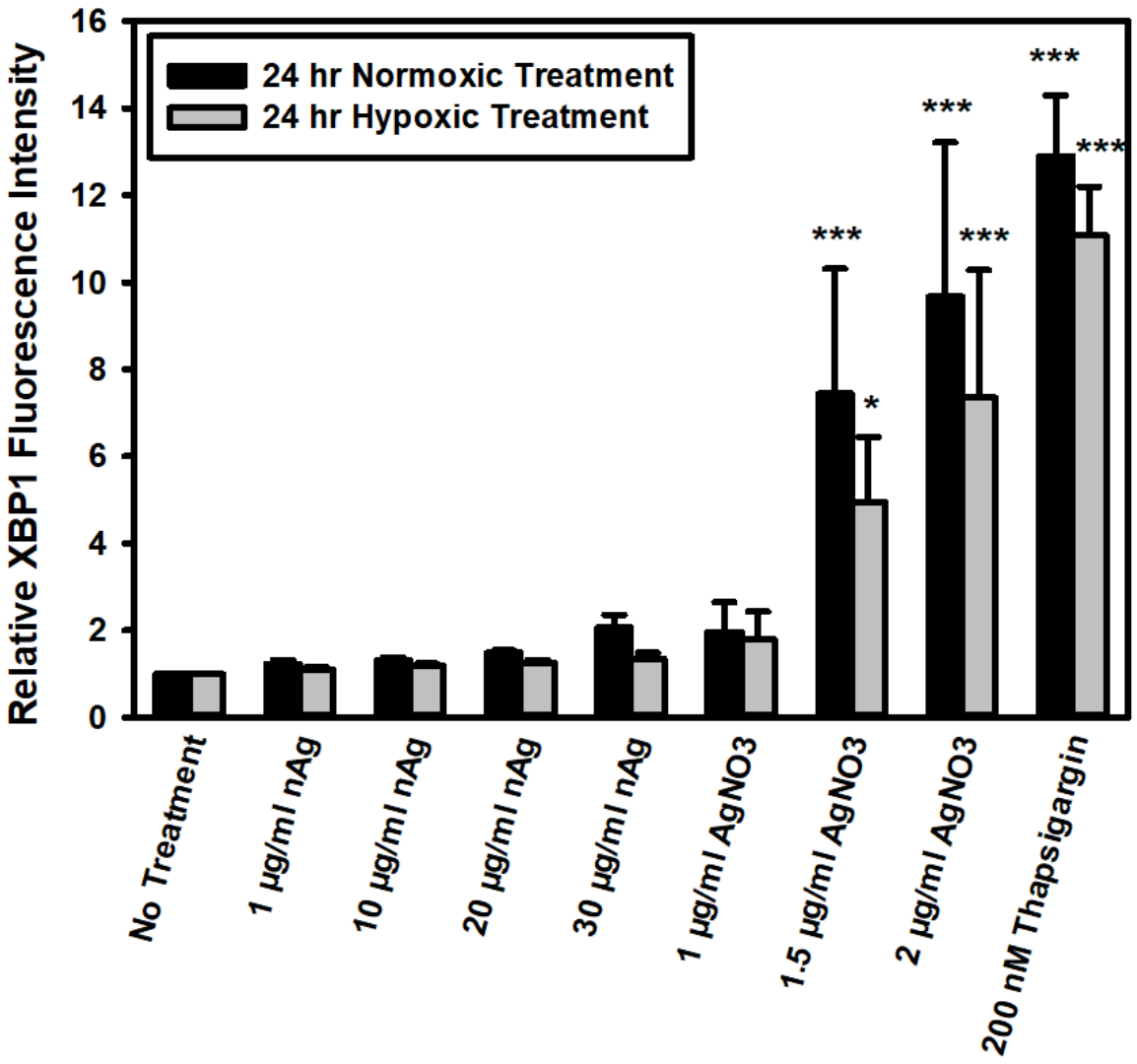

Figure 32. Determining the effect 10 nm PVP coated nanosilver (nAg) has on *XBP1* splicing in HCT116-XBP1 cells. All treatments were made up in HCT116 media. No treatment was only media. 4-12 replicates. 4-8 replicates. Standard error, one-way ANOVA, and the Dunnett's test (*p<0.05, **p<0.01, ***p<0.001) were used.

3.4.2 HCT116-ATF4

A time course experiment was conducted to determine optimal treatment time to determine the effects on the ER stress response in HCT116-ATF4 cells. HCT116-ATF4 cells were also treated with 200 nM thapsigargin, 10 μg/mL tunicamycin, and 3 mM DTT for 2, 4, 16, and 24 hours. The 24 hours of 200 nM thapsigargin treatment induced a significant and the greatest amount of fluorescence, with a 3.0-fold change relative to the control, just media with no treatment sample (Figure 33).

For the HCT116-ATF4, under both hypoxic and normoxic conditions, only 2.0 μg/mL $AgNO_3$, and 200 nM thapsigargin were statistically different ATF4 translation relative to the no treatment control. Attenuation of ER stress was seen under hypoxia for every treatment relative to the normoxic treatments (Figure 34).

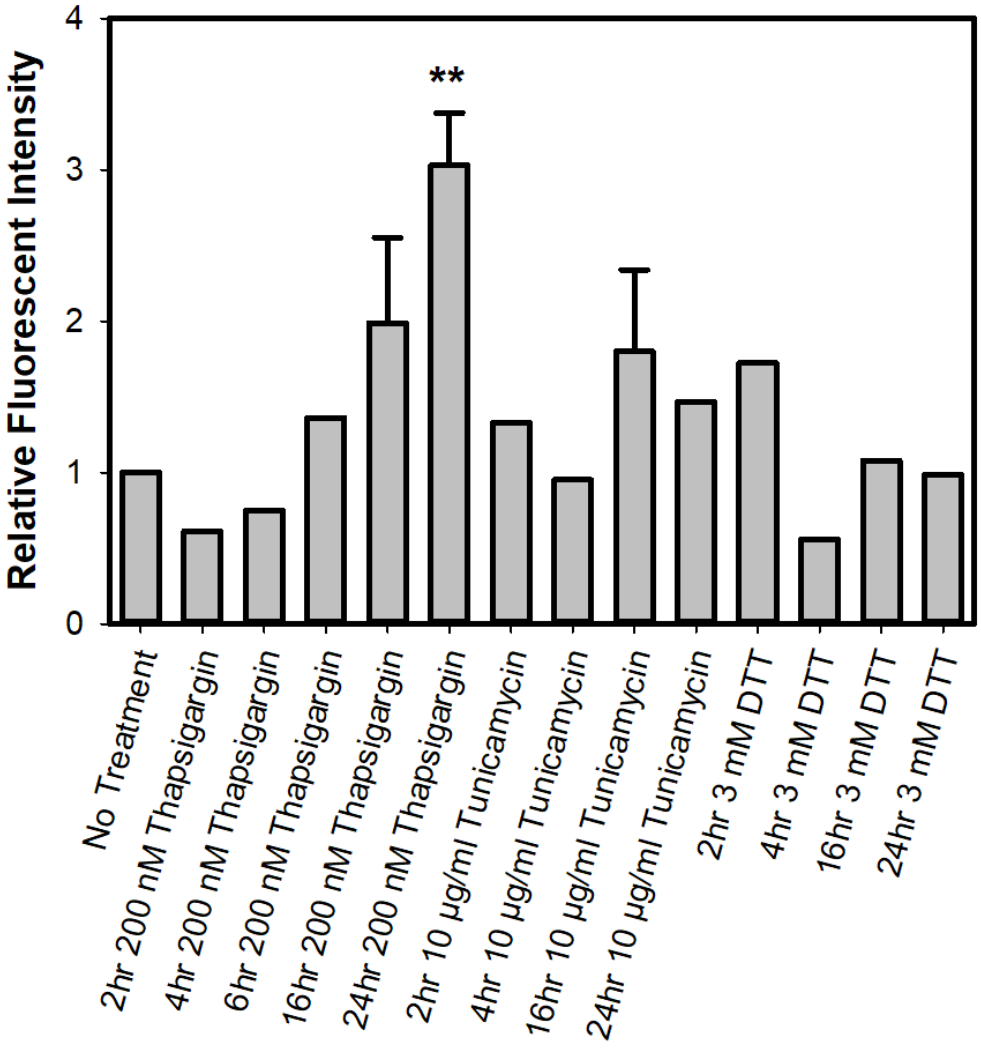

Figure 33. Time course treatment for effects of known ER stressors, thapsigargin, tunicamycin, and dithiothreitol (DTT) treatments in HCT-ATF4 cells for ATF4 translation. All treatments were made up in HCT116 media. No treatment was only media. 1-9 replicates. Standard error, one-way ANOVA, and Dunnett's test were used (*$p<0.05$, **$p<0.01$, ***$p<0.001$).

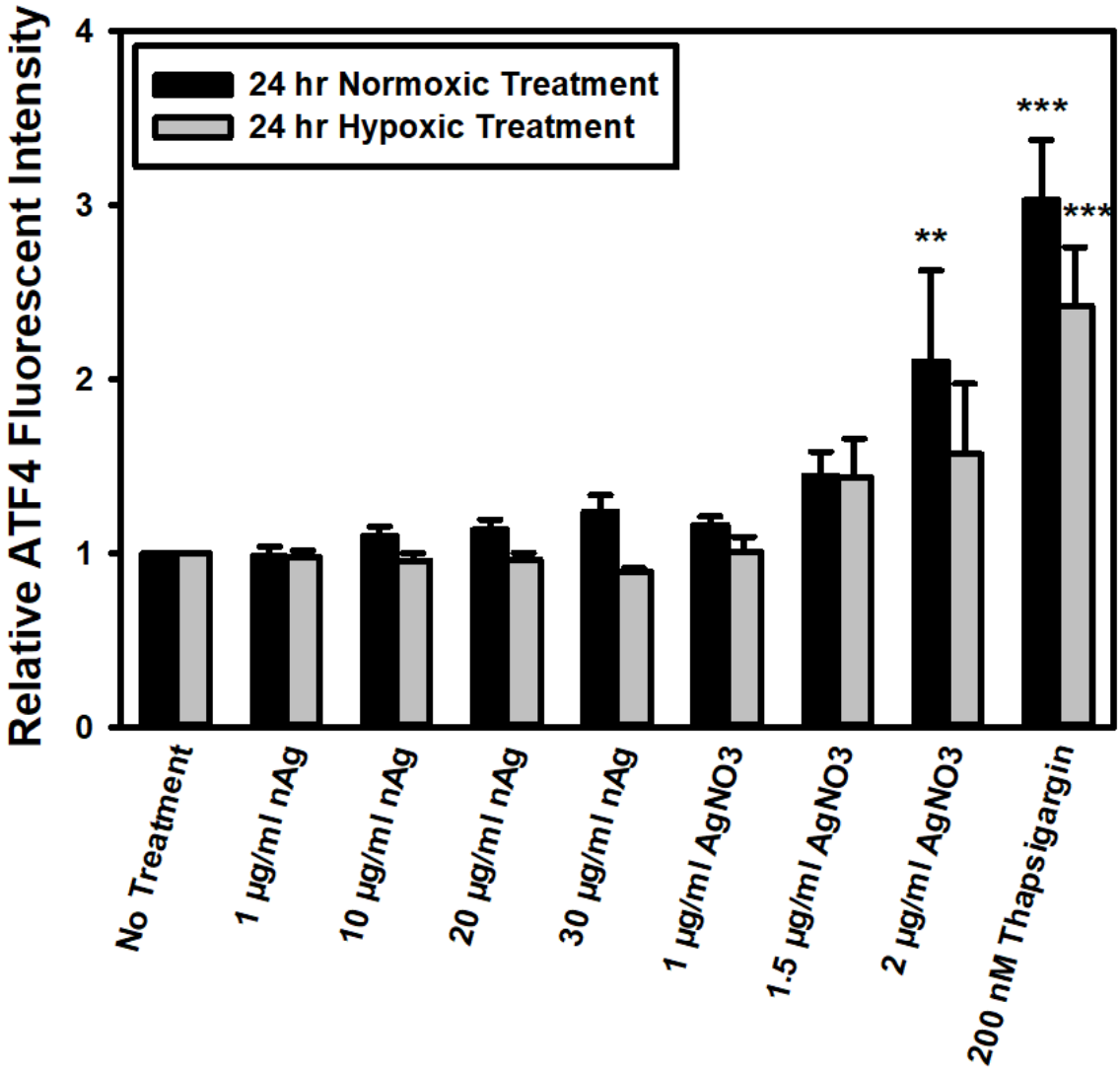

Figure 34. Determining the effect 10 nm PVP coated nanosilver (nAg) has on ATF4 translation in HCT116-ATF4 cells. All treatments were made up in HCT116 media. No treatment was only media. Normoxic treatments had 4-11 replicates. Thapsigargin was used as a positive control. Hypoxia treatments had 5-6 replicates. Standard error, one-way ANOVA, and Dunnett's test were used (*$p<0.05$, **$p<0.01$, ***$p<0.001$).

3.5 Nanosilver and the Cell Cycle

Using BrdU staining, the effects of nanosilver on HCT116 cells was determined with 24-hours of treatments. No significant changes to the S phase were observed in any of the treatments. The AgNP treatments resulted in a lower proportion of cells in the G1 phase and an increased proportion of cells in the G2/M phase of the cell cycle. No significant changes were induced by $AgNO_3$ treatment. A slight additive effect was seen with the SA co-treatment (Figure 35). There was no significant difference between 1 mM SA with 1 mM SA + 10 µg/mL AgNP and 1mM SA + 20 µg/mL AgNP using the Tukey's test.

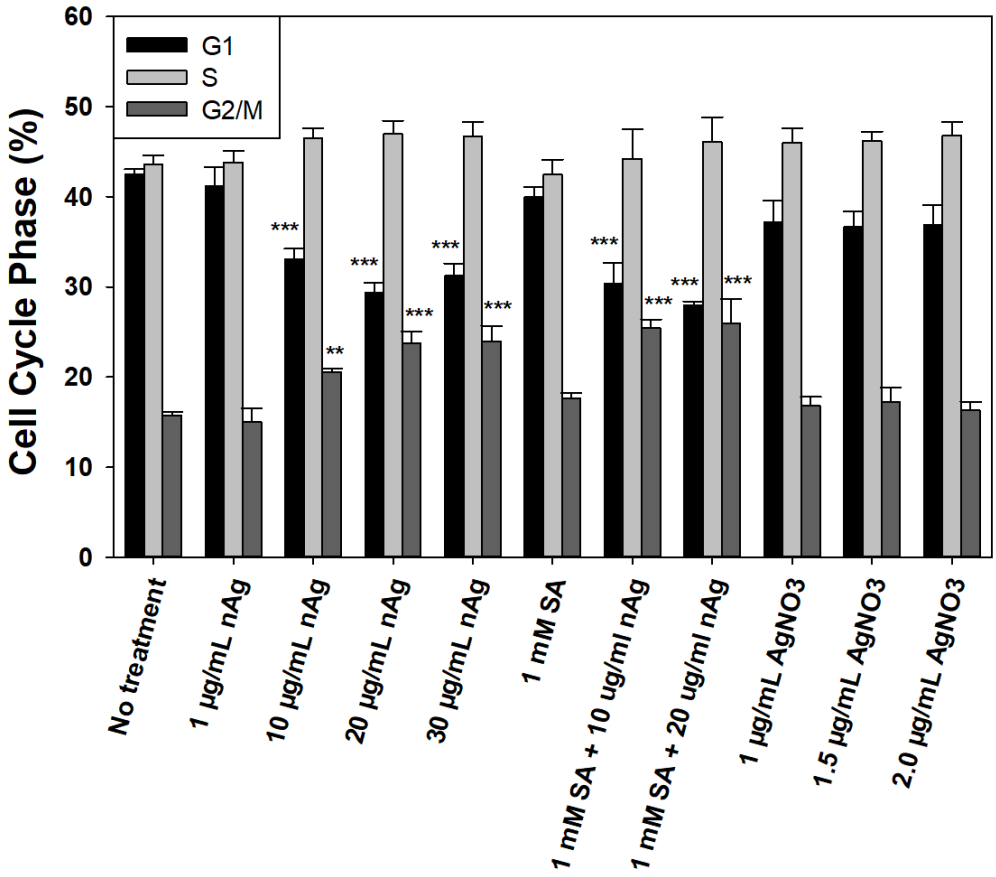

Figure 35. Determining the effect 10 nm PVP coated nanosilver (nAg) and sodium ascorbate (SA) co-treatment has on the cell cycle in HCT116 cells using BrdU staining. Cells were treated for 24 hours and stained with BrdU for 1 hour. All treatments were made up in HCT116 media. No treatment was only media. 7 replicates. Standard error, one-way ANOVA, and Dunnett's test were used (*$p<0.05$, **$p<0.01$, ***$p<0.001$). Tukey's test was used to compare 1 mM SA with 1 mM SA + 10 µg/mL nAg and 1mM SA + 20 µg/mL nAg.

3.6 Nanosilver and the Hypoxic Stress Response

3.6.1 HIF1-α Expression

Western blotting for HIF1-α protein expression for 4 hours of treatments in HCT116 showed 20 µg/mL AgNP and 1.32 µg/mL $AgNO_3$ induced a significant increase in HIF1-α expression. Positive control, hypoxia treatment and hypoxia with 20 µg/mL AgNP also significantly increased HIF1-α expression. Other treatments also increased expression of HIF1-α, except SA with AgNP co-treatment which slightly decreased HIF-1α expression relative to the 10 µg/mL AgNP treatment and SA treatment (Figure 28).

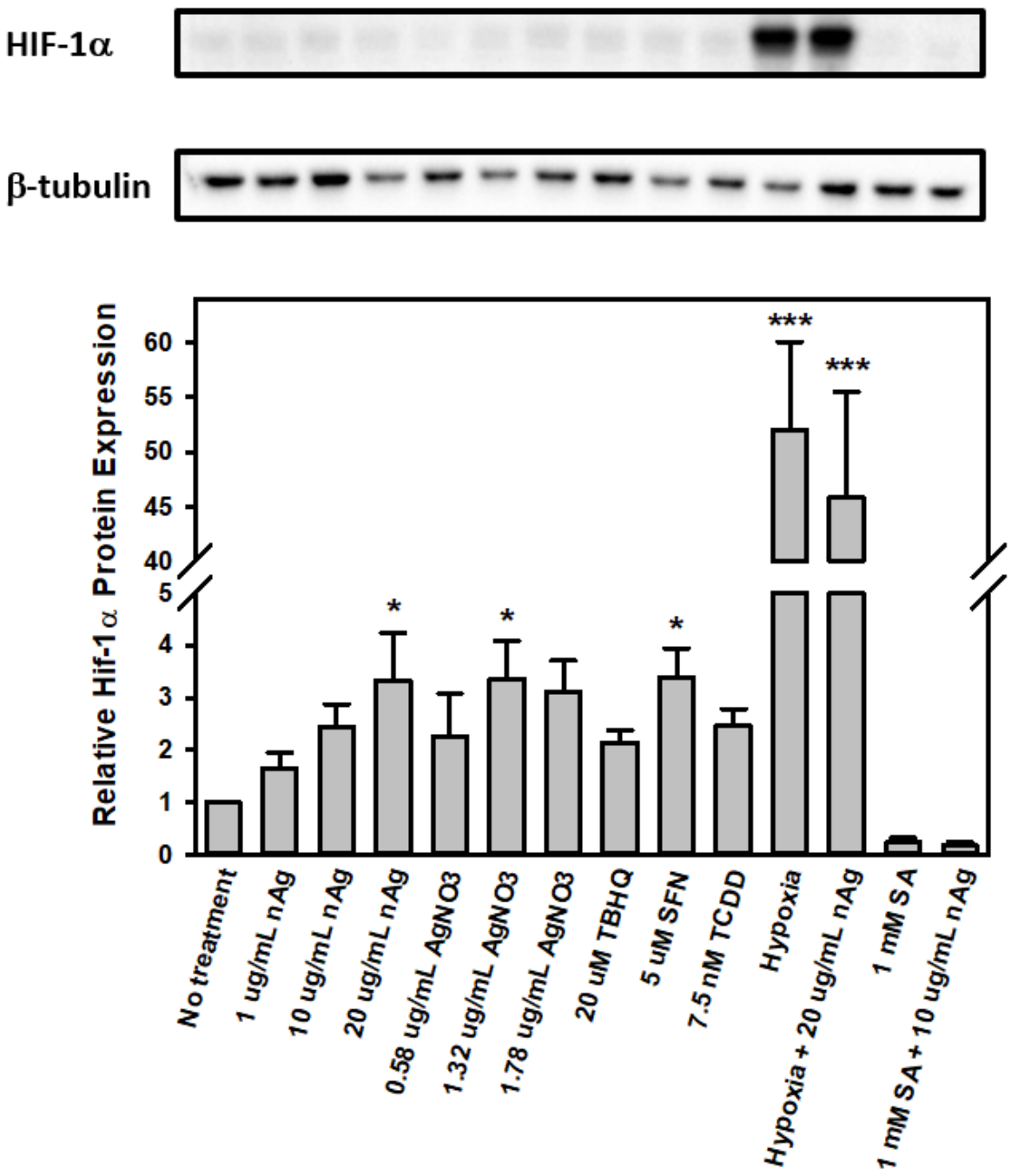

Figure 36. Western blotting for HIF1-α total protein expression through urea extraction from HCT116 cells treated for 4 hours. HIF1-α band at 120 kDa. Protein expression of each sample was normalized to β-tubulin. Standard error, one-way ANOVA, and the Dunnett's test (*p<0.05, **p<0.01, ***p<0.001). 3-4 replicates.

3.7 Nanosilver and Wnt Signaling

3.7.1 Wntless

Western blotting for Wntless protein expression for 4-hour treatments in HCT116 showed AgNP and $AgNO_3$ treatments induced an non-significant increase in Wntless expression. SA with 10 µg/mL AgNP had less expression of Wntless relative to the 10 µg/mL AgNP treatment. All other treatments, except 1 mM SA + 10 µg/mL AgNP also slightly increased Wntless expression. No changes were significant (Figure 37).

Using qPCR, Wntless gene expression did not significantly change in HCT116 treated for 4 hours (Figure 38).

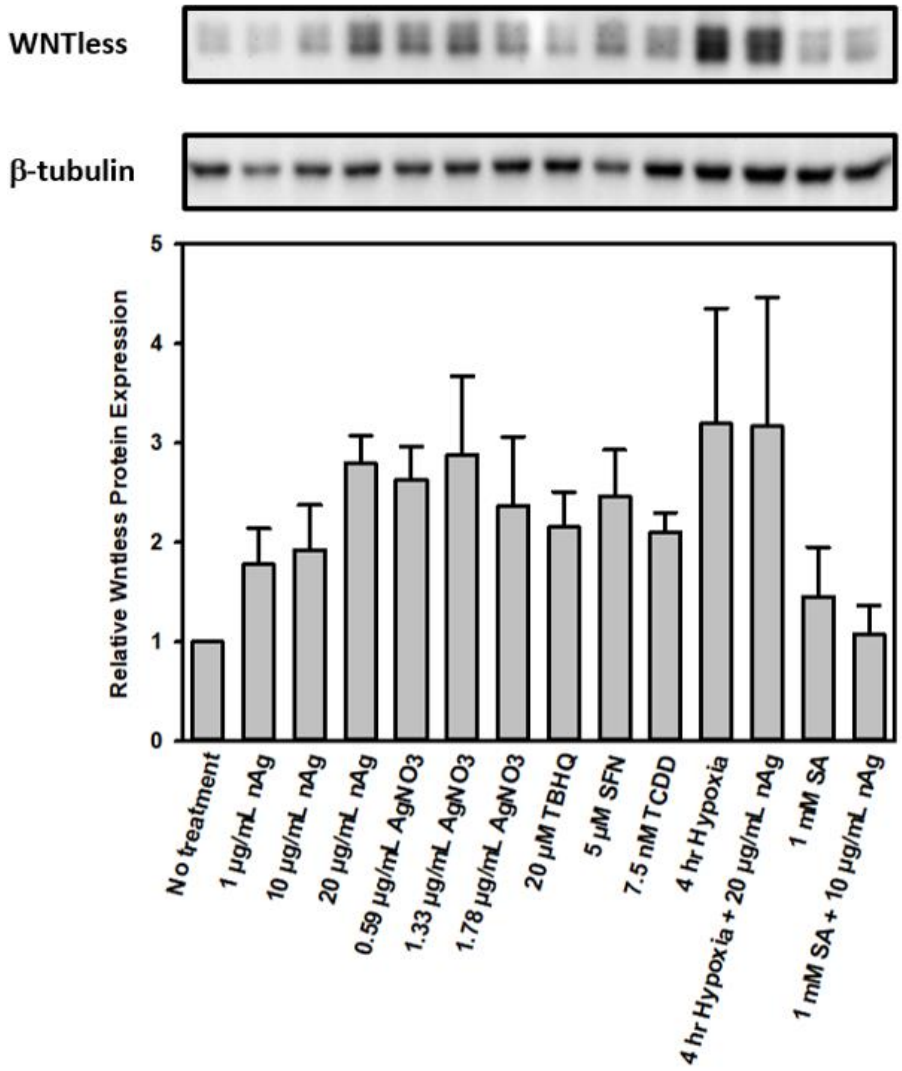

Figure 37. Western blotting for Wntless total protein expression through urea extraction from HCT116 cells treated for 4 hours. Wntless band at 37 kDa. Protein expression of each sample was normalized to β-tubulin. Standard error, one-way ANOVA, and the Dunnett's test were used. 4 replicates.

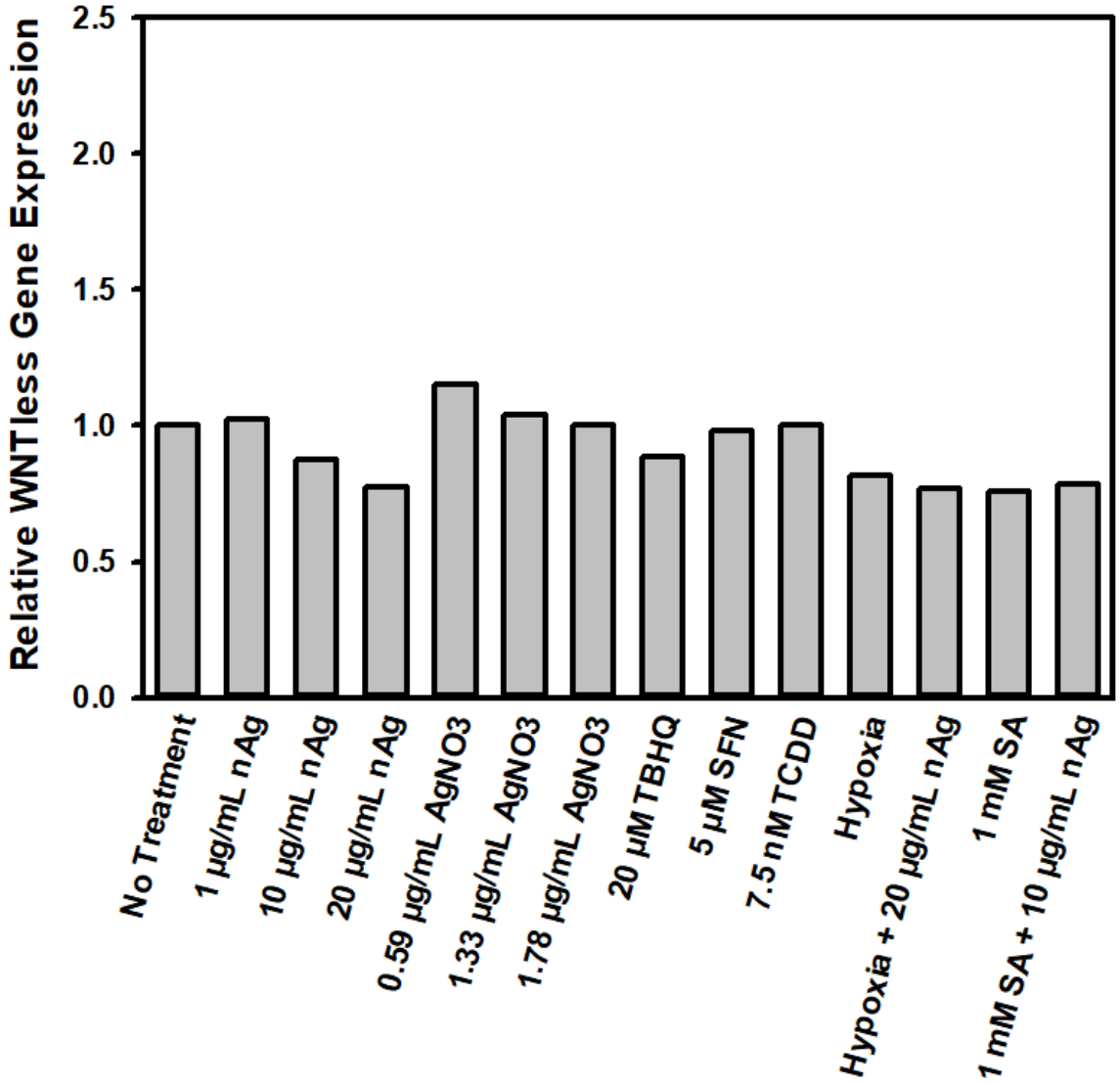

Figure 38. Using qPCR to determine Wntless gene expression in HCT116 cells treated for 4 hours. One-way ANOVA, and the Dunnett's test were used. 2 replicates.

3.7.2 β-catenin

Western blotting for β-catenin protein expression for 4 hour treatments in HCT116 showed all treatments slightly increased β-catenin expression except for the SA and SA + AgNP treatments. SA with AgNP co-treatment also decreased β-catenin expression relative to the 10 μg/mL AgNP treatment (Figure 39).

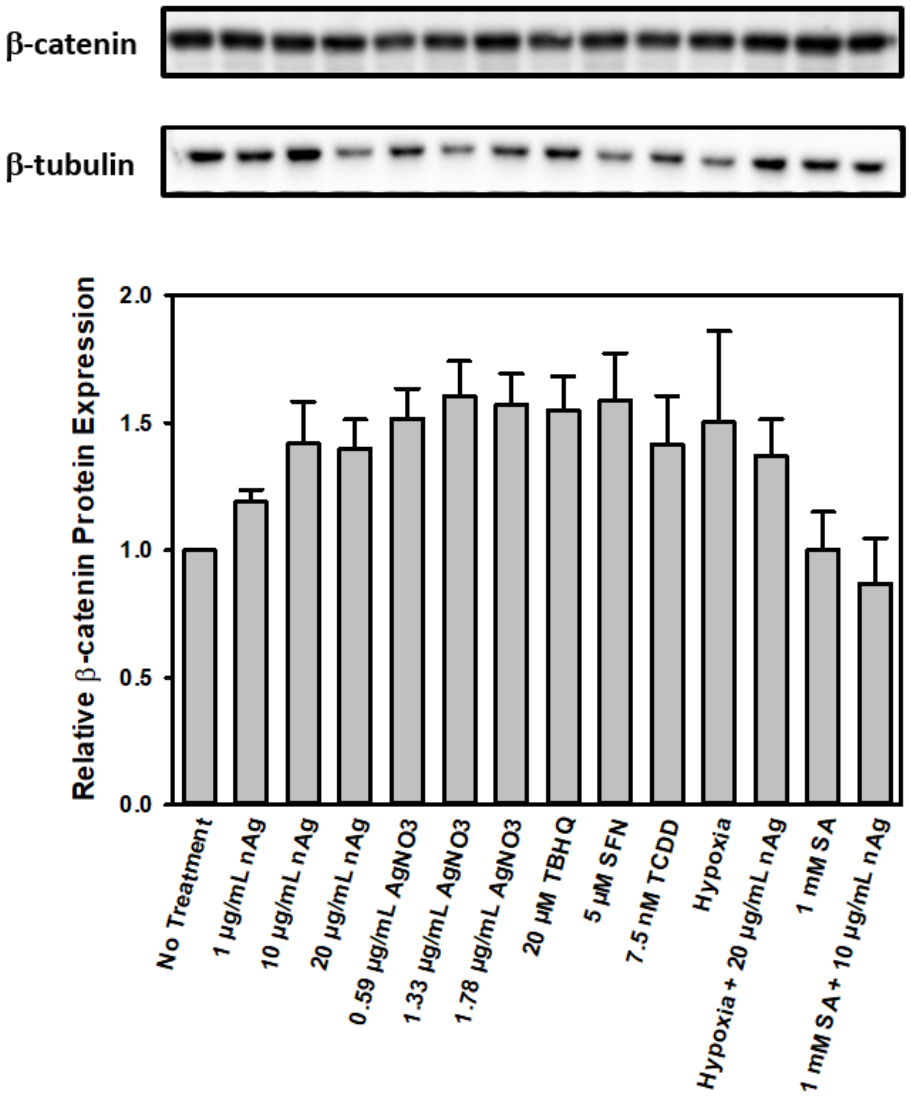

Figure 39. Western blotting for β-catenin total protein expression through urea extraction from HCT116 cells treated for 4 hours. β-catenin band at 100 kDa. Protein expression of each sample was normalized to β-tubulin. Standard error, one-way ANOVA, and the Dunnett's test. 3-4 replicates.

3.7.3 PORCN

Western blotting for PORCN protein expression for 4-hour treatments in HCT116 showed all treatments slightly increased PORCN expression except for hypoxia + 20 μg/mL AgNP, 1 mM SA, and 1 mM SA + 10 μg/mL AgNP. Only the SFN treatment significantly increased PORCN expression. SA with AgNP co-treatment decreased PORCN expression relative to the 10 μg/mL AgNP treatment (Figure 40).

Using qPCR, PORCN gene expression did not significantly change in HCT116 treated for 4 hours. (Figure 41).

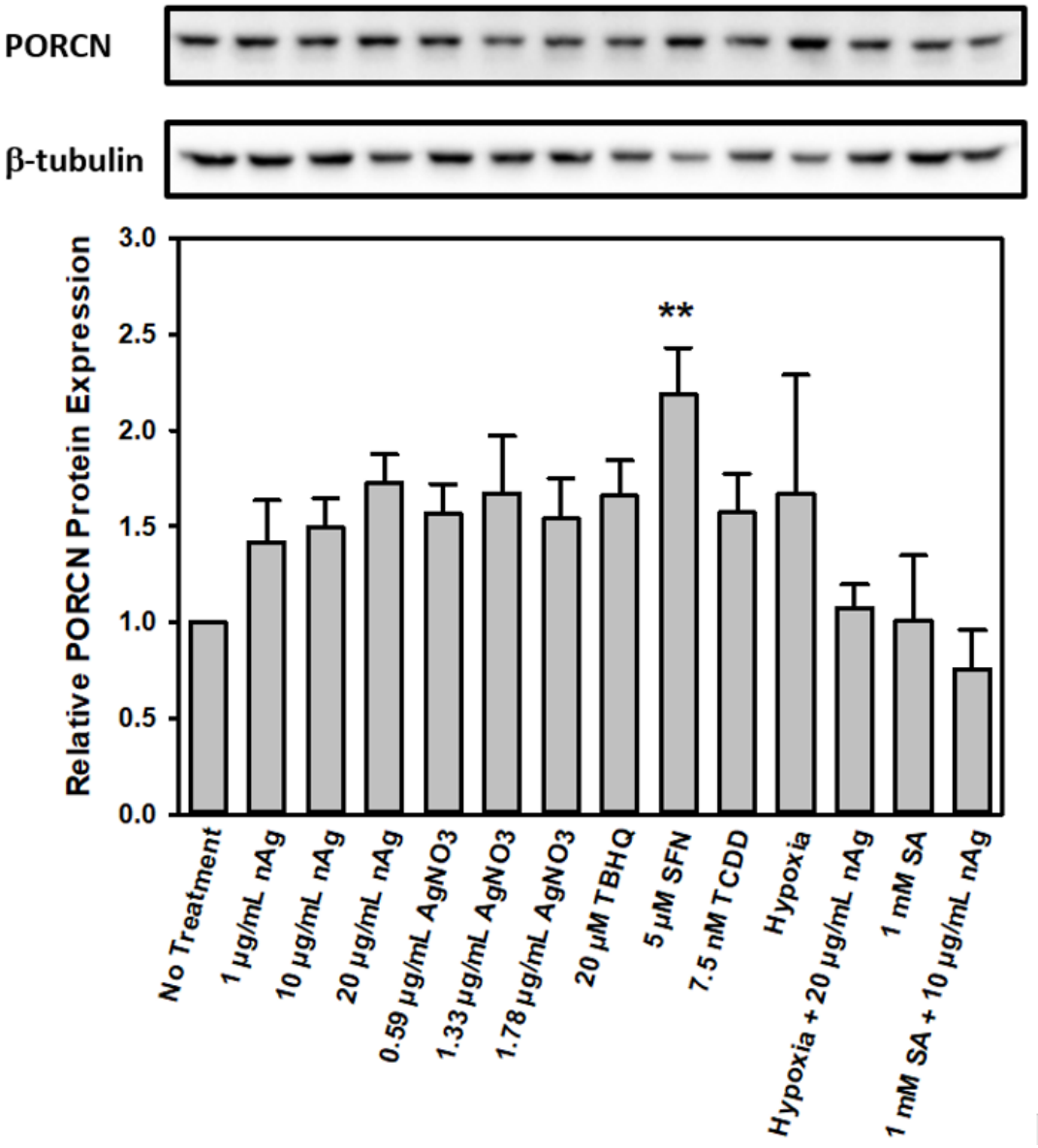

Figure 40. Western blotting for PORCN total protein expression through urea extraction from HCT116 cells treated for 4 hours. PORCN band at 63 kDa. Standard error, one-way ANOVA, and the Dunnett's test (*p<0.05, **p<0.01, ***p<0.001). 3-4 replicates.

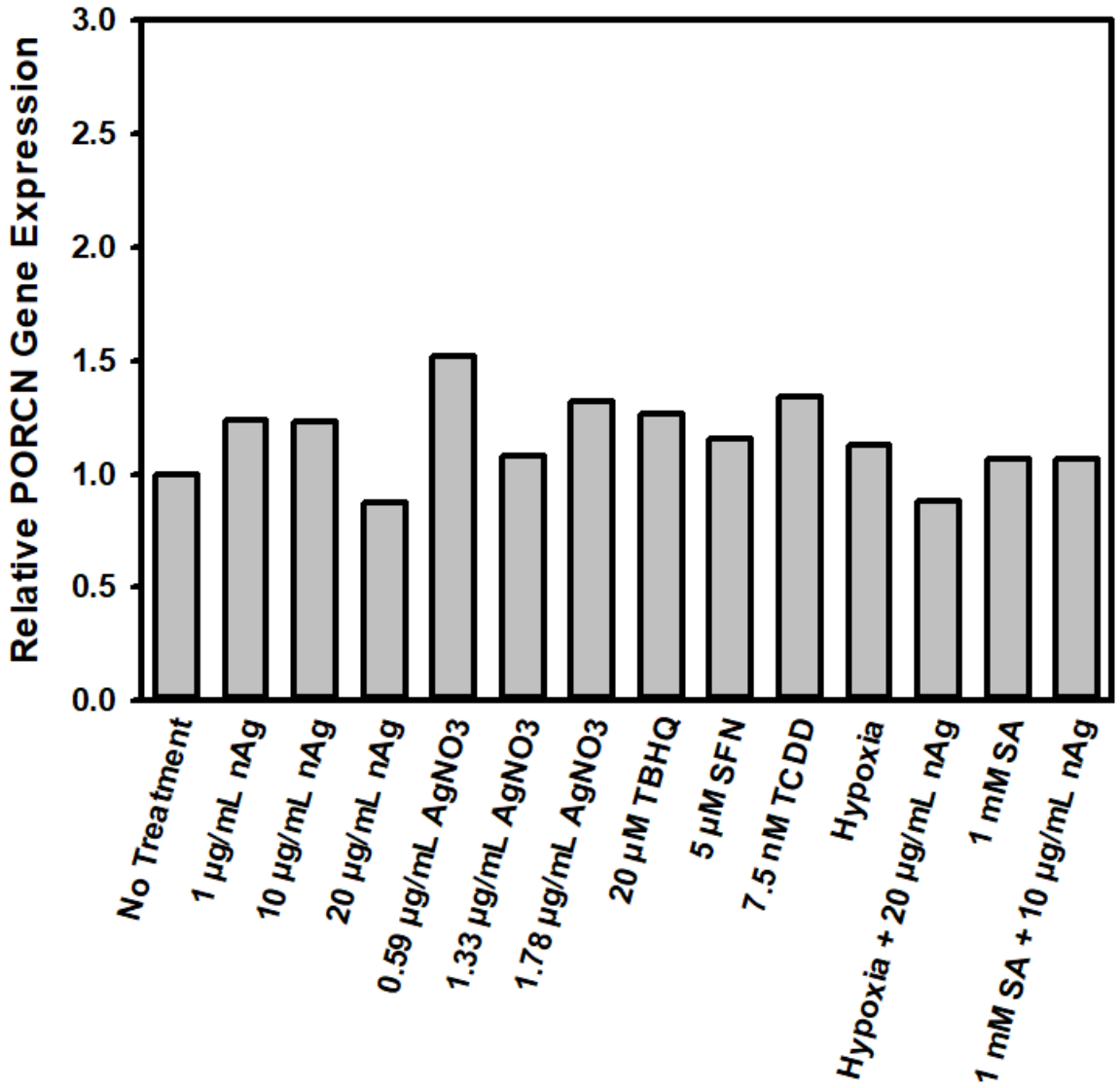

Figure 41. Using qPCR to determine PORCN gene expression in HCT116 cells treated for 4 hours. One-way ANOVA, and the Dunnett's test were used. 2 replicates.

3.7.4 Wnt3a

Western blotting for Wnt3a protein expression for 4-hour treatments in HCT116 showed AgNP and $AgNO_3$ treatments slightly increased Wnt3a expression. SA and SA + AgNP treatments increased Wnt3a expression. Hypoxia treatment slightly decreased Wnt3a expression. No significant differences were found (Figure 42).

Using qPCR, Wnt3a gene expression did not significantly change in HCT116 treated for 4 hours (Figure 43).

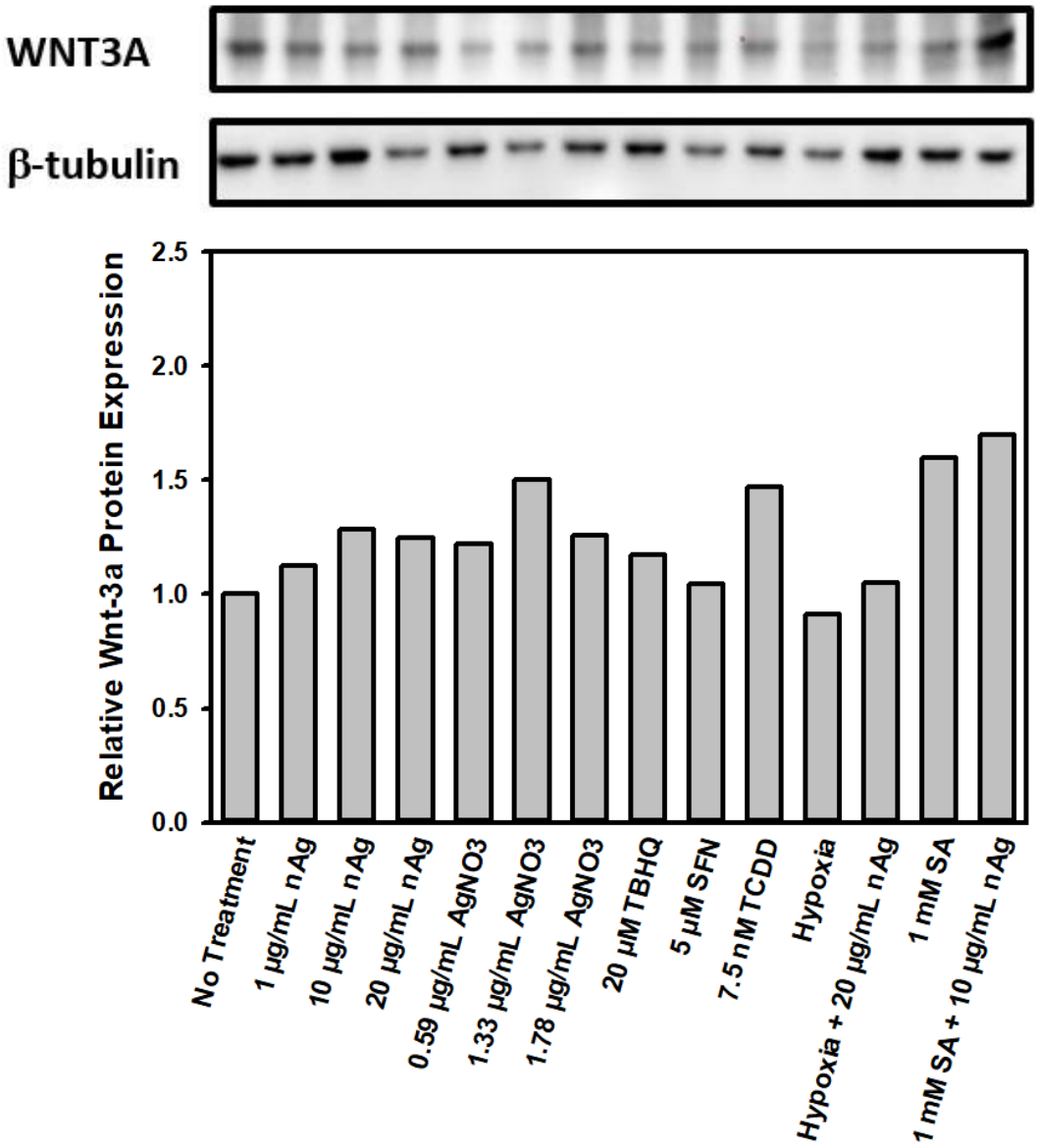

Figure 42. Western blotting for Wnt3a total protein expression through urea extraction from HCT116 cells treated for 4 hours. Wnt3a band at 37 kDa. One-way ANOVA, and the Dunnett's test were used. 2 replicates.

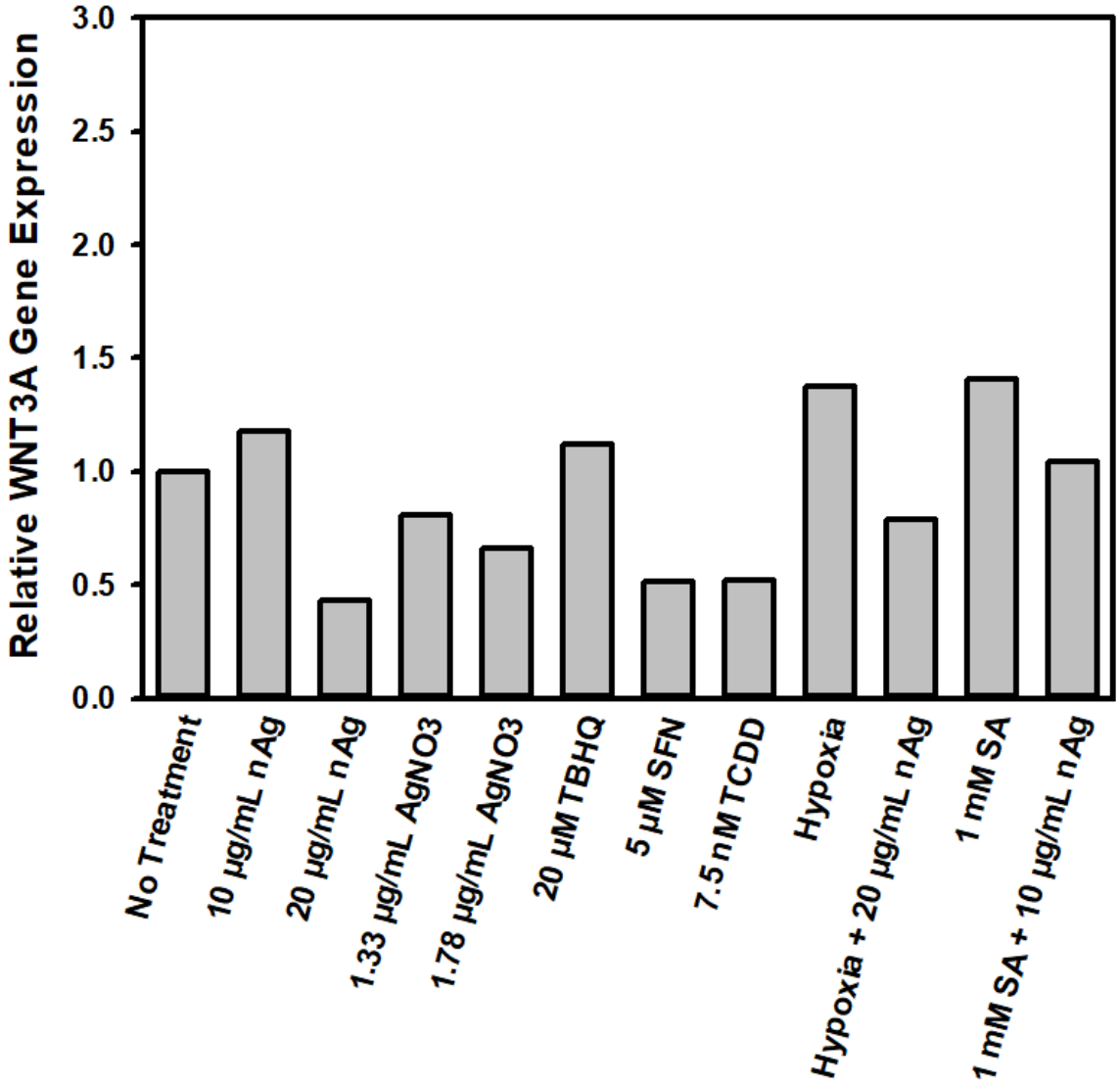

Figure 43. Using qPCR to determine Wnt3a gene expression in HCT116 cells treated for 4 hours. One-way ANOVA, and the Dunnett's test were used. 2 replicates.

3.7.5 Wnt5a

Western blotting for Wnt5a protein expression for 4-hour treatments in HCT116 showed AgNP and $AgNO_3$ treatment increased Wnt5a expression. Other treatments also slightly increased expression of Wnt5a except hypoxia, and the SA with AgNP co-treatment decreased Wnt5a expression relative to the 10 μg/mL AgNP treatment. No changes were significant (Figure 44).

Using qPCR, Wnt5a gene expression did not significantly change in HCT116 treated for 4 hours (Figure 45).

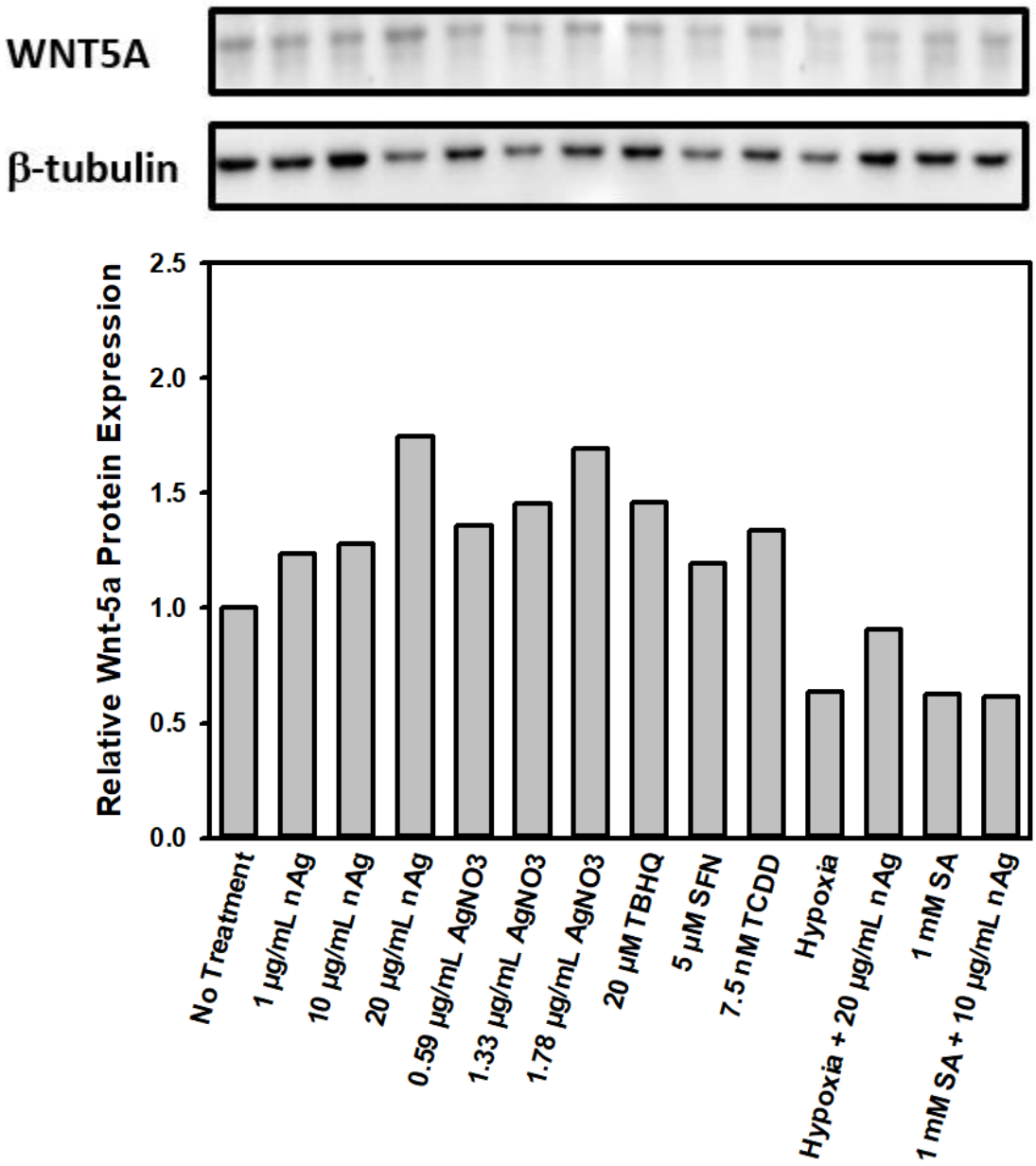

Figure 44. Western blotting for Wnt5a total protein expression through urea extraction from HCT116 cells treated for 4 hours. Wnt5a band at 39 kDa. One-way ANOVA, and the Dunnett's test were used. 2 replicates.

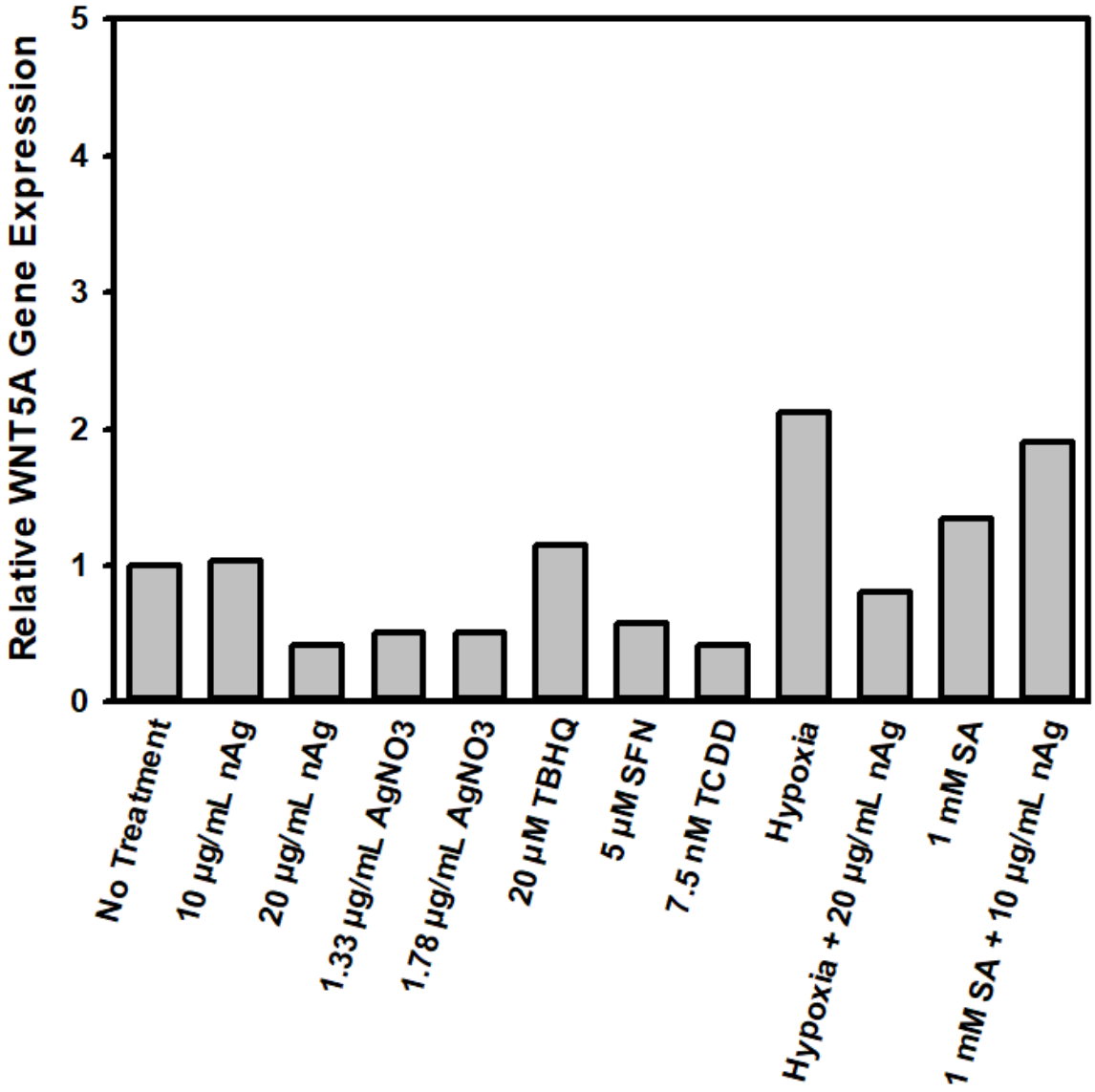

Figure 45. Using qPCR to determine Wnt5a gene expression in HCT116 cells treated for 4 hours. One-way ANOVA, and the Dunnett's test were used. 2 replicates.

3.8 Supplementary Data

The EC_{50} for SA treated for 1 hour with 24-hour recovery was 9.851 ± 0.0525 mM. Cell viability was statistically different at 1.75, 4, 7.5 mM and above. (Figure A14 Appendix). The 1-hour SA treatment followed by 24-hour recovery was to simulate the clearance of ascorbic acid in humans via intravenous treatment. Clearance occurs quickly with the half-life of ingested ascorbic acid being 30 minutes and clearance after intravenous treatment occurs within hours[151]. Although, the 24-hour treatment of SA elicited a stronger response, the very short 1-hour treatment decreased cell viability a relatively great amount. For the rest of the experiments, 24-hour treatment of SA was used instead as it elicited a greater response.

Aryl hydrocarbon receptor (AhR) is a transcription factor that plays a role in regulation of enzymes involved in metabolism such as cytochrome P450 enzymes. AhR may also play a role in regulation of growth, the immune system and development[152]. In our study, we showed that AgNPs increased an increase in nuclear and cytosolic AhR expression (Figure A12 in the Appendix). In the nuclear fraction, the $AgNO_3$ equivalent controls had higher expression than the AgNP treatments, indicating silver ions may play a role in the increase of AhR expression in the nucleus. However, in the cytosolic fraction, AhR expression is significantly increased with AgNP treatment where 20 μg/mL AgNP induced a 2.8-fold increase in AhR expression relative to the cytosolic no treatment control. The equivalent $AgNO_3$ treatments not increasing as much as the AgNP treatments, indicating that the effects seen are due to the AgNPs and not just the silver ions released. However, 2,3,7,8-tetrachlorodibenzo-p-dioxin (TCDD), a known AhR activator[152], did not significantly increase expression of AhR in neither the nuclear nor cytosolic fractions.

There are currently no studies looking at the relationship between AgNPs and AhR. For future experiments, the effects that AgNPs may play in the AhR pathway should be explored for potential mechanisms with AgNPs interacts with a biological system.

Using qPCR, the gene expression of AhR in HCT116 cells treated for 4 hours was observed. The AgNP treatments did not induce significant increases in AhR gene expression, therefore the increase in AhR protein levels in the cells did not result from upregulation of the AhR gene (Figure A13 in the Appendix).

A time course treatment for Nrf2 expression at 20 μM TBHQ was conducted to determine the optimal treatment time for protein determination via Western blotting. The 4-hour treatment elicited the greatest protein expression out of 0.5, 1, 2, 4, 6, 8, and 24 hours treatment, therefore, 4-hour treatments were used for Western blotting (Figure A15 in the Appendix).

Chapter 4: Discussion and Conclusion

There were many interesting findings I found in this study. AgNPs induced mitochondrial oxidative stress in the HCT116 cancer cells, but not in the non-cancer HIEC-6 cells. AgNPs induced a significant increase in Nrf2 protein expression with 4-hour treatment, however, no cytoplasmic or mitochondrial oxidative stress was induced by the AgNPs with 4-hour treatment. SA and AgNP treatment preferentially expired the cancer HCT116 cells compared to the non-cancer HIEC-6 cells. AgNPs disrupted the cell cycle and seemed to induce cell cycle arrest at the G1 and G2/M phases. I also found that hypoxia attenuated cytoplasmic oxidative stress induced by positive control, H_2O_2, and attenuated mitochondrial oxidative stress induced by both the AgNPs and positive control, antimycin A, in the HCT116 cells. Hypoxia also attenuated ER stress induced by the positive control thapsigargin. I also found that AgNPs induced an increase in cytosolic AhR protein expression. Table 3 shows a summary of all the results and main conclusions of the experiments conducted.

Table 3. Summary of results including experimental endpoint, treatment concentrations of nAg and $AgNO_3$, methods, and main conclusions.

Experimental Endpoint	**Treatment Concentrations of SA, nAg and $AgNO_3$**	**Methods**	**Conclusions**
Determine silver ion equivalents for $AgNO_3$ and nAg	nAg: 1 – 10 µg/mL $AgNO_3$: 0.05 – 5 µg/mL	ICP-MS	n/a
Cell morphology (HCT116, HIEC-6)	nAg: 1 – 30 µg/mL $AgNO_3$: 0.5 – 2 µg/mL	Microscopy	-High $AgNO_3$ and nAg concentrations induced morphological changes
Cell viability (HCT116, HIEC-6) -4 hr & 24 hr treatments	nAg: 0.5 – 100 µg/mL (HCT116), 1 – 125 µg/mL (HIEC-6) $AgNO_3$: 0.5 – 10 µg/mL (HCT116), 0.5 – 20 µg/mL (HIEC-6) SA: 0.01 – 30 mM Constant 10 µg/mL nAg: 0.05 – 10 mM SA Constant 1 mM SA: 0.5 – 100 µg/mL nAg	MTT assay	-HCT116 more susceptible to $AgNO_3$ and nAg than HIEC-6 -HCT116 more susceptible to SA & nAg co-treatments than HIEC-6
Cytoplasmic & mitochondrial oxidative stress (HEK293T) -2 hr treatments	nAg: 1 – 20 µg/mL $AgNO_3$: 0.48 – 1.22 µg/mL	Transfection with cyto-roGFP & mito-roGFP & flow cytometry	-No significant results
Cytoplasmic oxidative stress (HCT116 & HIEC-6) -4 hr and 24 hr treatments	nAg: 1 – 30 µg/mL $AgNO_3$: 0.5 – 2 µg/mL	CellROX stain & flow cytometry (normoxia & hypoxia)	-Hypoxia attenuated cytoplasmic oxidative stress in HCT116 & HIEC-6

Mitochondrial oxidative stress (HCT116 & HIEC-6) -4 hr and 24 hr treatments	nAg: 1 – 30 µg/mL AgNO3: 0.5 – 2 µg/mL	MitoSOX stain & flow cytometry (normoxia & hypoxia)	-nAg induced significant increase of mitochondrial oxidative stress in HCT116 -Hypoxia attenuated mitochondrial oxidative stress in HCT116
Nrf1 and Nrf2 protein/gene expression (HCT116) -4 hr treatments	nAg: 1 – 30 µg/mL AgNO3: 0.59 – 1.78 µg/mL SA: 1mM SA & 1mM SA + 10 µg/mL nAg (Nrf1)	Western blot & qPCR	-nAg induced non-significant increase in Nrf1 protein expression -nAg induced significant increase in nuclear Nrf2 protein expression -No significant changes to Nrf1 & Nrf2 gene expression
ER stress (HCT116) -24 hr treatments	nAg: 1 – 30 µg/mL AgNO3: 1 – 2 µg/mL	Stably transfected HCT116-ATF4 & HCT116-XBP1 cells & flow cytometry	-Hypoxia attenuated ER stress in HCT116-ATF4 & -XBP1 cells -nAg induced slight, non-significant increase in ER stress in both cell lines
Cell cycle (HCT116) -24 hr treatments	nAg: 1 – 30 µg/mL AgNO3: 1 – 2 µg/mL SA: 1mM SA & 1mM SA + 10 µg/mL nAg	BrdU stain & flow cytometry	-nAg induced significant decrease of percentage of cells in the G1 phase and increase in the G2/M phase of the cell cycle -SA co-treatment had additive effect
HIF-1α protein expression (HCT116) -4 hr treatments	nAg: 1 – 30 µg/mL AgNO3: 0.59 – 1.78 µg/mL SA: 1mM SA & 1mM SA + 10 µg/mL nAg	Western blot	-nAg induced significant increase in HIF-1α protein expression
Wnt signalling protein/gene expression (HCT116) -4 hr treatments	nAg: 1 – 30 µg/mL AgNO3: 0.59 – 1.78 µg/mL SA: 1mM SA & 1mM SA + 10 µg/mL nAg	Western blot & qPCR	-nAg induced non-significant increase in WNTless, β-catenin, PORCN, WNT3A, WNT5A -SA treatments decreased protein expression relative to the increases by nAg in WNTless, β-catenin, PORCN, WNT5A -No significant changes to gene expression
AhR protein expression (HCT116) -4 hr treatments	nAg: 1 – 30 µg/mL AgNO3: 0.59 – 1.78 µg/mL	Western blot & qPCR	-nAg induced significant increase in cytosolic AhR protein expression & non-significant increase in nuclear AhR -No significant changes to gene expression

4.1 General Toxicity of Nanosilver

A study looking at the cytotoxic effects of AgNPs on human colon cells and human colon cancer cells (HCT116) showed AgNP was slightly more toxic to the non-cancer colon cells than the HCT116 in an MTT assay, although they only went up to 60 µg/mL AgNP[153]. Another study that used an MTT assay on AgNP treated HCT116 showed a IC_{50} of 5.3 ppm (5.3 µg/mL), which is much lower than what was observed in this study, however, the study used AgNPs synthesized via thermal co-reduction with no coating, which could have increased the toxicity of the AgNPs[154]. Studies using biologically synthesized AgNPs also resulted in much lower IC_{50} (less than 10 µg/mL) in HCT116[155–157]. These AgNPs are not coated and may have different properties, making the biosynthetic AgNPs less stable and more toxic. No studies currently look at the effect AgNPs have on HIEC-6 cells specifically.

In this study, the HIEC-6 cells were also much more resistant to $AgNO_3$ and AgNP treatment compared to the HCT116 cells where the HIEC-6 EC_{50} was much higher. The HIEC-6 AgNP EC_{50} was greater than 125 µg/mL AgNP and the HCT116 AgNP EC_{50} was 78.431 ± 0.703 µg/mL. The HIEC-6 cells were also much more resistant to $AgNO_3$ (EC_{50} = 17.972 ± 0.356 µg/mL) than HCT116 (1.645 ± 0.0286 µg/mL). These results indicate that the HIEC-6 are more resistant to the toxic effects of both the AgNP and $AgNO_3$ treatments, which may indicate a cancer specific toxicity of the AgNP, making AgNPs a good candidate for anticancer therapy.

It is important to keep in mind that the MTT assay measures metabolic activity of cells: the MTT is converted into a purple product, formazan, by mitochondrial NAD(P)H-dependent cellular oxidoreductase enzymes. It is possible that differences in the cell lines

can be attributed to differences in mitochondrial activity. MTT results can also indicate mitophagy or mitochondrial biogenesis. For determination of sublethal AgNP and SA concentrations, however, the MTT assays were used as cell viability assays.

4.2 Nanosilver and Cellular Effects

4.2.1 Oxidative Stress

4.2.1.1 Mito- and Cyto-roGFP

Mito-roGFP is a redox sensitive fluorescent marker that is targeted to the mitochondria to measure mitochondrial oxidative stress. The mito-roGFP plasmid construct is shown in Figure A2 (Appendix). Cyto-roGFP is a redox sensitive fluorescent marker that is targeted to the cytosol to measure cytosolic oxidative stress. The cyto-roGFP plasmid construct is shown in Figure A3 (Appendix). No significant effects were seen with 2-hour treatments for any treatments in either of the mito- and cyto-roGFP transfected HEK293T cells. Even the positive controls, AA, DTT, and tBHP did not induce significant changes, which suggests the assay itself did not work as intended. The roGFPs are ratiometric sensors which produce fluorescent signals that fluoresce at 480 and 400 nm as a measure of the redox state of the environment using confocal imaging[158,159]. In these studies, live-cell imaging was conducted using confocal microscopy over a short time course of treatments[159]. It is likely that measurement with the flow cytometer does not work with this sensor. It's possible that the roGFPs may auto-fluoresce with long exposures and so studies using these roGFPs keep the exposure to the fluorescence short to avoid auto-fluorescence.

Protocols for the use of the mito-roGFP tends to be cell-specific and so there are various different protocols used by researchers[160]. In this study, I used similar concentrations of DTT and tBHP from existing mito-roGFP studies[159,160]. Treatment times of the positive controls DTT and tBHP for these studies ranged from 10 – 30 minutes[159,160]. Other cells that mito-roGFP experiments have been conducted in include rat muscle cells, embryonic chick cardiomyocytes, human lung fibroblasts, yeast cells, and human umbilical vein endothelial cells (HUVEC). One study used cyto-roGFP in pulmonary and systemic smooth muscle cells and similar protocols to the mito-roGFP were used[159].

Mito- and cyto-roGFP transfected HEK293T cells with 2-hour treatment and analysis via flow cytometry was ineffective at determining the effect AgNPs has on mitochondrial and cytoplasmic oxidative stress. For future experiments, confocal microscopy could be used instead of flow cytometry to measure cytosolic or mitochondrial oxidative stress using the mito- and cyto-roGFPs. Other oxidative stress markers or fluorescent probes may be better suited for measuring oxidative stress in longer treatments.

4.2.1.2 CellROX

CellROX Deep Red Reagent is a fluorescent probe that detects superoxides and hydroxyls in the cytoplasm of live cells using flow cytometry. In a reduced state, CellROX does not fluoresce and becomes fluorescent when oxidized by the ROS with emission maxima of approximately 665 nm[161]. Significant increase of fluorescence with the positive control H_2O_2, a known oxidative stress inducer, indicated that the CellROX was working as intended. The negative control 5 mM NAC pretreatment decreased the amount of

oxidative stress compared to just the H_2O_2 treatment, as predicted as NAC reduces the effects of oxidative stress[162].

No significant changes to cellular oxidative stress were seen in the 4-hour treated HCT116 cells, indicating that 4 hours may not be long enough to generate significant amounts of ROS, or the antioxidant machinery of the cells are able to clear any ROS generated at the tested concentrations of AgNP. The 24-hour normoxic treatment for HCT116 cells resulted in a slight increase in oxidative stress after AgNP treatment. Fluorescence of the equivalent $AgNO_3$ concentrations were less than the corresponding AgNP treatments for the HCT116 24-hour normoxic treatment and about the same as the AgNP treatments for the HIEC-6 24-hour hypoxic treatments, indicating it is possible the effects seen were due to the AgNPs rather than the silver ions released for the HIEC-6. Under hypoxia, I found hypoxic treatment in the HCT116 attenuated oxidative stress in all treatments compared to the normoxic treatments.

I did not find any significant changes in oxidative stress after 24-hours of AgNP treatment under normoxia in the HIEC-6 cells. I found the fluorescence of the equivalent $AgNO_3$ concentrations were greater than the corresponding AgNP treatments for the HIEC-6 24-hour normoxic treatment and was slightly lower than the AgNP treatments for the HIEC-6 24-hour normoxic treatments, indicating it is possible that the effects that were seen were due to the AgNPs, rather than the silver ions released. The hypoxic treatment of HIEC-6 attenuated oxidative stress in the positive control H_2O_2 treatment compared to the normoxic treatments.

AgNPs did not induce cytoplasmic ROS production in either of the HCT116 or HIEC-6 cells. The CellROX that we used detects superoxides and hydroxyl radicals in the

cytoplasm, so our results indicated that AgNPs did not induce cytoplasmic production of these ROS in HCT116 and HIEC-6 cells at the tested concentrations.

One study, using CellROX Green to measure cellular oxidative stress, showed toxic concentrations of AgNPs induced a slight increase in ROS for mouse neural cells and HUVEC cells[163]. An excellent review covering the effect AgNPs has on oxidative stress in various *in vivo* and *in vitro* studies showed AgNPs induce cellular oxidative stress, although the mechanisms by which AgNPs induces oxidative stress is unclear[164]. Studies have also showed AgNP treatment resulted in depletion of SOD levels, an antioxidant enzyme, within cells, resulting in an increase of ROS generation[164]. A study using human hepatoma cells showed after AgNP exposure, the AgNP was aggregated in the cytoplasm and nuclei of the cells where oxidative stress was induced[165]. Alveolar epithelial cells exposed to AgNPs also showed AgNPs accumulated in the cytoplasm of the cells[7]. The small amount of cellular oxidative stress induced by AgNPs using the CellROX experiments in the HCT116 could be explained by different cell lines reacting differently to the AgNPs or oxidative stress is induced through other compartments rather than the cytoplasm, such as the mitochondria. The results also showed that there are no cancer-cell specific ROS generation. Non-toxic, relatively low doses of AgNPs were also used in this study which could explain a lack of significant induction of oxidative stress.

4.2.1.3 MitoSOX

MitoSOX Red reagent is a fluorescent dye that targets the mitochondria where it can be quickly oxidized by superoxides, resulting in fluorescence[166]. The positive control, AA, was shown to significantly increase mitochondrial ROS in the 4- and 24-hour HCT116

normoxic experiments, indicating the MitoSOX was working as intended in detecting mitochondrial oxidative stress. NAC pretreatments slightly decreased amount of ROS produced relative to the AA treatments without NAC as predicted. The AA and NAC treatments had variable results in the 4-hour HIEC-6 treatments and were not significant. The positive control H_2O_2 treatment induced mitochondrial ROS produiction, although not to a significant level. In the 24-hour HIEC-6 normoxic treatments, AA treatments significantly increased mitochondrial ROS levels and NAC pretreatment reduced ROS levels as predicted.

In the HCT116 cells, MitoSOX 4-hour treatments under normoxia, results were slightly variable and non-significant, except for the positive control AA treatment, indicating that the 4-hour treatment may not be enough for AgNPs to induce significant amounts of mitochondrial ROS. Another possibility is that the antioxidant machinery of the cells is able to clear any ROS generated at the tested concentrations of AgNP. The HCT116 MitoSOX 24-hour treatment under normoxia showed that there is a significant dose-dependent increase in ROS generated by AgNP treatment. Both 20 and 30 µg/mL AgNP treatments were statistically different with 1.8- and 2.0-fold increases, relative to the no treatment. Only the highest $AgNO_3$ treatment induced a significant increase in ROS, the other $AgNO_3$ treatments did not induce any ROS production. It's possible that the effects seen are due to AgNPs rather than the release of silver ions from the AgNP as 2.0 µg/mL $AgNO_3$ is a toxic concentration to the HCT116 cells. I found that the hypoxic treatment in the HCT116 showed attenuated oxidative stress compared to the normoxic treatments, which indicates that hypoxic conditions alter the oxidative stress response. These experiments indicate that AgNP treatment induces mitochondrial superoxide generation in

HCT116 cells. The HIEC-6 MitoSOX 24-hour treatment under normoxia did not find any significant results, except for the positive control AA treatments.

Neither of the 4-hour normoxic treatment in the HCT116 and HIEC-6 cells had significant changes mitochondrial oxidative stress, except in the positive control AA. The 24-hour normoxic treatments in the HCT116 elicited greater mitochondrial ROS generation, compared to the HIEC-6 cells. This indicates that AgNPs may potentially harm the colon cancer cells more than the non-cancer colon cells via production of more mitochondrial oxidative stress.

Many studies have shown AgNPs can induce oxidative stress in various *in vitro* and *in vivo* models[2,18,24,39,53,78–82]. It has been suggested that disruption of mitochondrial function occurs through ROS production induced by AgNPs[2]. It has also been suggested that AgNPs induce mitochondrial ROS production, which can induce apoptosis in mouse fibroblast cells. In this study, the cells were treated with cyanide, which inhibits the electron transport chain, and showed an inhibition of AgNP-induced ROS generation, indicating that ROS generation was mitochondria-specific[24]. A study looking at HepG2 cells used the MitoSOX stain and treated with AgNPs for 4 and 24 hours. They showed an increase in mitochondrial ROS production for both AgNP treatments[167]. In a study looking at primary fibroblast and liver cells, it was shown through TEM that AgNPs were in the mitochondria of both cell types. This study also used MitoSOX and treatment of AgNP induced antioxidant mechanisms in the cells and so it is possible that the ROS responsible for triggering the antioxidant defense come from AgNP-induced ROS production in the mitochondria[168]. Localization of AgNPs in cells have been shown in the cytoplasm, nucleus, and mitochondria[7]. However, other studies have showed different cell lines did

not have AgNPs in the nucleus nor mitochondria and were instead found in endosomes or lysosomes in the cells[20].

Not many studies looking at oxidative stress induction by AgNPs look at cytoplasmic versus mitochondrial generated ROS. Our results indicate that for HCT116 and HIEC-6 cells, mitochondrial ROS contributes to cellular oxidative stress in addition to slight amount of cellular ROS production where the HCT116 generated more mitochondrial ROS than the HIEC-6. Our results agree with current literature that AgNP induces cellular oxidative stress. Generation of more ROS after AgNP treatment in the cancer HCT116 cells relative to the HIEC-6 non-cancer cells indicates that AgNP can harm HCT116 cells more via mitochondrial ROS production than in HIEC-6, which is important for the consideration of using AgNP as an anticancer agent.

4.2.1.4 Effect of Hypoxia on Oxidative Stress

Hypoxia has been shown to increase levels of HIF1α, induce production of ROS, decrease levels of reduced glutathione (GSH), increase protein oxidation and lipid peroxidation, increase nitric oxide, and increase the levels of antioxidant proteins heme oxygenase and metallothionein[169,170]. Previous studies found that hypoxia treatment decreases the antioxidant defense in the brain[170]. Hypoxia also activates the antioxidant response by inducing production of various antioxidant enzymes such as SOD, GPx, and GST in the cardiovascular system. In this study, heart tissue in rats were treated under hypoxia for two and five days. It was also found that the ROS generation was significant, but plateaued after a certain length of treatment time[169].

In hypoxic cells, the major source of ROS is from the mitochondria and so mitochondria play an important role under hypoxia. When faced with hypoxia, the balance of O_2 is disrupted in the mitochondrial respiratory chain which results in production of ROS and oxidation of macromolecules[171,172]. HIF1 plays an important role in prevention of excess production of ROS in the mitochondria when faced with hypoxia[172]. Studies have shown that HIF1 also reduces the production of cellular ROS via multiple pathways. These pathways that HIF1 activates all result in a decrease of ROS production: a subunit switch occurs in the cytochrome c oxidase to increase efficiency of complex IV in the mitochondria, induction of pyruvate dehydrogenase kinase 1, resulting in taking the pyruvate away from the mitochondria, triggering mitochondrial selective autophagy, and induction of a microRNA, resulting in blocking the assembly of iron/sulfur clusters required for oxidative phosphorylation[172]. A study using HUVEC and HepG2 cells showed a potential additional pathway which HIF1 decreases ROS. The study used mitochondria-targeted HIF1α and showed attenuated production of mitochondrial ROS by downregulation of mitochondrial mRNA and resulting in inhibition of respiratory chain activity and decrease in mitochondrial production of ROS[171].

In both the CellROX and MitoSOX experiments, attenuation of oxidative stress was seen with hypoxic treatment even with the positive control H_2O_2 treatments. Attenuation of oxidative stress was seen in the MitoSOX and CellROX HCT116 24-hour treatment under hypoxia conditions. Attenuation of oxidative stress under hypoxia in HIEC-6 cells was not as great in the CellROX experiment. Attenuation of oxidative stress in HIEC-6 cells did not occur in the HIEC-6 cells with the MitoSOX experiment, indicating that HIEC-6 may not be affected by hypoxia as much as the HCT116. HIF1 play an

important role in cancer cell survival and so targeting HIF1 has been proposed as a mechanism for anti-cancer therapies[173]. HIF expression is increased in many different cancers compared to non-cancer tissues or cells[174]. It's possible that the attenuation of oxidative stress in the HCT116 cells results from the higher levels of HIF1 in the HCT116 that aid in cell survival which results in higher levels of oxidative stress attenuation. These results in HCT116 cells agree with the studies previously finding that HIF1 decreases cellular ROS through various mechanisms. These mechanisms may explain the attenuation of oxidative stress seen in the CellROX and MitoSOX experiments on the HCT116 cells.

4.2.1.5 Nrf1 and Nrf2 Protein Expression

Nrf1 and Nrf2 are transcription factors involved in the oxidative stress response pathway and are activated by presence of ROS. Nrf1 and Nrf2 are the master regulators for signaling in the oxidative stress response[104,106,107,175]. Nrf2 is degraded in the cytoplasm and nucleus under normal functioning, but it has been showed that inhibition of degradation of the Nrf2 occurs more in the nucleus relative to the cytosol[176]. When there is oxidative stress in the cell, Nrf2 moves to the nucleus and is stabilized, hence the higher nuclear levels of Nrf2[177].

In HCT116 cells, significant increase in nuclear Nrf2 expression was induced by AgNP treatment in a dose-dependent fashion. AgNPs did not induce changes to gene expression. The 10 and 20 μg/mL AgNP treatment significantly increased nuclear Nrf2 protein expression relative to the no treatment control. The $AgNO_3$ treatments also increased nuclear Nrf2 expression, but not to significant levels, indicative that the increase in Nrf2 is possibly due to the AgNPs rather than silver ions released. Tert-

butylhydroquinone (TBHQ) and sulflurofane (SFN), known Nrf2 activators, induced significant increase in nuclear Nrf2 expression as predicted[178,179]. Significantly less Nrf2 expression occurred in the cytosol compared to the nuclear fraction. All tested concentrations of $AgNO_3$ had higher Nrf2 expression than the AgNP treatments. Neither TBHQ nor SFN treatments were significant in the cytosol. In the HCT116 cells, no significant changes were seen in total Nrf1 expression. No changes were observed for Nrf1 gene expression.

Studies showed AgNP treatment activated the Nrf2-mediated oxidative stress response in neurons, liver hepatocellular carcinoma cells, and human embryonic stem-cell-derived neural stem/progenitor cells[78,180–182]. Nrf2 protein expression was increased after exposure to non-toxic levels of AgNPs in K562 cells[81]. The Nrf2 results in this study are like those found in current literature where the current research agrees that AgNPs induces Nrf2 expression, therefore the oxidative stress response. There are currently no studies looking at the relationship between AgNP treatment and Nrf1 expression.

Although Nrf2 protein expression was increased at 4-hour treatment of AgNPs in HCT116 cells, the 4-hour treatment in the CellROX and MitoSOX experiment did not see a consistent dose-dependent increase in oxidative stress. This indicates the Nrf2 may not be being activated through generation of ROS, or at least not superoxide, from the mitochondria or it can be an indication that the MitoSOX and CellROX assays may lack sensitivity. Studies have showed AgNP treatment can induce changes to DNA and non-coding RNA expression[20]; it is possible that AgNPs could interact with the Nrf1 and Nrf2 genes or any related genes that may regulate Nrf1 and Nrf2. It is also possible for AgNPs to interact with and interfere with the Nrf2 degradation complex present in the cytosol to

prevent degradation of Nrf2. It's important to study the effect AgNPs has on oxidative stress and which mechanisms AgNP induces oxidative stress. It's also important to determine any differences in oxidative stress production and the mechanism in cancer versus non-cancer cells.

AgNP treatments had no effect on Nrf1 and Nrf2 gene expression, indicating that the increase of protein was not due to increased gene expression. These changes in protein level without change at the mRNA level could be explained by increased translation without change in mRNA level, decreased proteolysis, microRNAs, ribosomal binding proteins, RNA modification, or translational changes to the protein. Further studies could look at Nrf1 and Nrf2 protein and gene expression in HIEC-6 cells to compare with HCT116.

The majority of current research has showed AgNPs induces oxidative stress in various *in vivo* and *in vitro* model systems[2,18,24,39,53,78–82]. The main method of measuring AgNP-induced ROS production is the use of 2,7-dichlorodihydrofluorescein diacetate (H_2DCFDA), a non-polar dye that fluoresces strongly when oxidized. However, there are issues with the reliability of using H_2DCFDA to detect ROS[20]. Our experiments looking at the effect AgNPs have on oxidative stress in HCT116 and HIEC-6 cells indicates that AgNPs may induce oxidative stress through generation of superoxides in the mitochondria and generation of ROS in the cytoplasm. Hypoxic treatment in HCT116 cells resulted in attenuation of cytoplasmic and mitochondrial ROS levels. Hypoxic treatment in HIEC-6 resulted in slight attenuation of cytoplasmic ROS, but not mitochondrial ROS. In HCT116 cells, AgNPs were also showed to induce expression of Nrf1 and Nrf2 proteins from the oxidative stress response pathway.

4.2.2 Endoplasmic Reticulum Stress

4.2.2.1 HCT116-XBP1

XBP1 is an ER stress marker and the effect that AgNPs have on *XBP1* splicing was studied using stably transfected HCT116-XBP1 cells. The XBP1 mNeonGreen sensor fluoresces in response to *XBP1* mRNA splicing and so is an ER stress sensor for the IRE1α pathway[150]. The plasmid used for the HCT116-XBP1 is shown in Figure A5 of the Appendix.

With the time course treatment, 24-hour treatment elicited the strongest response from the positive control thapsigargin and so we used the 24-hour treatment time for the HCT116-XBP1 experiments. Thapsigargin is a known ER stressor and works by inhibiting the calcium (Ca^{2+}) pump in the sarcoplasmic/endoplasmic reticulum, resulting in reduction of Ca^{2+} in the ER. Under these conditions, calcium-dependent chaperones such as calnexin are unable to function properly, leading to ER stress[117].

The 24-hour AgNP treatment under normoxia did not induce significant *XBP1* splicing in HCT116-XBP1 cells. No significant changes to *XBP1* splicing was observed for all treatments except for the thapsigargin positive control.

A study has showed AgNP treatment in breast cancer cells increased levels of phosphorylated IRE1α, which is indicative of activation of the IRE1α pathway and can result in *XBP1* splicing[183]. One study showed AgNPs induced activation of the IREα pathway in rat cells[184]. Few studies look at the link between AgNPs and *XBP1* splicing or regulation. A study showed AgNPs induces ER stress which includes the upregulation of the *XBP1* gene in liver cells[20]. A study looking at zebrafish showed AgNP treatment

induced ER stress with significantly increased levels of spliced *XBP1*, however, a very high dosage of 500 µg/mL AgNP was used[185]. Other studies have also showed that AgNPs induced increased spliced *XBP1*[186,187]. Other *in vitro* models have also shown that AgNPs induce ER stress [20,89,188,189]. It's possible that ER stress is not mainly induced via the IRE1α pathway in HCT116 cells, the concentration of AgNPs was not high enough to elicit a great enough *XBP1* splicing response, or ER stress induced by AgNPs is mostly due to the release of silver ions.

4.2.2.2 HCT116-ATF4

ATF4 is also an ER stress marker and the effect that AgNPs has on ATF4 translation was studied using stably transfected HCT116-ATF4 cells. The ATF4 mScarlet is a sensor that fluoresces in response to ATF4 translation and so is an ER stress sensor for the PERK pathway[150]. The plasmid used for the HCT116-ATF4 is shown in Figure A7 of the Appendix. With the time course treatment, 24-hour treatment elicited the strongest response from the positive control thapsigargin and so we used the 24-hour treatment time for the HCT116-ATF4 experiments.

The 24-hour AgNP treatment under normoxia did not induce significant ATF4 translation in HCT116-ATF4 cells. The thapsigargin positive control induced significant ATF4 translation, indicating the HCT116-ATF4 fluoresce properly.

Studies have shown that AgNP treatment activates the PERK pathway from observations that ER stress markers involved in the PERK pathway are increased[189]. One study showed AgNPs induced upregulation of ATF4 levels in breast cancer cells[183]. Studies have showed AgNPs induce upregulation of phosphorylated PERK, a marker for potential

activation of the PERK pathway, which could lead to ATF4 translation[186,189,190]. One study found AgNP-induced activation of the PERK pathway in rat cells[184]. It's possible that ER stress is not mainly induced via the PERK pathway in HCT116 cells, the concentration of AgNPs was not high enough to elicit a great enough ATF4 translation, or ER stress induced by AgNPs is mostly due to the release of silver ions.

4.2.2.3 Effect of Hypoxia on ER Stress

Many studies have showed that ER stress can be induced by hypoxia and HIF1α[128,191–194]. The UPR can be activated by hypoxia as the low oxygen environment disrupts protein folding as oxygen is required for formation of disulphide links. Hypoxia also inhibits protein synthesis as hypoxic conditions result in hyperphosphorylation of PERK, which phosphorylates the initiation factor eIF2α, resulting in inhibition of protein translation[128,191]. Hypoxia can also inhibit mTOR, a protein responsible for regulation of protein translation in response to stress and/or lack of nutrients. The inhibition of mTOR is followed by hyperphosphorylate of its substrates which results in inhibition of protein translation[128]. Hypoxia also resulted in upregulation of ATF4 in *in vitro* and in human tumour studies. The ER stress response has been shown to aid in hypoxia tolerance in tumour cells[191].

One study looking at nucleus pulposus cells from the vertebral disc of mice found hypoxia and HIF1α attenuated the ER stress response. In this study, knockdown of HIF1α resulted in increased CHOP, PERK, and ATF6 and stabilization of HIF1α resulted in decreased expression of ER stress markers such as eIF2α. However, these cells normally

function at hypoxic microenvironments due to their location in the inner core of the vertebral disc[193].

In this study, the HCT116-XBP1 treated under hypoxia showed attenuation of *XBP1* splicing in all the treatments, including the thapsigargin positive control, compared to the normoxic treatments. The HCT116-ATF4 treated under hypoxia showed attenuation of ATF4 translation in all treatments, including the thapsigargin positive control, compared to the normoxic treatments. This is the opposite of what would be expected under hypoxia. The HCT116 cells are cancer cells that, like the nucleus pulposus cells, may normally survive under hypoxia and may find decrease of ER stress in a similar mechanism. Further studies should be conducted on the mechanism which hypoxia may attenuate ER stress in HCT116 cells. Further studies should also look at the effect AgNPs has on ER stress in non-cancer cells, such as the non-cancer HIEC-6 versus HCT116 cancer cells.

4.2.3 Hypoxic Stress

4.2.3.1 HIF1α Protein Expression

Using Western blotting, AgNPs induced a dose-dependent increase in HIF1α expression in 4-hour treated HCT116 cells. Significant increase at 20 μg/mL AgNP was observed at a 3.3-fold increase. $AgNO_3$ also increased HIF1α expression. It's possible that silver ion release plays a role in the increase of HIF1α expression. Hypoxia treatment significantly increased HIF1α expression with a 52-fold increase as predicted, as HIFs are transcription factors that are activated in response to hypoxic stress[108–110]. Hypoxia co-treated with 20 μg/mL AgNP showed a slightly lower HIF1α expression compared to the just hypoxia treatment.

Few studies have studied the effects of AgNPs on the hypoxic stress response and have found variable results. Two studies looking at lung cancer and human mesenchymal stem cells showed AgNP treatment increased HIF1α expression[82,195]. However, two other studies have showed AgNP treatment decreases HIF1α expression in human breast cancer cells and decreased HIF1α expression in mice[59]. The AgNP treatment in HCT116 cells induced a dose-dependent increase in HIF1α expression, which agrees with the first two studies mentioned. The study that found the decrease in HIF1α expression in breast cancer cells also showed that the combination treatment of hypoxia and AgNPs resulted in decreased HIF1α expression compared to the hypoxic only treatment[90] where, in HCT116 cells, the combined hypoxia and AgNP treatment decreased HIF1α expression relative to the hypoxic only treatment. Under normoxic conditions, AgNPs can increase HIF1α expression, however, under hypoxic conditions, AgNPs may inhibit HIF1α instead. HIF1α plays a role in cancer cell survival and cancer cells are normally in hypoxic microenvironments and so it is possible that AgNP treatment of colon cancer tumours can inhibit their growth and angiogenesis via HIF1α inhibition[90,109,114]. The AgNP treatment induces HIF1α expression, which can then induce the hypoxic stress response in HCT116 cells.

4.2.4 Effect of Nanosilver on the Cell Cycle

Using BrdU staining, the effects of AgNPs on cell cycle progression in HCT116 cells, treated for 24 hours, was determined. The AgNP treatments resulted in significant decreased proportion of cells in the G1 cells and increased proportion of cells in the G2/M phase with no significant change in $AgNO_3$ treatments, indicating that effects in the cell

cycle were due to the AgNPs rather than the silver ions released. The SA and AgNP treatment slightly decreased proportion of cells in the G1 phase and increased proportion of cells in the G2/M phase relative to just the SA treatment. AgNPs are able to significantly disrupt the cell cycle of HCT116 cells, which may be a mechanism which AgNPs induces toxicity.

A study looking at the effects AgNPs has on mouse macrophage cells found AgNPs interacted with DNA and induces G1 phase arrest and blocked the S phase, resulting in apoptosis[196]. Studies using HepG2 cells and human Jurkat cells showed AgNPs induced cell cycle arrest at the S phase[197–199]. Compounds that induce DNA damage are commonly showed to disrupt the cell cycle by inhibition of growth and accumulation of cells in the S phase[2,196]. A study looking at human liver cells showed AgNPs induced cell cycle arrest and a study using biosynthesized AgNP treatment in HCT116 cells also showed G1 phase arrest[155,199]. Another study using biosynthesized AgNPs and HCT116 cells showed AgNP treatment induced cell cycle arrest through interaction with genes that regulate the cell cycle[157]. A study using nuclear and cytoplasmic targeting AgNPs in a human tongue cancer cell line and human keratinocyte cell line, showed the nucleus targeted AgNPs increased the sub-G1 population, inducing apoptosis in the cancer cells. Accumulation of cells in the G2 phase was observed for both the cancer and non-cancer AgNPs treated cells[200]. A study using a non-cancer human intestinal epithelial cell line showed AgNP treatment induced an increase in of cells in the G2/M phase with a decrease of cells from the G1 phase[201]. Starch-coated AgNPs induces arrest of the G2/M phase and DNA damage in human glioblastoma cells and human fibroblasts[79]. Studies using human Jurkat T cells and mouse fibroblast cells found AgNPs induced cell cycle arrest at the G2/M phase[198,202].

G1 phase, which is the first phase and part of interphase in the cell cycle, arrest can occur due to inhibition of histone deacetylase[203]. Lack of nutrients in the cell growth medium can result in G1 phase arrest[204]. The G2 phase is right before mitosis and involves rapid cell growth and protein synthesis, and the M phase is when mitosis occurs where microtubules play a big role. Cyclins play a main role in the G2 phase and so any interference with cyclins can result in G2 phase arrest[205]. Prevention of disassembly or inhibition of formation of microtubules can result in cell cycle arrest at the M phase[206]. It is possible that AgNPs can interact with any of these components involved in the cell cycle to induce cell cycle arrest at the G1 and G2/M phases.

The results from this study showed AgNPs induced a decrease of cells in the G1 phase and increased cells in the G2/M phase. The previously mentioned studies mostly show AgNPs induced cell cycle arrest at the G2/M phase with one study also finding decreased proportion of cells in the G1 phase. The ability of AgNPs to suppress cell proliferation in cancer cells are beneficial in terms of incorporating use of AgNPs in anti-cancer treatments. Further studies looking at the mechanism which AgNPs affects the cell cycle should be conducted as well as studies looking at the difference of effects of AgNPs on cancer versus non-cancer cells such as in the HIEC-6 cells. Other cell cycle markers should be used to study the effects AgNP has on the cell cycle as well.

4.2.5 Wnt Signaling

4.2.5.1 Wntless

Using Western blotting, AgNPs induced a dose-dependent increase in HIF1α expression in 4-hour treated HCT116 cells. No significant changes were found. The highest

20 µg/mL AgNP treatment induced a 2.8-fold increase in Wntless expression. $AgNO_3$ also induced Wntless expression so silver ions may play a role in induction of Wntless expression and therefore, Wnt signaling. Hypoxia and hypoxia with AgNP treatments also increased Wntless expression at similar levels, indicating hypoxia can induce Wnt signaling via upregulation of Wntless protein expression. This is important as tumours are in hypoxic microenvironments, the upregulation of Wnt signaling under hypoxia can aid in the survival of cancer cells.

Using qPCR, the increases in Wntless protein expression could not be explained by upregulation of Wntless gene expression as there were no significant changes to Wntless gene expression with any of the treatments.

There are currently no studies that look at the effect silver nanoparticles may have on Wntless expression. Wntless plays a role in the secretion of various Wnt pathway proteins[137,138] and so upregulation of Wntless can result in activation of the Wnt signaling pathway where the Wnt signaling pathway plays a role in cancer cell survival[130,135]. A study that looked at Wntless expression in breast cancer cells found overexpression of Wntless which was associated with increase tumour size and so Wntless is found to play an important role in breast cancer cells[207]. AgNP seem to increase expression of Wntless proteins and so may activate Wnt signaling in HCT116 which may aid the cells in survival. The Wntless protein and gene expression should be studied in non-cancer cells as well such as the HIEC-6 cells.

4.2.5.2 β-catenin

I did not find any significant changes in β-catenin expression. All treatments slightly induced β-catenin expression so AgNPs may affect the Wnt signaling pathway. Hypoxia and the hypoxia co-treatment with AgNPs induced non-significant increases in β-catenin expression, resulting potential activation of the Wnt signaling pathway, which may be relevant as previously mentioned, the upregulation of Wnt signaling under hypoxia can aid in the survival of cancer cells. The increase in β-catenin expression can increase Wnt signaling through the Wnt/β-catenin pathway, potentially resulting in increase in cell adhesion, cell migration, and/or cell proliferation.

A study looking at zebrafish embryos found increase of β-catenin through immunohistochemical staining after treatment with AgNPs[143]. In bone marrow-derived mesenchymal stem cells, low level AgNP treatment induced significant protein and gene expression of β-catenin[208]. However, a study looking at the effect low level AgNPs has on neural stem cells showed that AgNPs induced aggregation of β-catenin and disrupted β-catenin signaling and found a decrease in cellular β-catenin levels[209]. Increased β-catenin can potentially induce tumourigenesis as the loss of the APC, which plays a major role in degradation of β-catenin, is a major factor for development of colon cancer[210,211] and so can aid in survivability of cancer cells. Our results indicate that AgNPs induce β-catenin expression in HCT116 cells and so can potentially activate the Wnt signaling pathway, aid in survivability of the cancer cells, and/or increase tumourigenesis.

4.2.5.3 PORCN

No significant changes in PORCN expression in the HCT116 were observed. AgNP and $AgNO_3$ treatments showed slight non-significant increase in PORCN expression. Hypoxia increased PORCN expression while hypoxia co-treated with AgNPs decreased PORCN expression relative to the hypoxia only treatment, indicating AgNPs may decrease PORCN expression under hypoxia. This is important as AgNP treatment under hypoxia may be more effective in preventing cancer cell survival and decrease Wnt signaling. No significant changes were found with PORCN gene expression in the HCT116. This may indicate that changes to the protein expression are not due to changes in gene expression.

There are currently no studies that look at the effect silver nanoparticles may have on PORCN expression. PORCN palmitoylates Wnt proteins and allows for extracellular export of these Wnt proteins, resulting in upregulation of downstream signaling[135,136] and so AgNPs can activate this pathway through increase of PORCN expression. However, cancer cells are often in hypoxic microenvironments and the results indicated that AgNP treatment under hypoxia decreased PORCN expression so AgNP treatment in tumours under hypoxia may instead decrease cancer cell survival via decrease of PORCN expression.

4.2.5.4 Wnt3a

No significant changes in Wnt3a expression in the HCT116 were observed. Hypoxic treatments did not induce significant changes to Wnt3a levels. Gene expression of Wnt3a did not significantly change with treatments either. The changes in protein level were likely not due to changes in gene expression.

One study using bone marrow-derived mesenchymal stem cells, low level AgNP treatment induced significant protein and gene expression of Wnt3[208]. Wnt3a plays a role in the canonical Wnt/β-catenin pathway and can aid in cancer cell survival [130]. However, in this study, Wnt3a was not significantly induced with AgNP treatment up to 20 μg/mL. The role AgNPs plays in Wnt3a protein expression may be minimal and any changes in protein level may be due to release of silver ions from the AgNPs and so AgNPs may not affect the Wnt signaling pathway through Wnt3a expression.

4.2.5.5 Wnt5a

No significant changes in Wnt3a expression in the HCT116 were observed. All treatments except for the hypoxia, hypoxia and co-treatment with AgNPs, SA, and SA co-treatment with AgNPs induced a slight, non-significant increase in Wnt5a expression. $AgNO_3$ also induced Wnt5a expression so the release silver ions may play a role in induction of Wnt5a expression. Hypoxia treatment decreased Wnt5a expression and hypoxia co-treated with AgNPs increased Wnt5a expression relative to the hypoxia only treatment. Under hypoxia, AgNPs increases levels of Wnt5a in HCT116 cells. Wnt5a gene expression did not significantly change. The changes in protein level were likely not due to changes in gene expression.

There are currently no studies that look at the effect silver nanoparticles may have on Wnt5a expression. Upregulation of Wnt5a has been shown to induce metastasis of pancreatic cancer cells[149]. Disruption of Wnt5a signaling has also been found to associated with inflammatory diseases such as atherosclerosis and arthritis[212].

Wnt proteins play an important roles in embryonic development, and tissue regeneration of bone marrow, skin, and the intestine[131,132]. Wnt signaling also plays an important role in cancer cell survival and so there are studies that look at targeting Wnt signaling for anti-cancer therapies[130,135,213]. AgNPs induced β-catenin, PORCN, Wnt5a, and slightly induced Wnt3a expression in HCT116 cells which indicates that the AgNPs can activate the Wnt signaling pathway, which can potentially aid in the survival of the cancer cells. Hypoxia treatments generally increased Wnt protein expression where hypoxia with AgNPs cotreatment a decrease in PORCN and Wnt5a expression and slight decrease in β-catenin, Wnt3a, and Nrf1 expression relative to the 20 μg/mL AgNP treatment was observed. This indicates that AgNP treatment under hypoxia may have lesser activation of the Wnt signaling pathway than under normoxia and can potentially decrease activation of Wnt signaling in cells in tumours under hypoxia, therefore decreasing cancer cell survival.

4.2.5.6 Environmental and Human Health Impact of Nanosilver Exposure

With the increase of industrial use of AgNPs, the concern for the environmental contamination and human exposure increases. The AgNPs can be released into the aquatic system after being washed off of various consumer products such as fabric and textile products that incorporate AgNPs into the products[8]. Human exposure to AgNPs can occur dermally, through ingestion, or inhalation through various ways such as from: food containers or packaging, cookware, cosmetics, or AgNP factories[3,9,201].

Predictions of current concentrations of AgNPs in surface water, sewage treatment plant waste, and sewage sludge are predicted to range from 0.03 – 111 ng/L, which are

much lower concentrations than what was tested in this study[50]. Concentrations of AgNPs in sediments in aquatic environments have been found to range from 0.19 – 470.65 µg/kg[48,49]. It is predicted that the AgNP concentration will increase exponentially[50]. Accumulation of AgNPs can occur in aquatic organisms that are exposed to AgNPs released into the aquatic system as waste[51,52]. Exposure to AgNPs can affect development, accumulate in the gills and intestines of fish, alter soil properties, and inhibit plant growth[50–53].

As the industrial use of AgNPs increases so does inadvertent release of AgNPs into the environment where AgNPs can accumulate. Currently environmental levels may not be high enough to induce significant or obvious damage, however, the concentrations of AgNPs in the environment continue to increase and chronic exposure to AgNPs may cause adverse effects in terrestrial and aquatic environments. In the CellROX and MitoSOX experiments, it was shown that at the lowest concentration of 1 µg/mL AgNPs was able to induce a small amount of oxidative stress is both HCT116 and HIEC-6 after 24-hour treatment. Chronic oxidative stress can result in chronic inflammation, resulting in potential progression of various diseases[71].

The low 1 and 10 µg/mL AgNP treatments induced a small amount of *XBP1* splicing and the slight increase in ATF4 translation indicates AgNP exposure can induce ER stress through these pathways. Chronic ER stress can result in apoptosis, irreversible ER stress-induced damage, and play a role in diseases such as cancer, diabetes, and neurodegeneration[118].

HIF1α plays a role in metabolism and so chronic exposure to AgNPs may affect metabolic pathways in aquatic and terrestrial organisms, and humans through upregulation

of HIF1α expression[114]. Studies have found HIF1α can induce cellular ER stress[128,194] and so it's possible that chronic exposure to AgNPs resulting in upregulation of HIF1α can result in generation of chronic ER stress.

Various studies have showed that AgNPs can damage DNA and suppress cell proliferation through disruption of the cell cycle, resulting in potential apoptosis[155,196,198,199,202]. This may have an effect on the development of aquatic and terrestrial organisms that may be exposed to AgNPs in the environment. In terms of human health, disruption of cell cycle regulation can potentially increase the risk of developing cancer[214].

Exposure to AgNPs in the environment and through consumer products can result in increase of Wnt signaling, affecting processes such as cell adhesion, cell proliferation, development, cell migration, and apoptosis[209]. A study looking at the development of zebrafish embryos showed AgNP treatment induced increased β-catenin levels through immunohistochemical staining, indicating AgNP treatment may affect development[143]. Other aquatic or terrestrial organisms that are exposed to AgNPs may also have their growth and development affected through the activation of the Wnt signaling pathway. The Wnt/β-catenin pathway plays a role in liver function[215] and AgNP exposure results in transportation of the AgNPs into the liver and blood[20,41] so AgNP exposure could result in disruption or alteration of liver function via the Wnt/β-catenin pathway.

Current environmental and human exposure to AgNPs may be relatively low with no acute adverse effects, however, there is not much knowledge on the chronic toxicity that low-dose AgNPs may have for relevant environmental models or for humans as most studies use acute and higher concentrations of AgNPs[216]. With growing concerns for

inadvertent environmental and human exposure to AgNPs released from consumer products, further studies should be conducted on the effects of chronic exposure of sub lethal concentrations of AgNPs in the context of both environmental and human health.

4.2.5.7 Nanosilver and Ascorbic Acid Co-treatment

Using the MTT to determine cell viability, various concentrations of SA and SA with AgNP co-treatment were tested in HCT116 and HIEC-6 cells. Sodium ascorbate, a mineral salt of ascorbic acid, was used to prevent significant pH changes to the media cells were incubated in if ascorbic acid was used. The HIEC-6 cells were slightly more sensitive to ascorbic acid treatment than the HCT116 cells (EC_{50} = 5.375 ± 0.918 mM SA) with a lower EC_{50} value of 3.775 ± 0.00803 mM SA. Treatment of varying SA with constant 10 µg/mL in HCT116 and HIEC-6 showed that the HCT116 cells were more sensitive at the lower range of SA concentrations below 2.5 mM and the HIEC-6 cells were more sensitive at the higher range of SA concentrations. This indicates that there is an optimal treatment concentration which the SA and AgNP co-treatment are more toxic to the HCT116 than the HIEC-6. The 1 mM + 10 µg/mL had the greatest difference between the HIEC-6 and HCT116 cell viability where the HCT116 had lower viability. Treatment of varying AgNP concentrations and constant 1 mM SA showed the HIEC-6 were much more resistant with an EC_{50} of greater than 100 µg/mL AgNP than the HCT116 which had an EC_{50} of 86.333 ± 2.696 µg/mL AgNP. The SA co-treatment with AgNPs also seemed to decrease the toxicity AgNPs induced slightly indicated by the higher EC_{50} of AgNPs with the constant SA treatment. This shows that the HCT116 were more susceptible to the combined treatment at constant 1 mM SA and varying AgNP concentrations. This indicates that SA

and AgNP may have potential for anti-cancer therapy as the AgNPs are more toxic to the cancer than non-cancer colon cells.

In the BrdU experiment looking at the effects of AgNPs on cell cycle, the 1 mM SA treatment on its own did not induce any significant changes to the percentage of cells in each cell cycle phase. However, the combined treatments of SA and AgNPs saw a slight additive effect. Using the Tukey's test, there was no significant difference between the 1 mM SA treatment with either of the SA co-treated with AgNPs to determine if the difference between the two treatments were significantly due to the AgNP co-treatment. A slightly greater decrease of cells in the G1 phase and a slightly greater increase induced by the 1 mM SA with 10 and 20 μg/mL AgNP treatment compared to just the 10 or 20 μg/mL AgNP treatments. This indicates that the SA co-treatment treatment slightly increases the effects that AgNPs have on the cell cycle in HCT116 cells and shows further potential for use of SA and AgNP for anti-cancer therapy. However, further studies should be done with HIEC-6 cells to determine if the SA and AgNP treatment affects the cancer cells more.

Using Western blotting, the effect that SA and SA co-treatment with AgNPs had on expression of Nrf1, HIF-1α, Wntless, β-catenin, PORCN, Wnt3a, and Wnt5a were observed. The SA treatment on its own increased expression of Nrf1, Wntless, and Wnt3a. None of the changes in expression were significantly different. For Nrf1, the SA co-treated with AgNP treatment did not find much difference in expression relative to the SA only treatment. For Wntless, the SA co-treated with AgNP treatment decreased protein expression slightly and did not change gene expression relative to the SA only treatment. For Wnt3a, the SA co-treated with AgNP treatment was very similar to the expression of

the SA only treatment. SA co-treatment with AgNP did not seem to change protein expression of Wntless or Nrf1 relative to the SA.

SA treatment on its own decreased HIF-1α and Wnt5a expression. For HIF-1α, the SA co-treated with AgNP treatment slightly decreased expression relative to the SA only treatment. SA treatment on its own did not change levels of expression of PORCN or β-catenin. SA with AgNP co-treatment also decreased HIF-1α, PORCN, β-catenin, and Wnt5a expression relative to the 10 μg/mL AgNP treatments. SA with AgNP co-treatment also slightly increased Nrf1 and had no change in Wnt3a expression relative to the 10 μg/mL AgNP treatments. The SA treatments had varying increase and decreases of Wnt signaling proteins, however, does not induce significant differences in protein or gene expression, indicating SA and SA with AgNP treatment has minimal effect on the Wnt signaling pathway.

As HIF-1α plays an important role in the survival of cancer cells[109,114], the ability of the SA and SA with AgNP treatment to decrease levels of HIF-1α indicates that they can inhibit cancer cell survival by targeting the downregulation of HIF-1α. Wnt signaling also plays an important role in cancer cell survival and so the SA co-treatment with AgNPs can dampen the induction of certain Wnt signaling proteins by the AgNPs, potentially decreasing or at least not increasing Wnt signaling in cancer cells. Further studies should look at the combination of AgNPs and SA treatment on the Wnt signaling pathway and cell cycle in cancer versus non-cancer cells.

SA treatments were done for later experiments only, resulting in many experiments not including the SA and SA/AgNP co-treatments. Further studies should look into the

effects that SA and SA/AgNP co-treatment has on oxidative stress, ER stress, and hypoxic stress responses in both cancer and non-cancer cells.

4.3 Conclusions

The AgNP treatments induced cellular stress responses and crosstalk of stress responses in HCT116 cells as predicted. AgNPs did not elicit significant ER stress response and no significant stress responses were seen with the HIEC-6. HIEC-6 cells were more resistant to both AgNPs and $AgNO_3$ than HCT116 determined by the MTT assay. The mito and cyto-roGFP flow cytometry experiments were ineffective and did not yield significant results regarding mitochondrial and cytoplasmic oxidative stress. Another method of measurement or use of other fluorescent probes or dyes would yield better results. The CellROX experiments showed AgNP treatment resulted in slight induction of similar levels of cytoplasmic ROS in both HCT116 and HIEC-6 cells. The MitoSOX experiments showed AgNP treatment resulted in significant, dose-dependent increase in mitochondrial ROS in the HCT116 cells while very little increase in mitochondrial ROS was seen in the HIEC-6. The AgNP treatment induced a non-significant increase in Nrf1 expression and a significant, dose-dependent increase in Nrf2 expression in HCT116 cells. Hypoxia co-treated with 20 μg/mL AgNP slightly decreased Nrf1 expression relative to the AgNP treatment. There is more evidence of cross-talk of stress responses occurring in the HCT116 than the HIEC-6 cell line: hypoxia treatment attenuated both cytoplasmic and mitochondrial ROS production in HCT116 cells and a slight attenuation of cytoplasmic ROS in the HIEC-6 cells, however, further research must be done. Slight increase in *xbp1* splicing and atf4 translation was seen in HCT116-XBP1 and HCT116-ATF4 cells treated

with AgNPs. Hypoxia treatment induced attenuation of both *xbp1* splicing and ATF4 translation in both the HCT116-XBP1 and HCT116-ATF4 cells. The AgNP treatment in HCT116 induced significant, dose-dependent increase in HIF1α expression. Cell cycle disruption was significantly induced by AgNP treatment. A dose-dependent decrease of cells in the G1 phase and increase of cells in the G2/M phase of the cell cycle of HCT116 cells was observed. Wnt signaling in HCT116 is also affected in AgNP treated HCT116 cells: AgNPs induced increased Wntless, β-catenin, PORCN, and Wnt5a expression and slight increase in Wnt3a expression.

Various observations indicate AgNPs has potential to be incorporated into anti-cancer therapies. The AgNP treatment induced more mitochondrial ROS in HCT116 cells compared to the non-cancer HIEC-6 cells, the HCT116 cells were more susceptible to AgNP toxicity than the non-cancer HIEC-6 cells, and the cell cycle is disrupted by AgNP treatment in HCT116 cells. Future studies could also determine if cancer cells have increased uptake of AgNPs, due to their rapid cell division and growth.

The AgNPs and SA was shown to act synergistically to enhance the effects AgNPs had on the HCT116 cells. Use of ascorbic acid co-treatment generally enhanced the effects that AgNP treatments had on the HCT116 cells where SA and AgNP treatment decreases expression of proteins involved in cancer cell survival and increasing cell cycle effects induced by AgNPs. SA and AgNP treatment had an additive effect in cell cycle disruption, at lower SA doses tested showed higher toxicity to HCT116 than HIEC-6 cells, decreased the effect AgNPs had on the expression of Wnt proteins, PORCN, β-catenin, and Wnt5a expression relative to the equivalent AgNP treatments, and decrease in HIF-1α expression.

These results indicate SA and AgNPs may be a good potential candidate for anti-cancer therapy.

As exposure of AgNPs increases in the environment and to humans through inadvertent contact with or release from consumer products is a concern as there is a lack of data on chronic low-dose exposure to AgNPs. Accumulation of AgNPs in aquatic or terrestrial systems or organisms is also a concern. Expression of HIF1α can be upregulated with AgNP exposure, which can result in activation of hypoxic stress response, which can induce ER stress, resulting in potential apoptosis or cellular damage. ROS generation is induced by AgNP exposure which can induce cellular damage, resulting in apoptosis and/or development of various oxidative stress-related diseases. The cell cycle is disrupted after AgNP exposure, resulting in potential apoptosis, increases risk of cancer, and may disrupt development. These effects that AgNPs may have can affect aquatic and terrestrial organisms and human health. Further studies need to be conducted to explore the environmental and human health impacts chronic exposure of low-dose AgNPs may have. Further studies should also focus on testing different cancer and non-cancer primary cell lines to further explore the potential of AgNP and ascorbic acid for anti-cancer therapy. The results shown in this study are preliminary and need further research to confirm and explore these results further.

Appendix

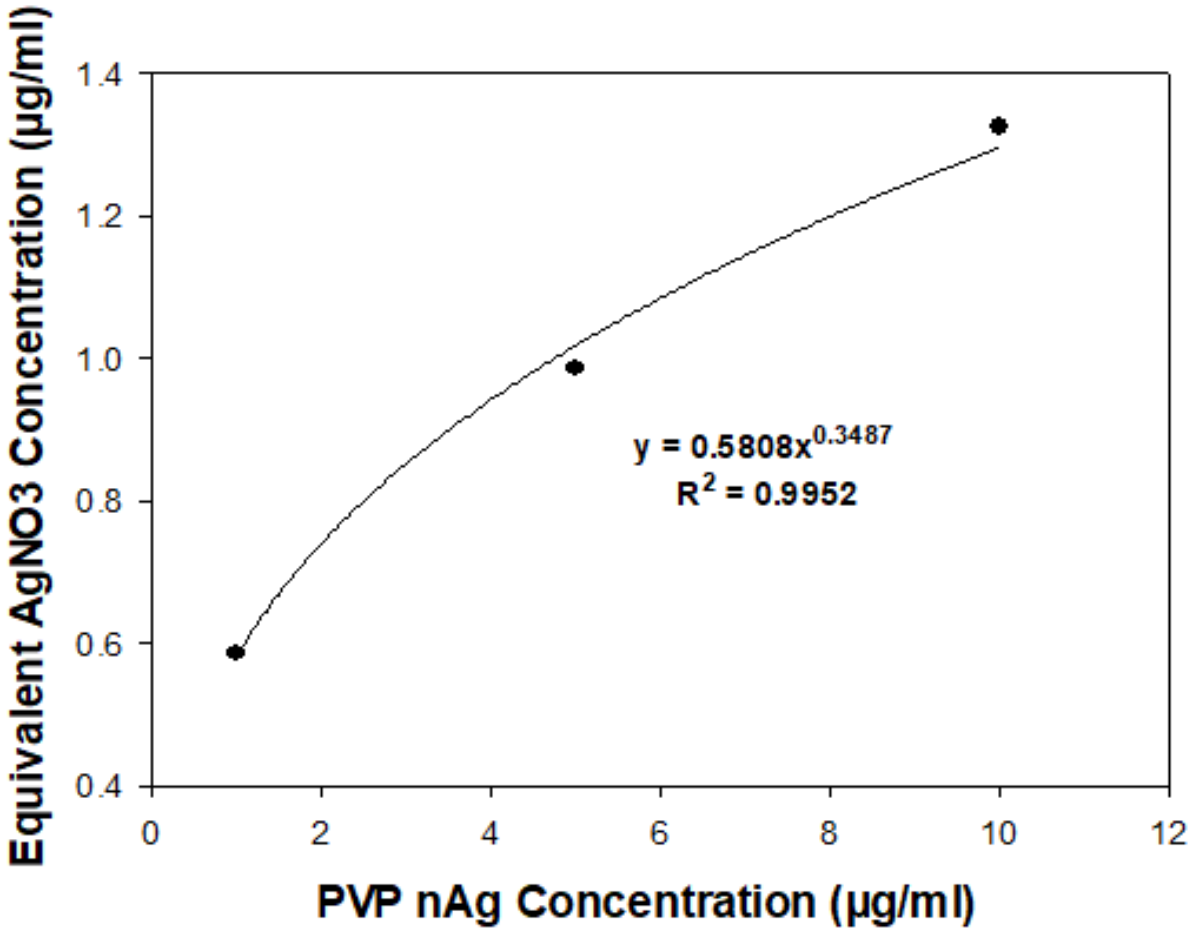

Figure A1. Using ICP-MS to determine equivalent concentrations of $AgNO_3$ for 30 µg/mL of 10 nm PVP coated nanosilver (nAg) at 4 hours. A power line of best fit was used: $y = 0.5808x^{0.3487}$, where $R^2 = 0.9952$. 1 replicate.

Sample Calculations

For proposed $AgNO_3$ at 20 µg/mL:

Determine percent increase from 5 µg/mL AgNP to 10 µg/mL AgNP:

$$\% \, increase = \frac{(AgNO_3 \; equivalent \; at \; 10 \; \mu g/mL)}{(AgNO_3 \; equivalent \; at \; 5 \; \mu g/mL)} * 100\%$$

$$= \frac{(1.326 \; \mu g/mL)}{(0.986 \; \mu g/mL)} * 100\%$$

$$= 134.493\%$$

Multiply percent increase by the $AgNO_3$ equivalent (µg/mL) at 10 µg/mL AgNP to get proposed $AgNO_3$ equivalent at 20 µg/mL AgNP:

$$Proposed \; AgNO3 \; equivalent \; at \; 20 \; \mu g/ml \; nAg \; = 0.134 * 1.326 \; \mu g/ml$$

$$= 1.783 \; \mu g/ml$$

For proposed $AgNO_3$ equivalent at 30 µg/mL AgNP, the line equation $y = 0.5808x^{0.3487}$ from Figure A1 (Appendix) was used instead, where y is the $AgNO_3$ equivalent concentration and x is the AgNP concentration.

$$Proposed \; AgNO_3 \; equivalent \; at \; 30 \; \mu g/ml \; nAg = 0.5808 * 30^{0.3487}$$

$$= 1.902 \; \mu g/ml$$

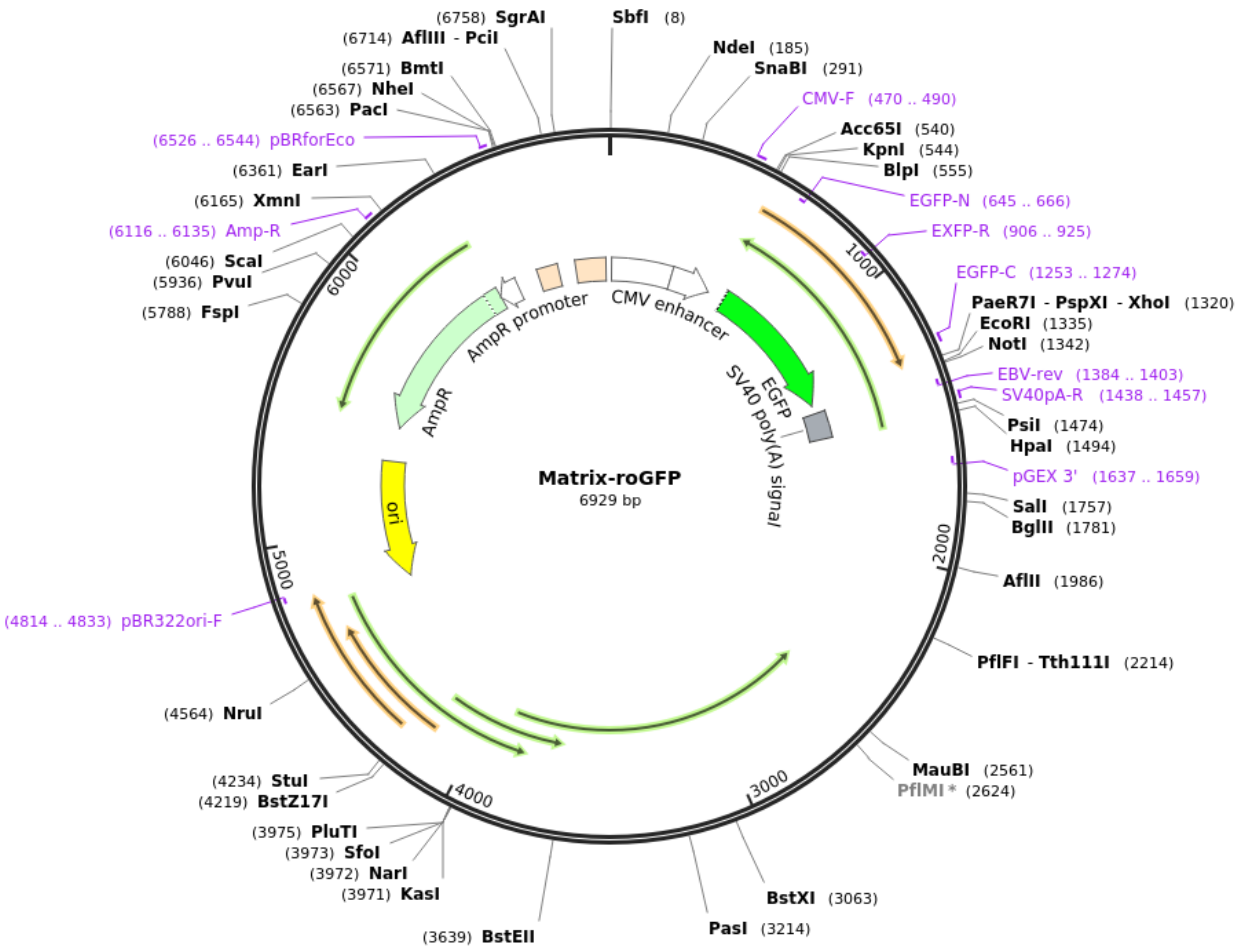

Figure A2. Representation of the Matrix-roGFP2 plasmid. HEK293T cells were transfected with this mitochondrial matrix oxidative stress sensor plasmid. Matrix-roGFP was a gift from Paul Schumacker (Addgene plasmid # 49437; http://n2t.net/addgene:49437; RRID:Addgene_49437)[159].

Figure A3. Representation of the plasmid. HEK293T cells were transfected with this mitochondrial oxidative stress sensor plasmid. The pMOS015: mito-roGFP2-Orp1 H_2O_2 oxidation sensor (mitochondrial) was a gift from Adam Cohen (Addgene plasmid # 163059; http://n2t.net/addgene:163059; RRID:Addgene_163059)[217].

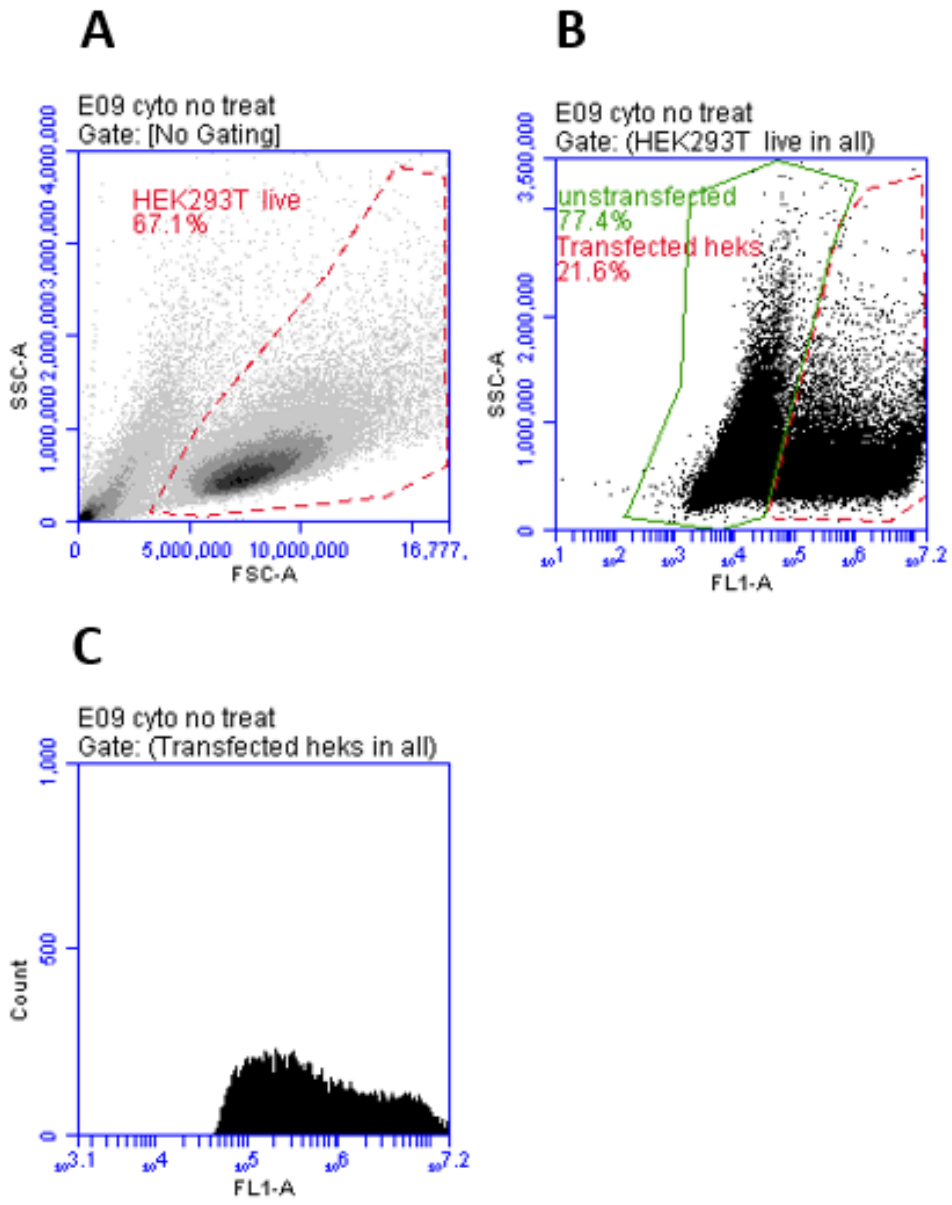

Figure A4. Example of flow cytometry data analysis from Cyto-roGFP experiments using the BD Acurri c6 software. Mito-roGFP transfected HEK293T cells were analyzed the same way as the Cyto-roGFP experiments. A) HEK293T cells were gated for the live cells. B) Live HEK293T cells were gated for transfected cells only. C) Mean fluorescence intensity was measured from the transfected cells on the FL1 channel.

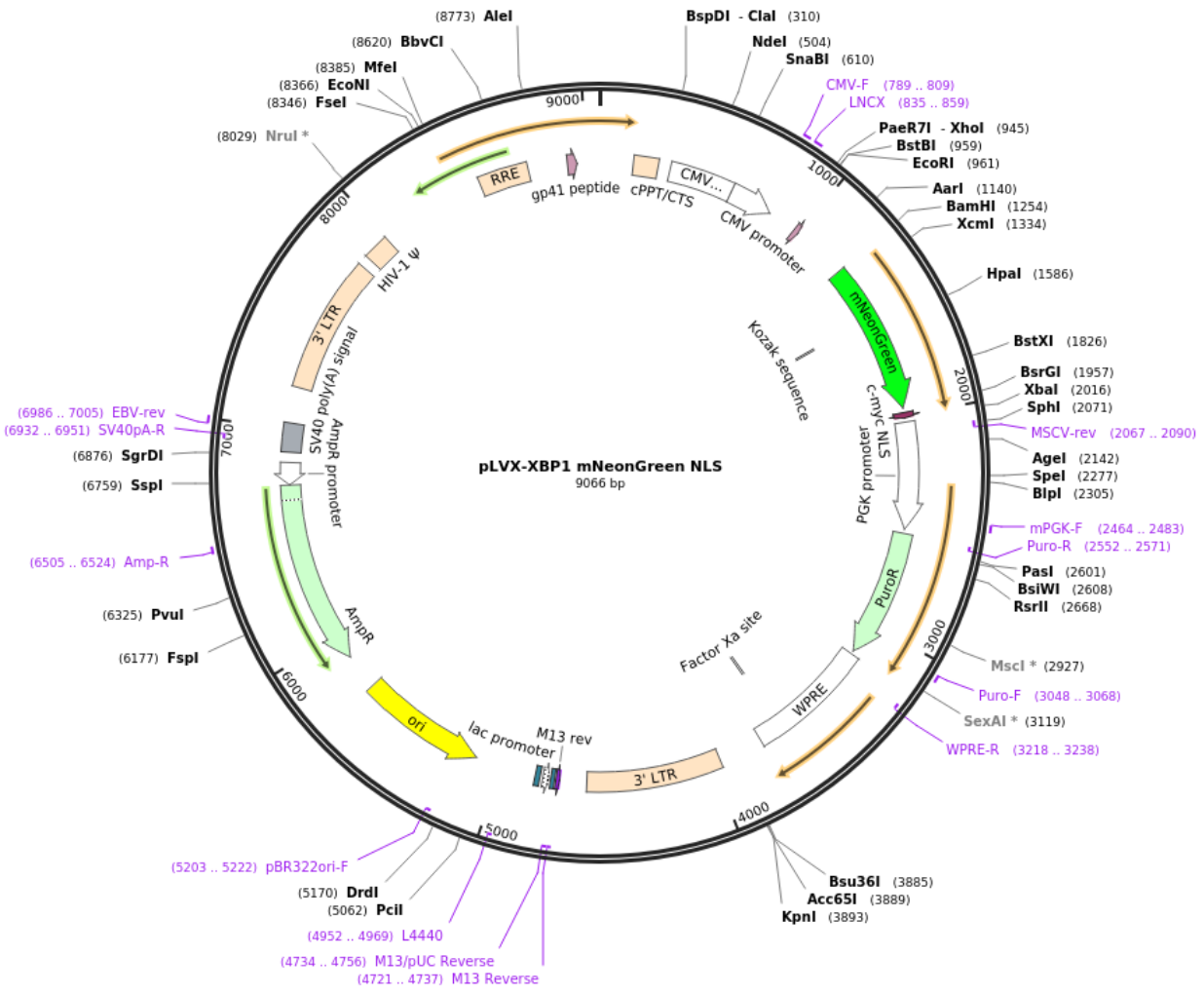

Figure A5. Representation of the pLVX-XBP1 mNEonGreen NLS plasmid. HCT116-XBP1 cells were transfected with this XBP1 splicing fluorescent reporter with mNeonGreen plasmid. The pLVX-XBP1 mNeonGreen NLS was a gift from David Andrews (Addgene plasmid # 115968; http://n2t.net/addgene:115968; RRID:Addgene_115968)[150].

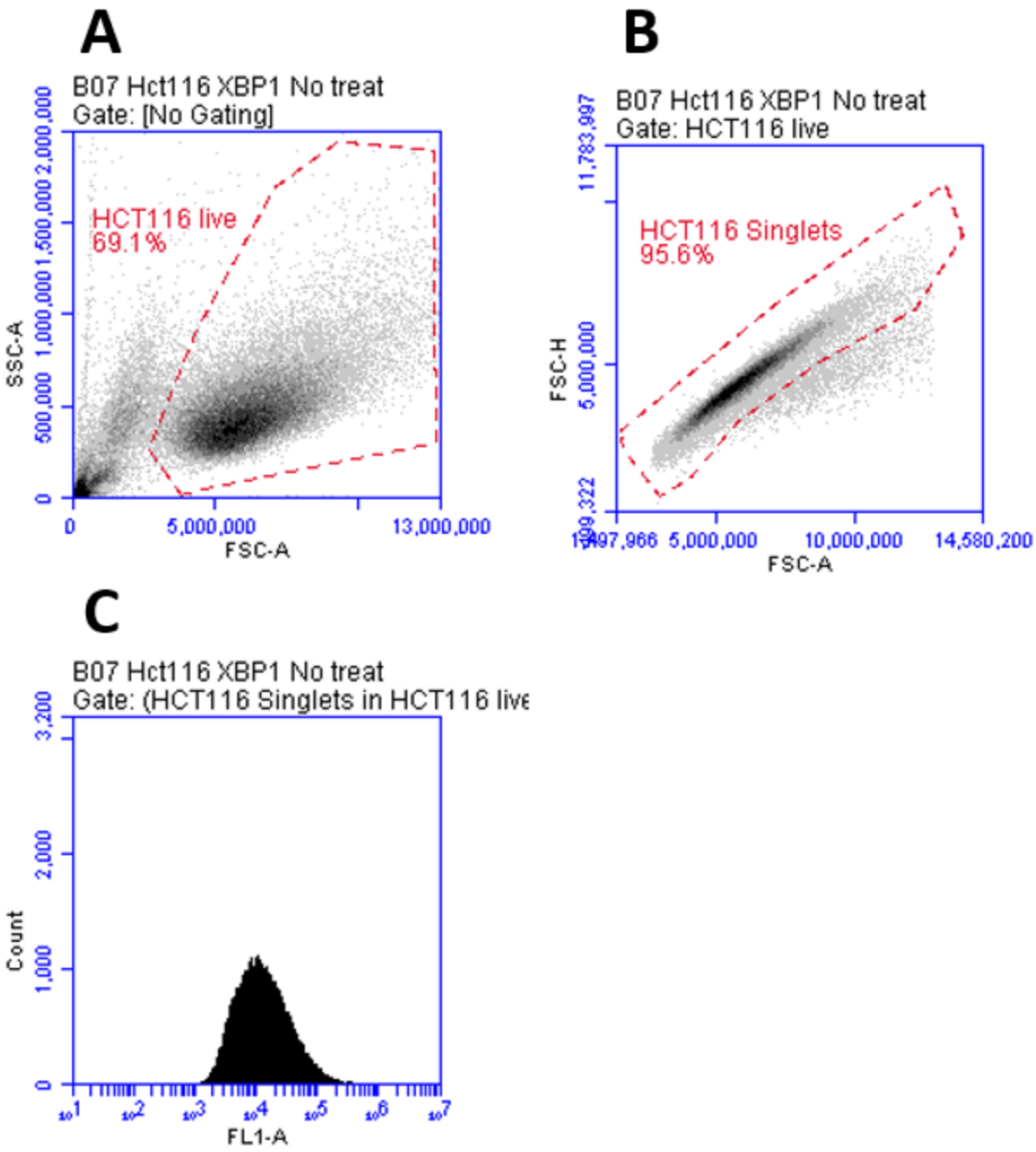

Figure A6. Example of flow cytometry data analysis from HCT116-XBP1 experiments using the BD Acuri c6 software. A) HCT116-XBP1 cells were gated for live cells. B) HCT116-XBP1 live cells were then gated for singlet cells. C) The singlet cells were then gated to measure mean fluorescence intensity on the FL1 channel.

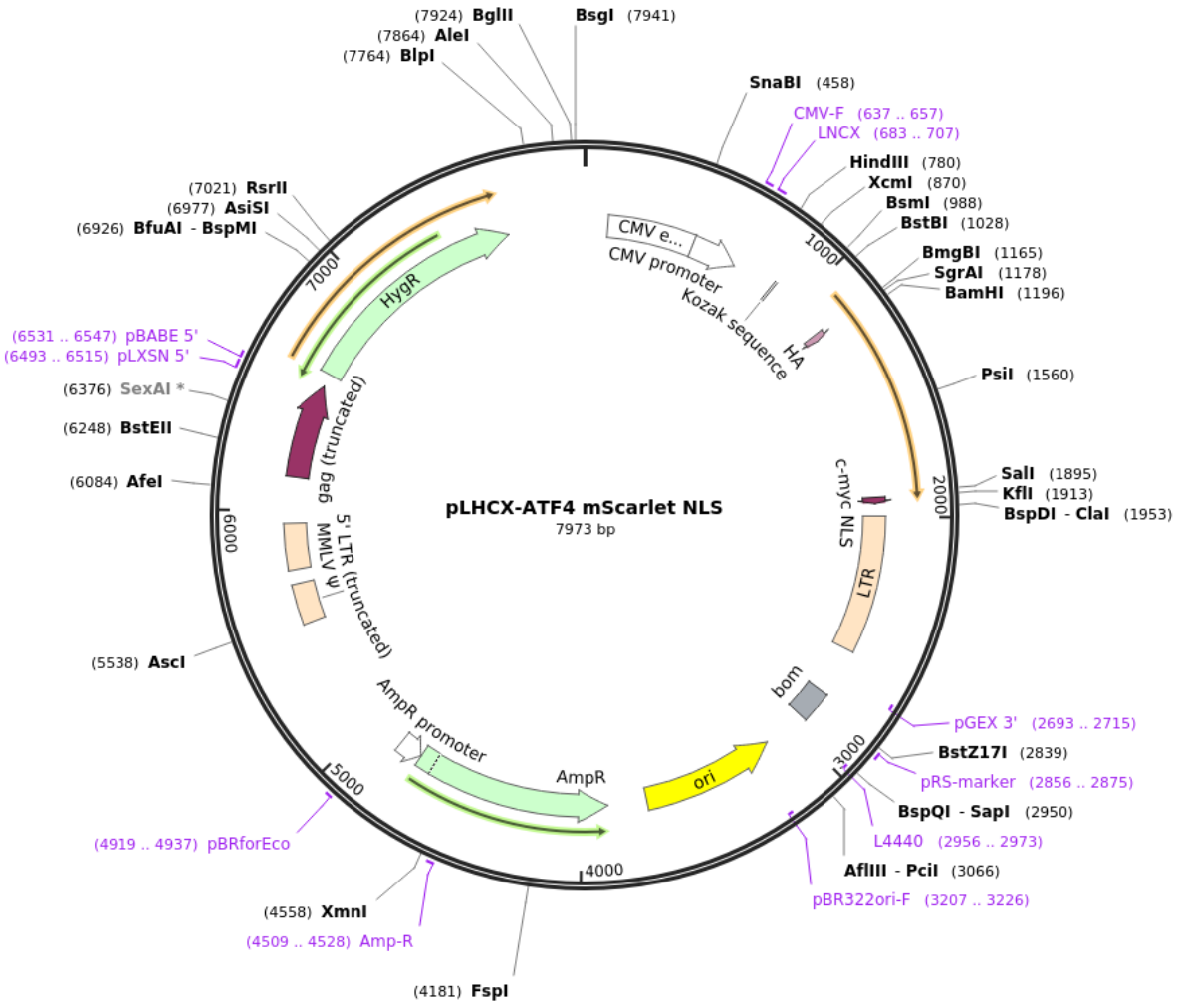

Figure A7. Representation of pLHCX-ATF4 mScarlet NLS plasmid. HCT116-ATF4 cells were transfected with this ATF4 translation at ORF3 fluorescent reporter with mScarlet-I (retroviral vector backbone) plasmid. The pLHCX-ATF4 mScarlet NLS was a gift from David Andrews (Addgene plasmid # 115970; http://n2t.net/addgene:115970; RRID:Addgene_115970)[150].

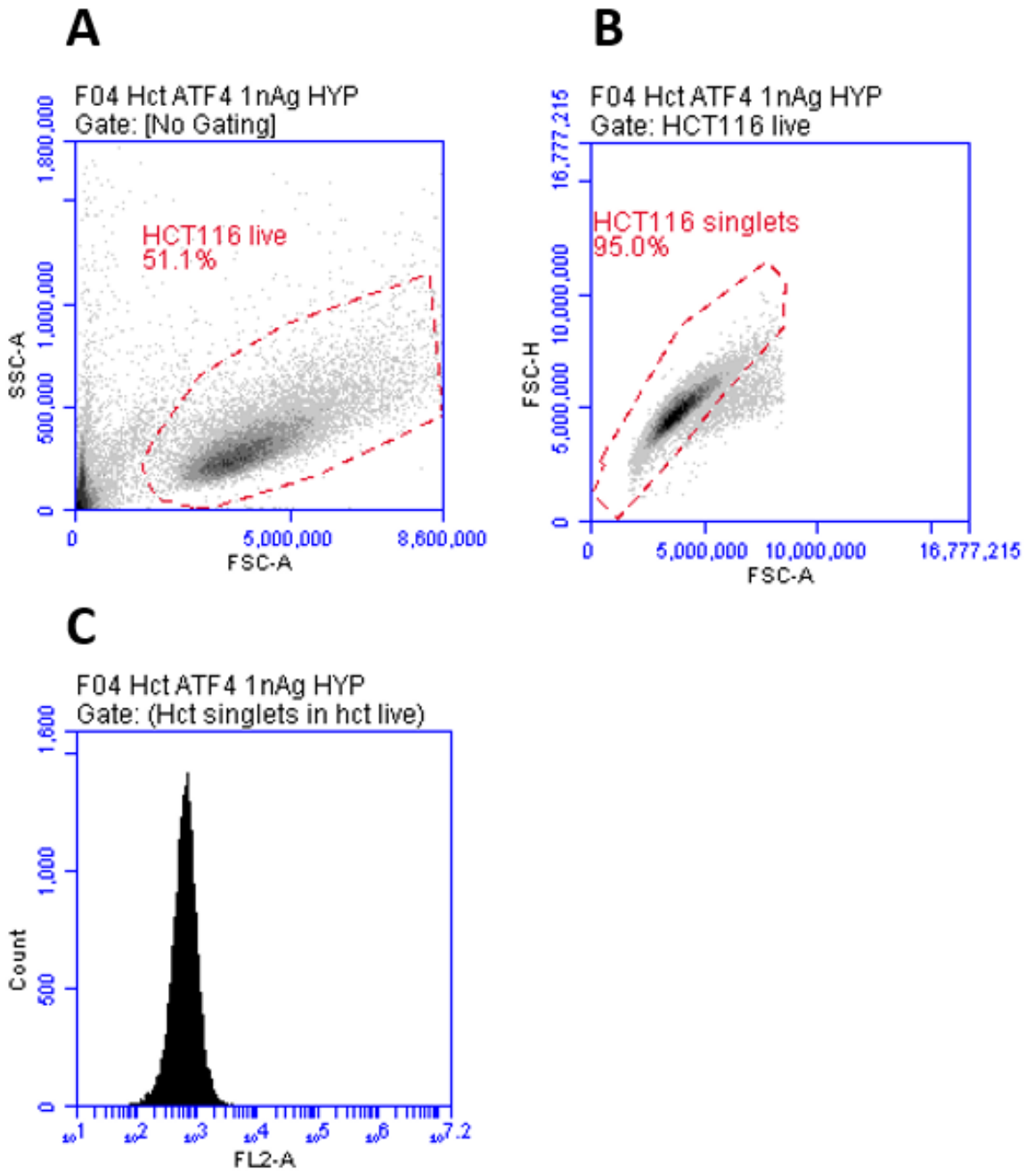

Figure A8. Example of flow cytometry data analysis from HCT116-ATF4 experiments using the BD Acuri c6 software. A) HCT116-ATF4 cells were gated for live cells. B) HCT116-ATF4 live cells were then gated for singlet cells. C) The singlet cells were then gated to measure mean fluorescence intensity on the FL2 channel.

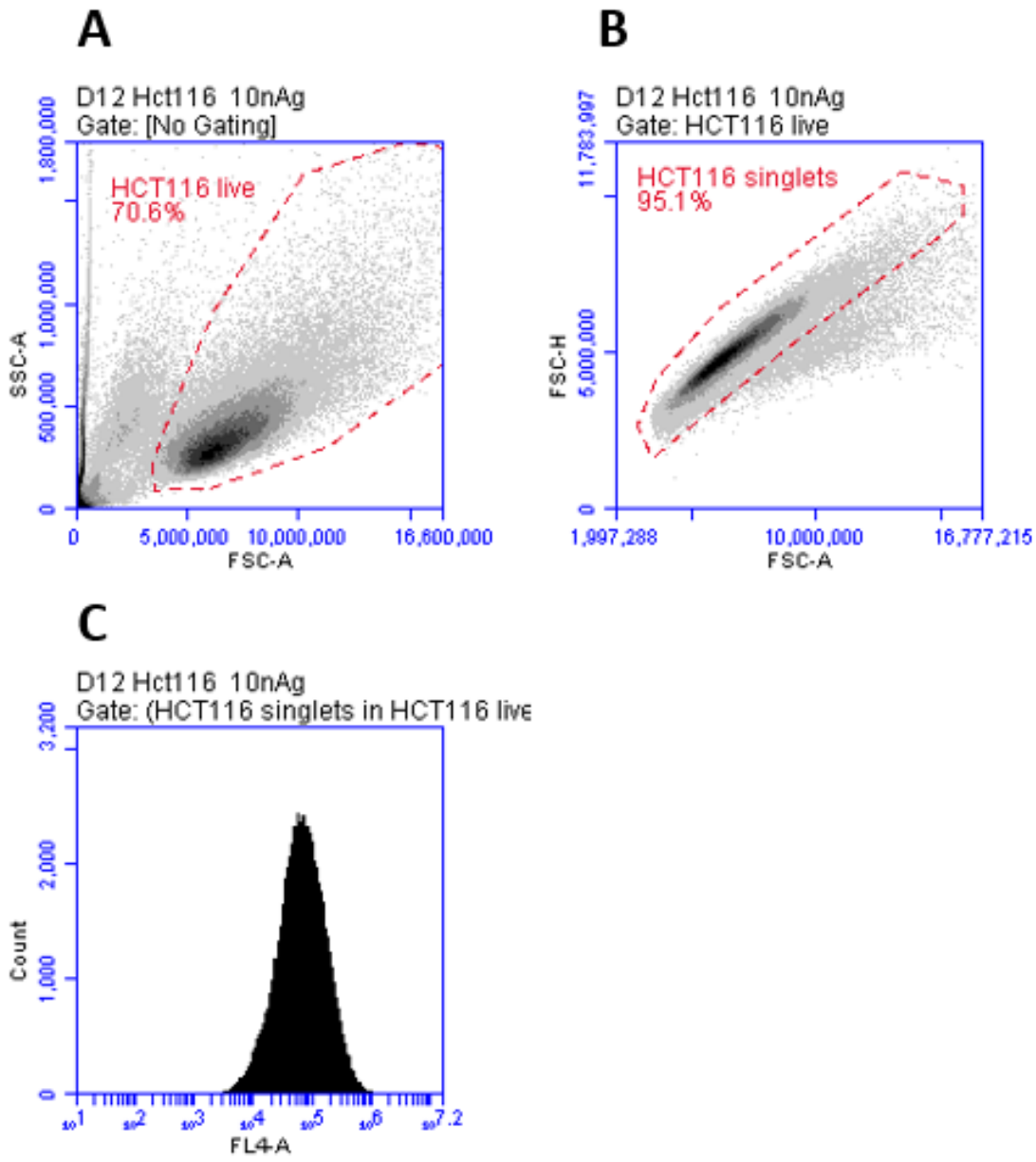

Figure A9. Example of flow cytometry data analysis from HCT116 CellROX experiments using the BD Accuri c6 software. A) HCT116 cells were gated for live cells. B) HCT116 live cells were then gated for singlet cells. C) The singlet cells were then gated to measure mean fluorescence intensity on the FL4 channel.

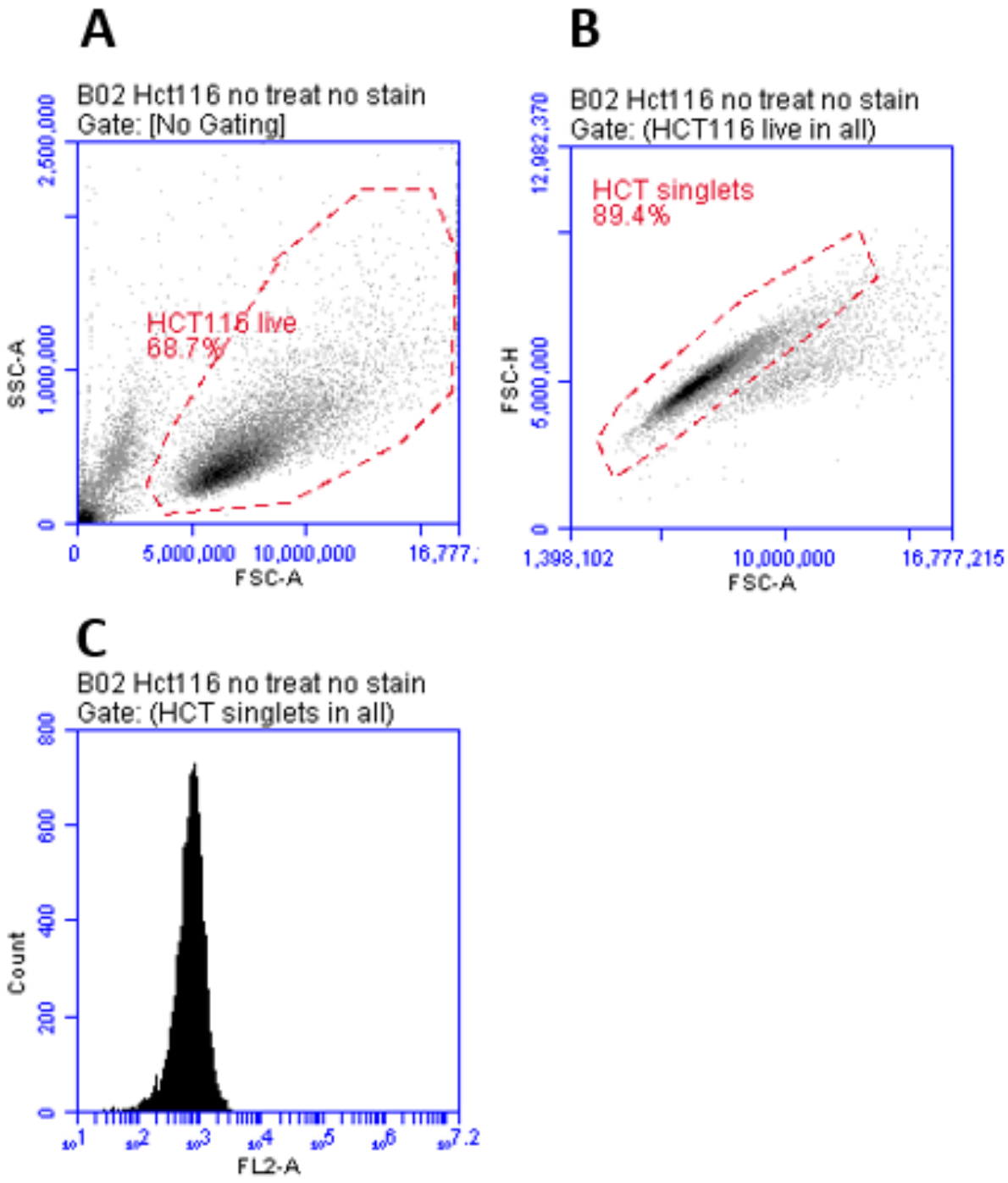

Figure A10. Example of flow cytometry data analysis from HCT116 MitoSOX experiments using the BD Accuri c6 software. A) HCT116 cells were gated for live cells. B) HCT116 live cells were then gated for singlet cells. C) The singlet cells were then gated to measure mean fluorescence intensity on the FL2 channel.

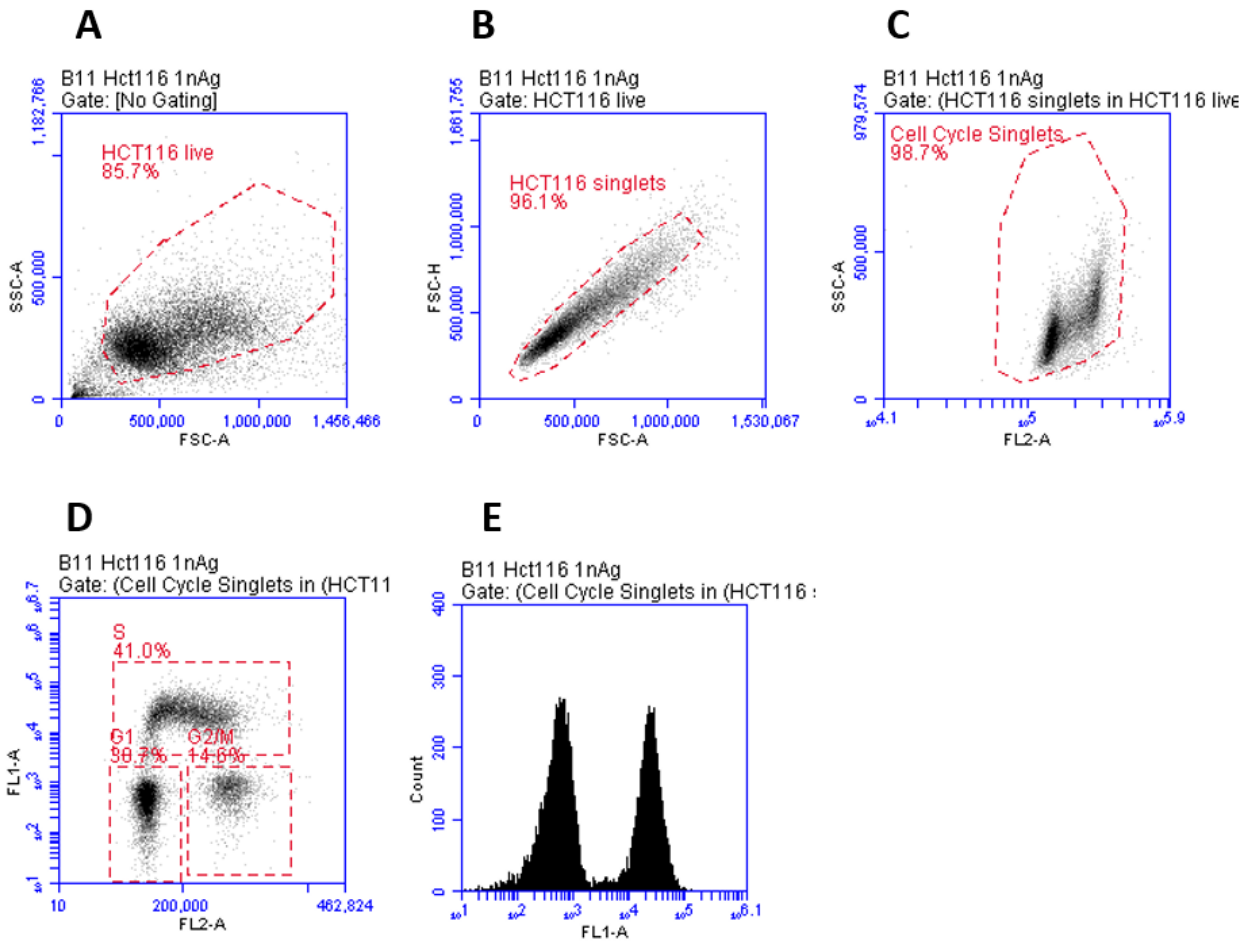

Figure A11. Example of flow cytometry data analysis from HCT116 BrdU experiments using the BD Accuri c6 software. A) HCT116 cells were gated for live cells. B) HCT116 live cells were then gated for singlet cells. C) Propidium iodide (PI) cells were stained and labeled the cell cycle singlets. D) Cells in the S, G1, and G2/M phases were gated to measure the percentage of PI and BrdU stained cells in each cell cycle phase. E) The singlet cells were gated to measure mean fluorescence intensity. Peaks in fluorescence confirm BrdU and/or PI staining.

Figure A12 shows the nuclear and cytosolic protein expression of AhR in HCT116 cells treated for 4 hours. The AgNP and $AgNO_3$ treatments induced an increase in nuclear AhR protein expression. TCDD, an AhR activator also induced an increase in nuclear AhR protein expression. No significant increase of nuclear AhR occurred. The 10 and 20 µg/mL AgNP treatments induced increase in cytosolic AhR. The 20 µg/mL induced a significant increase in cytosolic AhR. TCDD did not induce an increase in cytosolic AhR protein expression.

Figure A13 shows gene expression of AhR in HCT116 cells treated for 4 hours using qPCR. The lowest 0.59 µg/mL $AgNO_3$ induced significant AhR gene expression. The lowest 1 µg/mL AgNP treatment increased the most AhR gene expression out of all the nAg treatments.

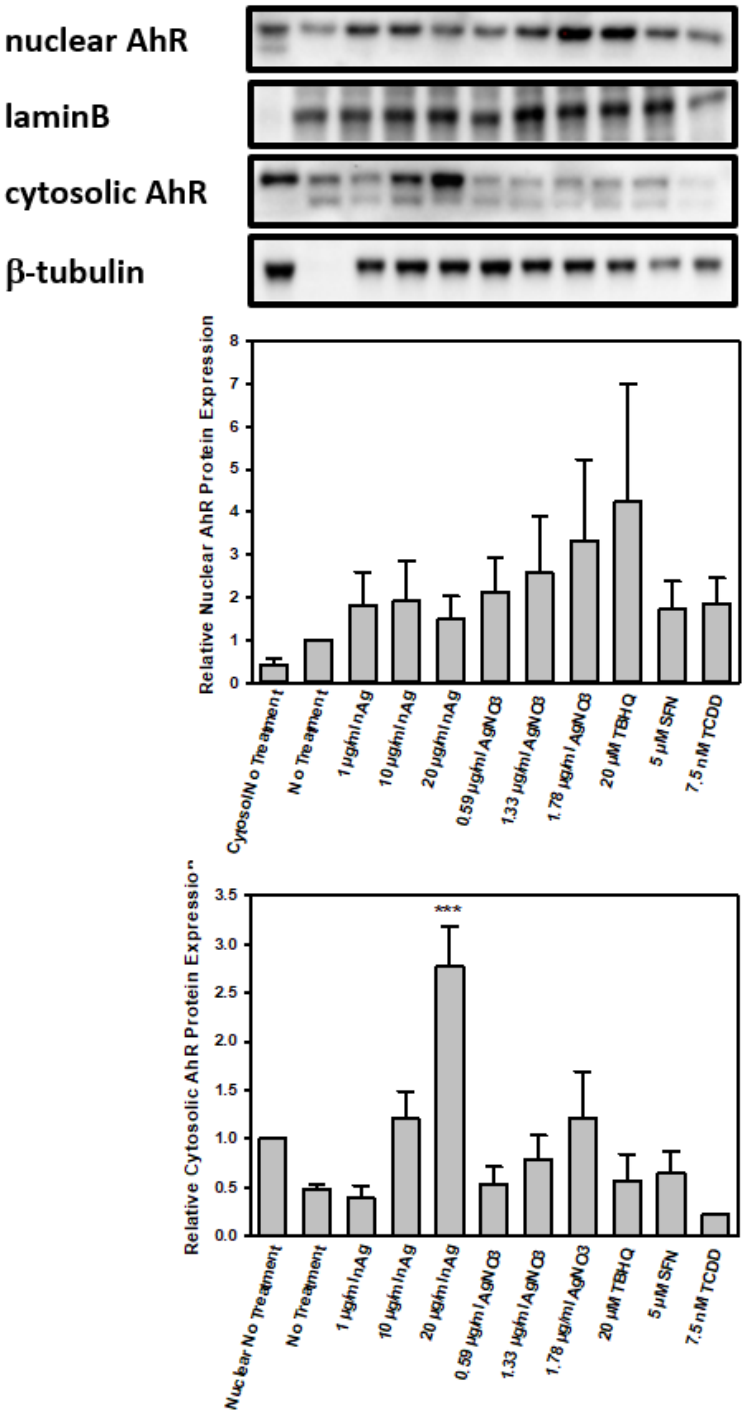

Figure A12. Western blotting for AhR protein expression in nuclear and cytosolic fractions from HCT116 cells treated for 4 hours. Protein expression of each sample was normalized to β-tubulin. Standard error, one-way ANOVA, and the Dunnett's test (*p<0.05, **p<0.01, ***p<0.001). 3 replicates.

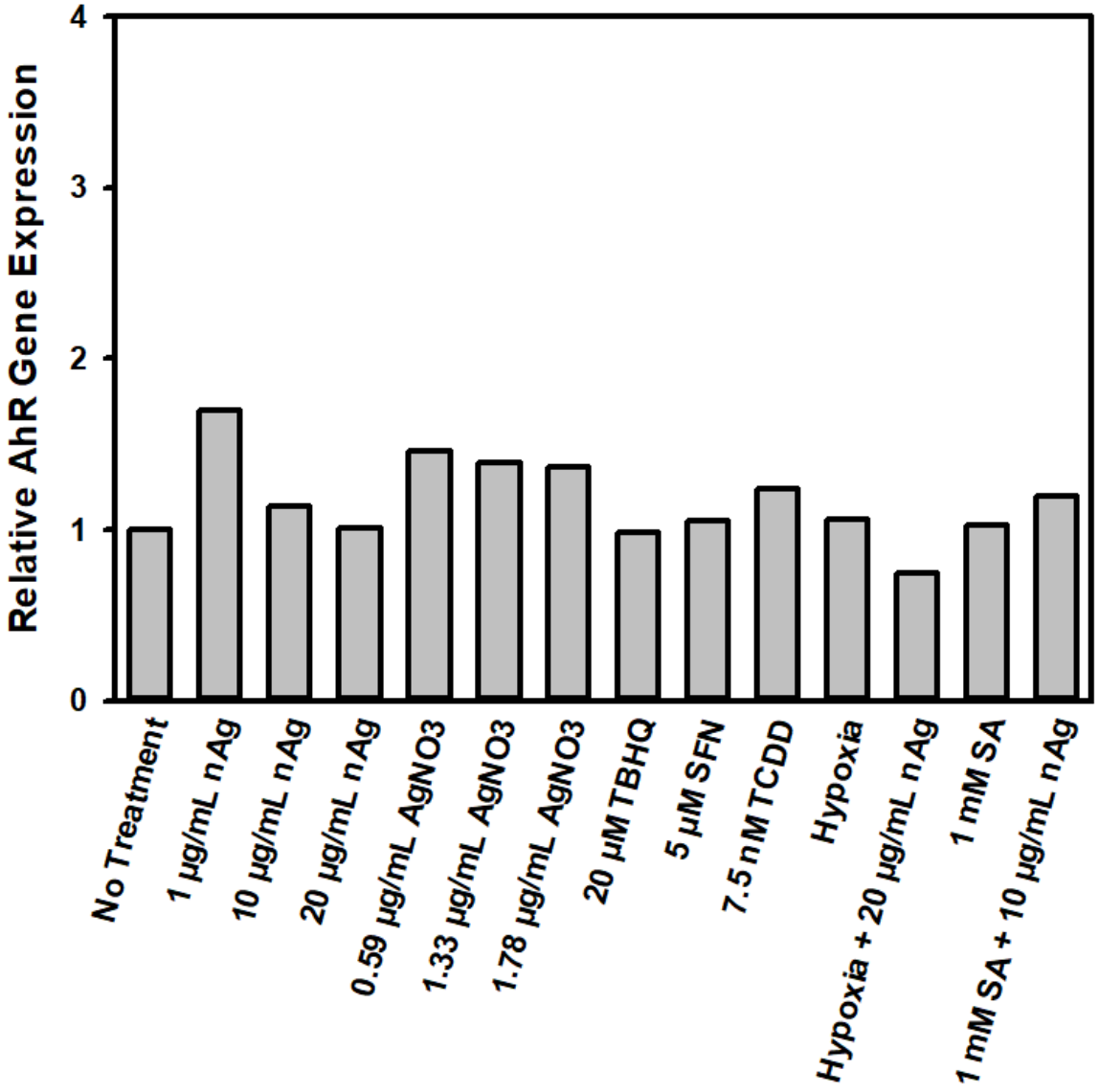

Figure A13. Using qPCR to determine AhR gene expression in HCT116 cells treated for 4 hours. One-way ANOVA, and the Dunnett's test were used (*$p<0.05$, **$p<0.01$, ***$p<0.001$). 3 replicates.

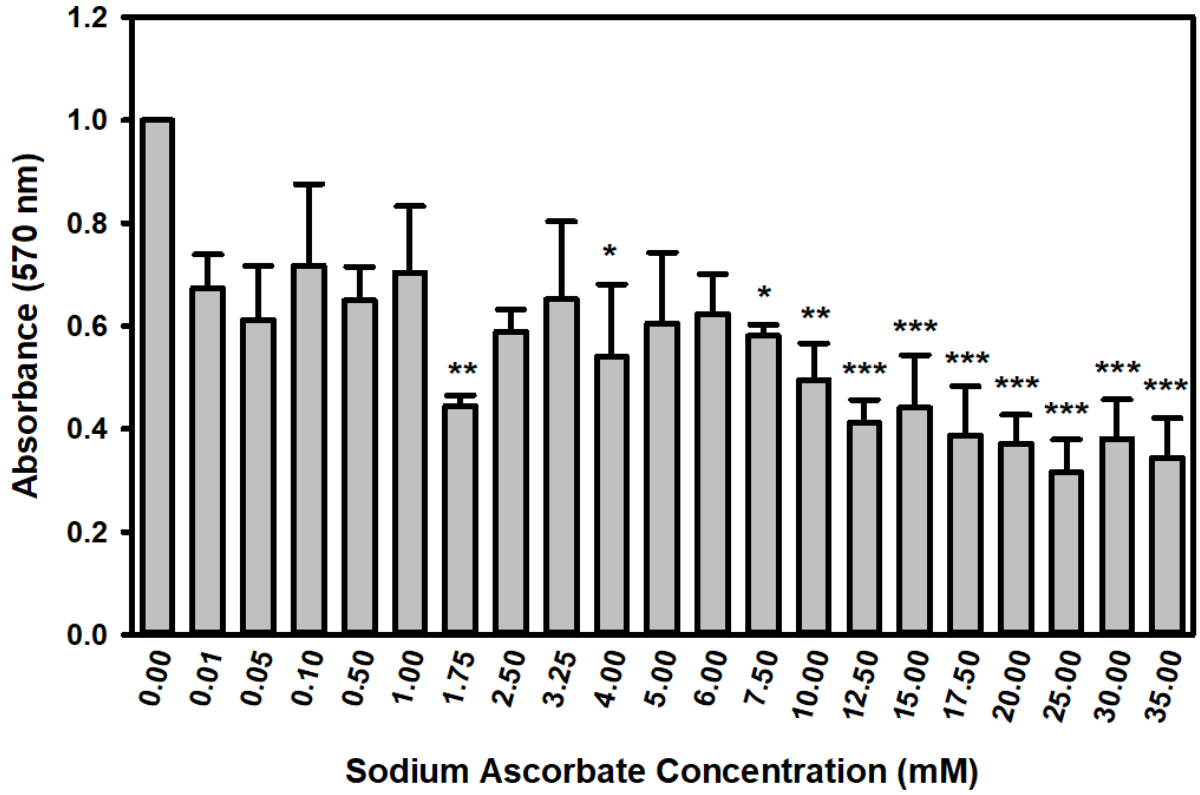

Figure A14. Determining cell viability in HCT116 cells using the MTT assay. HCT116 cells were treated with sodium ascorbate for 1 hour with 24-hour recovery. HCT116 SA EC_{50} = N/A. 1.75, 4.0, 7.5, 10.0, 12.5, 15.0, 17.50, 20.0, 25.0, 30.0, and 35.0 mM treatments were statistically different. Standard error, one-way ANOVA, and Dunnett's test were used (*$p<0.05$, **$p<0.01$, ***$p<0.001$). 4 replicates.

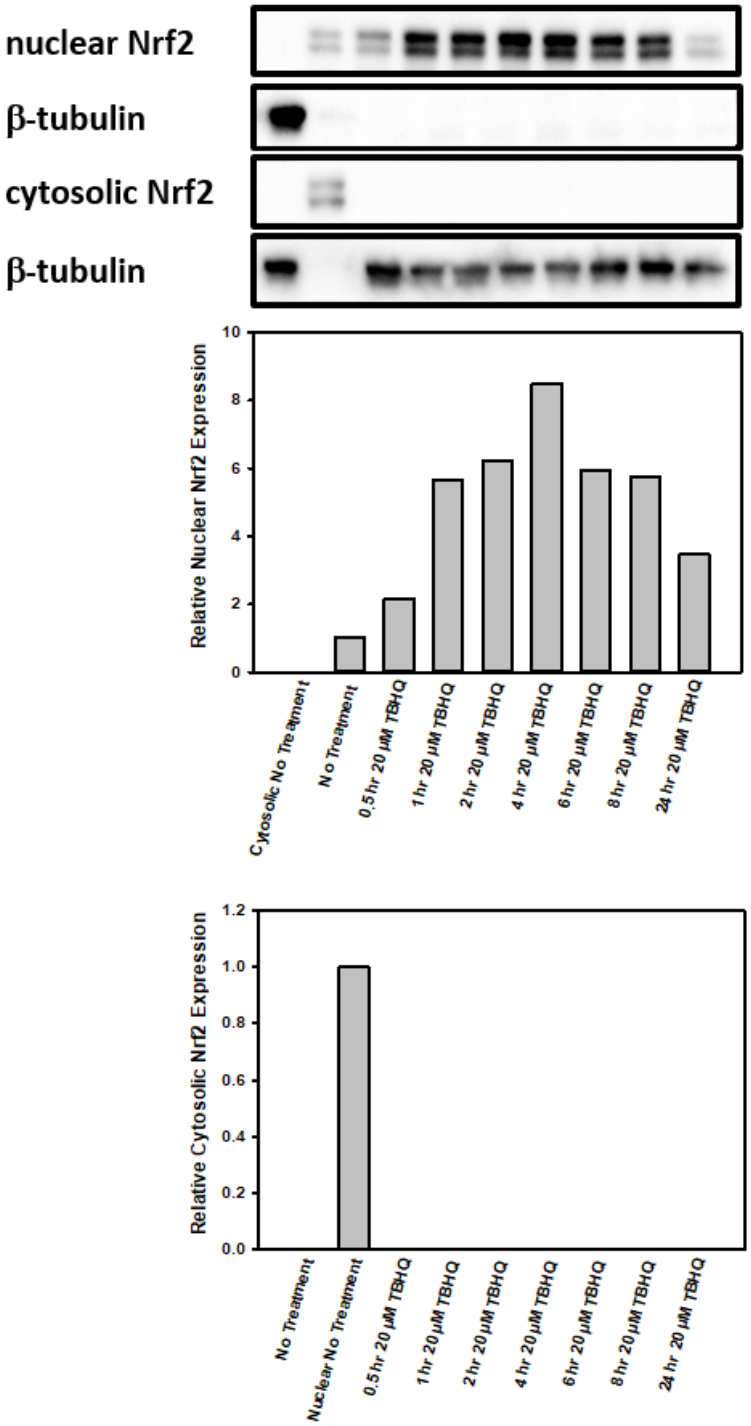

Figure A15. Western blotting for Nrf2 expression in HCT116 cells. Time course using various concentrations of TBHQ, a known Nrf2 activator. One-way ANOVA, and Dunnett's test were used (*$p<0.05$, **$p<0.01$, ***$p<0.001$). 2 replicates. Experiment conducted by S. Cameron at Carleton University.

References

1. Beer C, Foldbjerg R, Hayashi Y, Sutherland DS, Autrup H. Toxicity of silver nanoparticles - nanoparticle or silver ion? *Toxicol Lett*. 2012;208(3):286-292. doi:10.1016/j.toxlet.2011.11.002
2. Ahamed M, Alsalhi MS, Siddiqui MKJ. Silver nanoparticle applications and human health. *Clin Chim Acta*. 2010;411(23-24):1841-1848. doi:10.1016/j.cca.2010.08.016
3. Najahi-Missaoui W, Arnold RD, Cummings BS. Safe nanoparticles: are we there yet? *Int J Mol Sci*. 2020;22(1). doi:10.3390/ijms22010385
4. Fröhlich E. Europe PMC Funders Group Cellular targets and mechanisms in the cytotoxic action of non- biodegradable engineered nanoparticles. 2013;14(9):976-988.
5. Zhang W. Nanoparticle aggregation: principles and modeling. *Adv Exp Med Biol*. 2014;811:19-43. doi:10.1007/978-94-017-8739-0_2
6. Schrand AM, Rahman MF, Hussain SM, Schlager JJ, Smith DA, Syed AF. Metal-based nanoparticles and their toxicity assessment. *Wiley Interdiscip Rev Nanomed Nanobiotechnol*. 2010;2(5):544-568. doi:10.1002/wnan.103
7. Akter M, Sikder MT, Rahman MM, et al. A systematic review on silver nanoparticles-induced cytotoxicity: Physicochemical properties and perspectives. *J Adv Res*. 2018;9:1-16. doi:10.1016/j.jare.2017.10.008
8. Yu S, Yin Y, Liu J. Silver nanoparticles in the environment. *Environ Sci Process Impacts*. 2013;15(1):78-92. doi:10.1039/c2em30595j
9. Lewinski N, Colvin V, Drezek R. Cytotoxicity of nanoparticles. *Small*.

2008;4(1):26-49. doi:10.1002/smll.200700595

10. Chenthamara D, Subramaniam S, Ramakrishnan SG, et al. Therapeutic efficacy of nanoparticles and routes of administration. *Biomater Res*. 2019;23(1):1-29. doi:10.1186/s40824-019-0166-x

11. El-Sayed A, Kamel M. Advances in nanomedical applications: diagnostic, therapeutic, immunization, and vaccine production. *Environ Sci Pollut Res*. 2020;27(16):19200-19213. doi:10.1007/s11356-019-06459-2

12. Mitchell MJ, Billingsley MM, Haley RM, Wechsler ME, Peppas NA, Langer R. Engineering precision nanoparticles for drug delivery. *Nat Rev Drug Discov*. 2021;20(2):101-124. doi:10.1038/s41573-020-0090-8

13. Wolfram J, Zhu M, Yang Y, et al. Safety of nanoparticles in medicine. *Curr Drug Targets*. 2015;16(14):1671-1681. doi:10.2174/1389450115666140804124808

14. Bobo D, Robinson KJ, Islam J, Thurecht KJ, Corrie SR. Nanoparticle-based medicines: a review of fda-approved materials and clinical trials to date. *Pharm Res*. 2016;33(10):2373-2387. doi:10.1007/s11095-016-1958-5

15. Khanna P, Ong C, Bay BH, Baeg GH. Nanotoxicity: An interplay of oxidative stress, inflammation and cell death. *Nanomaterials*. 2015;5(3):1163-1180. doi:10.3390/nano5031163

16. Mariam J, Sivakami S, Dongre PM. Albumin corona on nanoparticles–a strategic approach in drug delivery. *Drug Deliv*. 2016;23(8):2668-2676. doi:10.3109/10717544.2015.1048488

17. Hewitt RE, Chappell HF, Powell JJ. Small and dangerous? Potential toxicity mechanisms of common exposure particles and nanoparticles. *Curr Opin Toxicol*.

2020;19:93-98. doi:10.1016/j.cotox.2020.01.006

18. Zhang X-F, Liu Z-G, Shen W, Gurunathan S. Silver Nanoparticles: Synthesis, characterization, properties, applications, and therapeutic approaches. *Int J Mol Sci*. 2016;17(9):1534. doi:10.3390/ijms17091534

19. Li W-R, Xie X-B, Shi Q-S, Zeng H-Y, Ou-Yang Y-S, Chen Y-B. Antibacterial activity and mechanism of silver nanoparticles on Escherichia coli. *Appl Microbiol Biotechnol*. 2010;85(4):1115-1122. doi:10.1007/s00253-009-2159-5

20. Cameron SJ, Hosseinian F, Willmore WG. A current overview of the biological and cellular effects of nanosilver. *Int J Mol Sci*. 2018;19(7):2030. doi:10.3390/ijms19072030

21. Jena P, Mohanty S, Mallick R, Jacob B, Sonawane A. Toxicity and antibacterial assessment of chitosan-coated silver nanoparticles on human pathogens and macrophage cells. *Int J Nanomedicine*. 2012;7:1805-1818. doi:10.2147/IJN.S28077

22. Rozhin A, Batasheva S, Kruychkova M, Cherednichenko Y, Rozhina E, Fakhrullin R. Biogenic Silver nanoparticles: synthesis and application as antibacterial and antifungal agents. *Micromachines*. 2021;12(12). doi:10.3390/mi12121480

23. Galdiero S, Falanga A, Vitiello M, Cantisani M, Marra V, Galdiero M. Silver nanoparticles as potential antiviral agents. *Molecules*. 2011;16(10):8894-8918. doi:10.3390/molecules16108894

24. Hsin Y-H, Chen C-F, Huang S, Shih T-S, Lai P-S, Chueh PJ. The apoptotic effect of nanosilver is mediated by a ROS- and JNK-dependent mechanism involving the mitochondrial pathway in NIH3T3 cells. *Toxicol Lett*. 2008;179(3):130-139.

doi:10.1016/j.toxlet.2008.04.015

25. Nate S. Nanosilver: Weighing the risks and benefits. *Environ Health Perspect*. 2013;121(7):a220-a225. doi:10.1289/ehp.121-a220

26. Liu J, Zhao Y, Guo Q, et al. TAT-modified nanosilver for combating multidrug-resistant cancer. *Biomaterials*. 2012;33(26):6155-6161. doi:10.1016/j.biomaterials.2012.05.035

27. Thompson EA, Graham E, MacNeill CM, et al. Differential response of MCF7, MDA-MB-231, and MCF 10A cells to hyperthermia, silver nanoparticles and silver nanoparticle-induced photothermal therapy. *Int J Hyperth Off J Eur Soc Hyperthermic Oncol North Am Hyperth Gr*. 2014;30(5):312-323. doi:10.3109/02656736.2014.936051

28. M JF, P L. Apoptotic efficacy of biogenic silver nanoparticles on human breast cancer MCF-7 cell lines. *Prog Biomater*. 2015;4(2-4):113-121. doi:10.1007/s40204-015-0042-2

29. Sathishkumar G, Gobinath C, Wilson A, Sivaramakrishnan S. Dendrophthoe falcata (L.f) Ettingsh (Neem mistletoe): a potent bioresource to fabricate silver nanoparticles for anticancer effect against human breast cancer cells (MCF-7). *Spectrochim Acta A Mol Biomol Spectrosc*. 2014;128:285-290. doi:10.1016/j.saa.2014.02.096

30. Raghunandan D, Ravishankar B, Sharanbasava G, et al. Anti-cancer studies of noble metal nanoparticles synthesized using different plant extracts. *Cancer Nanotechnol*. 2011;2(1-6):57-65. doi:10.1007/s12645-011-0014-8

31. Ma H, Huang S, Feng X, et al. Electrochemical synthesis and fabrication of gold

nanostructures based on poly(N-vinylpyrrolidone). *Chemphyschem*. 2006;7(2):333-335. doi:10.1002/cphc.200500398

32. Ahlberg S, Antonopulos A, Diendorf J, et al. PVP-coated, negatively charged silver nanoparticles: A multi-center study of their physicochemical characteristics, cell culture and in vivo experiments. *Beilstein J Nanotechnol*. 2014;5:1944-1965. doi:10.3762/bjnano.5.205

33. Firdhouse MJ, Lalitha P. Apoptotic efficacy of biogenic silver nanoparticles on human breast cancer MCF-7 cell lines. *Prog Biomater*. 2015;4(2-4):113-121. doi:10.1007/s40204-015-0042-2

34. Gopinath P, Gogoi SK, Sanpui P, Paul A, Chattopadhyay A, Ghosh SS. Signaling gene cascade in silver nanoparticle induced apoptosis. *Colloids Surf B Biointerfaces*. 2010;77(2):240-245. doi:10.1016/j.colsurfb.2010.01.033

35. Stensberg MC, Wei Q, McLamore ES, Porterfield DM, Wei A, Sepulveda MS. Toxicological studies on silver nanoparticles: challenges and opportunities in assessment, monitoring and imaging. *Nanomedicine (Lond)*. 2011;6(5):879-898. doi:10.2217/nnm.11.78

36. Burdusel A-C, Gherasim O, Grumezescu AM, Mogoanta L, Ficai A, Andronescu E. Biomedical applications of silver nanoparticles: an up-to-date overview. *Nanomater (Basel, Switzerland)*. 2018;8(9). doi:10.3390/nano8090681

37. Fedorenko S V, Grechkina SL, Mukhametshina AR, et al. Silica nanoparticles with Tb(III)-centered luminescence decorated by Ag(0) as efficient cellular contrast agent with anticancer effect. *J Inorg Biochem*. 2018;182:170-176. doi:10.1016/j.jinorgbio.2018.02.002

38. Wu W, Zhang R, McClements DJ, Chefetz B, Polubesova T, Xing B. Transformation and speciation analysis of silver nanoparticles of dietary supplement in simulated human gastrointestinal tract. *Environ Sci Technol*. 2018;52(15):8792-8800. doi:10.1021/acs.est.8b01393

39. Mohammadzadeh R. Hypothesis: silver nanoparticles as an adjuvant for cancertherapy. *Adv Pharm Bull*. 2012;2(1):133. doi:10.5681/apb.2012.020

40. McShan D, Ray PC, Yu H. Molecular toxicity mechanism of nanosilver. *J food drug Anal*. 2014;22(1):116-127. doi:10.1016/j.jfda.2014.01.010

41. Flores-López LZ, Espinoza-Gómez H, Somanathan R. Silver nanoparticles: Electron transfer, reactive oxygen species, oxidative stress, beneficial and toxicological effects. Mini review. *J Appl Toxicol*. 2019;39(1):16-26. doi:10.1002/jat.3654

42. Wang L, Zhang T, Li P, et al. Use of synchrotron radiation-analytical techniques to reveal chemical origin of silver-nanoparticle cytotoxicity. *ACS Nano*. 2015;9(6):6532-6547. doi:10.1021/acsnano.5b02483

43. Barcińska E, Wierzbicka J, Zauszkiewicz-Pawlak A, Jacewicz D, Dabrowska A, Inkielewicz-Stepniak I. Role of oxidative and nitro-oxidative damage in silver nanoparticles cytotoxic effect against human pancreatic ductal adenocarcinoma cells. *Oxid Med Cell Longev*. 2018;2018. doi:10.1155/2018/8251961

44. Teodoro JS, Simões AM, Duarte F V., et al. Assessment of the toxicity of silver nanoparticles in vitro: A mitochondrial perspective. *Toxicol Vitr*. 2011;25(3):664-670. doi:10.1016/j.tiv.2011.01.004

45. Ziemińska E, Stafiej A, Struzyńska L. The role of the glutamatergic NMDA

receptor in nanosilver-evoked neurotoxicity in primary cultures of cerebellar granule cells. *Toxicology*. 2014;315(1):38-48. doi:10.1016/j.tox.2013.11.008

46. Wang D, Lin Z, Wang T, et al. Where does the toxicity of metal oxide nanoparticles come from: The nanoparticles, the ions, or a combination of both? *J Hazard Mater*. 2016;308:328-334. doi:10.1016/j.jhazmat.2016.01.066

47. Abdal Dayem A, Hossain MK, Lee S Bin, et al. The role of reactive oxygen species (ros) in the biological activities of metallic nanoparticles. *Int J Mol Sci*. 2017;18(1). doi:10.3390/ijms18010120

48. Giese B, Klaessig F, Park B, et al. Risks, release and concentrations of engineered nanomaterial in the environment. *Sci Rep*. 2018;8(1):1565. doi:10.1038/s41598-018-19275-4

49. Zhao J, Wang X, Hoang SA, et al. Silver nanoparticles in aquatic sediments: Occurrence, chemical transformations, toxicity, and analytical methods. *J Hazard Mater*. 2021;418:126368. doi:10.1016/j.jhazmat.2021.126368

50. Courtois P, Rorat A, Lemiere S, et al. Ecotoxicology of silver nanoparticles and their derivatives introduced in soil with or without sewage sludge: A review of effects on microorganisms, plants and animals. *Environ Pollut*. 2019;253:578-598. doi:10.1016/j.envpol.2019.07.053

51. Jiang HS, Zhang Y, Lu ZW, Lebrun R, Gontero B, Li W. Interaction between silver nanoparticles and two dehydrogenases: role of thiol groups. *Small*. 2019;15(27):e1900860. doi:10.1002/smll.201900860

52. Fabrega J, Luoma SN, Tyler CR, Galloway TS, Lead JR. Silver nanoparticles: behaviour and effects in the aquatic environment. *Environ Int*. 2011;37(2):517-

531. doi:10.1016/j.envint.2010.10.012

53. Massarsky A, Abraham R, Nguyen KC, et al. Nanosilver cytotoxicity in rainbow trout (Oncorhynchus mykiss) erythrocytes and hepatocytes. *Comp Biochem Physiol C Toxicol Pharmacol*. 2014;159:10-21. doi:10.1016/j.cbpc.2013.09.008

54. Ale A, Galdopórpora JM, Desimone MF, de la Torre FR, Cazenave J. Nanosilver and Silver nitrate toxicity in ex vivo-exposed gills of fish and mitigation by humic acids. *Bull Environ Contam Toxicol*. 2021;107(3):421-426. doi:10.1007/s00128-021-03257-w

55. Banning NC, Maccarone LD, Fisk LM, Murphy D V. Ammonia-oxidising bacteria not archaea dominate nitrification activity in semi-arid agricultural soil. *Sci Rep*. 2015;5(1):11146. doi:10.1038/srep11146

56. Hadrup N, Sharma AK, Loeschner K. Toxicity of silver ions, metallic silver, and silver nanoparticle materials after in vivo dermal and mucosal surface exposure: A review. *Regul Toxicol Pharmacol*. 2018;98:257-267. doi:10.1016/j.yrtph.2018.08.007

57. Sung JH, Ji JH, Yoon JU, et al. Lung function changes in Sprague-Dawley rats after prolonged inhalation exposure to silver nanoparticles. *Inhal Toxicol*. 2008;20(6):567-574. doi:10.1080/08958370701874671

58. Gurunathan S, Lee K-J, Kalishwaralal K, Sheikpranbabu S, Vaidyanathan R, Eom SH. Antiangiogenic properties of silver nanoparticles. *Biomaterials*. 2009;30(31):6341-6350. doi:10.1016/j.biomaterials.2009.08.008

59. Jang S, Park JW, Cha HR, et al. Silver nanoparticles modify VEGF signaling pathway and mucus hypersecretion in allergic airway inflammation. *Int J*

Nanomedicine. 2012;7:1329-1343. doi:10.2147/IJN.S27159

60. Paladini F, Pollini M. Antimicrobial silver nanoparticles for wound healing application: progress and future trends. *Mater (Basel, Switzerland)*. 2019;12(16). doi:10.3390/ma12162540

61. Kalantari K, Mostafavi E, Afifi AM, et al. Wound dressings functionalized with silver nanoparticles: promises and pitfalls. *Nanoscale*. 2020;12(4):2268-2291. doi:10.1039/c9nr08234d

62. Gong C-P, Li S-C, Wang R-Y. Development of biosynthesized silver nanoparticles based formulation for treating wounds during nursing care in hospitals. *J Photochem Photobiol B*. 2018;183:137-141. doi:10.1016/j.jphotobiol.2018.04.030

63. Kang K, Lim D-H, Choi I-H, et al. Vascular tube formation and angiogenesis induced by polyvinylpyrrolidone-coated silver nanoparticles. *Toxicol Lett*. 2011;205(3):227-234. doi:10.1016/j.toxlet.2011.05.1033

64. Parveen R, Shamsi TN, Fatima S. Nanoparticles-protein interaction: Role in protein aggregation and clinical implications. *Int J Biol Macromol*. 2017;94(Pt A):386-395. doi:10.1016/j.ijbiomac.2016.10.024

65. Durán N, Silveira CP, Durán M, Martinez DST. Silver nanoparticle protein corona and toxicity: a mini-review. *J Nanobiotechnology*. 2015;13:55. doi:10.1186/s12951-015-0114-4

66. Wang M, Fu C, Liu X, Lin Z, Yang N, Yu S. Probing the mechanism of plasma protein adsorption on Au and Ag nanoparticles with FT-IR spectroscopy. *Nanoscale*. 2015;7(37):15191-15196. doi:10.1039/c5nr04498g

67. Armstrong N, Ramamoorthy M, Lyon D, Jones K, Duttaroy A. Mechanism of

silver nanoparticles action on insect pigmentation reveals intervention of copper homeostasis. *PLoS One*. 2013;8(1):e53186. doi:10.1371/journal.pone.0053186

68. Ilyechova EY, Saveliev AN, Skvortsov AN, et al. The effects of silver ions on copper metabolism in rats. *Metallomics*. 2014;6(10):1970-1987. doi:10.1039/c4mt00107a

69. Florianczyk B. Metallothioneins and its role in metal regulation, binding of reactive oxygen species, apoptosis and cell differentiation. *J Pre-clinical Clin Res*. 2007;1(1).

70. Ziemińska E, Strużyńska L. Zinc modulates nanosilver-induced toxicity in primary neuronal cultures. *Neurotox Res*. 2016;29(2):325-343. doi:10.1007/s12640-015-9583-3

71. Pizzino G, Irrera N, Cucinotta M, et al. Oxidative stress: harms and benefits for human health. *Oxid Med Cell Longev*. 2017;2017:8416763. doi:10.1155/2017/8416763

72. Li J, Cao F, Yin H-L, et al. Ferroptosis: past, present and future. *Cell Death Dis*. 2020;11(2):88. doi:10.1038/s41419-020-2298-2

73. Beg M, Maji A, Mandal AK, Das S, Jha PK, Hossain M. Spectroscopic investigation on interaction of biogenic, Croton bonplandianum leaves extract mediated potential bactericidal silver nanoparticles with human hemoglobin and human serum albumin. *J Biomol Struct Dyn*. 2018;36(3):711-723. doi:10.1080/07391102.2017.1294505

74. Mahato M, Pal P, Tah B, Ghosh M, Talapatra GB. Study of silver nanoparticle-hemoglobin interaction and composite formation. *Colloids Surf B Biointerfaces*.

2011;88(1):141-149. doi:10.1016/j.colsurfb.2011.06.024

75. Zolghadri S, Saboury AA, Golestani A, Divsalar A, Rezaei-Zarchi S, Moosavi-Movahedi AA. Interaction between silver nanoparticle and bovine hemoglobin at different temperatures. *J Nanoparticle Res*. 2008;11(7):1751. doi:10.1007/s11051-008-9538-1

76. Miyayama T, Arai Y, Suzuki N, Hirano S. Cellular distribution and behavior of metallothionein in mammalian cells following exposure to silver nanoparticles and silver ions. *Yakugaku Zasshi*. 2014;134(6):723-729. doi:10.1248/yakushi.14-00035-1

77. Liu W, Worms IAM, Herlin-Boime N, et al. Interaction of silver nanoparticles with metallothionein and ceruloplasmin: impact on metal substitution by Ag(i), corona formation and enzymatic activity. *Nanoscale*. 2017;9(19):6581-6594. doi:10.1039/c7nr01075c

78. Oh J-H, Son M-Y, Choi M-S, et al. Integrative analysis of genes and miRNA alterations in human embryonic stem cells-derived neural cells after exposure to silver nanoparticles. *Toxicol Appl Pharmacol*. 2016;299:8-23. doi:10.1016/j.taap.2015.11.004

79. Asharani P V, Hande MP, Valiyaveettil S. Anti-proliferative activity of silver nanoparticles. *BMC Cell Biol*. 2009;10:65. doi:10.1186/1471-2121-10-65

80. Lee Y-H, Cheng F-Y, Chiu H-W, et al. Cytotoxicity, oxidative stress, apoptosis and the autophagic effects of silver nanoparticles in mouse embryonic fibroblasts. *Biomaterials*. 2014;35(16):4706-4715. doi:10.1016/j.biomaterials.2014.02.021

81. Gao M, Zhao B, Chen M, et al. Nrf-2-driven long noncoding RNA ODRUL

contributes to modulating silver nanoparticle-induced effects on erythroid cells. *Biomaterials*. 2017;130:14-27. doi:10.1016/j.biomaterials.2017.03.027

82. Jeong J-K, Gurunathan S, Kang M-H, et al. Hypoxia-mediated autophagic flux inhibits silver nanoparticle-triggered apoptosis in human lung cancer cells. *Sci Rep*. 2016;6:21688. doi:10.1038/srep21688

83. Sahu SC, Zheng J, Graham L, et al. Comparative cytotoxicity of nanosilver in human liver HepG2 and colon Caco2 cells in culture. *J Appl Toxicol*. 2014;34(11):1155-1166. doi:10.1002/jat.2994

84. Wang Z, Liu S, Ma J, et al. Silver nanoparticles induced RNA polymerase-silver binding and RNA transcription inhibition in erythroid progenitor cells. *ACS Nano*. 2013;7(5):4171-4186. doi:10.1021/nn400594s

85. Qian Y, Zhang J, Hu Q, et al. Silver nanoparticle-induced hemoglobin decrease involves alteration of histone 3 methylation status. *Biomaterials*. 2015;70:12-22. doi:10.1016/j.biomaterials.2015.08.015

86. Chen Y, Wang Z, Xu M, et al. Nanosilver incurs an adaptive shunt of energy metabolism mode to glycolysis in tumor and nontumor cells. *ACS Nano*. 2014;8(6):5813-5825. doi:10.1021/nn500719m

87. Gabay C. Interleukin-6 and chronic inflammation. *Arthritis Res Ther*. 2006;8 Suppl 2(Suppl 2):S3. doi:10.1186/ar1917

88. Karlsson HL, Gliga AR, Calléja FMGR, et al. Mechanism-based genotoxicity screening of metal oxide nanoparticles using the ToxTracker panel of reporter cell lines. *Part Fibre Toxicol*. 2014;11:41. doi:10.1186/s12989-014-0041-9

89. Khan AA, Allemailem KS, Almatroudi A, et al. Endoplasmic reticulum stress

provocation by different nanoparticles: an innovative approach to manage the cancer and other common diseases. *Molecules*. 2020;25(22). doi:10.3390/molecules25225336

90. Yang T, Yao Q, Cao F, Liu Q, Liu B, Wang X-H. Silver nanoparticles inhibit the function of hypoxia-inducible factor-1 and target genes: insight into the cytotoxicity and antiangiogenesis. *Int J Nanomedicine*. 2016;11:6679-6692. doi:10.2147/IJN.S109695

91. Chen Y, Yang T, Chen S, Qi S, Zhang Z, Xu Y. Silver nanoparticles regulate autophagy through lysosome injury and cell hypoxia in prostate cancer cells. *J Biochem Mol Toxicol*. 2020;34(5):e22474. doi:10.1002/jbt.22474

92. Firdhouse MJ, Lalitha P. Biosynthesis of silver nanoparticles using the extract of Alternanthera sessilis-antiproliferative effect against prostate cancer cells. *Cancer Nanotechnol*. 2013;4(6):137-143. doi:10.1007/s12645-013-0045-4

93. Jha M, Shimpi NG. Green synthesis of zero valent colloidal nanosilver targeting A549 lung cancer cell: In vitro cytotoxicity. *J Genet Eng Biotechnol*. 2018;16(1):115-124. doi:10.1016/j.jgeb.2017.12.001

94. Chugh H, Sood D, Chandra I, Tomar V, Dhawan G, Chandra R. Role of gold and silver nanoparticles in cancer nano-medicine. *Artif cells, nanomedicine, Biotechnol*. 2018;46(sup1):1210-1220. doi:10.1080/21691401.2018.1449118

95. Kathiravan V, Ravi S, Ashokkumar S. Synthesis of silver nanoparticles from Melia dubia leaf extract and their in vitro anticancer activity. *Spectrochim Acta A Mol Biomol Spectrosc*. 2014;130:116-121. doi:10.1016/j.saa.2014.03.107

96. Head KA. Ascorbic acid in the prevention and treatment of cancer. *Altern Med*

Rev. 1998;3(3):174-186.

97. Reang J, Sharma PC, Thakur VK, Majeed J. Understanding the therapeutic potential of ascorbic acid in the battle to overcome cancer. *Biomolecules*. 2021;11(8). doi:10.3390/biom11081130

98. Carr AC, Cook J. Intravenous vitamin C for cancer therapy - identifying the current gaps in our knowledge. *Front Physiol*. 2018;9:1182. doi:10.3389/fphys.2018.01182

99. Taghyan SA, Messiry H El, Zainy MA El. Evaluation of the toxic effect of silver nanoparticles and the possible protective effect of ascorbic acid on the parotid glands of albino rats: An in vivo study. *Toxicol Ind Health*. 2020;36(6):446-453. doi:10.1177/0748233720933071

100. Brieger K, Schiavone S, Miller FJJ, Krause K-H. Reactive oxygen species: from health to disease. *Swiss Med Wkly*. 2012;142:w13659. doi:10.4414/smw.2012.13659

101. Dröge W. Free radicals in the physiological control of cell function. *Physiol Rev*. 2002;82(1):47-95. doi:10.1152/physrev.00018.2001

102. Truong TH, Carroll KS. Redox regulation of protein kinases. *Crit Rev Biochem Mol Biol*. 2013;48(4):332-356. doi:10.3109/10409238.2013.790873

103. He L, He T, Farrar S, Ji L, Liu T, Ma X. Antioxidants maintain cellular redox homeostasis by elimination of reactive oxygen species. *Cell Physiol Biochem Int J Exp Cell Physiol Biochem Pharmacol*. 2017;44(2):532-553. doi:10.1159/000485089

104. Saha S, Buttari B, Panieri E, Profumo E, Saso L. An overview of nrf2 signaling

pathway and its role in inflammation. *Molecules*. 2020;25(22). doi:10.3390/molecules25225474

105. Simmons SO, Fan C-Y, Ramabhadran R. Cellular stress response pathway system as a sentinel ensemble in toxicological screening. *Toxicol Sci*. 2009;111(2):202-225. doi:10.1093/toxsci/kfp140

106. Digaleh H, Kiaei M, Khodagholi F. Nrf2 and Nrf1 signaling and ER stress crosstalk: implication for proteasomal degradation and autophagy. *Cell Mol Life Sci*. 2013;70(24):4681-4694. doi:10.1007/s00018-013-1409-y

107. Ma Q. Role of nrf2 in oxidative stress and toxicity. *Annu Rev Pharmacol Toxicol*. 2013;53:401-426. doi:10.1146/annurev-pharmtox-011112-140320

108. Loboda A, Jozkowicz A, Dulak J. HIF-1 and HIF-2 transcription factors--similar but not identical. *Mol Cells*. 2010;29(5):435-442. doi:10.1007/s10059-010-0067-2

109. Lee J-W, Bae S-H, Jeong J-W, Kim S-H, Kim K-W. Hypoxia-inducible factor (HIF-1)alpha: its protein stability and biological functions. *Exp Mol Med*. 2004;36(1):1-12. doi:10.1038/emm.2004.1

110. Dengler VL, Galbraith M, Espinosa JM. Transcriptional regulation by hypoxia inducible factors. *Crit Rev Biochem Mol Biol*. 2014;49(1):1-15. doi:10.3109/10409238.2013.838205

111. Semenza GL. HIF-1 and mechanisms of hypoxia sensing. *Curr Opin Cell Biol*. 2001;13(2):167-171. doi:10.1016/s0955-0674(00)00194-0

112. Ke Q, Costa M. Hypoxia-inducible factor-1 (HIF-1). *Mol Pharmacol*. 2006;70(5):1469-1480. doi:10.1124/mol.106.027029

113. Albanese A, Daly LA, Mennerich D, Kietzmann T, Sée V. The role of hypoxia-

inducible factor post-translational modifications in regulating its localisation, stability, and activity. *Int J Mol Sci*. 2020;22(1). doi:10.3390/ijms22010268

114. Gonzalez FJ, Xie C, Jiang C. The role of hypoxia-inducible factors in metabolic diseases. *Nat Rev Endocrinol*. 2018;15(1):21-32. doi:10.1038/s41574-018-0096-z
115. Oakes SA, Papa FR. The role of endoplasmic reticulum stress in human pathology. *Annu Rev Pathol*. 2015;10:173-194. doi:10.1146/annurev-pathol-012513-104649
116. Anelli T, Sitia R. Protein quality control in the early secretory pathway. *EMBO J*. 2008;27(2):315-327. doi:10.1038/sj.emboj.7601974
117. Oslowski CM, Urano F. Measuring ER stress and the unfolded protein response using mammalian tissue culture system. *Methods Enzymol*. 2011;490:71-92. doi:10.1016/B978-0-12-385114-7.00004-0
118. Hetz C. The unfolded protein response: controlling cell fate decisions under ER stress and beyond. *Nat Rev Mol Cell Biol*. 2012;13(2):89-102. doi:10.1038/nrm3270
119. Fusakio ME, Willy JA, Wang Y, et al. Transcription factor ATF4 directs basal and stress-induced gene expression in the unfolded protein response and cholesterol metabolism in the liver. *Mol Biol Cell*. 2016;27(9):1536-1551. doi:10.1091/mbc.E16-01-0039
120. Yoshida H, Uemura A, Mori K. pXBP1(U), a negative regulator of the unfolded protein response activator pXBP1(S), targets ATF6 but not ATF4 in proteasome-mediated degradation. *Cell Struct Funct*. 2009;34(1):1-10. doi:10.1247/csf.06028
121. Uemura A, Oku M, Mori K, Yoshida H. Unconventional splicing of XBP1 mRNA occurs in the cytoplasm during the mammalian unfolded protein response. *J Cell*

Sci. 2009;122(16):2877-2886. doi:10.1242/jcs.040584

122. Liu Z, Lv Y, Zhao N, Guan G, Wang J. Protein kinase R-like ER kinase and its role in endoplasmic reticulum stress-decided cell fate. *Cell Death Dis*. 2015;6(7):e1822. doi:10.1038/cddis.2015.183

123. Wortel IMN, van der Meer LT, Kilberg MS, van Leeuwen FN. Surviving stress: modulation of atf4-mediated stress responses in normal and malignant cells. *Trends Endocrinol Metab*. 2017;28(11):794-806. doi:10.1016/j.tem.2017.07.003

124. Barrera M-J, Aguilera S, Castro I, et al. Pro-inflammatory cytokines enhance ERAD and ATF6α pathway activity in salivary glands of Sjögren's syndrome patients. *J Autoimmun*. 2016;75:68-81. doi:10.1016/j.jaut.2016.07.006

125. Hu H, Tian M, Ding C, Yu S. The C/EBP Homologous protein (CHOP) transcription factor functions in endoplasmic reticulum stress-induced apoptosis and microbial infection. *Front Immunol*. 2018;9:3083. doi:10.3389/fimmu.2018.03083

126. Dandekar A, Mendez R, Zhang K. Cross talk between ER stress, oxidative stress, and inflammation in health and disease. *Methods Mol Biol*. 2015;1292:205-214. doi:10.1007/978-1-4939-2522-3_15

127. Hasnain SZ. Endoplasmic reticulum and oxidative stress in immunopathology: understanding the crosstalk between cellular stress and inflammation. *Clin Transl Immunol*. 2018;7(7):e1035. doi:10.1002/cti2.1035

128. Díaz-Bulnes P, Saiz ML, López-Larrea C, Rodríguez RM. Crosstalk between hypoxia and er stress response: a key regulator of macrophage polarization. *Front Immunol*. 2019;10:2951. doi:10.3389/fimmu.2019.02951

129. Nusse R, Brown A, Papkoff J, et al. A new nomenclature for int-1 and related genes: the Wnt gene family. *Cell*. 1991;64(2):231. doi:10.1016/0092-8674(91)90633-a

130. Taciak B, Pruszynska I, Kiraga L, Bialasek M, Krol M. Wnt signaling pathway in development and cancer. *J Physiol Pharmacol an Off J Polish Physiol Soc*. 2018;69(2). doi:10.26402/jpp.2018.2.07

131. Nusse R. Wnt signaling in disease and in development. *Cell Res*. 2005;15(1):28-32. doi:10.1038/sj.cr.7290260

132. Duchartre Y, Kim Y-M, Kahn M. The Wnt signaling pathway in cancer. *Crit Rev Oncol Hematol*. 2016;99:141-149. doi:10.1016/j.critrevonc.2015.12.005

133. Logan CY, Nusse R. THE WNT SIGNALING PATHWAY IN DEVELOPMENT AND DISEASE. *Annu Rev Cell Dev Biol*. 2004;20(1):781-810. doi:10.1146/annurev.cellbio.20.010403.113126

134. Guan X, Fierke CA. Understanding protein palmitoylation: biological significance and enzymology. *Sci China Chem*. 2011;54(12):1888-1897. doi:10.1007/s11426-011-4428-2

135. Zhan T, Rindtorff N, Boutros M. Wnt signaling in cancer. *Oncogene*. 2017;36(11):1461-1473. doi:10.1038/onc.2016.304

136. Lombard AP, Liu C, Armstrong CM, et al. Wntless promotes cellular viability and resistance to enzalutamide in castration-resistant prostate cancer cells. *Am J Clin Exp Urol*. 2019;7(4):203-214.

137. Das S, Yu S, Sakamori R, Stypulkowski E, Gao N. Wntless in Wnt secretion: molecular, cellular and genetic aspects. *Front Biol (Beijing)*. 2012;7(6):587-593.

doi:10.1007/s11515-012-1200-8

138. Bänziger C, Soldini D, Schütt C, Zipperlen P, Hausmann G, Basler K. Wntless, a conserved membrane protein dedicated to the secretion of Wnt proteins from signaling cells. *Cell*. 2006;125(3):509-522. doi:10.1016/j.cell.2006.02.049

139. Zhang H, Zhang H, Zhang Y, et al. Dishevelled-DEP domain interacting protein (DDIP) inhibits Wnt signaling by promoting TCF4 degradation and disrupting the TCF4/beta-catenin complex. *Cell Signal*. 2010;22(11):1753-1760. doi:10.1016/j.cellsig.2010.06.016

140. Logan CY, Nusse R. The wnt signaling pathway in development and disease. *Annu Rev Cell Dev Biol*. 2004;20(1):781-810. doi:10.1146/annurev.cellbio.20.010403.113126

141. Nelson WJ, Nusse R. Convergence of Wnt, beta-catenin, and cadherin pathways. *Science*. 2004;303(5663):1483-1487. doi:10.1126/science.1094291

142. Veeman MT, Axelrod JD, Moon RT. A second canon. Functions and mechanisms of beta-catenin-independent Wnt signaling. *Dev Cell*. 2003;5(3):367-377. doi:10.1016/s1534-5807(03)00266-1

143. Eryılmaz O, Ateş PS, Ünal İ, et al. Evaluation of the interaction between proliferation, oxidant-antioxidant status, Wnt pathway, and apoptosis in zebrafish embryos exposed to silver nanoparticles used in textile industry. *J Biochem Mol Toxicol*. 2018;32(1). doi:10.1002/jbt.22015

144. Corda G, Sala A. Non-canonical WNT/PCP signalling in cancer: Fzd6 takes centre stage. *Oncogenesis*. 2017;6(7):e364-e364. doi:10.1038/oncsis.2017.69

145. Nishimura T, Honda H, Takeichi M. Planar cell polarity links axes of spatial

dynamics in neural-tube closure. *Cell*. 2012;149(5):1084-1097. doi:10.1016/j.cell.2012.04.021

146. MacDonald BT, Tamai K, He X. Wnt/beta-catenin signaling: components, mechanisms, and diseases. *Dev Cell*. 2009;17(1):9-26. doi:10.1016/j.devcel.2009.06.016

147. Komiya Y, Habas R. Wnt signal transduction pathways. *Organogenesis*. 2008;4(2):68-75. doi:10.4161/org.4.2.5851

148. Rao TP, Kühl M. An updated overview on Wnt signaling pathways: a prelude for more. *Circ Res*. 2010;106(12):1798-1806. doi:10.1161/CIRCRESAHA.110.219840

149. Bo H, Zhang S, Gao L, et al. Upregulation of Wnt5a promotes epithelial-to-mesenchymal transition and metastasis of pancreatic cancer cells. *BMC Cancer*. 2013;13:496. doi:10.1186/1471-2407-13-496

150. Nougarède A, Tesnière C, Ylanko J, Rimokh R, Gillet G, Andrews DW. Improved IRE1 and PERK pathway sensors for multiplex endoplasmic reticulum stress assay reveal stress response to nuclear dyes used for image segmentation. *Assay Drug Dev Technol*. 2018;16(6):350-360. doi:10.1089/adt.2018.862

151. Chen Q, Espey MG, Krishna MC, et al. Pharmacologic ascorbic acid concentrations selectively kill cancer cells: action as a pro-drug to deliver hydrogen peroxide to tissues. *Proc Natl Acad Sci U S A*. 2005;102(38):13604-13609. doi:10.1073/pnas.0506390102

152. Zhu K, Meng Q, Zhang Z, et al. Aryl hydrocarbon receptor pathway: Role, regulation and intervention in atherosclerosis therapy (Review). *Mol Med Rep*.

2019;20(6):4763-4773. doi:10.3892/mmr.2019.10748

153. Jia M, Zhang W, He T, et al. Evaluation of the genotoxic and oxidative damage potential of silver nanoparticles in human NCM460 and HCT116 cells. *Int J Mol Sci*. 2020;21(5). doi:10.3390/ijms21051618

154. Dasgupta N, Ranjan S, Mishra D, Ramalingam C. Thermal Co-reduction engineered silver nanoparticles induce oxidative cell damage in human colon cancer cells through inhibition of reduced glutathione and induction of mitochondria-involved apoptosis. *Chem Biol Interact*. 2018;295:109-118. doi:10.1016/j.cbi.2018.07.028

155. Javed B, Mashwani Z-U-R. Synergistic effects of physicochemical parameters on bio-fabrication of mint silver nanoparticles: structural evaluation and action against HCT116 colon cancer cells. *Int J Nanomedicine*. 2020;15:3621-3637. doi:10.2147/IJN.S254402

156. Deepika S, Selvaraj CI, Roopan SM. Screening bioactivities of Caesalpinia pulcherrima L. swartz and cytotoxicity of extract synthesized silver nanoparticles on HCT116 cell line. *Mater Sci Eng C Mater Biol Appl*. 2020;106:110279. doi:10.1016/j.msec.2019.110279

157. Gurunathan S, Qasim M, Park C, Yoo H, Kim J-H, Hong K. Cytotoxic potential and molecular pathway analysis of silver nanoparticles in human colon cancer cells HCT116. *Int J Mol Sci*. 2018;19(8). doi:10.3390/ijms19082269

158. Liao P-C, Yang EJ, Pon LA. Live-cell imaging of mitochondrial redox state in yeast cells. *STAR Protoc*. 2020;1(3):100160. doi:10.1016/j.xpro.2020.100160

159. Waypa GB, Marks JD, Guzy R, et al. Hypoxia triggers subcellular compartmental

redox signaling in vascular smooth muscle cells. *Circ Res*. 2010;106(3):526-535. doi:10.1161/CIRCRESAHA.109.206334

160. Teixeira RB, Karbasiafshar C, Sabra M, Abid MR. Optimization of mito-roGFP protocol to measure mitochondrial oxidative status in human coronary artery endothelial cells. *STAR Protoc*. 2021;2(3):100753. doi:10.1016/j.xpro.2021.100753

161. Themo Fisher Scientific. CellROX™ Deep Red Reagent, for oxidative stress detection. https://www.thermofisher.com/order/catalog/product/C10422. Accessed December 1, 2021.

162. Alnahdi A, John A, Raza H. N-acetyl cysteine attenuates oxidative stress and glutathione-dependent redox imbalance caused by high glucose/high palmitic acid treatment in pancreatic Rin-5F cells. *PLoS One*. 2019;14(12):e0226696. doi:10.1371/journal.pone.0226696

163. Manshian BB, Pfeiffer C, Pelaz B, et al. High-content imaging and gene expression approaches to unravel the effect of surface functionality on cellular interactions of silver nanoparticles. *ACS Nano*. 2015;9(10):10431-10444. doi:10.1021/acsnano.5b04661

164. Kim S, Ryu D-Y. Silver nanoparticle-induced oxidative stress, genotoxicity and apoptosis in cultured cells and animal tissues. *J Appl Toxicol*. 2013;33(2):78-89. doi:10.1002/jat.2792

165. Kim S, Choi JE, Choi J, et al. Oxidative stress-dependent toxicity of silver nanoparticles in human hepatoma cells. *Toxicol In Vitro*. 2009;23(6):1076-1084. doi:10.1016/j.tiv.2009.06.001

166. Thermo Fisher Scientific. MitoSOX™ Red Mitochondrial Superoxide Indicator, for live-cell imaging. https://www.thermofisher.com/order/catalog/product/M36008#:~:text=MitoSOX™ Red reagent is,maxima%3A ~510%2F580 nm. Accessed December 1, 2021.

167. Miranda RR, Bezerra AGJ, Oliveira Ribeiro CA, et al. Toxicological interactions of silver nanoparticles and non-essential metals in human hepatocarcinoma cell line. *Toxicol In Vitro*. 2017;40:134-143. doi:10.1016/j.tiv.2017.01.003

168. Arora S, Jain J, Rajwade JM, Paknikar KM. Interactions of silver nanoparticles with primary mouse fibroblasts and liver cells. *Toxicol Appl Pharmacol*. 2009;236(3):310-318. doi:10.1016/j.taap.2009.02.020

169. Singh M, Thomas P, Shukla D, Tulsawani R, Saxena S, Bansal A. Effect of subchronic hypobaric hypoxia on oxidative stress in rat heart. *Appl Biochem Biotechnol*. 2013;169(8):2405-2419. doi:10.1007/s12010-013-0141-2

170. Coimbra-Costa D, Alva N, Duran M, Carbonell T, Rama R. Oxidative stress and apoptosis after acute respiratory hypoxia and reoxygenation in rat brain. *Redox Biol*. 2017;12:216-225. doi:10.1016/j.redox.2017.02.014

171. Li H-S, Zhou Y-N, Li L, et al. HIF-1α protects against oxidative stress by directly targeting mitochondria. *Redox Biol*. 2019;25:101109. doi:10.1016/j.redox.2019.101109

172. Semenza GL. Hypoxia-inducible factor 1: regulator of mitochondrial metabolism and mediator of ischemic preconditioning. *Biochim Biophys Acta*. 2011;1813(7):1263-1268. doi:10.1016/j.bbamcr.2010.08.006

173. Semenza GL. Targeting HIF-1 for cancer therapy. *Nat Rev Cancer*.

2003;3(10):721-732. doi:10.1038/nrc1187

174. Jun JC, Rathore A, Younas H, Gilkes D, Polotsky VY. Hypoxia-inducible factors and cancer. *Curr sleep Med reports*. 2017;3(1):1-10. doi:10.1007/s40675-017-0062-7

175. Schultz MA, Abdel-Mageed AB, Mondal D. The nrf1 and nrf2 balance in oxidative stress regulation and androgen signaling in prostate cancer cells. *Cancers (Basel)*. 2010;2(2):1354-1378. doi:10.3390/cancers2021354

176. Li Y, Paonessa JD, Zhang Y. Mechanism of chemical activation of Nrf2. *PLoS One*. 2012;7(4):e35122. doi:10.1371/journal.pone.0035122

177. Niture SK, Kaspar JW, Shen J, Jaiswal AK. Nrf2 signaling and cell survival. *Toxicol Appl Pharmacol*. 2010;244(1):37-42. doi:10.1016/j.taap.2009.06.009

178. Zagorski JW, Turley AE, Dover HE, VanDenBerg KR, Compton JR, Rockwell CE. The Nrf2 activator, tBHQ, differentially affects early events following stimulation of Jurkat cells. *Toxicol Sci*. 2013;136(1):63-71. doi:10.1093/toxsci/kft172

179. Kubo E, Chhunchha B, Singh P, Sasaki H, Singh DP. Sulforaphane reactivates cellular antioxidant defense by inducing Nrf2/ARE/Prdx6 activity during aging and oxidative stress. *Sci Rep*. 2017;7(1):14130. doi:10.1038/s41598-017-14520-8

180. Prasad RY, McGee JK, Killius MG, et al. Investigating oxidative stress and inflammatory responses elicited by silver nanoparticles using high-throughput reporter genes in HepG2 cells: effect of size, surface coating, and intracellular uptake. *Toxicol In Vitro*. 2013;27(6):2013-2021. doi:10.1016/j.tiv.2013.07.005

181. Chorley B, Ward W, Simmons SO, Vallanat B, Veronesi B. The cellular and

genomic response of rat dopaminergic neurons (N27) to coated nanosilver. *Neurotoxicology*. 2014;45:12-21. doi:10.1016/j.neuro.2014.08.010

182. Sahu SC, Zheng J, Yourick JJ, Sprando RL, Gao X. Toxicogenomic responses of human liver HepG2 cells to silver nanoparticles. *J Appl Toxicol*. 2015;35(10):1160-1168. doi:10.1002/jat.3170

183. Simard J-C, Durocher I, Girard D. Silver nanoparticles induce irremediable endoplasmic reticulum stress leading to unfolded protein response dependent apoptosis in breast cancer cells. *Apoptosis*. 2016;21(11):1279-1290. doi:10.1007/s10495-016-1285-7

184. Persaud I, Shannahan JH, Raghavendra AJ, Alsaleh NB, Podila R, Brown JM. Biocorona formation contributes to silver nanoparticle induced endoplasmic reticulum stress. *Ecotoxicol Environ Saf*. 2019;170:77-86. doi:10.1016/j.ecoenv.2018.11.107

185. Christen V, Fent K. Silica nanoparticles induce endoplasmic reticulum stress response and activate mitogen activated kinase (MAPK) signalling. *Toxicol reports*. 2016;3:832-840. doi:10.1016/j.toxrep.2016.10.009

186. Li L, Cui J, Liu Z, et al. Silver nanoparticles induce SH-SY5Y cell apoptosis via endoplasmic reticulum- and mitochondrial pathways that lengthen endoplasmic reticulum-mitochondria contact sites and alter inositol-3-phosphate receptor function. *Toxicol Lett*. 2018;285(September 2017):156-167. doi:10.1016/j.toxlet.2018.01.004

187. Huo L, Chen R, Zhao L, et al. Silver nanoparticles activate endoplasmic reticulum stress signaling pathway in cell and mouse models: The role in toxicity evaluation.

Biomaterials. 2015;61:307-315. doi:10.1016/j.biomaterials.2015.05.029

188. De Jong WH, Van Der Ven LTM, Sleijffers A, et al. Systemic and immunotoxicity of silver nanoparticles in an intravenous 28 days repeated dose toxicity study in rats. *Biomaterials*. 2013;34(33):8333-8343. doi:10.1016/j.biomaterials.2013.06.048

189. Zhang R, Piao MJ, Kim KC, et al. Endoplasmic reticulum stress signaling is involved in silver nanoparticles-induced apoptosis. *Int J Biochem Cell Biol*. 2012;44(1):224-232. doi:10.1016/j.biocel.2011.10.019

190. Chen R, Zhao L, Bai R, et al. Silver nanoparticles induced oxidative and endoplasmic reticulum stresses in mouse tissues: implications for the development of acute toxicity after intravenous administration. *Toxicol Res (Camb)*. 2016;5(2):602-608. doi:10.1039/c5tx00464k

191. Koumenis C. ER stress, hypoxia tolerance and tumor progression. *Curr Mol Med*. 2006;6(1):55-69. doi:10.2174/156652406775574604

192. Zhang N, Ji N, Jiang W-M, et al. Hypoxia-induced autophagy promotes human prostate stromal cells survival and ER-stress. *Biochem Biophys Res Commun*. 2015;464(4):1107-1112. doi:10.1016/j.bbrc.2015.07.086

193. Novais EJ, Choi H, Madhu V, et al. Hypoxia and Hypoxia-Inducible Factor-1α Regulate Endoplasmic Reticulum Stress in Nucleus Pulposus Cells: Implications of Endoplasmic Reticulum Stress for Extracellular Matrix Secretion. *Am J Pathol*. 2021;191(3):487-502. doi:10.1016/j.ajpath.2020.11.012

194. Feldman DE, Chauhan V, Koong AC. The unfolded protein response: a novel component of the hypoxic stress response in tumors. *Mol Cancer Res*.

2005;3(11):597-605. doi:10.1158/1541-7786.MCR-05-0221

195. Jung SK, Kim JH, Kim HJ, Ji YH, Kim JH, Son SW. Silver nanoparticle-induced hMSC proliferation is associated with HIF-1α-mediated upregulation of IL-8 expression. *J Invest Dermatol*. 2014;134(12):3003-3007. doi:10.1038/jid.2014.281

196. Park E-J, Yi J, Kim Y, Choi K, Park K. Silver nanoparticles induce cytotoxicity by a Trojan-horse type mechanism. *Toxicol In Vitro*. 2010;24(3):872-878. doi:10.1016/j.tiv.2009.12.001

197. Liu W, Wu Y, Wang C, et al. Impact of silver nanoparticles on human cells: effect of particle size. *Nanotoxicology*. 2010;4(3):319-330. doi:10.3109/17435390.2010.483745

198. Eom H-J, Choi J. p38 MAPK activation, DNA damage, cell cycle arrest and apoptosis as mechanisms of toxicity of silver nanoparticles in Jurkat T cells. *Environ Sci Technol*. 2010;44(21):8337-8342. doi:10.1021/es1020668

199. Piao MJ, Kang KA, Lee IK, et al. Silver nanoparticles induce oxidative cell damage in human liver cells through inhibition of reduced glutathione and induction of mitochondria-involved apoptosis. *Toxicol Lett*. 2011;201(1):92-100. doi:10.1016/j.toxlet.2010.12.010

200. Austin LA, Ahmad S, Kang B, et al. Cytotoxic effects of cytoplasmic-targeted and nuclear-targeted gold and silver nanoparticles in HSC-3 cells - A mechanistic study. *Toxicol Vitr*. 2015;29(4):694-705. doi:10.1016/j.tiv.2014.11.003

201. McCracken C, Zane A, Knight DA, Hommel E, Dutta PK, Waldman WJ. Oxidative stress-mediated inhibition of intestinal epithelial cell proliferation by silver nanoparticles. *Toxicol In Vitro*. 2015;29(7):1793-1808.

doi:10.1016/j.tiv.2015.07.017

202. Wei L, Tang J, Zhang Z, Chen Y, Zhou G, Xi T. Investigation of the cytotoxicity mechanism of silver nanoparticles in vitro. *Biomed Mater*. 2010;5(4):44103. doi:10.1088/1748-6041/5/4/044103

203. O'Grady S, Lawless MW. Chapter 12 - Liver Cancer (Hepatocellular Carcinoma). In: Gray SGBT-ECT, ed. Boston: Academic Press; 2015:269-288. doi:https://doi.org/10.1016/B978-0-12-800206-3.00012-4

204. Krek W, DeCaprio JABT-M in E. [7] Cell synchronization. In: *Oncogene Techniques*. Vol 254. Academic Press; 1995:114-124. doi:https://doi.org/10.1016/0076-6879(95)54009-1

205. Murray AW, Kirschner MW. Cyclin synthesis drives the early embryonic cell cycle. *Nature*. 1989;339(6222):275-280. doi:10.1038/339275a0

206. Kuhn M. The microtubule depolymerizing drugs nocodazole and colchicine inhibit the uptake of Listeria monocytogenes by P388D1 macrophages. *FEMS Microbiol Lett*. 1998;160(1):87-90. doi:10.1111/j.1574-6968.1998.tb12895.x

207. Zheng D, Jiang C, Yan N, et al. Wntless (Wls): A prognostic index for progression and patient survival of breast cancer. *Onco Targets Ther*. 2020;13:12649-12659. doi:10.2147/OTT.S265324

208. Adibkia K, Ehsani A, Jodaei A, Fathi E, Farahzadi R, Barzegar-Jalali M. Silver nanoparticles induce the cardiomyogenic differentiation of bone marrow derived mesenchymal stem cells via telomere length extension. *Beilstein J Nanotechnol*. 2021;12:786-797. doi:10.3762/bjnano.12.62

209. Cooper RJ, Menking-Colby MN, Humphrey KA, Victory JH, Kipps DW, Spitzer

N. Involvement of β-catenin in cytoskeleton disruption following adult neural stem cell exposure to low-level silver nanoparticles. *Neurotoxicology*. 2019;71:102-112. doi:10.1016/j.neuro.2018.12.010

210. Drost J, van Jaarsveld RH, Ponsioen B, et al. Sequential cancer mutations in cultured human intestinal stem cells. *Nature*. 2015;521(7550):43-47. doi:10.1038/nature14415

211. Matano M, Date S, Shimokawa M, et al. Modeling colorectal cancer using CRISPR-Cas9-mediated engineering of human intestinal organoids. *Nat Med*. 2015;21(3):256-262. doi:10.1038/nm.3802

212. Bhatt PM, Malgor R. Wnt5a: a player in the pathogenesis of atherosclerosis and other inflammatory disorders. *Atherosclerosis*. 2014;237(1):155-162. doi:10.1016/j.atherosclerosis.2014.08.027

213. Katoh M, Katoh M. Molecular genetics and targeted therapy of WNT-related human diseases (Review). *Int J Mol Med*. 2017;40(3):587-606. doi:10.3892/ijmm.2017.3071

214. Rünger TM, Vergilis I, Sarkar P, DePinho RA, Sharpless NE. How disruption of cell cycle regulating genes might predispose to sun-induced skin cancer. *Cell Cycle*. 2005;4(5):643-645. doi:10.4161/cc.4.5.1673

215. Russell JO, Monga SP. Wnt/β-Catenin signaling in liver development, homeostasis, and pathobiology. *Annu Rev Pathol*. 2018;13:351-378. doi:10.1146/annurev-pathol-020117-044010

216. Wang Z, Xia T, Liu S. Mechanisms of nanosilver-induced toxicological effects: more attention should be paid to its sublethal effects. *Nanoscale*.

2015;7(17):7470-7481. doi:10.1039/c5nr01133g

217. Werley CA, Boccardo S, Rigamonti A, Hansson EM, Cohen AE. Multiplexed optical sensors in arrayed islands of cells for multimodal recordings of cellular physiology. *Nat Commun*. 2020;11(1):3881. doi:10.1038/s41467-020-17607-5